Pacific Community
Communauté du Pacifique

Climate Change in the Pacific 2022:

Historical and Recent Variability, Extremes and Change

Climate and Oceans Support Program in the Pacific

Australian Government
Bureau of Meteorology

SPREP
Secretariat of the Pacific Regional Environment Programme

Australian Aid

NEW ZEALAND
FOREIGN AFFAIRS & TRADE
Aid Programme

Climate Change in the Pacific 2022:

Historical and Recent Variability, Extremes and Change

Simon McGree, Grant Smith, Elise Chandler, Nicholas Herold, Zulfikar Begg, Yuriy Kuleshov, Philip Malsale and Mathilde Ritman

Pacific Community
Communauté du Pacifique

Suva, Fiji, 2022

Original text: English

Pacific Community Cataloguing-in-publication data

McGree, Simon

Climate Change in the Pacific 2022: historical and recent variability, extremes and change / Simon McGree, Grant Smith, Elise Chandler, Nicholas Herold, Zulfikar Begg, Yuriy Kuleshov, Philip Malsale and Mathilde Rittman

1. Climatic changes — Oceania.

2. Climatic changes — Management — Oceania.

3. Climate change mitigation — Oceania.

4. Rain and rainfall — Oceania.

5. Temperature — Oceania.

6. Sea level — Oceania.

7. Cyclones — Oceania.

8. Environment — Management — Oceania.

I. McGree, Simon II. Smith, Grant III. Chandler, Elise IV. Herold, Nicholas V. Begg, Zulfikar VI. Malsale, Philip VII. Rittman, Mathilde VIII. Title IX. Pacific Community

577.220995 AACR2

ISBN: 978-982-00-1479-4

Prepared for publication and printed at SPC Suva Regional Office
Private Mail Bag, Suva, Fiji
www.spc.int

Contents

Abbreviations

CliDE	Climate Data for the Environment
COSPPac	Climate and Oceans Support Program in the Pacific
CSIRO	(Australian) Commonwealth Scientific and Industrial Research Organisation
ECMWF	European Centre for Medium-Range Weather Forecasts
EEZ	exclusive economic zone
ENSO	El Niño–Southern Oscillation
ERA5	European Centre for Medium-Range Weather Forecasts reanalysis version 5
FSM	Federated States of Micronesia
GA	Geoscience Australia
GPD	generalized Pareto distribution
IPCC	Intergovernmental Panel on Climate Change
IPO	Interdecadal Pacific Oscillation
ITCZ	Intertropical Convergence Zone
MJO	Madden–Julian Oscillation
NIWA	(New Zealand) National Institute of Water and Atmospheric
NOAA	(United States) National Oceanic and Atmospheric Administration
PACCSAP	Pacific–Australia Climate Change Science and Adaptation Planning
PCCM	Pacific Climate Change Monitor
PCCSP	Pacific Climate Change Science Program
PDO	Pacific Decadal Oscillation
PNG	Papua New Guinea
PSLGM	Pacific Sea Level and Geodetic Monitoring
RCC	Regional Climate Centre
RMI	Republic of the Marshall Islands
SHTC	Southern Hemisphere Tropical Cyclone
SPC	Pacific Community (formerly South Pacific Commission)
SPCZ	South Pacific Convergence Zone
SPEI	Standardised Rainfall Evapotranspiration Index
SPREP	(Secretariat of the) Pacific Regional Environment Programme
SST	sea surface temperature
The Bureau	(Australian) Bureau of Meteorology
WMO	World Meteorological Organization
WPM	West Pacific Monsoon

Acknowledgments

This report is an outcome of the high degree of cooperation and collaboration that exists between the implementing partners of the Australian Aid-funded Climate and Oceans Support Program in the Pacific (COSPPac), specifically the Bureau of Meteorology (BoM), the Pacific Community (SPC) and Pacific Regional Environmental Programme (SPREP), together with the valuable ongoing support from the national meteorological services in the 15 partner countries and territories.

Coordinating lead authors
Simon McGree, Grant Smith and Elise Chandler

Lead authors
Nicholas Herold, Zulfikar Begg, Yuriy Kuleshov, Philip Malsale, Mathilde Ritman and Ben Hague

Peer review
Andy Taylor, The Bureau
David Jones, The Bureau
Chalapan Kaluwin, University of Papua New Guinea
Awnesh Singh, The University of the South Pacific

Other reviewers
Andrew Jones, The Bureau
COSPPac partner country and territory national meteorological services

Editorial committee and support
Celine Becker, Merana Kitione and Azarel Mariner (COSPPac), Neil Conning & Associates, New Zealand Aid Programme, SPC Publications team

How to cite this report
McGree, S., G. Smith, E. Chandler, N. Herold, Z. Begg, Y. Kuleshov, P. Malsale and M. Ritman. 2022. Climate Change in the Pacific 2022: Historical and Recent Variability, Extremes and Change. Climate and Oceans Support Program in the Pacific. Pacific Community, Suva, Fiji.

Executive summary

About this report

This report presents key scientific findings from the second phase of the Climate and Oceans Support Program in the Pacific (COSPPac, July 2018–June 2023), Seasonal Prediction and the Pacific Sea Level and Geodetic Monitoring (PSLGM) Projects. The report contributes to COSPPac's aim for Pacific Island national meteorological services to understand and use climate, ocean and sea level data and information to develop and disseminate useful products and services to Pacific Island governments and communities, building resilience against the impact of climate change, climate variability and disasters.

The report also provides an update of scientific understanding of large-scale climate processes, variability and extremes in the western tropical Pacific first presented in the Pacific Climate Change Science Program (PCCSP) *Climate Change in the Pacific: Scientific Assessment and New Research, Volume 2, Country Reports* (2011) and the Pacific–Australia Climate Change Science and Adaptation Planning (PACCSAP) Program *Climate Variability, Extremes and Change in the Western Tropical Pacific: New Science and Updated Country Reports* (2014).

The work is designed to complement the recently released 'NextGen' Projections for the Western Tropical Pacific country reports and provide finer-scale partner country historical climate change information not presented in the Intergovernmental Panel on Climate Change (IPCC)'s Sixth Assessment Report (AR6), *Climate Change 2021: The Physical Science Basis,* and World Meteorological Organization (WMO) Regional Association Five (RA-V) Pacific Regional Climate Centre (RCC) Network's *Pacific Climate Change Monitor* (PCCM) Report (2022).

Chapter 1 provides a general introduction to the content, structure and methods used for each country report in subsequent chapters. Each subsequent country chapter has nine sections that provide: (1) a climate and ocean summary; (2) country description; (3) data availability; (4) rainfall seasonal cycle and observed trends; (5) air temperature seasonal cycle and observed trends; (6) tropical cyclone seasonal cycle and observed trends; (7) sea surface temperature (SST) seasonal cycle and observed trends; (8) sea level seasonal cycle and observed trends; and (9) wave climate, seasonal cycle, trends, and extreme value analysis. Trend lengths vary depending on data availability and quality.

It is anticipated that this report, associated products and capacity-building activities will provide decision-makers and other stakeholders in the partner countries, as well as the wider scientific community, with up-to-date, robust climate change science information for the region and the individual countries.

While producing this report, the authors identified a decline in the quality and quantity of Pacific Island climate data and metadata beginning in the 1990s. Few Pacific national meteorological services are documenting equipment maintenance/change, calibration, exposure and site changes. More than half of the countries represented in this report currently have less than two stations near-complete maximum and minimum temperature time series from the 1980s to 2020. In some cases, this represents a national network decline of greater than 80% in 30 years. Pacific Island governments and donors are requested to prioritise climate and ocean observations for the purposes of ongoing climate change monitoring in the Pacific.

Regional summary

Climate variability and current climate

Communities in COSPPac partner countries and territories experience climate and ocean variability at weekly, seasonal and longer timescales. They also experience extreme events such as droughts, tropical cyclones, coastal and river flooding, and coral bleaching. The occurrence of extreme events, and in some cases multiple events simultaneously, as well as global warming, can have devastating impacts.

An important aspect of understanding and adapting to climate change in the region is being able to differentiate between climate variability and long-term change and being able to correctly attribute extreme events to climate variability or anthropogenic climate change. This report provides communities in COSPPac partner countries and territories information on seasonal cycles, the impact of the major modes of variability and long-term change for key variables at a country scale, expanding on information provided in the WMO RA V Pacific RCC Network PCCM (2022).

El Niño and La Niña have perhaps the strongest influence on year-to-year climate variability in the Pacific. These phenomena are a part of a natural cycle known as El Niño–Southern Oscillation (ENSO) and are associated with a sustained period (many months) of warming (El Niño) or cooling (La Niña) in the central and/or eastern tropical Pacific. The ENSO cycle operates over timescales from two to seven years.

ENSO is strongly linked with variations in other climate features, such as the Pacific Warm Pool, Intertropical Convergence Zone (ITCZ), South Pacific Convergence Zone (SPCZ), West Pacific Monsoon (WPM) and trade winds associated with the subtropical belt. During La Niña events, the SPCZ is displaced southwest of its normal position, while the ITCZ moves further north of the equator. These variations influence the amount of rainfall countries in the vicinity receive. Sea level, SST, ocean waves and currents, air temperature and tropical cyclone genesis are also impacted. All COSPPac partner countries and territories experience climate and ocean variability due to ENSO, although the magnitude and timing of this influence varies.

ENSO behaviour is modified at decadal timescales by the Interdecadal Pacific Oscillation, which includes the closely related Pacific Decadal Oscillation (PDO). Understanding decadal variability is important as some Pacific climate data records are short, such as tropical cyclones and sea level, making the detection of long-term trends difficult.

The following is a summary of climate and ocean trends presented in this report that are based on updated or improved datasets.

Rainfall

- Station records show large year-to-year and decade-to-decade variability. However, long-term trends in total annual and seasonal rainfall show little change at most locations over the last 70 years.
- Trends in the extreme rainfall indices, including the standardised rainfall-evapotranspiration index (drought) and maximum one-day rainfall indices, also show little change at most locations.

Air temperature

- Station records show notable warming of mean maximum daytime and mean minimum night-time temperatures over the last 70 years (and over shorter periods). There have been significantly more warm days and nights, and fewer cool days and nights.
- There have been strong increases in the cooling degree day index across the region, suggesting that energy requirements for air conditioning have increased significantly over the last 70 years.

Tropical cyclones

- There has been little change in the total number of tropical cyclones occurring in the Southwest Pacific over the last 40 years. Over the same period, there has been a decline in the total number of severe tropical cyclones and a marginal decline in the proportion of tropical cyclones reaching severe status.
- The decline in the total number of severe tropical cyclones identified in this report differs from that for the same region and period in the WMO RA V Pacific RCC Network PCCM (2022). The PCCM reports that trends in severe tropical cyclones in the Southwest Pacific are not statistically significant. This report uses The Bureau Southern Hemisphere Tropical Cyclone (SHTC) archive, while the PCCM uses International Best Track Archive for Climate Stewardship. Reasons for the notable difference in severe tropical cyclone numbers in these datasets are unclear at this time. Further research is required to resolve this issue. The key message from both reports is that trends in severe tropical cyclones in the Southwest Pacific have not increased over the last 40 years.
- In the Northwest Pacific, there has been little change in the total number of tropical cyclones, severe tropical cyclones and proportion of tropical cyclones reaching severe status.

Sea (ocean) surface temperature

- Satellite observations show rapid warming of sea surface temperatures over the last 40 years in COSPPac partner countries and territories in the western tropical Pacific.

Sea level

- Sea level observations from satellite altimetry over the last 30 years show increases across the western tropical Pacific, but these rates vary due to large-scale climate processes. In many countries, the rate of sea-level rise is higher than the global average for the same period.
- Tide-gauge observations show higher rates of sea-level rise where land subsidence is occurring, including New Guinea Islands (PNG), Samoa, Tonga, Federated States of Micronesia (FSM), Kiribati and Nauru.

Ocean waves

- Mean annual wave height has remained unchanged at most locations over the last 44 years. Waves change from month to month with the seasons, but they also change from year to year with climate oscillations such as ENSO.

Extreme ocean waves

- Extreme wave analysis was undertaken for selected locations by defining a severe height threshold and fitting a generalized Pareto distribution. The number of wave events reaching or exceeding a particular threshold is reported over a 42-year wave record for each selected location. Average recurrence (1–100-year) interval wave heights are also presented.

1 Introduction to the country reports

© 75CentralPhotography

1.1 Summary

Climate and ocean summaries presented at the beginning of each country chapter provide an overview of the climate and ocean observations for the relevant country.

1.2 Country description

The country description provides brief details for the relevant country. This includes location in the Pacific region, island type, land area, exclusive economic zone (EEZ) size, number of islands, provinces/administrative divisions, primary sources of foreign exchange and current population.

1.3 Data

This section provides details on the meteorological and oceanographic data used in this report.

Meteorological data length, completeness and quality differs from country to country. Where data are available, the analysis start date is 1 January 1951. While some station records have data for a much longer period, 1951 was selected as the start year as the formalisation of meteorological operations for most Pacific countries and territories began during or just after the Second World War. A rapid increase in station numbers occurred in the late 1940s with a peak occurring around the early 1950s, which is the second reason for selecting 1951. For many observation sites there have been changes in station position, instrumentation and local environment that have produced inhomogeneities resulting in non-climatic step-changes in the data. For rainfall, only records or parts of records that have passed homogeneity tests are used in this report. For temperature, where possible, inhomogeneities have been identified and corrected using statistical techniques. Details on the quality control and homogenisation procedures for temperature and rainfall are presented in McGree et al. (2019). The raw and homogenised meteorological data used in this report is archived in the Pacific Climate Change Data Portal http://www.bom.gov.au/climate/pccsp.

Insufficient station daily rainfall and temperature data for Nauru and temperature data for Tokelau were available for this report. For both these countries it was determined that the European Centre for Medium-Range Weather Forecasts (ECMWF) reanalysis version 5 (ERA5) (Hersbach et al. 2020) was suitable for calculating temperature trends. Reanalysis products combine a global weather model with global ocean, land and atmospheric observations, and offer the most complete picture of historical climate. However, they also share the same limitations as models. ERA5 is a state-of-the-art reanalysis dataset providing global data at a resolution of approximately 30 km. Comparison with station data for a Pacific Island showed that ERA5 captures temperature trends well. Furthermore, temperatures do not typically vary by large amounts over small distances, particularly in oceanic environments, so grid cell temperatures from ERA5 are likely to be representative of any islands contained within them. Therefore, there is high confidence that trends from the ERA5 reanalysis are representative of station trends for small Pacific Islands.

Tropical cyclone data were provided by the Australian Tropical Cyclone Warning Centres (Brisbane, Darwin and Perth) for the Australian region (90–160°E) and by the meteorological services of Fiji and New Zealand for the eastern South Pacific Ocean (east of 160°E). Tropical cyclone tracks from these archives were merged into one archive, ensuring consistency of track data when tropical cyclones cross regional borders. For the Northwest Pacific, data were obtained from the Regional Specialised Meteorological Centre, Tokyo. These data are archived in the SHTC Data Portal http://www.bom.gov.au/cyclone/history/tracks/index.shtml and Western North Pacific Tropical Cyclone Data Portal http://www.bom.gov.au/cyclone/history/tracks/beta/?region=wnp.

Sea surface temperature (SST) data were obtained via the daily Optimum Interpolation SST version 2.1 (OISST v2.1) dataset from the National Oceanic and Atmospheric Administration (NOAA) (Reynolds et al. 2007; Banzon et al. 2016). In situ ocean temperature and sea level data were obtained from

the COSPPac PSLGM Project http://www.bom.gov.au/pacific/projects/pslm and are also available via the Pacific Ocean Portal http://oceanportal.spc.int/portal/ocean.html.

Wave data were sourced from the PACCSAP wave hindcast (Smith et al. 2021), available hourly from 1979 to present, with a grid resolution near Pacific Island countries of 7 km.

Regional sea level data were obtained from the Commonwealth Scientific and Industrial Research Organisation (CSIRO) satellite altimetry (updated by Benoit Legresy, Church and White 2011), with correction for seasonal signals, inverse barometer effect and glacial isostatic adjustment. In situ sea level data were obtained from local tide-gauges where available.

1.4 Rainfall

1.4.1 Seasonal cycle

Rainfall climatology for the selected locations is presented in this section. Influences of the main climate drivers and orography are also presented.

1.4.2 Trends

Where gaps in the daily timeseries exist and monthly values were available, there were used to extend and fill gaps in the monthly total timeseries (subject to passing quality control and homogeneity checks). Seasonal and annual totals are only presented where each month of the season/year is available. Trends in total rainfall have been calculated from monthly data.

Graphs in this section as well as the section on tropical cyclones are colour coded to differentiate El Niño, La Niña and El Niño–Southern Oscillation (ENSO) neutral years. These years are defined using the The Bureau official ENSO record http://www.bom.gov.au/climate/history/enso. Since this record ends in 2016, the status for subsequent years was obtained from the ENSO Outlook alert system http://www.bom.gov.au/climate/enso/outlook/#tabs=ENSO-Outlook-history.

The influence of ENSO on the climate of the partner countries is not always clear. This is because: (1) these events often start in the middle of one year and continue into the next; (2) the impact of ENSO on local rainfall and air temperature is not always simultaneous (that is, there can be a lag of a few months between ENSO development and impact at some locations); and (3) in some countries, ENSO does not have a major influence.

Eleven climate indices are used to characterise trends in annual and seasonal rainfall and temperature extremes. These indices are defined in Table 1.1 and are recommended by the World Meteorological Organization (WMO) Expert Team on Climate Information for Decision-Making (ET-CID) and calculated from daily data using the Climpact software (University of New South Wales 2022). To maintain statistical robustness, any months with more than three missing days of data were not computed, and any years with more than 15 missing days were also not computed. Further, linear trends were not computed when there were insufficient years or months in the timeseries. Some temperature and rainfall indices involve a comparison of each year to a baseline period. This baseline period is 1961–1990 for station observations and 1981–2010 for reanalysis data, which was used in the case of Nauru, Samoa and Tokelau (see Section 1.3).

Table 1.1:
Temperature and rainfall extremes indices used in the following chapters. All indices are calculated yearly except for the standardised rainfall evapotranspiration index.

Variable	Index	Definition	Units
Rainfall	Number of wet days	The number of days each year with rainfall of at least 1 mm	Days
	Contribution to total rainfall from extreme events	The percentage of total annual wet day rainfall that occurs on days with rainfall above the 95th percentile for 1961–1990*	%
	Consecutive dry days	The longest stretch of consecutive days without rain	Days
	Maximum 1-day rainfall	The maximum rain that falls on a single day	mm
Temperature	Number of hot days	The number of days with maximum temperatures above the 90th percentile for 1961–1990*	Days
	Number of cool days	The number of days with maximum temperatures below the 10th percentile for 1961–1990*	Days
	Number of warm nights	The number of days with minimum temperatures above the 90th percentile for 1961–1990*	Nights
	Number of cold nights	The number of days with minimum temperatures below the 10th percentile for 1961–1990*	Nights
	Cooling degree days	The difference between daily mean temperature and 25 °C, summed over the entire year, with the assumption that air conditioners are generally turned on at this temperature. If daily mean temperature is below 25 °C, a value of zero is used for the corresponding day	Degree days
	Daily temperature range	The average difference between daily maximum and minimum temperatures	°C
Mixed	Standardised rainfall evapotranspiration index (SPEI)	SPEI is a drought index that uses both temperature and rainfall data, and can be calculated on a range of timescales from 1–48 months. It can be used for determining the onset, duration and magnitude of drought conditions with respect to normal conditions in a variety of natural and managed systems, such as crops, ecosystems, rivers, water resources, etc. The May–October and November–April periods are presented in this study. Negative values indicate drier conditions compared to 1961–1990*	Unitless

*This base period is 1981–2010 when using ERA5 reanalysis data for Nauru, Samoa and Tokelau.

Sen's slope was used to represent linear trends in annual, seasonal and extreme rainfall and temperature (Sen 1968). This method of linear trend analysis minimises the effect of outliers. Statistical significance of trends was determined using the Mann–Kendall test at a 95% significance level. Prewhitening of each timeseries using 'Zhang's method' (Bronaugh and Werner 2019) was conducted prior to trend analysis to remove the effect of autocorrelation. For statistical robustness, only station records with at least 20 valid data points and that are at least 70% complete after prewhitening have trends calculated.

1.5 Air temperature

1.5.1 Seasonal cycle

Air temperature climatology for the selected locations is presented in this section. Where possible, the long-term average is presented for the current WMO Normal period (1991–2020), which is compared with the long-term average for 1961–1990, the reference period for climate change assessment recommended by WMO at present.

1.5.2 Trends

This section provides revised and updated analyses of observed trends for mean and extreme annual and seasonal maximum and minimum temperatures. Methodological information is provided in Section 1.4.2.

1.6 Tropical cyclones

1.6.1 Seasonal cycle

Section 1.6.1 provides the number of tropical cyclones that developed within or crossed a country or territory EEZ between the 1969/70 and 2017/18 seasons in the southern hemisphere, and 1969–2018 seasons in the northern hemisphere. Year-to-year changes in tropical cyclone occurrence are characterised by ENSO phases.

A graph with annual occurrences and an 11-year running mean shows the interannual and interdecadal behaviour of tropical cyclones. For most countries, the interannual variability in the number of tropical cyclones is large. For some, especially those close to the equator, only a small number of tropical cyclones occur within the EEZ boundary. Statistical analysis of such small numbers of tropical cyclone occurrences at a national scale cannot provide reliable estimates of long-term trends in tropical cyclone frequency and intensity (Kuleshov et al. 2010), and this information is therefore not presented in this report.

Some analysed tropical cyclone tracks include the tropical depression stage (sustained winds ≤34 knots) before and/or after tropical cyclone formation. For an event to be counted, it must become a 'tropical cyclone' within the respective country EEZ.

1.6.2 Trends

Trends in total number of tropical cyclones (<995 hPa) and severe tropical cyclones (<970 hPa) are presented for the period 1981/82–2020/21 for the greater western North Pacific (125°E–180°W; 0–20°N) and Southwest Pacific (135°E–120°W; 0–50°S). In this report, 995 hPa and 970 hPa thresholds were used to define a tropical cyclone and a severe tropical cyclone, respectively, based on central pressure estimates as recommended in the literature (Nicholls et al. 1998; Kuleshov et al. 2010).

Records of tropical cyclones exist from the late 1800s in some countries. Satellite-based observations began in the Southwest Pacific in the early 1970s, with consistent coverage and reliable intensity estimates only available since the early 1980s. Confidence in tropical cyclone trends is moderate as the definition of a tropical cyclone has changed and satellite observation methods have continued to improve over the last 40 years. The trend is calculated using linear least-squares regression with a 95% confidence interval.

1.7 Sea surface temperature

1.7.1 Seasonal cycle

SST climatology for available in situ tide-gauges in the respective country or territory is presented in this section. Statistics are derived from hourly data over monthly timescales. In the absence of in situ data, daily satellite SST is used at the grid cell nearest to the country capital with a resolution of approximately 27 km and averaged monthly.

1.7.2 Trends

SST trends from satellite observations are provided for the country or territory EEZ from 1981 to 2021. The data temporal interval is daily and averaged across all grid cells in the EEZ prior to trend calculation. Grid cell spatial resolution is approximately 27 km. The trend is calculated using linear least-squares regression with a 95% confidence interval.

1.8 Sea level

1.8.1 Seasonal cycle

Sea level exceedance of the 99th percentile on a monthly basis is presented in this section for available tide-gauges in the respective country or territory. The 99th percentile threshold is calculated across all months and years. Exceedance values are presented as hours of exceedance spilt into years and a percentage of total hours exceedance for all years available.

1.8.2 Trends

Sea level trends from satellite altimeters are provided for the country or territory EEZ from 1993 to 2020 in the form of a thematic map and compared with the global average trend and tide-gauge trends (where available). Temporal interval of data is monthly and spatial resolution is 1° (approximately 110 km in the tropics). The trend is calculated using linear least-squares regression with a 95% confidence interval.

1.9 Waves

1.9.1 Seasonal cycle

The average wave climate for key locations in each country or territory is defined by the significant wave height, peak period and peak direction. The significant wave height is the mean wave height (from trough to crest) of the highest one third of waves and corresponds to the wave height that would be reported by an experienced observer. Peak period is the time interval between two waves of the dominant wave period. Peak direction is the direction from which the dominant waves are coming. Annual wave roses categorise the directional wave data into 20° bins. Seasonal averages are presented monthly for wave height, peak period and direction.

1.9.2 Trends

Trends in wave height and period are presented for key locations in each country from 1979 to 2021 in the form of a timeseries plot to assess whether a trend can be observed.

1.9.3 Extreme waves

Extreme wave return periods are estimated from fitting a generalized Pareto distribution to the wave height data, which can then be used to calculate the average return (recurrence) interval (ARI) for 1-, 10-, 20-, 50- and 100-year return periods.

2 Cook Islands

2.1 Summary

2.1.1 Climate

- Changes in air temperature from season to season are relatively small and strongly linked to changes in the surrounding ocean temperature. The Cook Islands have two distinct seasons – a warm wet season from November to April and a cooler dry season from May to October.
- The seasonal cycle is strongly affected by the South Pacific Convergence Zone (SPCZ), which is most intense during the wet season.
- Annual and seasonal air temperatures at Rarotonga increased over the period 1951–2020. The annual number of hot days and warm nights has increased, while the number of cool days and cold nights has decreased. The energy required for cooling indoor environments has increased and the difference between daytime and night-time temperatures has decreased.
- Annual rainfall has decreased at Rarotonga. Most of this has occurred during May to October. The annual number of wet days has also decreased.
- Tropical cyclones usually affect the Cook Islands between November and April. Over the period 1969–2018, an average of 16 cyclones passed within the Cook Islands' exclusive economic zone (EEZ) per decade. Tropical cyclones were most frequent in El Niño years and least frequent in La Niña years. Year-to-year variability is large, ranging from no tropical cyclones in some seasons to six.
- There has been little change in the total number of tropical cyclones in the Southwest Pacific since 1981/82. The number of severe tropical cyclones has declined over the same period/region.

2.1.2 Ocean

- Highest sea levels typically occur from October to April.
- Sea-level rise within the Cook Islands EEZ, measured by satellite altimeters from 1993 to mid-2020, ranges from about 2.5 to 5.5 mm per year across the majority of the EEZ, with highest estimates in the far south.
- Monthly average ocean temperature, as measured by the Rarotonga tide-gauge, ranges from 24.5 °C in August to 28 °C in February and March. However, monthly temperatures in any given year can be up to ±2 °C of these averages.
- Sea surface temperature increased within the Cook Islands EEZ by 0.21 °C per decade from 1981 to 2021.
- Dominant wave direction is from 190° (south), with an average significant wave height of 2.04 m and average wave period of 12.64 s.
- Severe wave height was defined as 4.01 m, with an average of three severe events per year.
- Peak average significant wave height occurs around June.

2.2 Country description

The Cook Islands are located in the tropical western South Pacific Ocean between latitudes 9°S and 23°S, and longitudes 157°W and 166°W (Figure 2.1). The country is made up of 15 islands divided into two distinct north and south groups. The total land area is 237 km^2 and the Cook Islands have an EEZ of about 2.0 million km^2. The chief town Avarua (the capital, referred to as Rarotonga) is located on the island of Rarotonga (67 km^2) in the Southern Cook Islands. The highest elevation is 652 m above sea level on Rarotonga. The Cook Islands population is approximately 17,000 and about 13,000 live on Rarotonga.

Figure 2.1:
Cook Islands and the locations of the climate stations used in this report

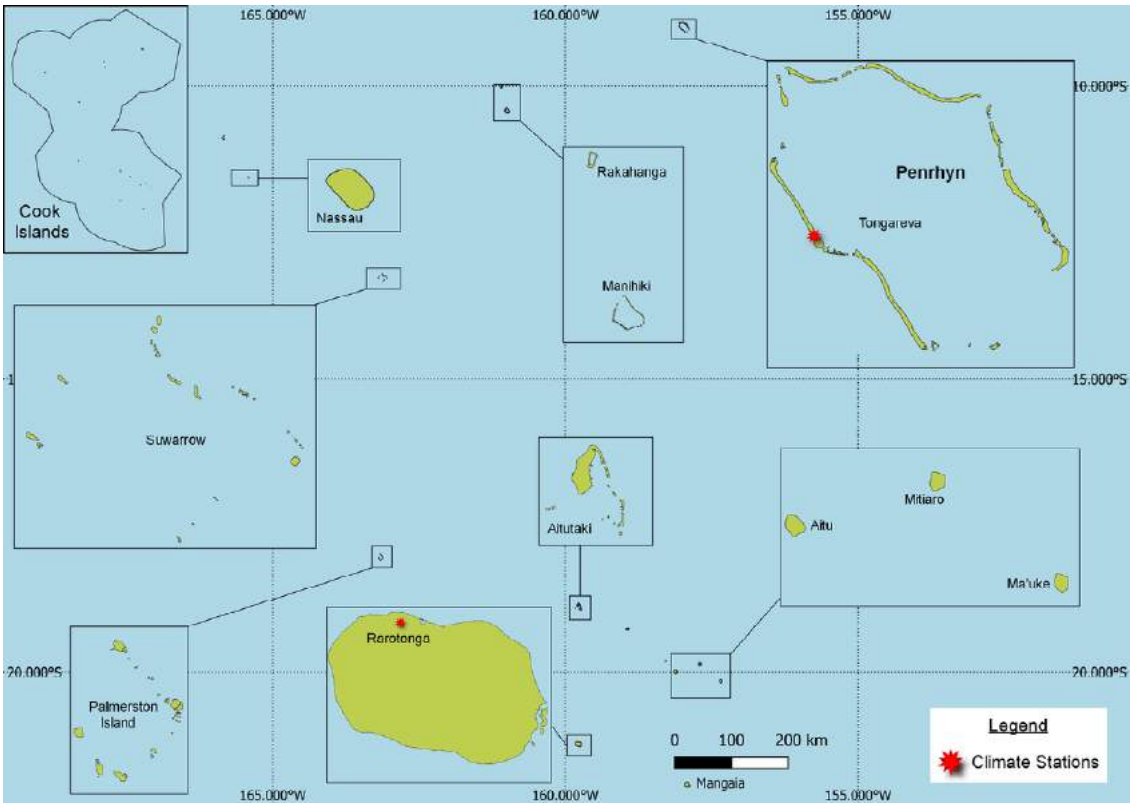

2.3 Data

Daily historical rainfall and air temperature records for Penrhyn (northern Cook Islands) and Rarotonga (southern Cook Islands) from 1951 were obtained from the Cook Islands Meteorological Service. These records have undergone data quality and homogeneity assessment. Where the maximum or minimum air temperature records were found to have discontinuities, these records were adjusted to make them homogeneous (further information is provided in Chapter 1). Additional information on historical climate trends for the Cook Islands can be found in the Pacific Climate Change Data Portal http://www.bom.gov.au/climate/pccsp.

Tropical cyclone data and historical tracks starting from the 1969/70 season are available from the SHTC Data Portal http://www.bom.gov.au/cyclone/history/tracks/index.shtml.

Sea surface temperature (SST) covering the EEZ for the Cook Islands was obtained via the daily Optimum Interpolation SST version 2.1 (OISST v2.1) dataset from NOAA (Reynolds et al. 2007; Banzon et al. 2016). In situ ocean temperature data were obtained from the PSLGM Project tide-gauge located at Rarotonga, with data spanning from 1993 to 2021.

Wave data were obtained from the PACCSAP wave hindcast (Smith et al. 2021), available hourly from 1979 to 2021, with a grid resolution near the Cook Islands of 7 km.

Regional sea level data were obtained from CSIRO satellite altimetry (updated by Benoit Legresy, Church and White 2011), with correction for seasonal signals, inverse barometer effect and glacial isostatic adjustment. Tide-gauge data were sourced from the Rarotonga tide-gauge station, spanning from 1993 to 2021 at hourly intervals.

2.4 Rainfall

2.4.1 Seasonal cycle

Rainfall in the Cook Islands is strongly affected by the SPCZ and is centred close to or over the Southern Cook Islands (Southern Group) from December to April, when the SPCZ is most active and furthest south. From November to March, the SPCZ is wide and strong enough for the Northern Group to also receive significant rainfall.

The percentage of rainfall received in Penrhyn during the wet season months from November to April is 61%. Similarly, Rarotonga receives 64% of its annual rainfall during the wet season (Figure 2.2). The driest months of the year in the Cook Islands are from June to October. During these months, there is a significant reduction in rainfall in the northern and southern Cook Islands.

Figure 2.2:
Mean annual rainfall at Penrhyn and Rarotonga

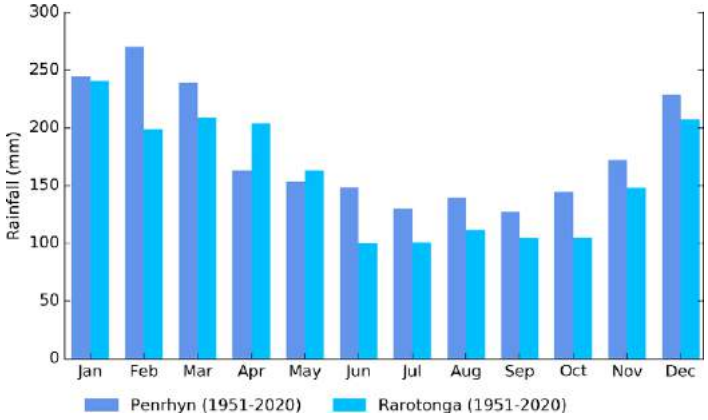

2.4.2 Trends

Annual rainfall has decreased significantly at Rarotonga since 1951. This is attributed to decreases during May to October (Figure 2.3, Table 2.1). Correspondingly, the number of wet days at Rarotonga has also decreased. Annual and seasonal rainfall at Penrhyn has not changed significantly. Year-to-year variability associated with El Niño–Southern Oscillation (ENSO) is evident at Rarotonga, with La Niña years typically experiencing higher rainfall than El Niño years (Figure 2.3). Pronounced decade-to-decade variability is evident at Penrhyn. Annual rainfall has varied from approximately 1100 to 3000 mm at Rarotonga and from approximately 800 to 4700 mm at Penrhyn.

Figure 2.3:
Annual rainfall (bar graph) and number of wet days (where rainfall is at least 1 mm; line graph) at Rarotonga (left) and Penrhyn (right). Straight lines indicate linear trends for annual rainfall (in black) and number of wet days (in blue). The magnitudes of the trends are presented in Table 2.1. Diamonds indicate years with insufficient data for one or both variables.

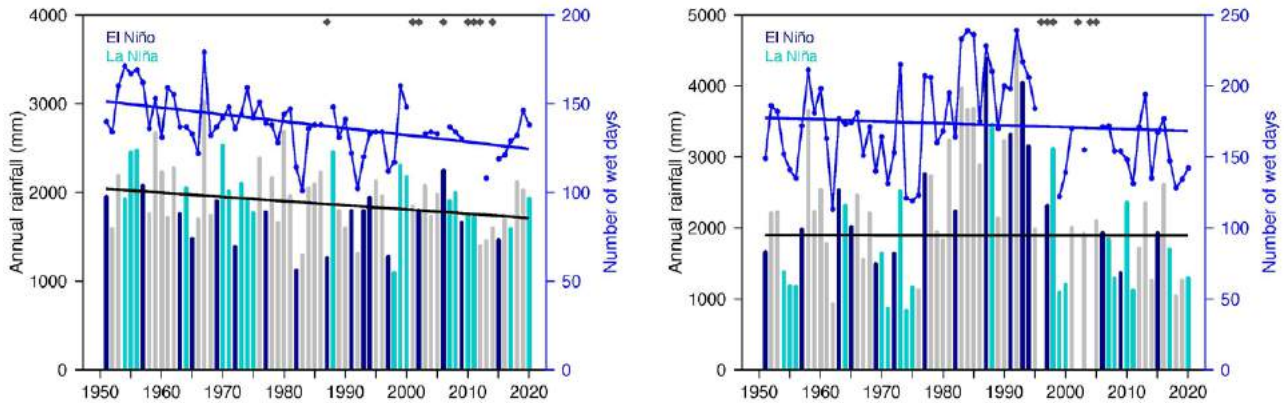

Table 2.1:
Trends in annual, seasonal and extreme rainfall at Rarotonga and Penrhyn. The 95% confidence intervals are shown in parentheses, and trends significant at the 95% level are shown in bold. The contribution to total rainfall from extreme events and the standardised rainfall evapotranspiration index are measured relative to 1961–1990 (see Chapter 1 for details). The standardised rainfall evapotranspiration index is not available for Penrhyn due to daily temperature observations not being available for this site.

	Rarotonga	Penrhyn
	1951–2020	
Annual rainfall (mm/decade)	**-47.59** (-90.85, -3.13)	-1.03 (-249.20, +191.97)
November–April (mm/decade)	-23.12 (-66.6, +20.94)	+18.66 (-94.19, +111.76)
May–October (mm/decade)	**-21.54** (-37.45, -3.50)	-38.36 (-109.18, +27.36)
Number of wet days (days/decade)	**-3.87** (-6.44, -1.08)	-1.35 (-7.54, +5.05)
Contribution to total rainfall from extreme events (%/decade)	-0.77 (-2.03, +0.71)	+0.71 (-1.60, +2.68)
Consecutive dry days (days/decade)	+0.39 (0.00, +0.87)	+0.14 (-0.47, +0.74)
Maximum one-day rainfall (mm/decade)	+1.50 (-3.22, +5.91)	+1.72 (-3.59, +8.34)
Standardised rainfall evapotranspiration index (November–April)	-0.08 (-0.22, +0.07)	-
Standardised rainfall evapotranspiration index (May–October)	-0.12 (-0.24, +0.02)	-

With the exception of the Number of wet days at Rarotonga no significant trends in extreme rainfall indices, including the standardised rainfall evapotranspiration drought index, are present at Rarotonga and Penrhyn (Table 2.1). Figure 2.4 shows change and variability in the longest run of days without rain and maximum daily rainfall at both sites. Variability associated with ENSO is evident at Penrhyn, with longer dry spells and lower daily rainfall maximums occurring during La Niña years compared to El Niño years.

Figure 2.4:
Annual longest run of consecutive dry days (bar graph) and maximum daily rainfall (line graph) at Rarotonga (left) and Penrhyn (right). Straight lines indicate linear trends for dry days (in black) and maximum daily rainfall (in blue). The magnitudes of these trends are presented in Table 2.1. Diamonds indicate years with insufficient data for one or both variables.

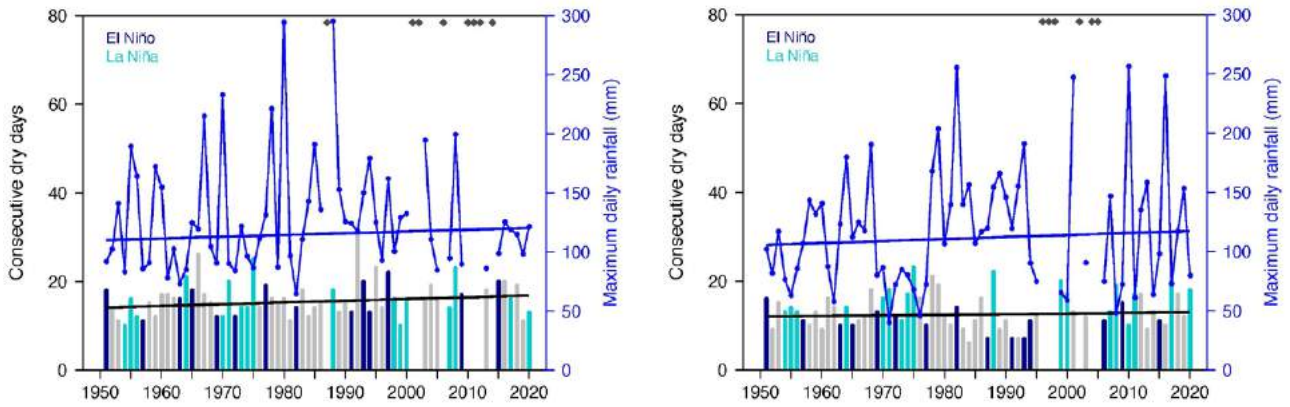

2.5 Air temperature

2.5.1 Seasonal cycle

There is a significant difference in seasonal temperatures between the northern and southern Cook Islands. The position of the northern Cook Islands (Northern Group) so close to the equator results in fairly constant temperatures throughout the year, while in the southern Cook Islands (Southern Group), temperatures cool off during the dry season. Changes in temperatures are strongly linked to changes in the surrounding ocean temperature. The range in average monthly maximum temperature is 1.1 °C at Penrhyn in the Northern Group and 4.4 °C at Rarotonga in the Southern Group (Figure 2.5). The range in average monthly minimum temperature at Penrhyn is 0.75 °C and at Rarotonga, it is 4.7 °C.

There has been a clear shift towards warmer average monthly temperatures between the climatology periods of 1961–1990 and 1991–2020 (Figure 2.5), with warmer average air temperatures occurring in all months throughout the year for Rarotonga.

Figure 2.5:
Maximum and minimum air temperature seasonal cycle for Penrhyn (purple) and Rarotonga (green), and for the periods 1961–1990 (dotted lines) and 1991–2020 (solid lines)

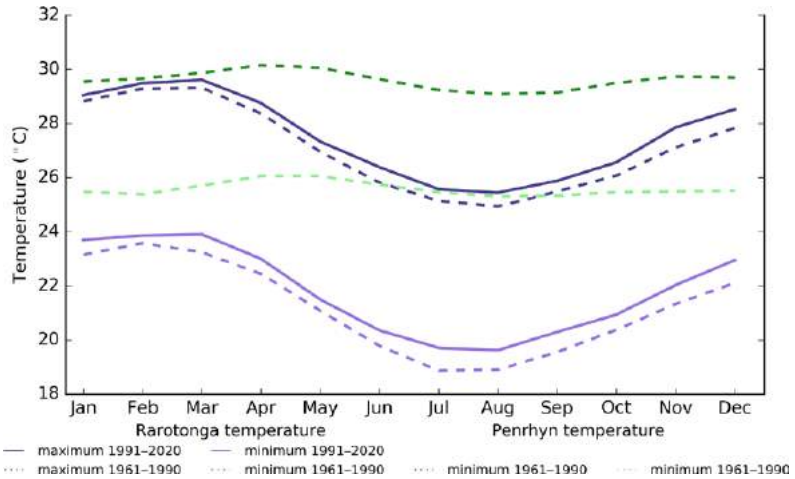

2.5.2 Trends

Average annual and seasonal temperatures have increased significantly at Rarotonga (Figure 2.6). November–April temperatures are warming at approximately the same rate as May–October temperatures (Table 2.2). Daily minimum temperatures are warming faster than daily maximum temperatures.

Figure 2.6:
Average annual, November–April and May–October temperatures for Rarotonga. Straight lines indicate linear trends. The magnitudes of the trends are presented in Table 2.2. Diamonds indicate years with insufficient data for one or more variables.

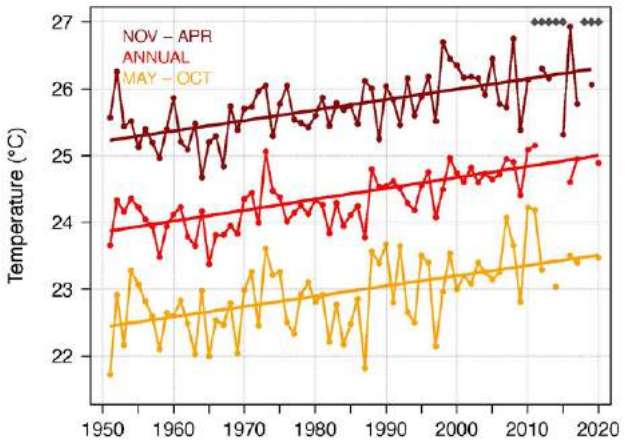

Table 2.2:
Trends in annual and seasonal air temperatures at Rarotonga. The 95% confidence intervals are shown in parentheses, and trends significant at the 95% level are shown in bold.

	Rarotonga Tmax (°C/decade)	Rarotonga Tmin (°C/decade)	Rarotonga Tmean (°C/decade)
	1951–2020		
Annual	**+0.14** (+0.06, +0.21)	**+0.18** (+0.14, +0.23)	**+0.16** (+0.11, +0.21)
November–April	**+0.13** (+0.07, +0.19)	**+0.18** (+0.13, +0.23)	**+0.16** (+0.11, +0.20)
May–October	**+0.11** (+0.04, +0.20)	**+0.18** (+0.13, +0.25)	**+0.15** (+0.08, +0.22)

The number of hot days and warm nights has increased, and the number of cool days and cold nights has decreased at Rarotonga (Table 2.3, Figure 2.7).

The cooling degree days index provides a measure of the energy demand needed to cool a building down to 25 °C, with the assumption that air conditioners are generally turned on at this temperature. There has been an increase in the cooling degree index, suggesting the energy needed for cooling has increased significantly since 1951. The difference between daytime and night-time temperatures at Rarotonga has been decreasing.

Table 2.3:
Trends in annual temperature extremes at Rarotonga. The 95% confidence intervals are shown in parentheses, and trends significant at the 95% level are shown in bold. Hot and cool days, and warm and cold nights are measured relative to 1961–1990 (see Chapter 1 for details).

	Rarotonga
	1951–2020
Number of hot days (days/decade)	**+6.92** (+0.52, +13.34)
Number of warm nights (nights/decade)	**+6.81** (+4.69, +9.28)
Number of cool days (days/decade)	**-4.12** (-6.40, -1.75)
Number of cold nights (nights/decade)	**-5.12** (-6.86, -3.65)
Cooling degree days (degree days/decade)	**+22.34** (+14.50, +29.72)
Daily temperature range (°C/decade)	**-0.08** (-0.16, -0.01)

Figure 2.7:
Annual number of hot days and cold nights at Rarotonga. Straight lines indicate linear trends. The magnitudes of the trends are presented in Table 2.3. Diamonds indicate years with insufficient data for one or both variables.

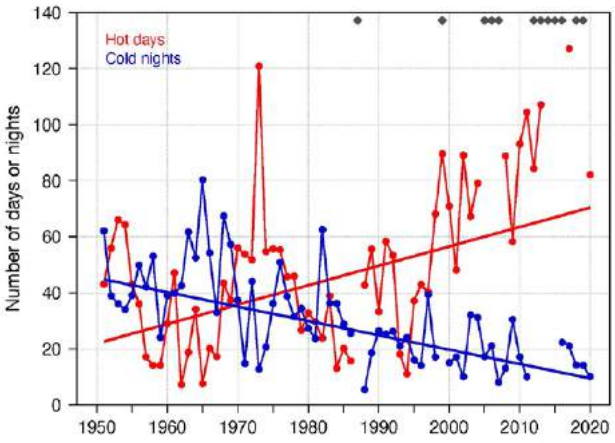

2.6 Tropical cyclones

2.6.1 Seasonal cycle

Tropical cyclones usually affect the Cook Islands during the southern hemisphere tropical cyclone season, which is from November to April, but also occasionally occur outside the tropical cyclone season. The tropical cyclone archive of the southern hemisphere indicates that between the 1969/70 and 2017/18 seasons, 79 tropical cyclones (Figure 2.8) passed within the Cook Islands EEZ. This represents an average of 16 cyclones per decade. Tropical cyclones were most frequent in El Niño years (25 cyclones per decade), followed by neutral years (17 cyclones per decade) and least frequent in La Niña years (7 cyclones per decade).

Interannual variability in the number of tropical cyclones in the EEZ is large, ranging from zero in some seasons to six in 1980/81, 1997/98 and 2004/05 (Figure 2.8). High interannual variability and the small number of tropical cyclones occurring in the EEZ make reliable identification of long-term trends in frequency and intensity difficult.

Some tropical cyclone tracks analysed in this section include the tropical depression stage (sustained winds ≤34 knots) before and/or after tropical cyclone formation.

Figure 2.8:
Number of tropical cyclones passing within the Cook Islands EEZ per season. Each season is defined by the ENSO status, with light blue being an El Niño year, dark blue a La Niña year and grey showing a neutral ENSO year. The 11-year moving average is presented as a purple line and considers all years.

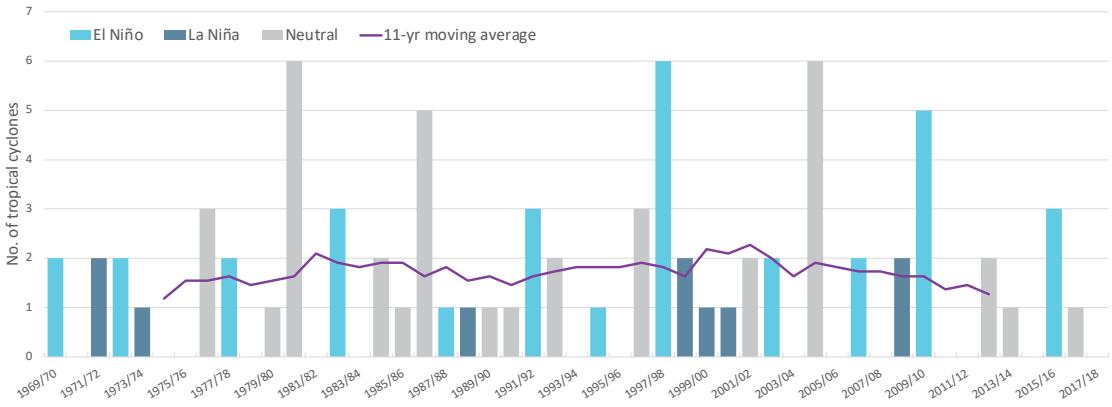

2.6.2 Trends

Trends in total number of tropical cyclones (<995 hPa) and severe tropical cyclones (<970 hPa) are presented for the period 1981/82–2020/21 for the greater Southwest Pacific (135°E–120°W; 0– 50°S). Trends are presented at a regional scale as the number of tropical cyclones occurring within Pacific Island EEZs is insufficient for reliable long-term trend analysis.

For the total number of tropical cyclones, the trend (and 95% confidence interval) is -0.92 (-1.85, 0.01) tropical cyclones/decade. There has been little change/marginal decline in the total number of tropical cyclones over the last 40 seasons. This trend is not statistically significant.

For the total number of severe tropical cyclones, the trend is -0.80 (-1.32, -0.29) tropical cyclones/decade. There is a negative trend in the number of severe tropical cyclones over the last 40 seasons. There has been little change/marginal decline in the proportion of tropical cyclones reaching severe status. The trend is -0.04 (-0.08, 0.00) tropical cyclones/decade. The negative trend is statistically significant.

Records of tropical cyclones exist from the late 1800s in some countries in the Southwest Pacific, but trends in tropical cyclones have only been presented from 1981/82. Satellite-based observations began in the Southwest Pacific in the early 1970s, but consistent coverage and reliable intensity estimates have only been available since the early 1980s. Confidence in tropical cyclone trends is moderate as the definition of a tropical cyclone has changed and satellite observation methods have continued to improve over the last 40 years.

2.7 Sea surface temperature

2.7.1 Seasonal cycle

Ocean temperature, as measured by the Rarotonga tide-gauge from 1993 to 2021, reaches on average a maximum of almost 28 °C in February/March but can get as high as 30 °C (Figure 2.9). Minimum average temperature reaches a low of approximately 24.5 °C in August. Hourly temperatures can be up to 2 °C higher or lower than these monthly averages, although 50% of hourly observations fall within 1 °C of the average.

Figure 2.9:
Annual temperatures measured at the Rarotonga tide-gauge. Blue dots show the monthly average, and shaded boxes show the middle 50% of hourly observations. Lines show the top and bottom 25% of hourly observations..

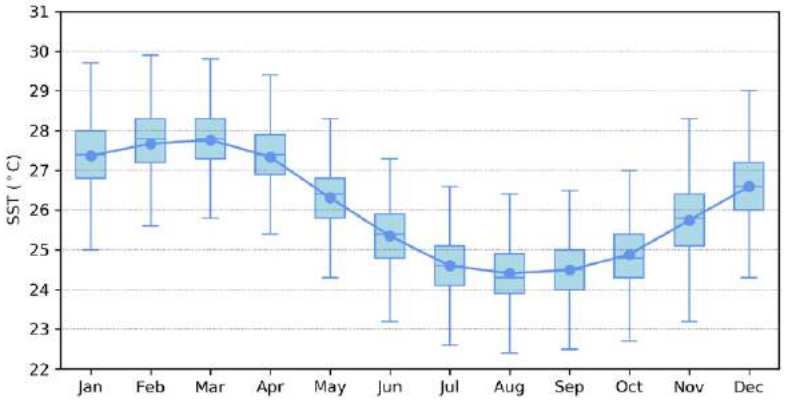

2.7.2 Trends

Figure 2.10 shows the 1981–2021 SST from satellite observations averaged over the Cook Islands EEZ. The data show a trend of 0.21 °C per decade with a 95% confidence interval of ±0.06 °C.

Figure 2.10:
Sea surface temperature from satellite observations averaged across the Cook Islands EEZ, shown as the orange line. The blue line shows the linear regression trend.

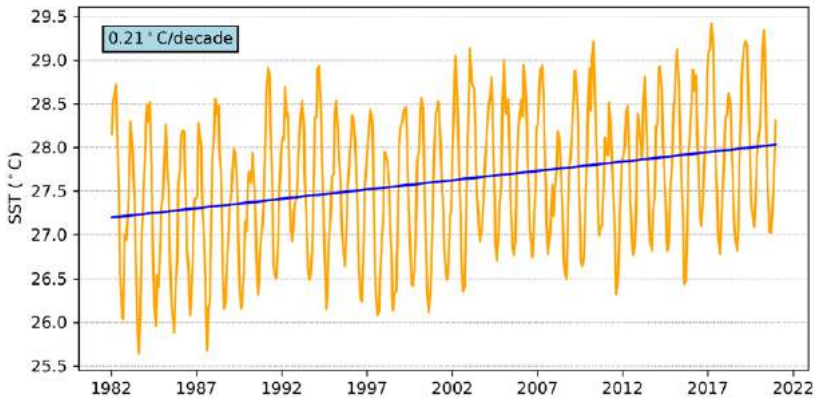

2.8 Sea level

2.8.1 Seasonal cycle

The Cook Islands experience a semidiurnal tidal cycle, meaning two high and two low tides per day. The highest predicted tides of the year typically occur during the wet season months of November to April. Figure 2.11 shows the number of hours the 99th percentile (1.15 m) sea level threshold is exceeded per month across the entire sea level record at Rarotonga. Peak sea levels typically occur over a significant portion of the year ranging from October to April. Since approximately 2006, increasingly more hours each year exceed the 2.0 m sea level threshold. This is due to a combination of sea-level rise and minor subsidence occurring at Rarotonga (Brown et al. 2020).

Figure 2.11:
Number of hours exceeding 99th percentile sea level threshold per month from 1993 to 2021 at the Rarotonga tide-gauge. Blue shading indicates the number of hours, and the final row provides a percentage summary of all the years.

Number of hours exceeding 1.15 m (Avatiu, Cook Islands)

	Jan	Feb	Mar	Apr	May	Jun	Jul	Aug	Sep	Oct	Nov	Dec	Annual
1993	0	0	0	0	0	0	0	0	0	0	0	0	0
1994	0	0	0	0	0	0	0	0	0	0	0	0	0
1995	0	0	0	0	0	0	0	0	0	0	0	0	0
1996	0	0	0	0	0	0	0	0	0	0	0	0	0
1997	0	0	6	0	0	0	0	0	0	0	0	6	12
1998	0	0	0	0	0	0	0	0	0	0	0	0	0
1999	0	0	0	0	0	0	1	0	0	0	0	2	3
2000	0	0	0	0	0	0	0	0	0	0	0	0	0
2001	0	0	0	0	0	0	0	0	0	0	0	0	0
2002	0	0	0	0	0	0	0	0	0	0	0	0	0
2003	0	0	0	0	0	0	0	0	0	0	0	0	0
2004	0	0	0	0	0	0	0	0	0	0	0	0	0
2005	0	2	0	0	0	0	0	0	0	0	0	0	2
2006	5	3	5	0	0	0	0	0	0	0	0	0	13
2007	4	0	0	1	0	0	0	0	0	2	6	0	13
2008	0	0	0	0	0	0	0	0	0	0	0	0	0
2009	1	0	0	0	0	0	0	0	0	0	0	0	1
2010	5	2	0	0	0	0	0	0	0	0	0	0	7
2011	1	0	0	2	0	0	0	6	0	6	0	1	16
2012	0	0	0	0	0	0	0	0	0	0	0	12	12
2013	0	0	0	0	0	0	0	0	0	0	0	0	0
2014	0	0	0	0	0	0	0	0	0	0	0	0	0
2015	0	0	5	0	0	0	0	0	0	0	0	0	5
2016	0	0	8	0	0	0	0	2	0	5	0	0	15
2017	0	0	0	2	0	0	0	0	0	0	0	1	3
2018	0	0	0	0	0	0	0	0	0	0	0	0	0
2019	6	1	1	0	0	0	0	0	0	4	0	0	12
2020	0	5	4	9	0	0	0	0	0	1	0	0	19
2021	0	0	8	6	11	1	0	0	0	5	2	8	41
Monthly Totals (%)	13	7	21	11	6	1	1	5	0	13	5	17	

2.8.2 Trends

Sea level at Cook Islands, measured by satellite altimeters (Figure 2.12) since 1993, has risen 2.5–5.5 mm per year across most of the EEZ, with a 95% confidence interval of ±0.4 mm in the south and up to ±0.8 mm in the north. Trend estimates in the south are higher, ranging from 3.5 to 5.5 mm per year, which is larger than the global average of 3.1 ± 0.4 mm per year (von Schuckmann et al. 2021). This rise is partly linked to a pattern related to climate variability from year to year and decade to decade.

Figure 2.12:
Satellite altimetry annual trend for the Pacific from 1993 to 2020, with the Cook Islands EEZ highlighted. The star symbol indicates the location of the tide-gauge at Rarotonga.

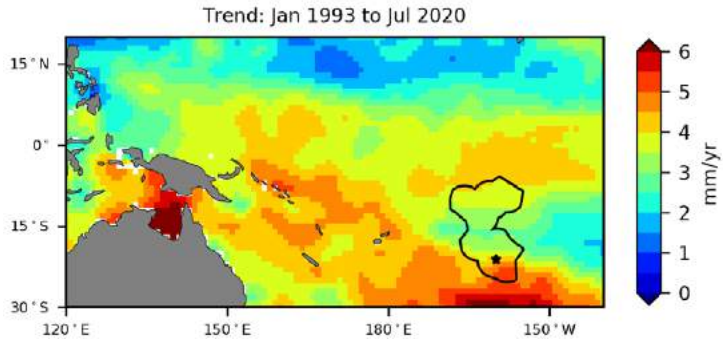

Trend estimates at the Rarotonga tide-gauge over a similar time span to the altimetry observations (February 1993 to July 2020) are provided in the PSLGM Monthly Data Report for July 2020 (http://www.bom.gov.au/ntc/IDO60101/IDO60101.202007.pdf).

For Rarotonga, the trend is reported as 3.9 mm per year, very similar to the altimetry trends shown in Figure 2.12 (tide-gauge indicated by star symbol).

2.9 Waves

2.9.1 Seasonal cycle

The average wave climate at Rarotonga is defined by the significant wave height, peak period and peak direction. The significant wave height is the mean wave height (from trough to crest) of the highest one third of waves and corresponds to the wave height that would be reported by an experienced observer. Peak period is the time interval between two waves of the dominant wave period. Peak direction is the direction from which the dominant waves are coming.

The average sea state is dominated by swells from the south. The annual mean wave height is 2.04 m, the annual mean wave direction is 190° and the annual mean wave period is 12.64 s. In the Pacific, waves often come from multiple directions and for different periods at a time. In Rarotonga, there are often more than six different wave direction/period components coming from the southeast to southwest (Figure 2.13).

Figure 2.13:
Annual wave rose for Rarotonga. Note that direction is where the wave is coming from.

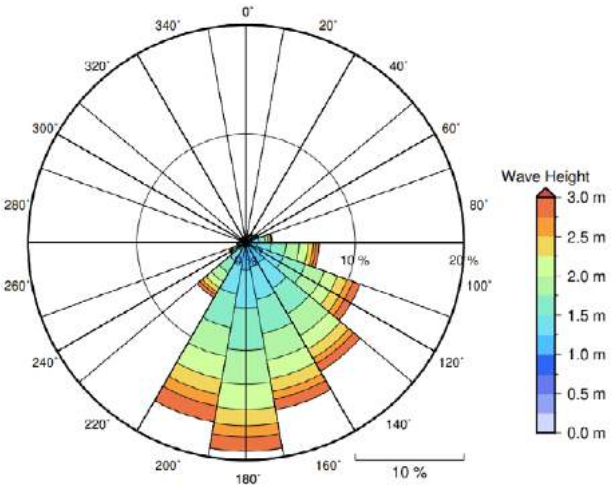

Seasonal wave height peak is in June, whereas the seasonal wave period peaks in May (Figure 2.14). This is related to the intensification of the Southern Ocean storm track during winter. Conversely, there is slightly reduced wave activity between November and December.

Figure 2.14:
Monthly wave height (black line), wave period (red line) and wave direction (arrows). The grey area represents the range of wave height between calm periods (10% of lowest wave height) and large wave events (10% of highest wave height).

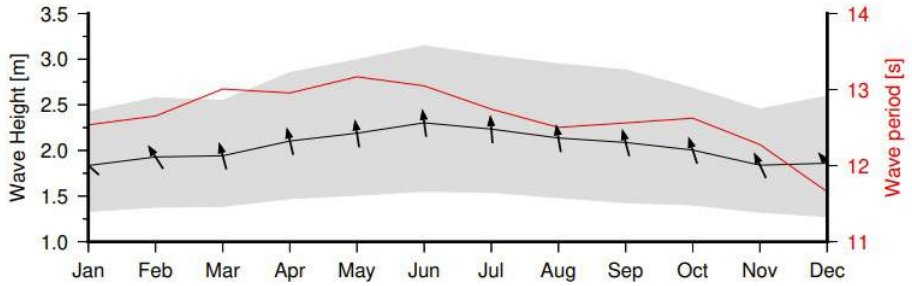

2.9.2 Trends

Waves change from month to month with the seasons, but they also change from year to year with climate oscillations. Typically, these changes are smaller than the seasonal changes but can be important during phenomena such as ENSO. At Rarotonga, the mean annual wave height has remained unchanged since 1979 (Figure 2.15). The mean annual wave height in Rarotonga is not significantly correlated with the main climate indicators of the region.

Figure 2.15:
Annual wave height (black line), wave period (red line) and wave direction (arrows). The grey area represents the range of wave height between calm periods (10% of lowest wave height) and large wave events (10% of highest wave height).

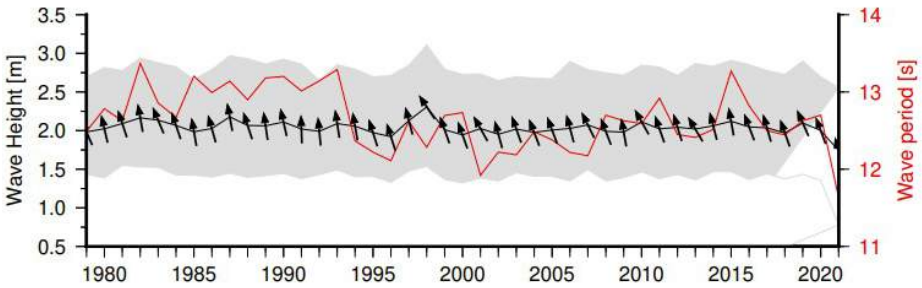

2.9.3 Extreme waves

Extreme wave analysis completed for Rarotonga was done by defining a severe height threshold and fitting a generalized Pareto distribution (GPD). The optimum threshold selected was 4.01 m. In the 42-year wave hindcast, 127 wave events reached or exceeded this threshold, averaging three per year. The GPD was fitted to the largest wave height reached during each of these events (Figure 2.16, Table 2.4). Extreme wave analysis is a very useful tool but is not always accurate because the analysis is very sensitive to the data available, the type of distribution fitted and the threshold used. For example, this analysis does not accurately account for tropical cyclone waves. More in-depth analysis is required to obtain results appropriate for designing coastal infrastructure and coastal hazard planning.

Figure 2.16:
Extreme wave distribution for Rarotonga. The crosses represent the wave events that have occurred since 1979. The solid line is the statistical distribution that best fits past wave events. The dashed lines show the upper and lower confidence limits of the fit. There is a 95% chance that the fitted distribution lies between the two dashed lines. Note that the annual return interval is in logarithmic scale.

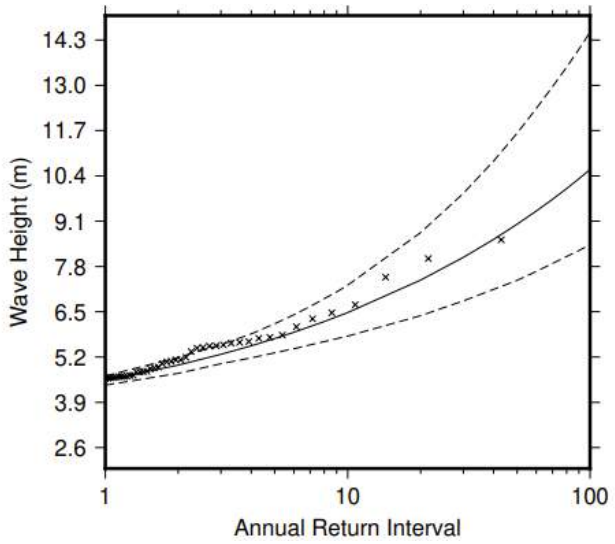

Table 2.4:
Summary of the results of extreme wave analysis for Rarotonga

Large wave height (90th percentile)	2.79 m
Severe wave height (99th percentile)	3.75 m
1-year ARI wave height	4.53 m
10-year ARI wave height	6.48 m
20-year ARI wave height	7.41 m
50-year ARI wave height	9.01 m
100-year ARI wave height	10.58 m

3 Federated States of Micronesia

3.1 Summary

3.1.1 Climate

- Changes in air temperature from season to season are relatively small and strongly linked to changes in the surrounding ocean temperature. The Federated States of Micronesia (FSM) has two seasons – the wet season from May to October and the dry season from November to April.
- The seasonal cycle is strongly affected by the Intertropical Convergence Zone (ITCZ) and West Pacific Monsoon (WPM), which are most intense during the wet season.
- Annual and seasonal air temperatures at Pohnpei and Chuuk increased over the period 1952–2020. The number of hot days and warm nights has increased at both sites, while the number of cool days and cold nights has decreased. The energy required for cooling indoor environments has also increased at both sites.
- May to October rainfall has decreased at Pohnpei since 1952. All other trends in annual and seasonal rainfall at Pohnpei and Chuuk are not statistically significant.
- Tropical cyclones affect FSM year-round. Over the period 1969–2017, an average of 74 cyclones passed within the FSM exclusive economic zone (EEZ) per decade. Tropical cyclones were most frequent in El Niño years and least frequent in La Niña years. Year-to-year variability is large, ranging from no tropical cyclones in some years to 14 in 1974.
- There has been little change in the number of severe tropical cyclones or the total number of tropical cyclones in the Northwest Pacific since 1981.

3.1.2 Ocean

- Highest sea levels typically occur in the months October to January. La Niña brings noticeably higher sea levels in the months leading up to winter (October–December).
- Sea-level rise within the EEZ, measured by satellite altimeters from 1993 to mid-2020, ranges from about 3 to 4.5 mm (0.11 to 0.18 in) per year, with highest estimates in the southeast.
- Monthly average ocean temperature, as measured by the Pohnpei tide-gauge, ranges from approximately 29 °C (84.2 °F) in February to 30 °C (86.0 °F) from August to November. However, monthly temperatures in any given year can be up to ±2 °C (±3.6 °F) of these averages.
- The sea surface temperature (SST) trend within the EEZ is 0.25 °C (0.45 °F) per decade.
- Dominant wave direction is from 23° (NNE), with an average significant wave height of 1.20 m (3.94 ft) and average wave period of 10.23 s.
- Severe wave height was defined as 2.45 m (8.04 ft), with an average of 3.8 severe events per year.
- Peak average significant wave height occurs between November and March.

3.2 Country description

Located in the equatorial/tropical North Pacific Ocean, FSM consists of four states. From west to east, these are Yap, Chuuk, Pohnpei and Kosrae (Figure 3.1). The nation has approximately 607 islands that cover a longitudinal distance of 2700 km located between latitudes 1°N and 11°N, and longitudes 136°E and 164°E. FSM has a total land area of 702 km^2 and an EEZ of 2.6 million km^2. The four states are centred on one or more main high islands, and all but Kosrae include numerous outlying atolls. The nation's capital is Palikir, located on Pohnpei Island. The largest city is Weno, located in Chuuk State. The highest elevation is 782 m (2566 ft) above sea level on Pohnpei. FSM's population is approximately 104,000, with about 11% residing in Yap, 47% in Chuuk, 35% in Pohnpei and 7% in Kosrae.

Figure 3.1:
Federated States of Micronesia and the locations of the climate stations used in this report

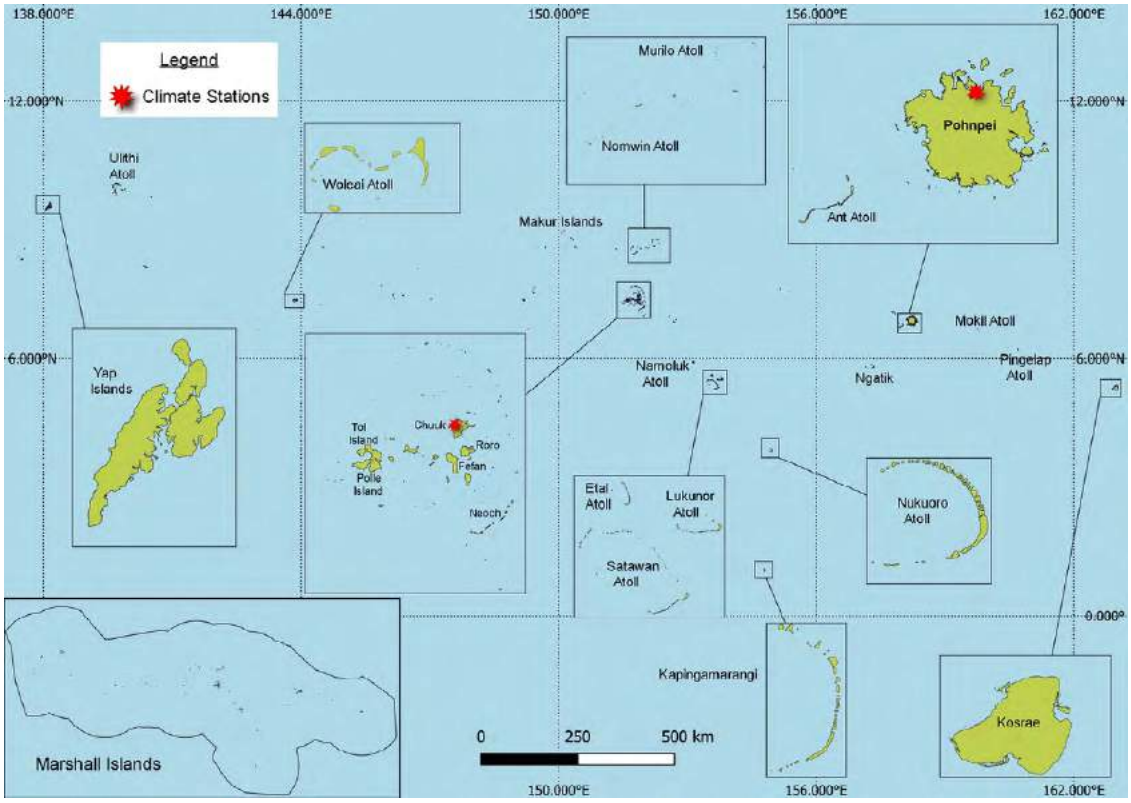

3.3 Data

Daily historical rainfall and air temperature records for Chuuk and Pohnpei from 1951 were obtained from the Pohnpei Weather Service Office of the United States National Oceanic and Atmospheric Administration. These records have undergone data quality and homogeneity assessment. Where the maximum or minimum air temperature records were found to have discontinuities, these records have been adjusted to make them homogeneous (further information is provided in Chapter 1). Additional information on historical climate trends for FSM can be found in the Pacific Climate Change Data Portal http://www.bom.gov.au/climate/pccsp.

Tropical cyclone data and historical tracks starting from the 1969 season are available from the Western North Pacific Tropical Cyclone Data Portal http://www.bom.gov.au/cyclone/history/tracks/beta/?region=wnp.

SST covering the EEZ was obtained via the daily Optimum Interpolation SST version 2.1 (OISST v2.1) dataset from NOAA (Reynolds et al. 2007; Banzon et al. 2016). In situ ocean temperature data were obtained from the PSLGM Project tide-gauge located at Pohnpei, with data spanning from 1993 to 2021.

Wave data were obtained from the PACCSAP wave hindcast (Smith et al. 2021), available hourly from 1979 to 2021, with a grid resolution near FSM of 7 km (4.3 mi).

Regional sea level data were obtained from CSIRO satellite altimetry (updated by Benoit Legresy, Church and White 2011), with correction for seasonal signals, inverse barometer effect and glacial isostatic adjustment. Tide-gauge data were sourced from the Pohnpei tide-gauge station, spanning from 2001 to 2020 at hourly intervals.

3.4 Rainfall

3.4.1 Seasonal cycle

The wet season occurs between May and October at Chuuk, while the dry season is from November to April. At Pohnpei, the wettest months are April and May, with January and February being the driest months (Figure 3.2). Wet season rainfall is driven by the ITCZ, which is strongest during the middle of the year and located furthest north, close to FSM. Chuuk receives 57% of its annual rainfall, over 2000 mm (78.7 in) of rain, during the wet season. Rainfall in Chuuk is lower than Pohnpei due to its location further west and away from the ITCZ. Pohnpei receives over 4700 mm (185.0 in) of rainfall annually, with a monthly average of nearly 500 mm (19.7 in) in May.

The WPM also affects rainfall in FSM, bringing additional rainfall during the wet season. This influence is strongest across the western islands and weaker in Pohnpei and the islands in the east.

Figure 3.2:
Mean annual rainfall at Chuuk and Pohnpei

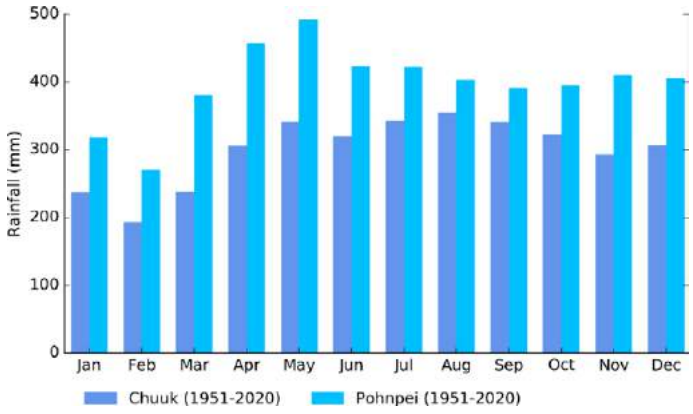

3.4.2 Trends

May to October rainfall has been decreasing at Pohnpei since 1952 (Table 3.1). All other trends in annual and seasonal rainfall at Pohnpei and Chuuk are not statistically significant (Figure 3.3, Table 3.1). Annual rainfall has varied from approximately 3300 to 6300 mm (129.9 to 248.0 in) at Pohnpei and 2300 to 4500 mm (90.6 to 177.2 in) at Chuuk.

Figure 3.3:
Annual rainfall (bar graph) and number of wet days (where rainfall is at least 1 mm; line graph) at Pohnpei (left) and Chuuk (right). Straight lines indicate linear trends for annual rainfall (in black) and number of wet days (in blue). The magnitudes of the trends are presented in Table 3.1. Diamonds indicate years with insufficient data for one or both variables.

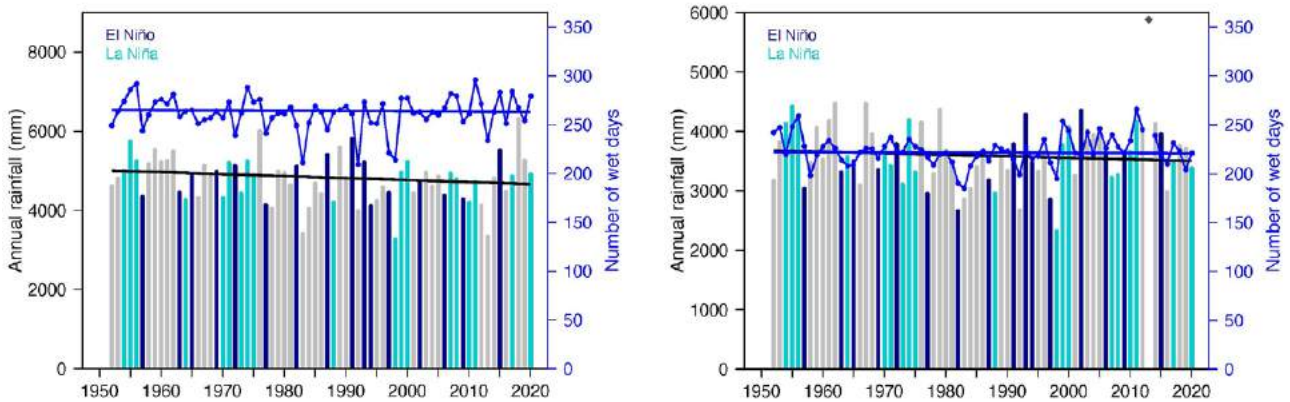

Table 3.1:
Trends in annual, seasonal and extreme rainfall at Pohnpei (left) and Chuuk (right). The 95% confidence intervals are shown in parentheses, and trends significant at the 95% level are shown in bold. The contribution to total rainfall from extreme events and the standardised rainfall evapotranspiration index are measured relative to 1961–1990 (see Chapter 1 for details).

	Pohnpei	Chuuk
	1952–2020	
Annual rainfall (mm/decade)	-50.06 (-118.75, +14.42)	-26.04 (-102.27, +52.03)
November–April (mm/decade)	-18.74 (-81.22, +48.80)	+0.60 (-44.39, +43.77)
May–October (mm/decade)	**-44.32** (-88.84, -0.60)	-23.81 (-79.33, +33.43)
Number of wet days (days/decade)	-0.31 (-2.18, +1.95)	-0.21 (-2.76, +2.71)
Contribution to total rainfall from extreme events (%/decade)	-0.21 (-1.09, +0.77)	-0.40 (-1.37, +0.60)
Consecutive dry days (days/decade)	0.00 (-0.38, 0.00)	0.00 (-0.43, +0.18)
Maximum one-day rainfall (mm/decade)	+2.08 (-3.57, +8.25)	0.00 (-4.08, +3.70)
Standardised rainfall evapotranspiration index (November–April)	-0.08 (-0.20, +0.09)	-0.02 (-0.14, +0.11)
Standardised rainfall evapotranspiration index (May–October)	-0.12 (-0.27, 0.00)	-0.07 (-0.26, +0.10)

Figure 3.4 shows change and variability in the longest run of days without rain and maximum daily rainfall at Pohnpei and Chuuk. Both sites rarely experience more than two weeks without rain. Unusually high maximum daily rainfall at Pohnpei in 1957 was likely associated with Typhoon Lola, and the high daily rainfall in 2002 at Chuuk was associated with tropical storm Chataan (Figure 3.4).

Figure 3.4:
Annual longest run of consecutive dry days (bar graph) and maximum daily rainfall (line graph) at Pohnpei (left) and Chuuk (right). Straight lines indicate linear trends for dry days (in black) and maximum daily rainfall (in blue). The magnitudes of the trends are presented in Table 3.1. Diamonds indicate years with insufficient data for one or both variables.

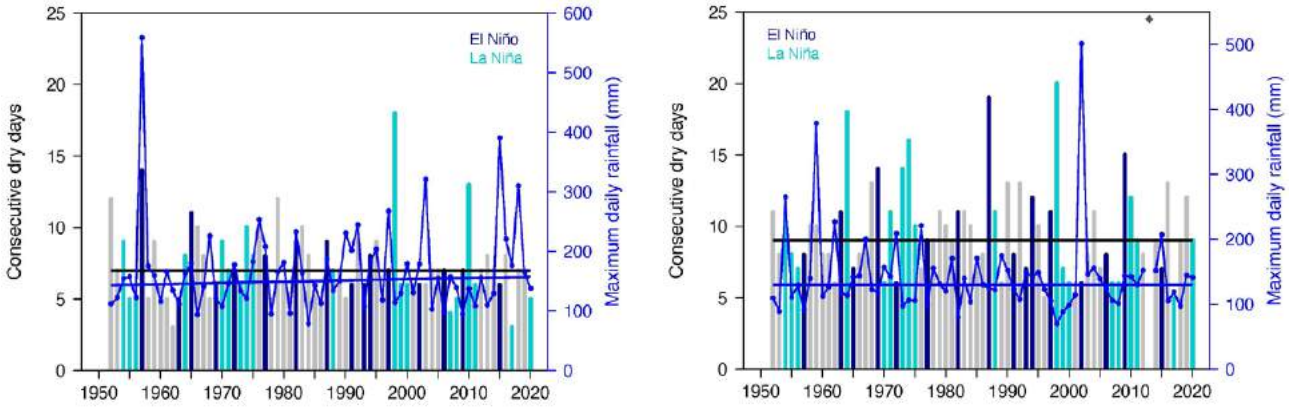

3.5 Air temperature

3.5.1 Seasonal cycle

Seasonal variations in monthly maximum and minimum air temperatures are less than 1.5°C (2.7 °F) between the average warmest and coolest months for Chuuk and Pohnpei. There has been a clear shift towards warmer average monthly temperatures between the climatology periods of 1961–1990 and 1991–2020 (Figure 3.5), with warmer average air temperatures occurring in all months throughout the year for both locations. The largest increase in average monthly maximum temperatures occurs at Pohnpei and is in excess of 1°C (1.8 °F) for August to October. Seasonal variations in air temperatures are driven by the surrounding SST.

Figure 3.5:
Maximum and minimum air temperature seasonal cycle for Chuuk (purple) and Pohnpei (green), and for the periods 1961–1990 (dotted lines) and 1991–2020 (full lines)

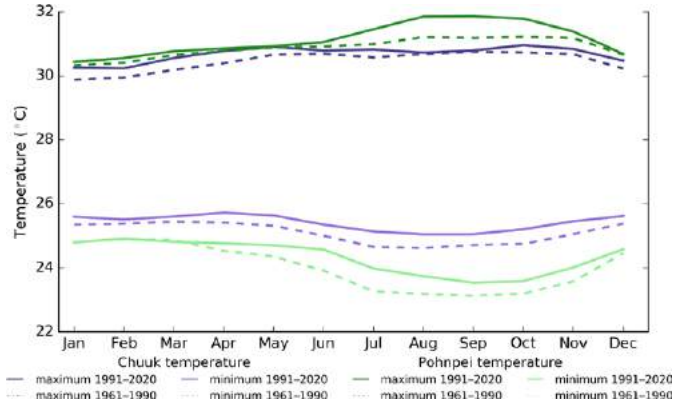

3.5.2 Trends

Average annual and seasonal temperatures have increased significantly at Pohnpei and Chuuk (Figure 3.6, Table 3.2). At Pohnpei, substantial decade-to-decade variability is evident, and May–October temperatures are warming faster than November–April temperatures (Figure 3.6).

Figure 3.6:
Average annual, November–April and May–October temperatures for Pohnpei (left) and Chuuk (right). Straight lines indicate linear trends. The magnitudes of the trends are presented in Table 3.2. Diamonds indicate years with insufficient data for one or more variables.

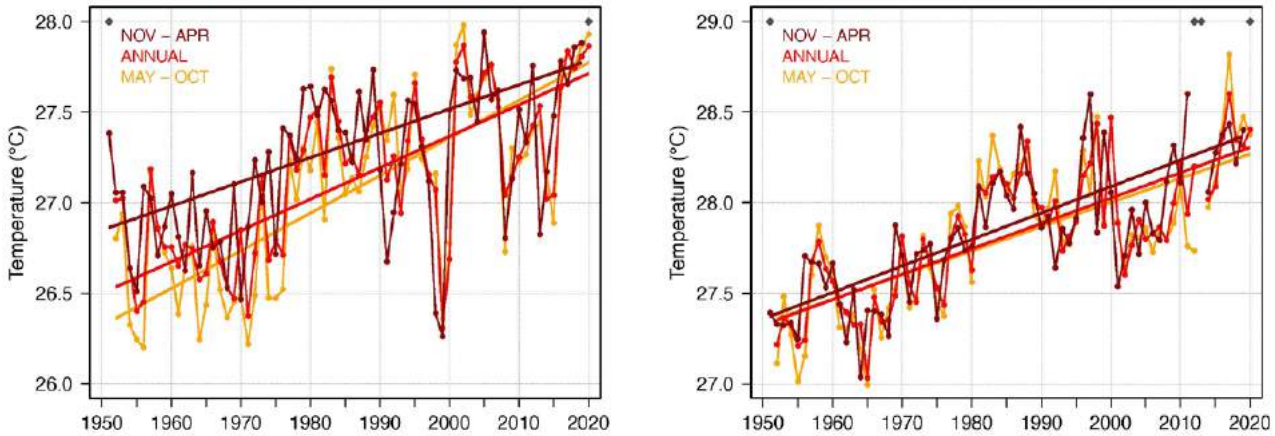

Table 3.2:
Trends in annual and seasonal air temperatures at Pohnpei (top) and Chuuk (bottom). The 95% confidence intervals are shown in parentheses, and trends significant at the 95% level are shown in bold.

	Pohnpei Tmax (°C/decade)	Pohnpei Tmin (°C/decade)	Pohnpei Tmean (°C/decade)	Chuuk Tmax (°C/10yrs)	Chuuk Tmin (°C/10yrs)	Chuuk Tmean (°C/10yrs)
	1952–2020					
Annual	**+0.18** (+0.12, +0.23)	**+0.14** (+0.06, +0.22)	**+0.17** (+0.11, +0.23)	**+0.15** (+0.07, +0.24)	**+0.12** (+0.07, +0.17)	**+0.14** (+0.08, +0.19)
November–April	**+0.16** (+0.10, +0.23)	**+0.10** (+0.02, +0.18)	**+0.13** (+0.07, +0.19)	**+0.20** (+0.11, +0.30)	**+0.10** (+0.06, +0.14)	**+0.15** (+0.10, +0.19)
May–October	**+0.20** (+0.14, +0.25)	**+0.19** (+0.09, +0.28)	**+0.21** (+0.14, +0.27)	**+0.12** (+0.03, +0.20)	**+0.14** (+0.08, +0.20)	**+0.13** (+0.07, +0.20)

The number of hot days and warm nights has increased, and the number of cool days and cold nights has decreased at Pohnpei and Chuuk (Figure 3.7, Table 3.3). Large variability is evident, particularly at Pohnpei. For example, some years experienced fewer than 20 hot days while others experienced over 100 hot days. This may be partly attributed to the tropical location of both sites, which makes only small temperature increases necessary for a day to be considered hot, i.e., to be in the hottest 10% of days compared to 1961–1990 (see Chapter 1 for details). However, quality issues may also be affecting these records.

The cooling degree days index provides a measure of the energy demand needed to cool a building down to 25 °C (77.0 °F), with the assumption that air conditioners are generally turned on at this temperature. At both Pohnpei and Chuuk, there has been a strong increase in the cooling degree index, suggesting the energy needed for cooling has increased significantly since 1952.

Table 3.3:
Trends in annual temperature extremes at Pohnpei (left) and Chuuk (right). The 95% confidence intervals are shown in parentheses, and trends significant at the 95% level are shown in bold. Hot and cool days, and warm and cold nights are measured relative to 1961–1990 (see Chapter 1 for details).

	Pohnpei	Chuuk
	1952–2020	
Number of hot days (days/decade)	**+12.23** (+6.02, +17.17)	**+10.79** (+3.69, +20.63)
Number of warm nights (nights/decade)	**+8.69** (+4.69, +13.51)	**+8.05** (+2.66, +13.47)
Number of cool days (days/decade)	**-5.87** (-7.59, -4.11)	**-4.37** (-6.38, -2.22)
Number of cold nights (nights/decade)	**-4.81** (-9.24, -0.50)	**-5.79** (-8.93, -2.22)
Cooling degree days (degree days/decade)	**+61.25** (+39.72, +81.18)	**+48.7** (+30.24, +65.11)
Daily temperature range (°C/decade)	+0.05 (-0.03, +0.13)	+0.05 (-0.02, +0.15)

Figure 3.7:
Annual number of hot days and cold nights at Pohnpei (left) and Chuuk (right). Straight lines indicate linear trends. The magnitudes of these trends are presented in Table 3.3. Diamonds indicate years with insufficient data for one or both variables.

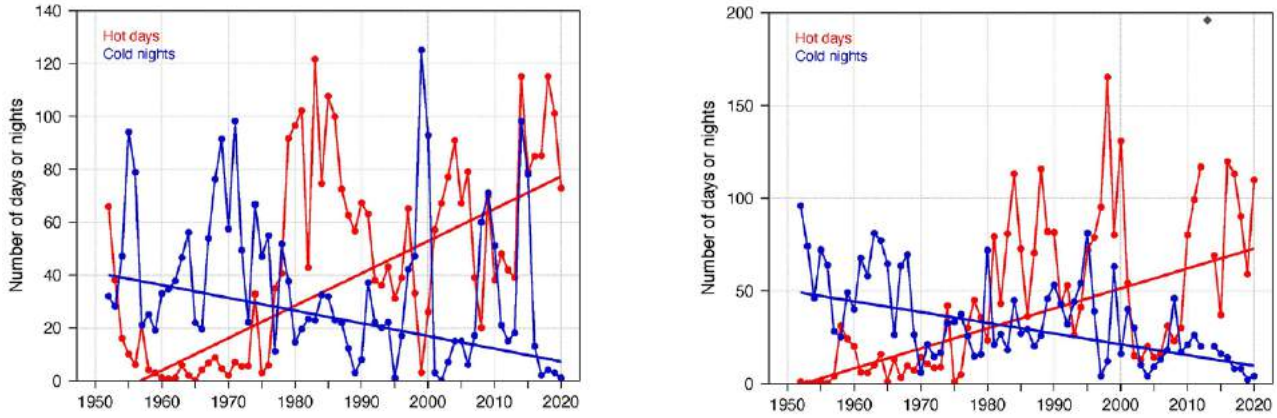

3.6 Tropical cyclones

3.6.1 Seasonal cycle

Tropical cyclones affect FSM year-round. The tropical cyclone archive of the western North Pacific indicates that between the 1969 and 2017 seasons, 364 tropical cyclones (Figure 3.8) passed within the EEZ. This represents an average of 74 cyclones per decade. Tropical cyclones were most frequent in El Niño years (95 cyclones per decade), followed by neutral years (78 cyclones per decade) and least frequent in La Niña years (46 cyclones per decade).

Interannual variability in the number of tropical cyclones in the EEZ is large, ranging from zero in 1999 to 14 in 1974 (Figure 3.8). High interannual variability and the small number of tropical cyclones occurring in the EEZ make reliable identification of long-term trends in frequency and intensity difficult.

Some tropical cyclone tracks analysed in this section include the tropical depression stage (sustained winds ≤34 knots) before and/or after tropical cyclone formation.

Figure 3.8:
Number of tropical cyclones passing within the FSM EEZ per season. Each season is defined by the El Niño–Southern Oscillation (ENSO) status, with light blue being an El Niño year, dark blue a La Niña year and grey showing a neutral ENSO year. The 11-year moving average is presented as a purple line and considers all years.

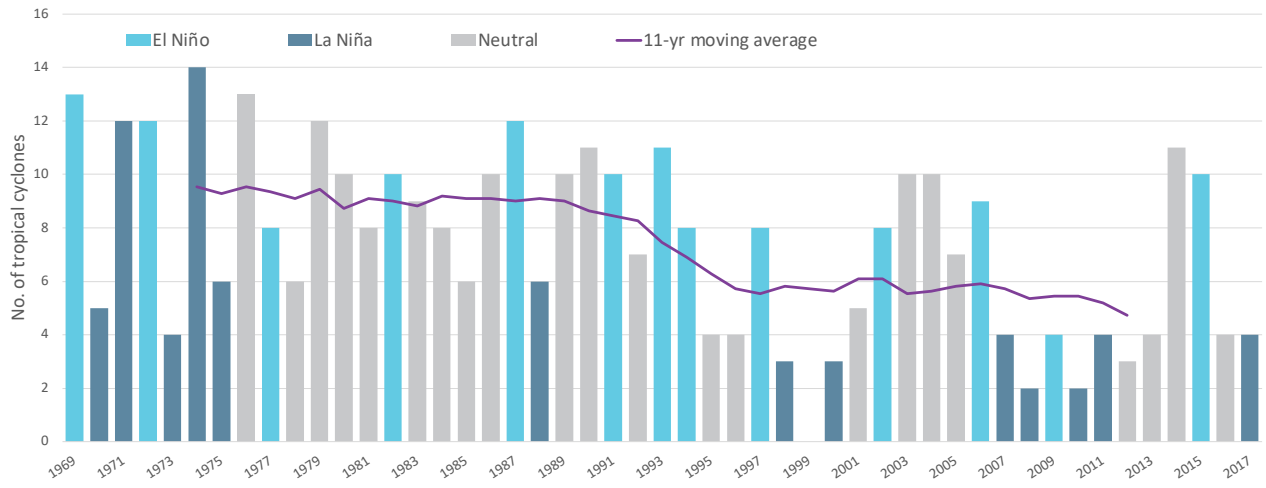

3.6.2 Trends

Trends in total number of tropical cyclones (<995 hPa) and severe tropical cyclones (<970 hPa) are presented for the period 1981–2021 for the Northwest Pacific (125°E–180°W; 0–20°N). Trends are presented at a regional scale as the number of tropical cyclones occurring within Pacific Island EEZs is insufficient for reliable long-term trend analysis.

For the total number of tropical cyclones, the trend (and 95% confidence interval) is -0.56 (-1.84, 0.72) tropical cyclones/decade. There has been little change in the total number of tropical cyclones over the last 41 seasons.

For the total number of severe tropical cyclones, the trend is -0.15 (-1.19, 0.89) tropical cyclones/decade. There has been little change in the number of severe tropical cyclones over the last 41 seasons. There has also been little change in the proportion of tropical cyclones reaching severe status. The trend is 0.01 (-0.04, 0.05) tropical cyclones/decade.

Records of tropical cyclones exist from the late 1800s in some countries in the Northwest Pacific, but trends in tropical cyclones have only been presented from 1981/82. Satellite-based observations began in the early 1970s, but consistent coverage and reliable intensity estimates have only been available since the early 1980s. Confidence in tropical cyclone trends is moderate as the definition of a tropical cyclone has changed and satellite observation methods have continued to improve over the last 41 years.

3.7 Sea surface temperature

3.7.1 Seasonal cycle

Ocean temperature, as measured by the Pohnpei tide-gauge from 2001 to 2021, reaches on average a maximum of approximately 30.0 °C (86.0 °F) from August to November but can get as high as 31.5 °C (88.7 °F) in September. Minimum average temperature dips below 29.0 °C (84.2 °F) in February. Hourly temperatures can be up to 1.5 °C (2.7 °F) higher or lower than these monthly averages in the warmer months. In cooler months, the temperature range is usually within ±1 °C (±1.8 °F), although 50% of hourly observations fall within 0.8 °C (1.4 °F) of the monthly average..

Figure 3.9:
Annual temperatures measured at the Pohnpei tide-gauge. Blue dots show the monthly average, and shaded boxes show the middle 50% of hourly observations. Lines show the top and bottom 25% of hourly observations.

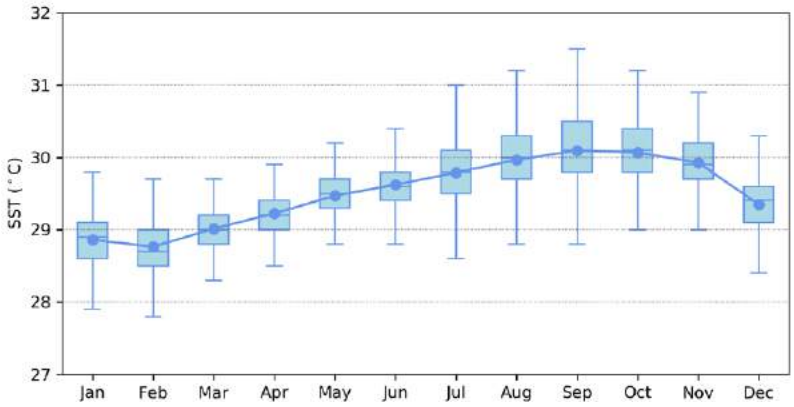

3.7.2 Trends

Figure 3.10 shows the 1981–2021 SST from satellite observations averaged over the FSM EEZ. The data show a trend of 0.25 °C (0.45 °F) per decade with a 95% confidence interval of ±0.04 °C (±0.07 °F).

Figure 3.10:
Sea surface temperature from satellite observations averaged across the FSM EEZ, shown as the orange line. The blue line shows the linear regression trend.

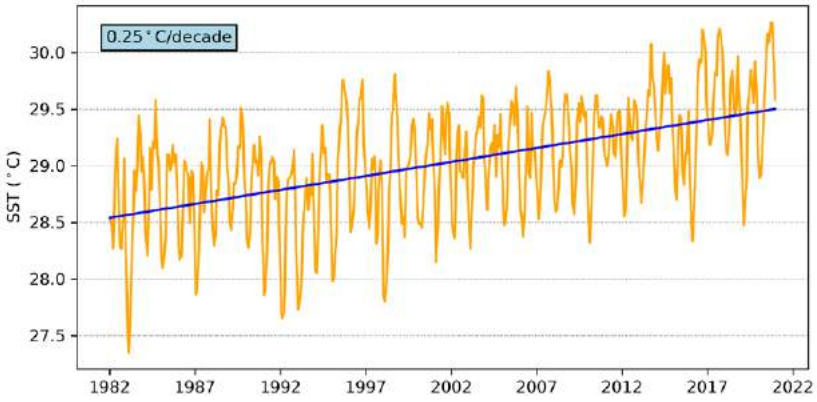

3.8 Sea level

3.8.1 Seasonal cycle

Tidal analysis of Pohnpei sea level data shows that it experiences a mixed tidal cycle. Typically, there are two high and two low tides a day during the new moon and full moon. However, there is only one high tide a day around the first and last quarter moons. The highest predicted tides of the year typically occur in both May/June as well as December/January. Figure 3.11 shows the number of hours the 99th percentile (1.64 m, 5.38 ft) sea level threshold is exceeded per month across the entire sea level record at Pohnpei. Peak sea levels typically occur from October to January. La Niña years typically have higher sea levels from October to December during a developing La Niña (2007, 2017, 2020).

Figure 3.11:
Number of hours exceeding 99th percentile sea level threshold per month from 2001 to 2020 at the Pohnpei tide-gauge. Blue shading indicates the number of hours, and the final row provides a percentage summary of all the years.

Number of hours exceeding 1.64 m (Dekehtik, Federated States of Micronesia)

	Jan	Feb	Mar	Apr	May	Jun	Jul	Aug	Sep	Oct	Nov	Dec	Annual
2001	0	0	0	0	0	0	0	0	0	0	0	0	0
2002	0	0	0	0	0	0	0	0	0	0	0	0	0
2003	0	0	0	0	0	0	0	0	0	0	0	0	0
2004	0	0	0	0	0	0	0	0	0	0	0	0	0
2005	0	0	0	0	0	0	0	0	0	0	0	0	0
2006	0	2	0	0	0	0	0	0	0	0	0	0	2
2007	0	0	0	0	0	1	0	0	0	9	11	2	23
2008	0	0	0	0	1	0	0	0	0	0	0	3	4
2009	1	0	0	0	0	0	0	0	0	0	0	0	1
2010	0	0	0	0	0	0	0	0	0	0	2	0	2
2011	3	0	0	1	0	0	0	0	0	2	2	1	9
2012	0	0	0	1	0	4	0	0	0	0	0	1	6
2013	0	0	0	3	0	0	0	0	0	0	1	0	4
2014	1	0	0	0	0	0	0	0	0	0	0	0	1
2015	0	0	0	0	0	0	0	0	0	0	0	0	0
2016	0	0	0	0	0	0	0	0	0	1	7	0	8
2017	0	0	0	0	0	0	0	0	0	0	17	0	17
2018	3	4	0	0	0	0	0	0	0	0	0	0	7
2019	0	0	0	0	0	0	1	0	0	0	0	0	1
2020	0	0	0	0	0	0	0	0	0	1	9	6	16
Monthly Totals (%)	8	6	0	5	1	5	1	0	0	13	49	13	

3.8.2 Trends

Sea level at FSM, measured by satellite altimeters (Figure 3.12) since 1993, has risen between 3 and 4.5 mm (0.12 and 0.18 in) per year. Trend estimates in the southeast are highest, ranging from 4 to 4.5 mm (0.16 to 0.18 in) per year, which is larger than the global average of 3.1 ± 0.4 mm (0.12 ± 0.02 in) per year (von Schuckmann et al. 2021). The 95% confidence interval is as high has ±1.6 mm (±0.06 in) in the west and down to 0.6 mm (0.02 in) in the southeast. This rise is partly linked to a pattern related to climate variability from year to year and decade to decade.

Figure 3.12:
Satellite altimetry annual trend for the Pacific from 1993 to 2020, with the FSM EEZ highlighted. The star symbol indicates the location of the tide-gauge at Pohnpei.

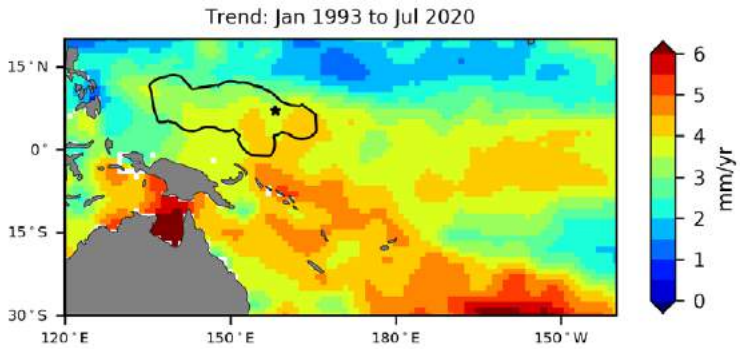

Trend estimates at the Pohnpei tide-gauge over a shorter time span than for the altimetry observations (December 2001 to July 2020) are provided in the PSLGM Monthly Data Report for July 2020 (http://www.bom.gov.au/ntc/IDO60101/IDO60101.202007.pdf). For Pohnpei, the trend is reported as 4.9 mm (0.19 in) per year, higher than the altimetry trends shown in Figure 3.12 (tide-gauge indicated by star symbol). This discrepancy could be an artefact of the different data time spans but can also be attributed to subsidence occurring at Pohnpei (Brown et al. 2020).

3.9 Waves

3.9.1 Seasonal cycle

The average wave climate at Pohnpei is defined by the significant wave height, peak period and peak direction. The significant wave height is the mean wave height (from trough to crest) of the highest one third of waves and corresponds to the wave height that would be reported by an experienced observer. Peak period is the time interval between two waves of the dominant wave period. Peak direction is the direction from which the dominant waves are coming.

The average sea state is dominated by winds from the northeast. The annual mean wave height is 1.20 m (3.9 ft), the annual mean wave direction is 23° and the annual mean wave period is 10.23 s. In the Pacific, waves often come from multiple directions and for different periods of time. In Pohnpei, there are often more than four different wave direction/period components coming from the northeast (Figure 3.13).

Figure 3.13:
Annual wave rose for Pohnpei. Note that direction is where the wave is coming from.

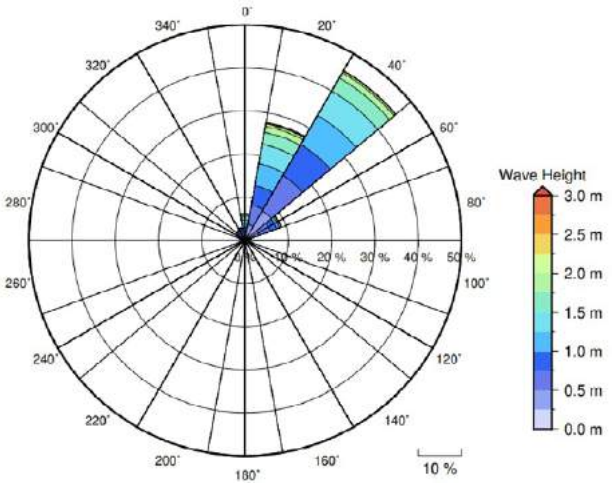

Seasonal wave activity peaks between November and March in terms of both wave height and period (Figure 3.14) due to North Pacific extra-tropical storm activity. Conversely, there is a distinct lull from late autumn to midsummer in terms of wave activity.

Figure 3.14:
Monthly wave height (black line), wave period (red line) and wave direction (arrows). The grey area represents the range of wave height between calm periods (10% of lowest wave height) and large wave events (10% of highest wave height).

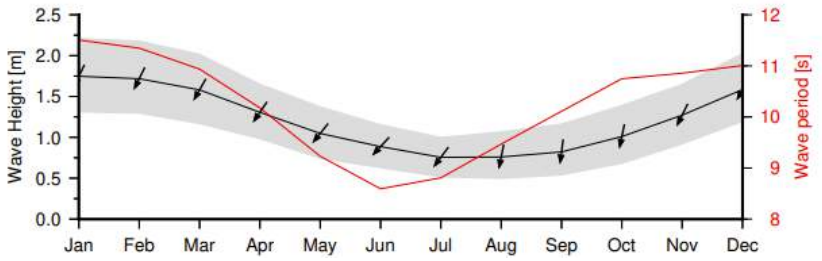

3.9.2 Trends

Waves change from month to month with the seasons, but they also change from year to year with climate oscillations. Typically, these changes are smaller than the seasonal changes but can be important during phenomena such as ENSO. In Pohnpei, the mean annual wave height has remained unchanged since 1979 (Figure 3.15). The mean annual wave height in Pohnpei is not significantly correlated with the main climate indicators of the region.

Figure 3.15:
Annual wave height (black line), wave period (red line) and wave direction (arrows). The grey area represents the range of wave height between calm periods (10% of lowest wave height) and large wave events (10% of highest wave height).

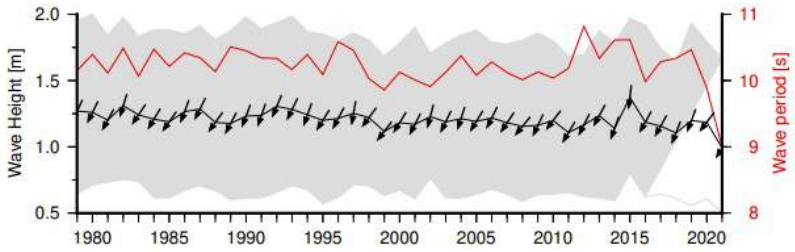

3.9.3 Extreme waves

Extreme wave analysis for Pohnpei was done by defining a severe height threshold and fitting a generalized Pareto distribution (GPD). The optimum threshold selected was 2.45 m (8.04 ft). In the 42-year wave hindcast, 162 wave events reached or exceeded this threshold, averaging 3.9 per year. The GPD was fitted to the largest wave height reached during each of these events (Figure 3.16, Table 3.4). Extreme wave analysis is a very useful tool but is not always accurate because the analysis is very sensitive to the data available, the type of distribution fitted and the threshold used. For example, this analysis does not accurately account for tropical cyclone waves. More in-depth analysis is required to obtain results appropriate for designing coastal infrastructure and coastal hazard planning.

Figure 3.16:
Extreme wave distribution for Pohnpei. The crosses represent the wave events that have occurred since 1979. The solid line is the statistical distribution that best fits past wave events. The dashed lines show the upper and lower confidence limits of the fit. There is a 95% chance that the fitted distribution lies between the two dashed lines. Note that the annual return interval is in logarithmic scale.

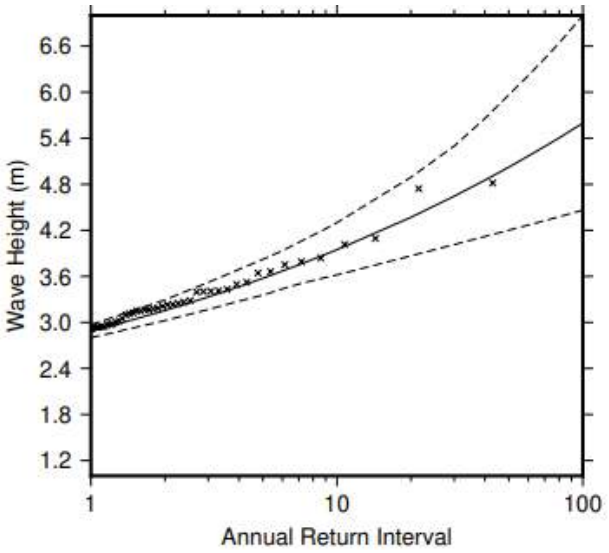

Table 3.4:
Summary of the results from extreme wave analysis in Pohnpei

Large wave height (90th percentile)	1.84 m (6.04 ft)
Severe wave height (99th percentile)	2.44 m (8.01 ft)
1-year ARI wave height	2.88 m (9.45 ft)
10-year ARI wave height	3.95 m (12.96 ft)
20-year ARI wave height	4.37 m (14.38 ft)
50-year ARI wave height	5.02 m (16.47 ft)
100-year ARI wave height	5.60 m (18.37 ft)

4 Fiji

4.1 Summary

4.1.1 Climate

- Changes in air temperature from season to season are relatively small and strongly linked to changes in the surrounding ocean temperature. Fiji has two distinct seasons – a warm wet season from November to April and a cooler dry season from May to October.
- The seasonal cycle is strongly affected by the South Pacific Convergence Zone (SPCZ), which is most intense during the wet season.
- Annual and seasonal air temperatures at Suva and Nadi Airport increased over the period 1951–2020. The number of hot days and warm nights has increased at Suva and Nadi Airport, while the number of cool days and cold nights has decreased.
- The energy required for cooling indoor environments has increased at Suva and Nadi Airport, and the difference between daytime and night-time temperatures has decreased at Nadi Airport.
- There has been little change in annual, seasonal and extreme rainfall at Suva and Nadi Airport.
- Tropical cyclones usually affect Fiji between November and April. Over the period 1969–2018, an average of 28 cyclones passed within the Fiji exclusive economic zone (EEZ) per decade. Tropical cyclones were most frequent in El Niño years and least frequent in La Niña years. Year-to-year variability is large, ranging from no tropical cyclones in some seasons to six.
- There has been little change in the total number of tropical cyclones in the Southwest Pacific since 1981/82. The number of severe tropical cyclones has declined over the same period/region.

4.1.2 Ocean

- Highest sea levels typically occur in the months October to March. La Niña brings noticeably higher sea levels outside the austral summer, specifically March/April and September/October.
- Sea-level rise within the EEZ, measured by satellite altimeters from 1993 to mid-2020, ranges from 4 to 5 mm per year, with highest trend estimates in the far north.
- Monthly average ocean temperature, as measured by the Lautoka tide-gauge, ranges from 26.4 °C in August to 30 °C in December to March. However, monthly temperatures in any given year can be up to ±2 °C of these averages.
- The sea surface temperature (SST) trend in the EEZ is 0.26 °C per decade.
- Highest waves at Fiji occur in the winter (June–August) months, with a distinct lull during summer (December–February).
- Dominant wave direction is from 185° (south), with an average significant wave height of 0.88 m and average wave period of 12.67 s.
- Severe wave height is defined as 1.97 m, with an average of 2.7 severe events per year.
- Peak average significant wave height occurs during the austral winter.

4.2 Country description

The Republic of Fiji is located in the tropical South Pacific Ocean between latitudes 12°S and 21°S, and longitudes 176°E and 178°W (Figure 4.1). Fiji is an archipelago of more than 330 islands, of which about 110 are permanently inhabited. There are more than 500 islets. Fiji has a total land area of 18,272 km^2 and an EEZ of 1.3 million km^2.

The two largest islands are Viti Levu and Vanua Levu, which account for 87.5% of the land area. The other islands consist of small volcanic islands, low-lying atolls and elevated reefs. The highest elevation is 1324 m above sea level on Viti Levu. Fiji's population is approximately 885,000. About 87% of the population live on the two main islands.

Figure 4.1:
Fiji and the locations of the climate stations used in this report

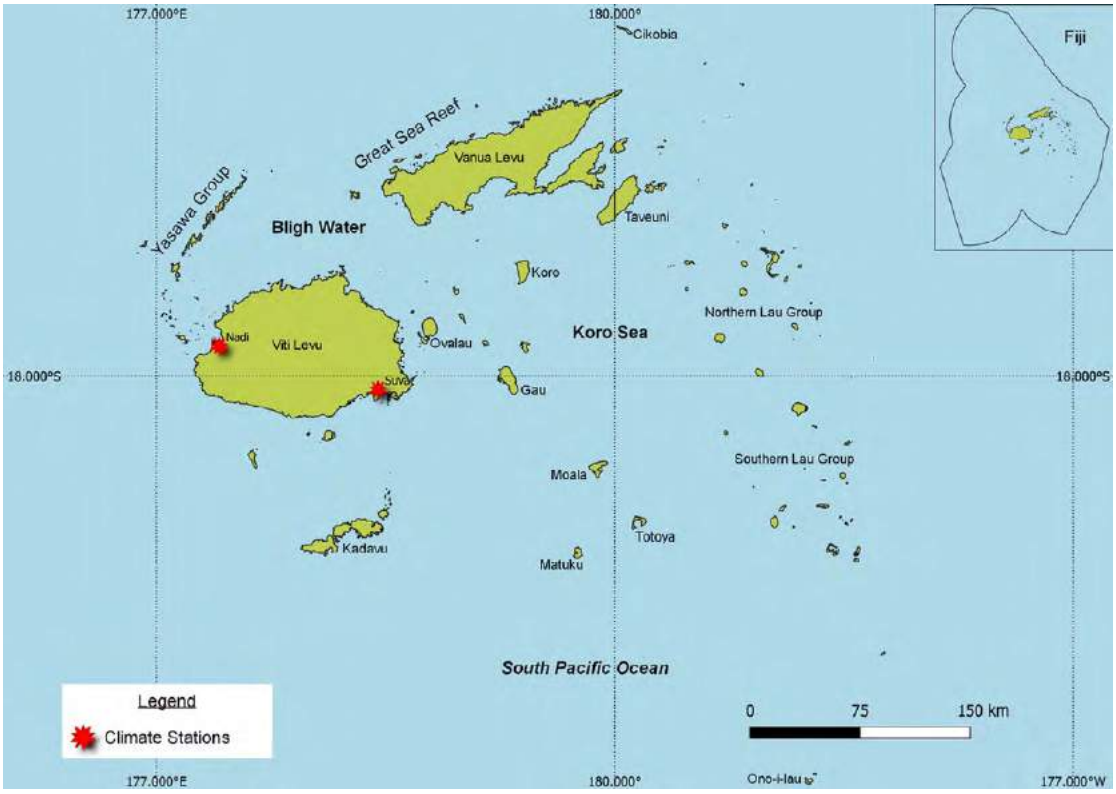

4.3 Data

Daily historical rainfall and air temperature records for Laucala Bay, Suva and Nadi Airport from 1951 were obtained from the Fiji Meteorological Service. These records have undergone data quality and homogeneity assessment. Where the maximum or minimum air temperature records were found to have discontinuities, these records have been adjusted to make them homogeneous (further information is provided in Chapter 1). Additional information on historical climate trends for Fiji can be found in the Pacific Climate Change Data Portal http://www.bom.gov.au/climate/pccsp.

Tropical cyclone data and historical tracks starting from the 1969/70 season are available from the SHTC Data Portal http://www.bom.gov.au/cyclone/history/tracks/index.shtml.

SST covering the EEZ was obtained via the daily Optimum Interpolation SST version 2.1 (OISST v2.1) dataset from NOAA (Reynolds et al. 2007; Banzon et al. 2016). In situ ocean temperature data were obtained from the PSLGM Project tide-gauge located at Lautoka, with data spanning from 1992 to 2021. The primary PSLGM tide-gauge in Fiji is located at Lautoka and has a longer data record than the tide-gauge at Suva.

Wave data were obtained from the PACCSAP wave hindcast (Smith et al. 2021), available hourly from 1979 to 2021, and for a grid resolution near Fiji of 7 km.

Regional sea level data were obtained from CSIRO satellite altimetry (updated by Benoit Legresy, Church and White 2011), with correction for seasonal signals, inverse barometer effect and glacial isostatic adjustment. Tide-gauge data were sourced from the Lautoka tide-gauge station, spanning from 1992 to 2021 at hourly intervals.

4.4 Rainfall

4.4.1 Seasonal cycle

In the cooler/drier half of the year (May–October), less energy is received from the sun and subtropical high-pressure systems move north bringing cooler, drier conditions. During the wetter/warmer half of the year, the SPCZ is most active and the southern edge usually lies close to Fiji, leading to about 63% of Suva's and 78% of Nadi Airport's rain falling during this period (Figure 4.2).

The effects of large-scale climate features such as the SPCZ and trade winds are modified on some islands due to the influence of mountains. Those regions exposed to the trade winds can receive mean annual rainfall in excess of 4000 mm, while leeward regions to the northwest receive on average less than 2000 mm annually, with less than 25% of annual rainfall between May and October. Several weather features have a notable impact on Fiji's climate. Active phases of the Madden–Julian Oscillation (MJO) near Fiji can be associated with significant rainfall for several days in the wet season. In addition, late afternoon convective thunderstorms contribute significant rainfall to the central and western parts of Viti Levu. In the dry season, cold fronts, which are usually weak by the time they reach Fiji's latitude, occasionally merge with troughs in the upper atmosphere, resulting in widespread rainfall.

Figure 4.2:
Mean annual rainfall at Nadi Airport and Suva

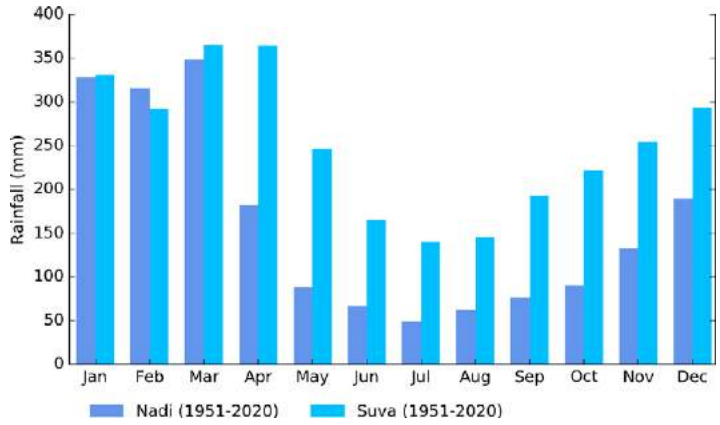

4.4.2 Trends

Trends in annual and seasonal rainfall since 1951 are not statistically significant at Suva and Nadi Airport (Figure 4.3, Table 4.1). This means there has been little change in annual and seasonal rainfal at these sites. Notable year-to-year variability associated with El Niño–Southern Oscillation (ENSO) is evident at Nadi Airport, with higher rainfall typically occurring during La Niña years compared to El Niño years (Figure 4.3). Annual rainfall since 1951 has varied from approximately 1600 to 4400 mm at Suva and from approximately 900 to 3500 mm at Nadi Airport.

Figure 4.3:
Annual rainfall (bar graph) and number of wet days (where rainfall is at least 1 mm; line graph) at Suva (left) and Nadi Airport (right). Straight lines indicate linear trends for annual rainfall (in black) and number of wet days (in blue). The magnitudes of the trends are presented in Table 4.1.

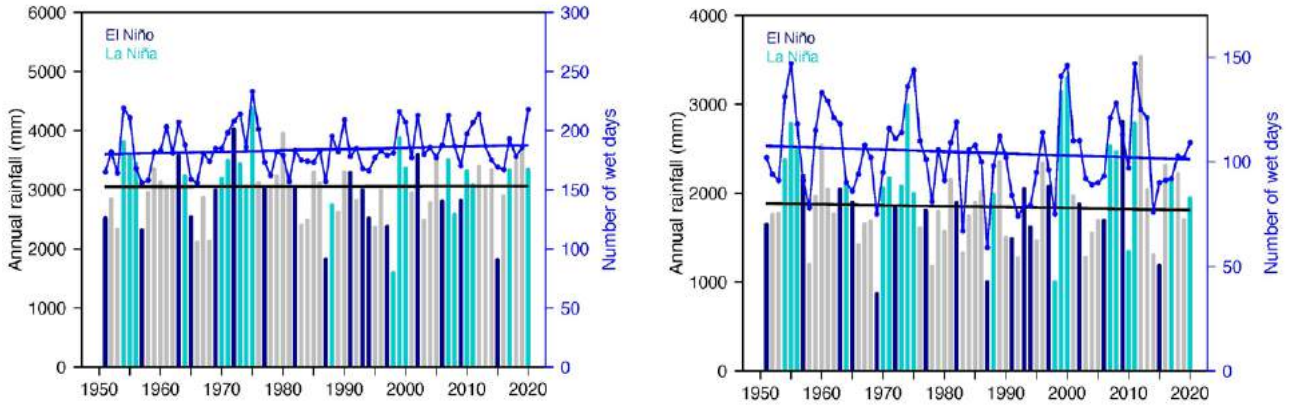

Table 4.1:
Trends in annual, seasonal and extreme rainfall at Suva (left) and Nadi Airport (right). The 95% confidence intervals are shown in parentheses. The contribution to total rainfall from extreme events and the standardised rainfall evapotranspiration index are measured relative to 1961–1990 (see Chapter 1 for details).

	Suva	Nadi Airport
	1951–2020	
Annual rainfall (mm/decade)	+1.76 (-68.20, +68.79)	-10.53 (-92.75, +75.19)
November–April (mm/decade)	-13.33 (-74.06, +46.91)	+11.92 (-51.27, +74.66)
May–October (mm/decade)	+1.30 (-51.81, +48.18)	-4.59 (-25.90, +21.75)
Number of wet days (days/decade)	+1.13 (-1.71, +3.72)	-0.93 (-4.45, +2.80)
Contribution to total rainfall from extreme events (%/decade)	-0.53 (-1.63, +0.66)	+0.71 (-0.67, +2.21)
Consecutive dry days (days/decade)	-0.31 (-0.73, 0.00)	+0.40 (-1.10, +2.28)
Maximum one-day rainfall (mm/decade)	-1.76 (-9.33, +5.04)	+0.89 (-4.97, +6.44)
Standardised rainfall evapotranspiration index (November–April)	-0.03 (-0.16, +0.10)	+0.02 (-0.14, +0.18)
Standardised rainfall evapotranspiration index (May–October)	+0.02 (-0.13, +0.15)	-0.01 (-0.15, +0.13)

Like annual and seasonal rainfall, no significant trends in extreme rainfall indices, including the standardised rainfall evapotranspiration drought index, were detected (Table 4.1). Figure 4.4 shows change and variability in the longest run of days without rain and maximum daily rainfall at Suva and Nadi Airport. Nadi Airport experiences longer dry spells compared to Suva, and both sites experience high interannual variability in maximum daily rainfall.

Figure 4.4:
Annual longest run of consecutive dry days (bar graph) and maximum daily rainfall (line graph) at Suva (left) and Nadi Airport (right). Straight lines indicate linear trends for dry days (in black) and maximum daily rainfall (in blue). The magnitudes of the trends are presented in Table 4.1.

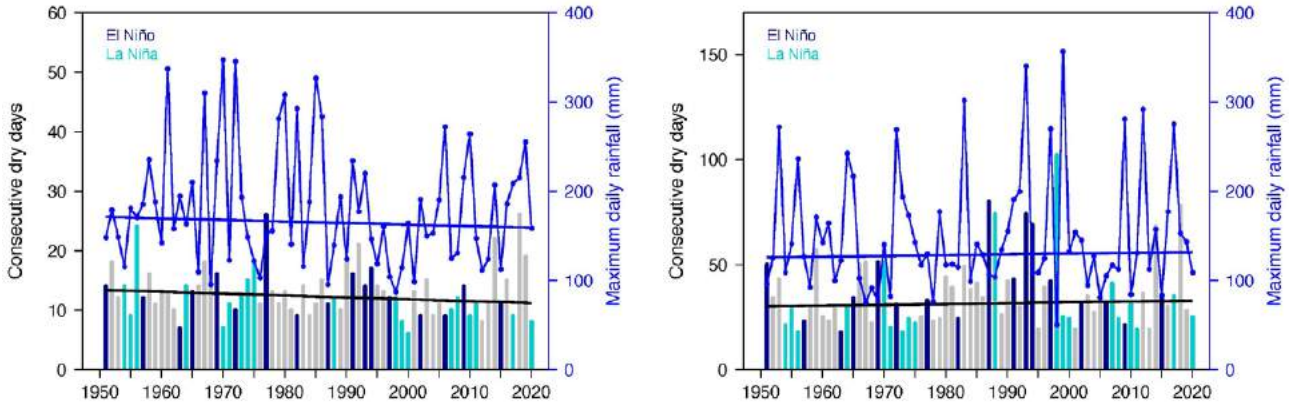

4.5 Air temperature

4.5.1 Seasonal cycle

The range in average monthly maximum temperatures throughout the year is about 5 °C for Suva and 3 °C for Nadi Airport. The average monthly minimum temperature range is about 3 °C for Suva and 4 °C for Nadi Airport for 1991–2020. There has been a clear shift towards warmer average monthly temperatures between the climatology periods of 1961–1990 and 1991–2020 (Figure 4.5), with warmer average temperatures occurring in all months throughout the year for both Suva and Nadi Airport, with the exception of average maximum temperatures at Nadi Airport between June and September. The largest increase in average monthly temperatures for both locations occurs at the end of the warmer/wetter season (November to April).

Figure 4.5:
Maximum and minimum air temperature seasonal cycle for Nadi Airport (purple) and Suva (green), and for the periods 1961–1990 (dotted lines) and 1991–2020 (full lines)

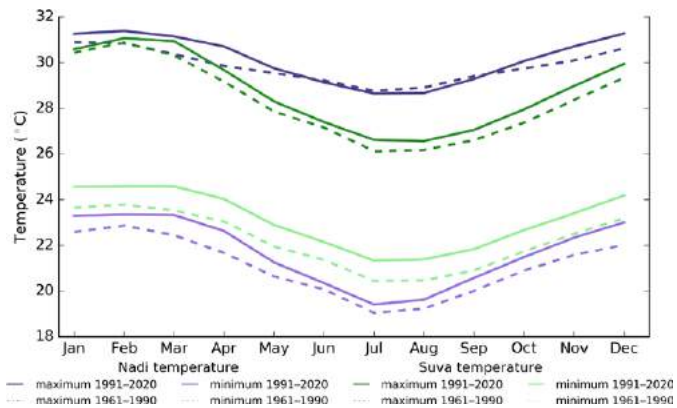

4.5.2 Trends

Average annual and seasonal temperatures have increased significantly at Suva and Nadi Airport (Figure 4.6). November–April temperatures are increasing faster than May–October temperatures at Nadi Airport (Table 4.2).

Figure 4.6:
Average annual, November–April and May–October temperatures for Suva (left) and Nadi Airport (right). Straight lines indicate linear trends. The magnitudes of the trends are presented in Table 4.2. Diamonds indicate years with insufficient data for one or more variables.

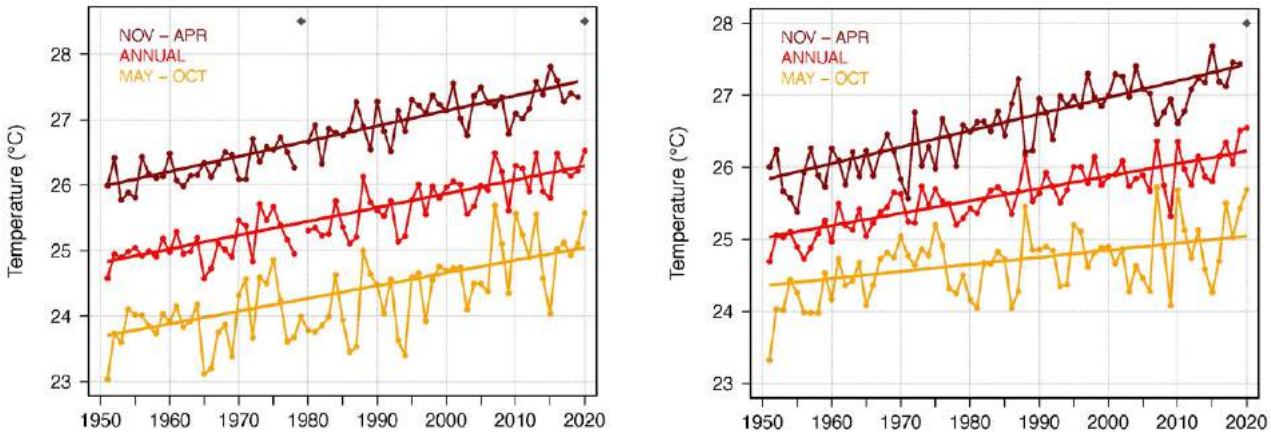

Table 4.2:
Trends in annual and seasonal air temperatures at Suva (top) and Nadi Airport (bottom). The 95% confidence intervals are shown in parentheses, and trends significant at the 95% level are shown in bold.

	Suva Tmax (°C/decade)	Suva Tmin (°C/decade)	Suva Tmean (°C/decade)	Nadi Airport Tmax (°C/10yrs)	Nadi Airport Tmin (°C/10yrs)	Nadi Airport Tmean (°C/10yrs)
			1951–2020			
Annual	**+0.18** (+0.13, +0.23)	**+0.24** (+0.19, +0.30)	**+0.21** (+0.18, +0.25)	**+0.15** (+0.11, +0.19)	**+0.20** (+0.16, +0.24)	**+0.17** (+0.15, +0.20)
November–April	**+0.21** (+0.15, +0.27)	**+0.26** (+0.22, +0.30)	**+0.23** (+0.20, +0.26)	**+0.22** (+0.16, +0.28)	**+0.25** (+0.22, +0.28)	**+0.23** (+0.19, +0.27)
May–October	**+0.15** (+0.08, +0.22)	**+0.24** (+0.15, +0.33)	**+0.19** (+0.12, +0.26)	**+0.07** (+0.01, +0.14)	**+0.16** (+0.07, +0.23)	**+0.10** (+0.05, +0.16)

The number of hot days and warm nights has increased, and the number of cool days and cold nights has decreased at Suva and Nadi Airport (Table 4.3). Increases in heat extremes have been particularly strong at Nadi Airport, with multiple recent years experiencing over 100 hot days (Figure 4.7).

The cooling degree days index provides a measure of the energy demand needed to cool a building down to 25 °C, with the assumption that air conditioners are generally turned on at this temperature. At Suva and Nadi Airport, there has been a strong increase in the cooling degree day index, suggesting the energy needed for cooling has increased significantly since 1951. The difference between daytime and night-time temperatures at Nadi Airport has been decreasing, and while a similar trend exists at Suva, it is not statistically significant (Table 4.3).

Table 4.3:
Trends in annual temperature extremes at Suva (left) and Nadi Airport (right). The 95% confidence intervals are shown in parentheses, and trends significant at the 95% level are shown in bold. Hot and cool days, and warm and cold nights are measured relative to 1961–1990 (see Chapter 1 for details).

	Suva	Nadi Airport
	1951–2020	
Number of hot days (days/decade)	**+7.66** (+3.88, +11.64)	**+11.69** (+9.72, +13.51)
Number of warm nights (nights/decade)	**+14.35** (+10.26, +18.91)	**+17.95** (+15.69, +20.17)
Number of cool days (days/decade)	**-5.69** (-7.02, -4.27)	**-5.62** (-9.53, -1.92)
Number of cold nights (nights/decade)	**-6.75** (-8.53, -5.14)	**-6.07** (-8.90, -3.26)
Cooling degree days (degree days/decade)	**+50.06** (+44.84, +55.32)	**+53.98** (+48.70, +60.01)
Daily temperature range (°C/decade)	-0.06 (-0.16, +0.03)	**-0.05** (-0.10, -0.01)

Figure 4.7:
Annual number of hot days and cold nights at Suva (left) and Nadi Airport (right). Straight lines indicate linear trends. The magnitudes of the trends are presented in Table 4.3. Diamonds indicate years with insufficient data for one or both variables.

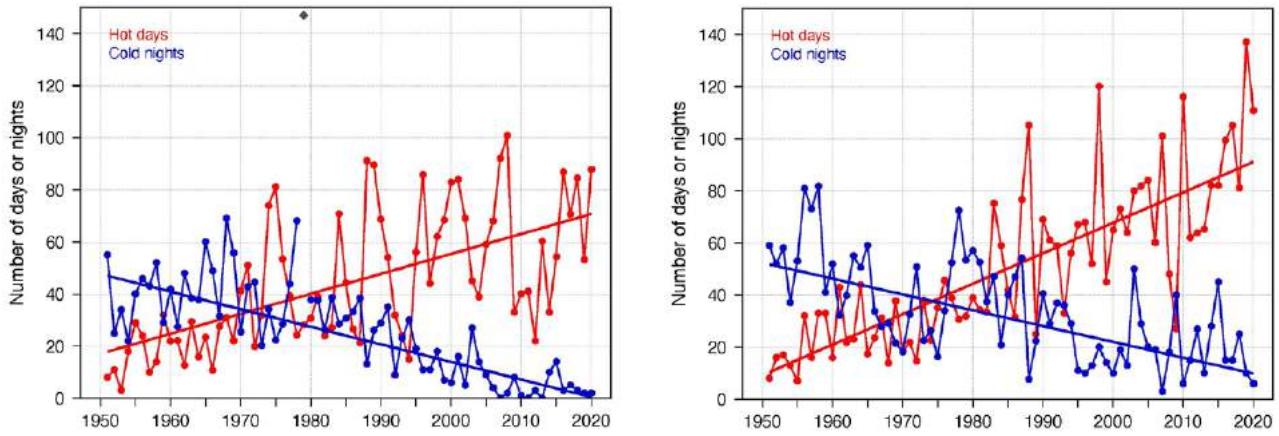

4.6 Tropical cyclones

4.6.1 Seasonal cycle

Tropical cyclones usually affect Fiji during the southern hemisphere tropical cyclone season, which is from November to April. Tropical cyclones also occasionally occur in October and May of El Niño years. The tropical cyclone archive of the southern hemisphere indicates that between the 1969/70 and 2017/18 seasons, 135 tropical cyclones (Figure 4.8) passed within the EEZ. This represents an average of 28 cyclones per decade. Tropical cyclones are most frequent in neutral years (29 cyclones per decade), and then equally likely during El Niño and La Niña years (26 cyclones per decade).

Interannual variability in the number of tropical cyclones in the EEZ is large, ranging from zero in the 1994/95 season to six in 1979/80 and 1992/93 (Figure 4.8). High interannual variability and the small number of tropical cyclones occurring in the EEZ make reliable identification of long-term trends in frequency and intensity difficult.

Some tropical cyclone tracks analysed in this section include the tropical depression stage (sustained winds ≤34 knots) before and/or after tropical cyclone formation.

Figure 4.8:
Number of tropical cyclones passing within the Fiji EEZ per season. Each season is defined by ENSO status, with light blue being an El Niño year, dark blue a La Niña year and grey showing a neutral ENSO year. The 11-year moving average is presented as a purple line and considers all years.

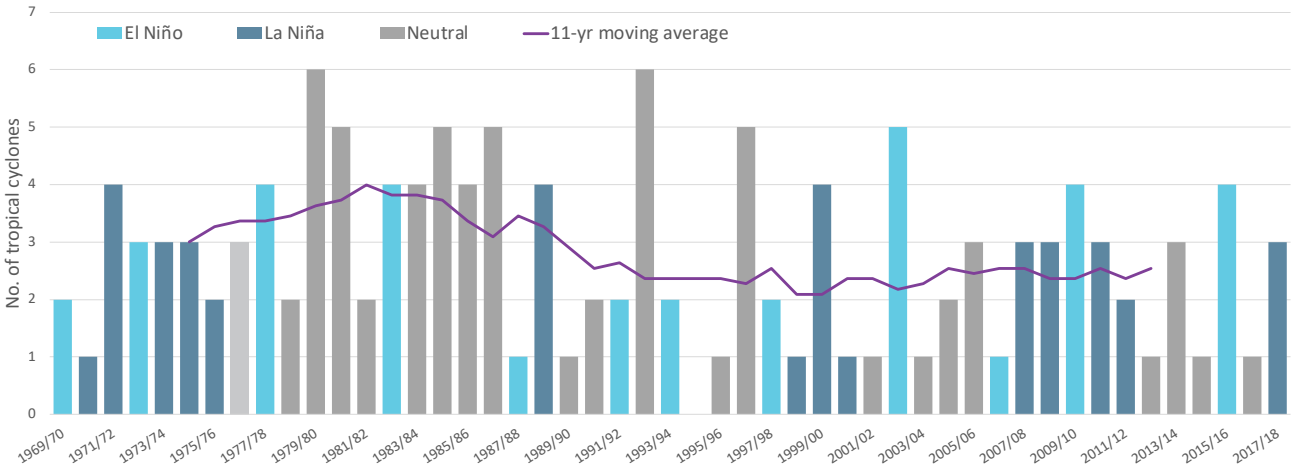

4.6.2 Trends

Trends in total number of tropical cyclones (<995 hPa) and severe tropical cyclones (<970 hPa) are presented for the period 1981/82–2020/21 for the greater Southwest Pacific (135°E–120°W; 0–50°S). Trends are presented at a regional scale as the number of tropical cyclones occurring within Pacific Island EEZs is insufficient for reliable long-term trend analysis.

For the total number of tropical cyclones, the trend (and 95% confidence interval) is -0.92 (-1.85, 0.01) tropical cyclones/decade. There has been little change/marginal decline in the total number of tropical cyclones over the last 40 seasons. This trend is not statistically significant.

For the total number of severe tropical cyclones, the trend is -0.80 (-1.32, -0.29) tropical cyclones/decade. There is a negative trend in the number of severe tropical cyclones over the last 40 seasons. There has been little change/marginal decline in the proportion of tropical cyclones reaching severe status. The trend is -0.04 (-0.08, 0.00) tropical cyclones/decade. The negative trend is statistically significant.

Records of tropical cyclones exist from the late 1800s in some countries in the Southwest Pacific, but trends in tropical cyclones have only been presented from 1981/82. Satellite-based observations began in the Southwest Pacific in the early 1970s, but consistent coverage and reliable intensity estimates have only been available since the early 1980s. Confidence in tropical cyclone trends is moderate as the definition of a tropical cyclone has changed and satellite observation methods have continued to improve over the last 40 years.

4.7 Sea surface temperature

4.7.1 Seasonal cycle

Ocean temperature, as measured by the Lautoka tide-gauge from 1992 to 2021, reaches on average a maximum of approximately 30 °C from December to March (Figure 4.9), but individual months can get as high as 32 °C. Minimum average temperature reaches a low of 26.4 °C in August. Hourly temperatures can be up to 2 °C higher or lower than these monthly averages, although 50% of hourly observations fall within 1 °C of the average.

Figure 4.9: Annual temperatures measured at the Lautoka tide-gauge. Blue dots show the monthly average, and shaded boxes show the middle 50% of hourly observations Lines show the top and bottom 25% of hourly observations

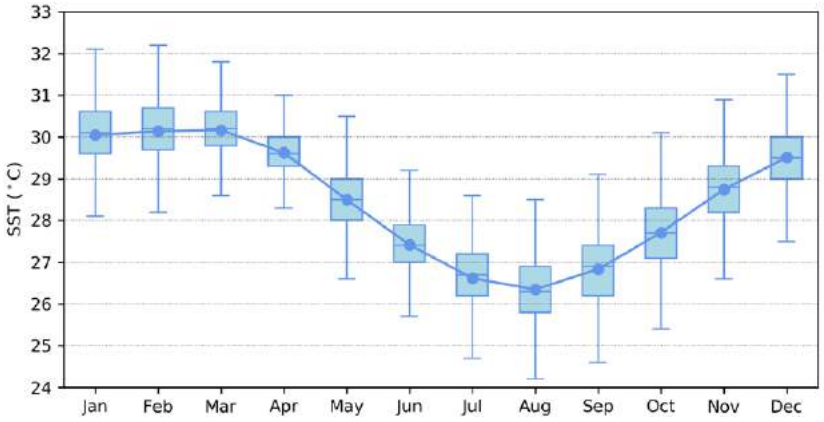

4.7.2 Trends

Historical changes in SST around Fiji are consistent with the broad-scale changes in the region. Water temperatures remained relatively constant from the 1950s to the late 1980s. This was followed by a period of more rapid warming. Figure 4.10 shows the 1981–2021 SST from satellite observations averaged over the EEZ. The data show a trend of 0.26 °C per decade with a 95% confidence interval of ±0.10 °C.

Figure 4.10: Sea surface temperature from satellite observations averaged across the Fiji EEZ, shown as the orange line. The blue line shows the linear regression trend.

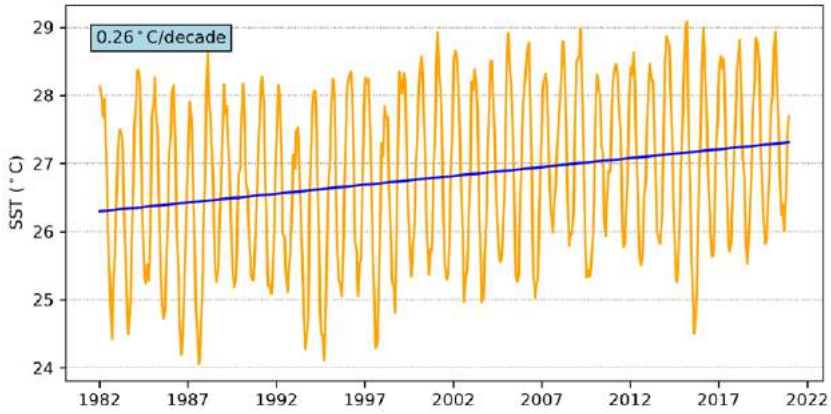

4.8 Sea level

4.8.1 Seasonal cycle

Fiji experiences a semidiurnal tidal cycle, meaning two high and two low tides per day. The highest predicted tides of the year typically occur during the wet season months of December–February. Figure 4.11 shows the number of hours the 99th percentile (2.39 m) sea level threshold is exceeded per month across the entire sea level record at Lautoka. Peak sea levels typically occur over a significant portion of the year from October to March. La Niña years typically have higher sea levels outside the austral summer, specifically March/April and September/October.

Since approximately 2009, the number of hours where sea level exceeds the 2.39 m sea level threshold has increased steadily. This is due to a combination of sea-level rise and subsidence occurring at Fiji (Brown et al. 2020).

Figure 4.11: Number of hours exceeding 99th percentile sea level threshold per month from 1992 to 2021 at the Lautoka tide-gauge. Blue shading indicates the number of hours, and the final row provides a percentage summary of all the years.

Number of hours exceeding 2.39 m (Lautoka, Fiji)

	Jan	Feb	Mar	Apr	May	Jun	Jul	Aug	Sep	Oct	Nov	Dec	Annual
1992	0	0	0	0	0	0	0	0	0	0	0	2	2
1993	0	0	0	0	0	0	0	0	0	0	0	0	0
1994	0	0	0	0	0	0	0	0	0	0	0	0	0
1995	0	0	0	0	0	0	0	0	0	0	0	2	2
1996	1	0	0	0	0	0	0	0	0	0	0	0	1
1997	0	4	15	0	0	0	0	0	0	0	0	0	19
1998	0	0	0	0	0	0	0	0	0	0	0	0	0
1999	0	0	0	0	0	0	0	0	0	0	0	0	0
2000	5	0	0	0	0	0	0	0	0	0	0	0	5
2001	0	2	0	0	0	0	0	0	0	0	0	0	2
2002	0	0	0	0	0	0	0	0	0	1	1	0	2
2003	0	0	0	0	0	0	0	0	0	0	0	0	0
2004	0	0	0	0	0	0	0	0	0	0	0	0	0
2005	0	0	0	0	0	0	0	0	0	0	0	0	0
2006	0	0	0	0	0	0	0	0	0	0	0	0	0
2007	0	0	0	0	0	0	0	0	1	0	0	0	1
2008	0	0	0	0	0	0	0	0	0	0	0	1	1
2009	5	3	0	0	0	0	0	1	0	0	0	0	9
2010	2	1	1	0	0	0	0	0	0	0	0	0	4
2011	0	0	1	0	0	0	0	0	5	6	0	0	12
2012	0	0	1	4	6	0	1	0	0	1	2	9	24
2013	7	0	0	0	0	0	0	0	0	0	0	2	9
2014	11	1	0	0	0	0	0	0	0	0	0	0	12
2015	0	3	0	0	0	0	0	0	0	0	6	0	9
2016	0	0	0	0	0	0	0	0	0	1	0	0	1
2017	0	0	0	0	0	0	0	0	0	0	0	0	0
2018	2	2	0	1	0	0	0	0	0	0	0	0	5
2019	0	0	0	0	0	0	0	0	0	2	0	2	4
2020	0	0	0	5	0	0	0	0	0	5	3	2	15
2021	0	0	2	4	1	0	0	0	0	0	2	8	17
Monthly Totals (%)	21	10	13	9	4	0	1	1	4	10	9	18	

4.8.2 Trends

Sea level at Fiji, measured by satellite altimeters (Figure 4.12) since 1993, has risen between 4 and 5 mm per year across the EEZ, with a 95% confidence interval of ±0.4 mm in the south and up to ±1.0 mm in the far north. This is larger than the global average of 3.1 ± 0.4 mm per year (von Schuckmann et al. 2021). This rise is partly linked to a pattern related to climate variability from year to year and decade to decade.

Trend estimates at the Lautoka tide-gauge over a similar time span to the altimetry observations (October 1992 to July 2020) are provided in the PSLGM Monthly Data Report for July 2020 (http://www.bom.gov.au/ntc/IDO60101/IDO60101.202007.pdf). For Lautoka, the trend is reported as 3.5 mm per year, very similar to the altimetry trends shown in Figure 4.12 (tide-gauge indicated by star symbol).

Figure 4.12: Satellite altimetry annual trend for the Pacific from 1993 to 2020, with the Fiji EEZ highlighted. The star symbol indicates the location of the tide-gauge at Lautoka.

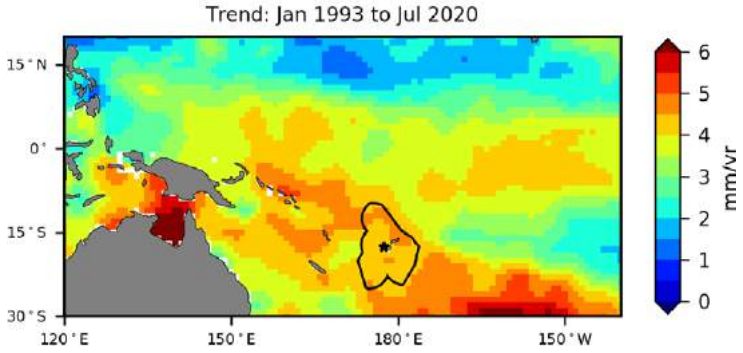

4.9 Waves

4.9.1 Seasonal cycle

The average wave climate at Suva is defined by the significant wave height, peak period and peak direction. The significant wave height is the mean wave height (from trough to crest) of the highest one third of waves and corresponds to the wave height that would be reported by an experienced observer. Peak period is the time interval between two waves of the dominant wave period. Peak direction is the direction from which the dominant waves are coming.

The average sea state is dominated by swells from the south. The annual mean wave height is 0.88 m, the annual mean wave direction is 185° and the annual mean wave period is 12.67 s. In the Pacific, waves often come from multiple directions and for different periods of time. In Suva, there are often more than four different wave direction/period components coming from the southeast to southwest (Figure 4.13).

Figure 4.13: Annual wave rose for Suva. Note that direction is where the wave is coming from.

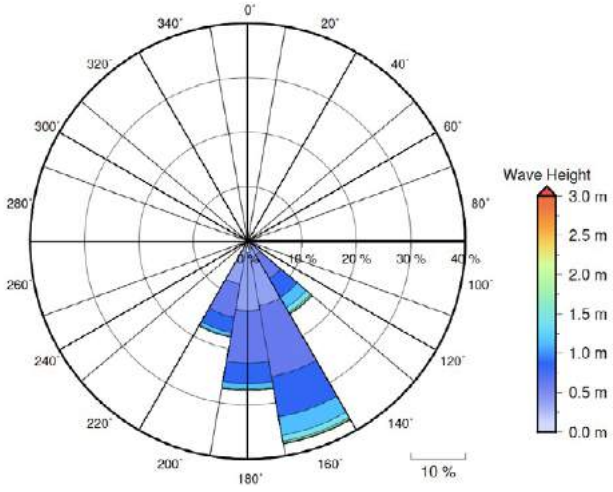

Seasonal wave activity peaks in the winter (June–August) months in terms of both wave height and period (Figure 4.14). This is related to the intensification of the Southern Ocean storm track during the austral winter. Conversely, there is slightly reduced significant wave height during summer (December–February) months, with wave period reduced significantly during this period.

Figure 4.14: Monthly wave height (black line), wave period (red line) and wave direction (arrows). The grey area represents the range of wave height between calm periods (10% of lowest wave height) and large wave events (10% of highest wave height).

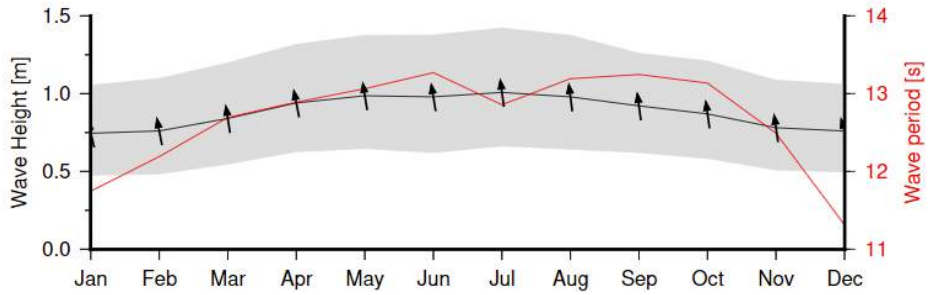

4.9.2 Trends

Waves change from month to month with the seasons, but they also change from year to year with climate oscillations. Typically, these changes are smaller than the seasonal changes but can be important during phenomena such as ENSO. In Suva, the mean annual wave height has remained unchanged since 1979 (Figure 4.15). The mean annual wave height in Suva is not significantly correlated with the main climate indicators of the region.

Figure 4.15: Annual wave height (black line), wave period (red line) and wave direction (arrows). The grey area represents the range of wave height between calm periods (10% of lowest wave height) and large wave events (10% of highest wave height).

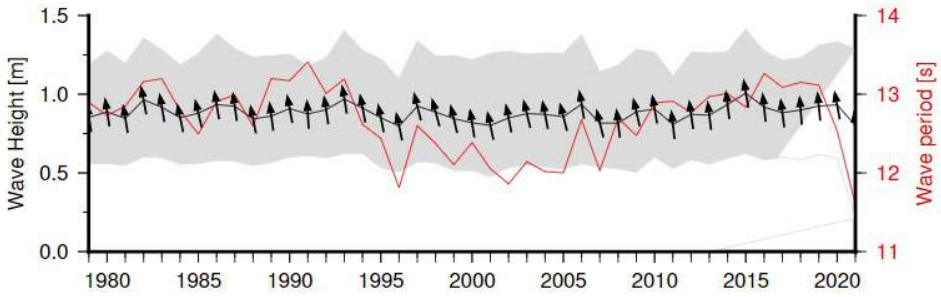

4.9.3 Extreme waves

Extreme wave analysis for Suva was done by defining a severe height threshold and fitting a generalized Pareto distribution (GPD). The optimum threshold selected was 1.97 m. In the 42-year wave hindcast, 112 wave events reached or exceeded this threshold, averaging 2.7 per year. The GPD was fitted to the largest wave height reached during each of these events (Figure 4.16, Table 4.3). Extreme wave analysis is a very useful tool but is not always accurate because the analysis is very sensitive to the data available, the type of distribution fitted and the threshold used. For example, this analysis does not accurately account for tropical cyclone waves. More in-depth analysis is required to obtain results appropriate for designing coastal infrastructure and coastal hazard planning.

Figure 4.16: Extreme wave distribution for Suva. The crosses represent the wave events that have occurred since 1979. The solid line is the statistical distribution that best fits past wave events. The dashed lines show the upper and lower confidence limits of the fit. There is a 95% chance that the fitted distribution lies between the two dashed lines. Note that the annual return interval is in logarithmic scale.

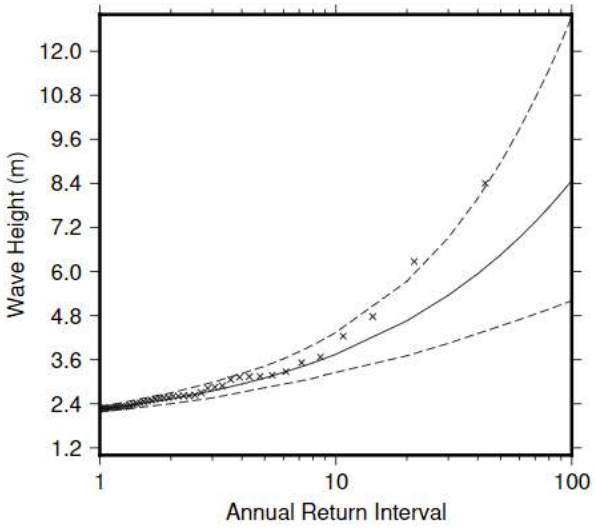

Table 4.3: Summary of the results from extreme wave analysis in Suva

Large wave height (90th percentile)	1.26 m
Severe wave height (99th percentile)	1.74 m
1-year ARI wave height	2.24 m
10-year ARI wave height	3.75 m
20-year ARI wave height	4.66 m
50-year ARI wave height	6.46 m
100-year ARI wave height	8.48 m

5 Kiribati

© Quentin Hanich

5.1 Summary

5.1.1 Climate

- Kiribati has a hot, humid climate with relatively small changes in air temperature from season to season and strong links to changes in the surrounding ocean temperature. The seasonal cycle of rainfall is variable across the large region. The wettest months at Kiritimati are March and April and at Tarawa between December and April.
- The seasonal cycle of rainfall is affected by the Intertropical Convergence Zone (ITCZ), with the strongest impact at Tarawa.
- Annual and seasonal air temperatures at Tarawa increased over the period 1951–2019.
- Annual and seasonal rainfall trends, as well as trends in rainfall extremes, show little change at Tarawa and Kiritimati. There is a strong influence from the El Niño–Southern Oscillation (ENSO) on annual rainfall and the duration of dry spells at both sites.
- As the Kiribati Islands are located within a few degrees of the equator, tropical cyclones rarely form within or pass through Kiribati waters.

5.1.2 Ocean

- Highest sea levels typically occur between January and March and in August/September. El Niño years typically have higher sea levels during February/March.
- Sea-level rise in the Kiribati exclusive economic zone (EEZ), as measured by satellite altimeters from 1993 to mid-2020, ranges from about 3 to 4 mm per year in the vicinity of the Gilbert and Phoenix Islands, and up to 4.5 mm per year in the vicinity of the Line Islands.
- Monthly average ocean temperature, as measured by the Tarawa tide-gauge, ranges from 29 °C in February to 30 °C in the months from June to October. Monthly ocean temperatures in any given year can be up to ±2.5 °C of these averages.
- The sea surface temperature (SST) trend across the EEZ is 0.21 °C per decade.
- Dominant wave direction is from 209° (SSW), with an average significant wave height of 0.78 m and average wave period of 12.17 s.
- Severe wave height was defined as 1.41 m, with an average of 3.9 severe events per year.
- Peak average wave period occurs from January to June, with little seasonal change in the significant wave height.

5.2 Country description

The Republic of Kiribati is located in the equatorial Pacific Ocean, with islands north and south of the equator and both west and east of the 180th meridian (Figure 5.1). Kiribati comprises 32 atolls and one raised coral island between latitudes 5°N and 12°S, and longitudes 120°E and 150°W. The groups of islands include Banaba Island between Nauru and the Gilbert Islands (16 atolls), Phoenix Islands (8 atolls and coral islands) and the Line Islands (8 atolls and a reef). Kiribati has a total land area of 811 km^2 and an EEZ of 3.4 million km^2. Tarawa, the largest atoll at 31 km^2, includes the capital, South Tarawa. The highest elevation is 81 m above sea level on Banaba. Kiribati's population is approximately 120,000. About 90% of the population live in the Gilbert Islands, with more than 50% in South Tarawa (Betio).

Figure 5.1:
Kiribati Gilbert Islands (top left), Phoenix Islands (top right) and Line Islands (bottom center) and the locations of the climate stations used in this report

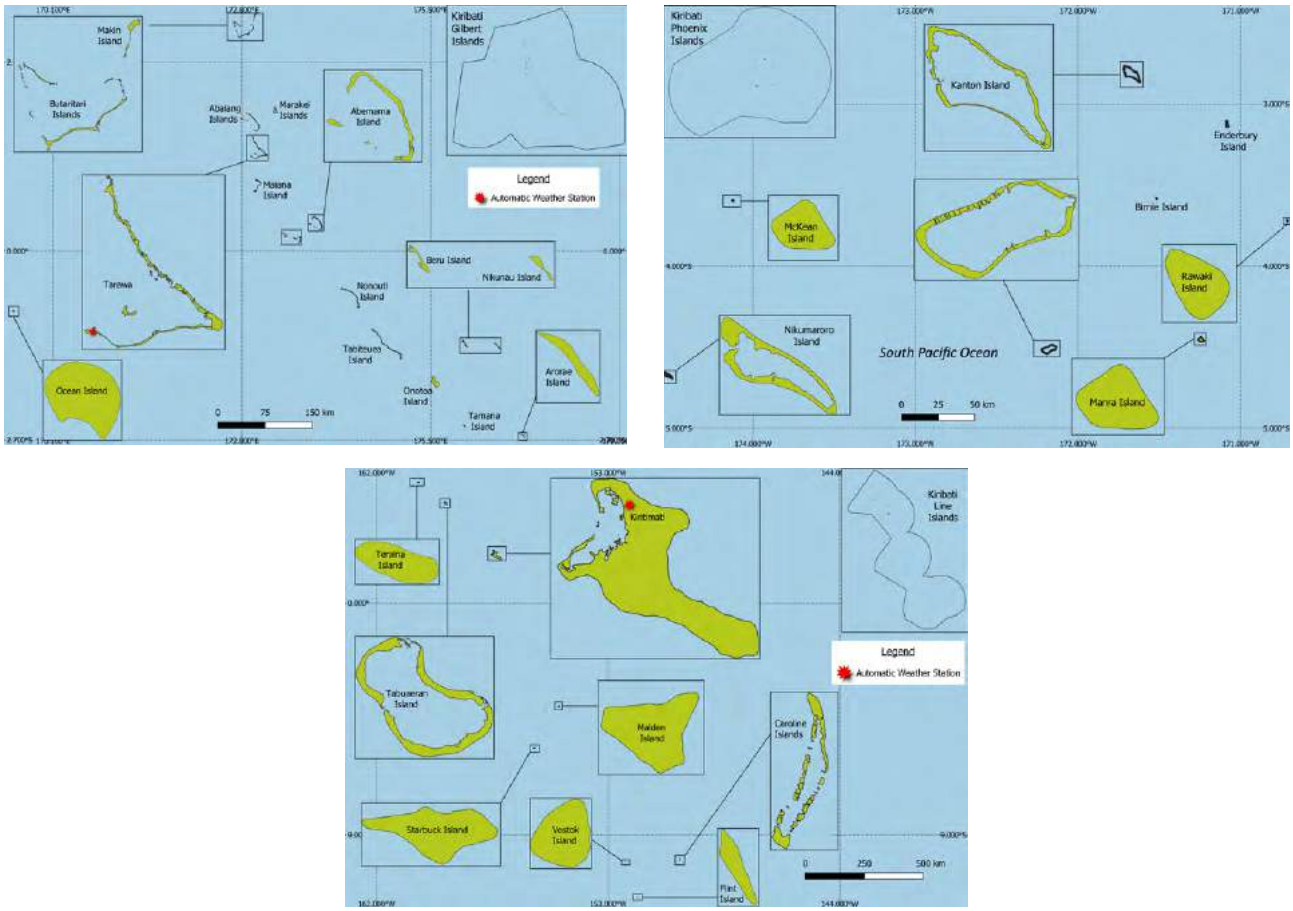

5.3 Data

Daily historical rainfall and air temperature records for Tarawa (Gilbert Islands) and Kiritimati (Line Islands) from 1951 were obtained from the Kiribati Meteorological Service. These records have undergone data quality and homogeneity assessment. Where the maximum or minimum air temperature records were found to have discontinuities, these records have been adjusted to make them homogeneous (further information is provided in Chapter 1). Additional information on historical climate trends for Kiribati can be found in the Pacific Climate Change Data Portal http://www.bom.gov.au/climate/pccsp.

Tropical cyclone data and historical tracks starting from the 1969/70 season are available from the SHTC Data Portal http://www.bom.gov.au/cyclone/history/tracks/index.shtml.

SST covering the EEZ was obtained via the daily Optimum Interpolation SST version 2.1 (OISST v2.1) dataset from NOAA (Reynolds et al. 2007; Banzon et al. 2016). In situ ocean temperature data were obtained from the PSLGM Project tide-gauge located at Tarawa, with data spanning from 1993 to 2021.

Wave data were obtained from the PACCSAP wave hindcast (Smith et al. 2021), available hourly from 1979 to 2021, with a grid resolution near Kiribati of 7 km.

Regional sea level data were obtained from CSIRO satellite altimetry (updated by Benoit Legresy, Church and White 2011), with correction for seasonal signals, inverse barometer effect and glacial isostatic adjustment. Tide-gauge data were sourced from the Tarawa tide-gauge station, spanning from 1993 to 2020 at hourly intervals.

5.4 Rainfall

5.4.1 Seasonal cycle

The driest and wettest periods in the year vary from location to location. The driest six-month period at Tarawa is June–November, known locally as Aumaiaki, with the driest month of October averaging 115 mm. The wettest season, Aumeang, lasts from December to approximately May, with peak rainfall in January averaging 255 mm. Approximately 58% of rainfall falls during the December to May period (Figure 5.2). The wettest months of the year occur when the ITCZ is furthest south and close to Tarawa.

At Kiritimati Island, the peak rainfall month is April, with the lowest rainfall months during the last five months of the year. Approximately 69% of rainfall occurs during the wettest season.

Figure 5.2:
Mean annual rainfall at Tarawa and Kiritimati

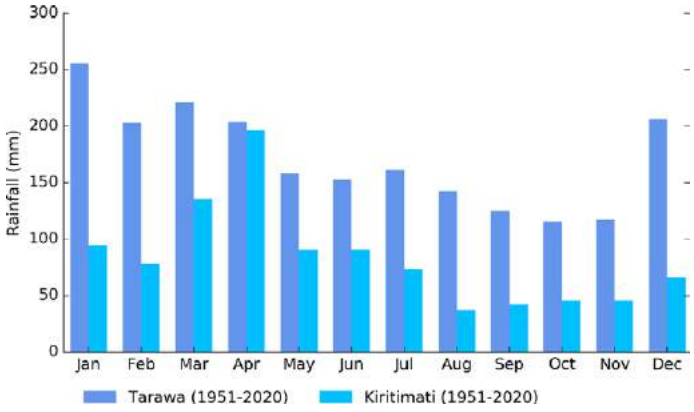

5.4.2 Trends

Trends in annual and seasonal rainfall since 1951 are not statistically significant at Tarawa and Kiritimati (Figure 5.3, Table 5.1). This means there has been little change in annual and seasonal rainfall at these sites. Strong variability associated with ENSO is evident at both sites, with El Niño years generally experiencing much higher rainfall than La Niña years. Annual rainfall varies from approximately 500 to 4400 mm at Tarawa and from approximately 200 to 3700 mm at Kiritimati.

Figure 5.3:
Annual rainfall (bar graph) and number of wet days (where rainfall is at least 1 mm; line graph) at Tarawa (left) and Kiritimati (right). Straight lines indicate linear trends for annual rainfall (in black) and number of wet days (in blue). Criteria for statistical robustness were not met for determining a linear trend for number of wet days at Kiritimati. The magnitudes of the trends are presented in Table 5.1. Diamonds indicate years with insufficient data for one or both variables.

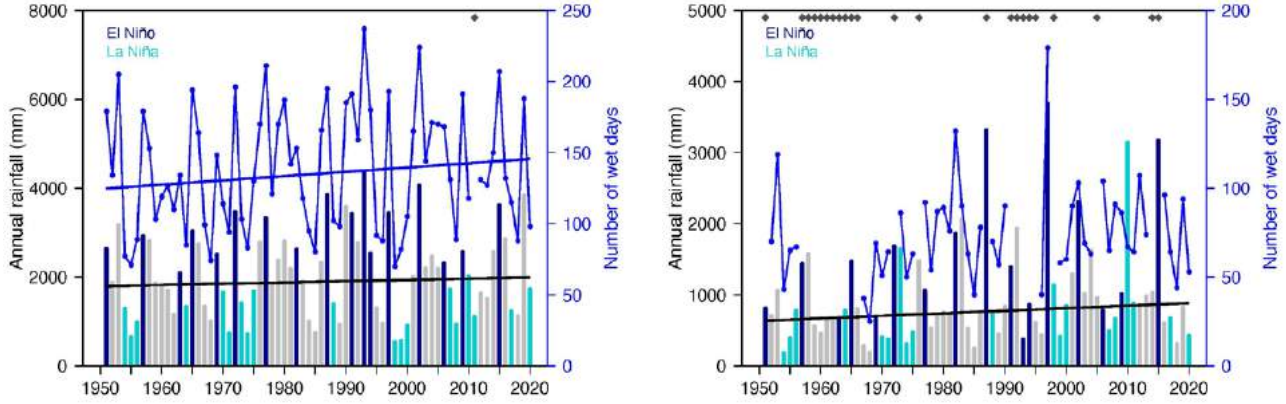

Table 5.1:
Trends in annual, seasonal and extreme rainfall at Tarawa (left) and Kiritimati (right). The 95% confidence intervals are shown in parentheses. The contribution to total rainfall from extreme events and the standardised rainfall evapotranspiration index are measured relative to 1961–1990 (see Chapter 1 for details). Criteria for statistical robustness were not met for determining linear trends for rainfall extremes at Kiritimati. The standardised rainfall evapotranspiration index is not available for Kiritimati due to the unavailability of daily temperature observations at this site.

	Tarawa	Kiritimati
	1951–2020	
Annual rainfall (mm/decade)	+28.30 (-102.38, +160.96)	+35.82 (-12.65, +86.68)
November–April (mm/decade)	+2.46 (-92.75, +94.50)	+35.32 (-0.43, +70.60)
May–October (mm/decade)	+23.78 (-30.94, +76.87)	+3.00 (-18.00, +26.34)
Number of wet days (days/decade)	+3.03 (-2.44, +9.07)	-
Contribution to total rainfall from extreme events (%/decade)	-0.14 (-1.32, +1.08)	-
Consecutive dry days (days/decade)	-0.49 (-2.11, +0.75)	-
Maximum one-day rainfall (mm/decade)	+1.12 (-4.56, +6.56)	-
Standardised rainfall evapotranspiration index (November–April)	0.00 (-0.19, +0.19)	-
Standardised rainfall evapotranspiration index (May–October)	+0.07 (-0.06, +0.18)	-

Numerous gaps exist in the daily rainfall record for Kiritimati, which prevents the robust calculation of trends in rainfall extremes (Table 5.1). No significant trends in extreme rainfall were detected at Tarawa. Figure 5.4 shows change and variability in the longest run of days without rain and maximum daily rainfall at Tarawa and Kiritimati. At both sites, variability associated with ENSO is evident, with La Niña years experiencing much longer dry spells than El Niño years. Year-to-year variability in consecutive dry days is higher at Kiritimati than Tarawa, with several years experiencing over four months without rain.

Figure 5.4:
Annual longest run of consecutive dry days (bar graph) and maximum daily rainfall (line graph) at Tarawa (left) and Kiritimati (right). Straight lines indicate linear trends for dry days (black) and maximum daily rainfall (blue). The magnitudes of the trends are presented in Table 5.1. Criteria for statistical robustness were not met for determining linear trends at Kiritimati. Diamonds indicate years with insufficient data for one or both variables.

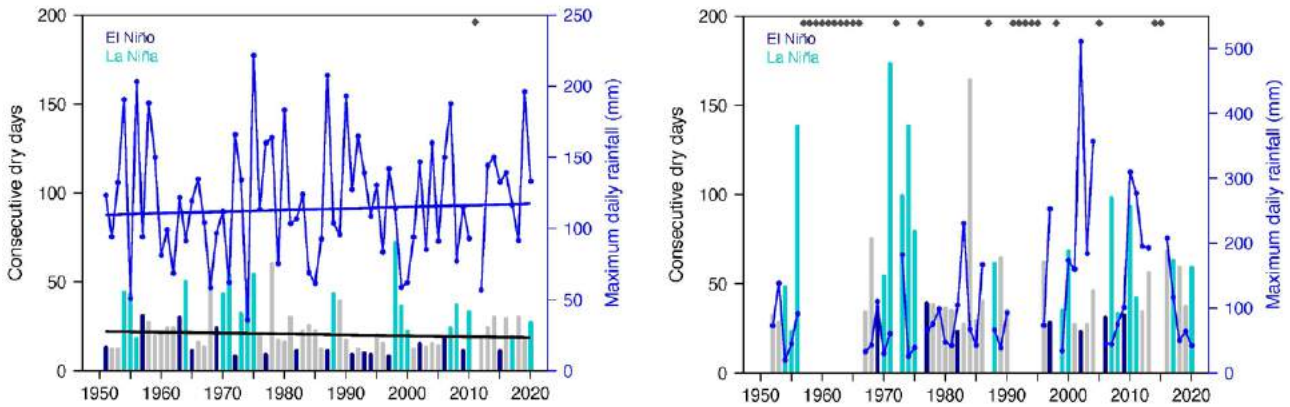

5.5 Air temperature

5.5.1 Seasonal cycle

Kiribati has a hot, humid tropical climate, with air temperatures very closely related to the temperature of the oceans surrounding the small islands and atolls. At both Tarawa and Kiritimati Island, average maximum and minimum air temperatures are highly stable throughout the year, with a range of less than 1 °C (Figure 5.5).

There has been a clear shift towards warmer average monthly temperatures between 1961–1990 and 1991–2020, with warmer average air temperatures occurring in all months throughout the year for Tarawa.

Figure 5.5:
Maximum and minimum air temperature seasonal cycle for Tarawa (purple) and Kiritimati (green), and for the periods 1961–1990 (dotted lines) and 1991–2020 (solid lines)

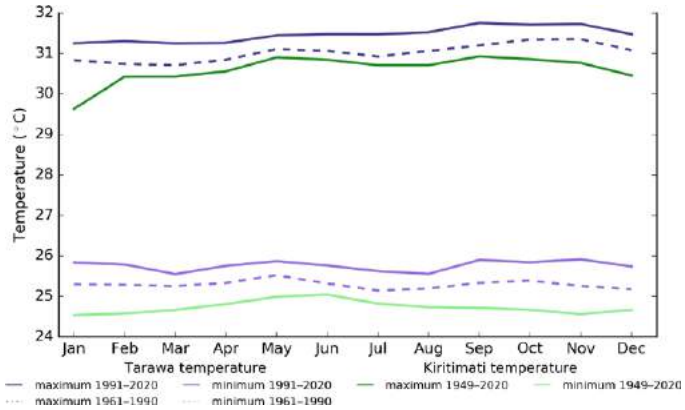

** High amount of missing temperature data for Kiritimati. The average 1949–2020 temperature cycle is available.

5.5.2 Trends

Average annual and seasonal temperatures have increased significantly at Tarawa (Figure 5.6, Table 5.2). The relatively small size of year-to-year fluctuations in temperature at Tarawa can be attributed to its equatorial location.

Figure 5.6:
Average annual, November–April and May–October temperatures for Tarawa. Straight lines indicate linear trends. The magnitudes of the trends are presented in Table 1.2. Diamonds indicate years with insufficient data for one or more variables.

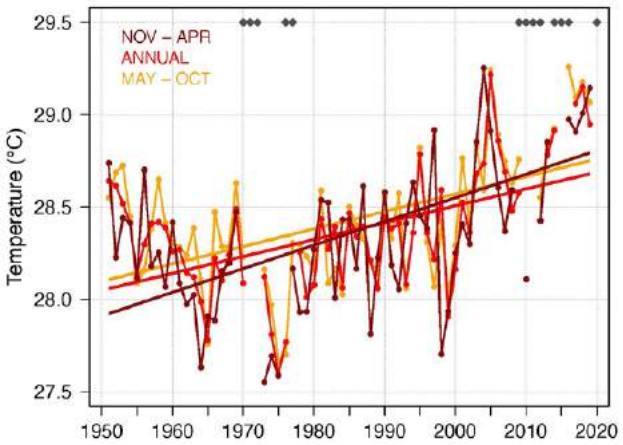

Table 5.2:
Trends in annual and seasonal air temperatures at Tarawa. The 95% confidence intervals are shown in parentheses, and trends significant at the 95% level are shown in bold.

	Tarawa Tmax (°C/decade)	Tarawa Tmin (°C/decade)	Tarawa Tmean (°C/decade)
	1951–2019		
Annual	**+0.12** (+0.02, +0.22)	**+0.11** (+0.03, +0.19)	**+0.09** (+0.01, +0.17)
November–April	**+0.13** (+0.04, +0.21)	**+0.11** (+0.05, +0.18)	**+0.13** (+0.05, +0.20)
May–October	**+0.11** (0.00, +0.21)	**+0.10** (+0.02, +0.16)	**+0.09** (+0.02, +0.17)

Numerous gaps exist in the daily temperature record at Tarawa, which prevents the robust calculation of trends for most temperature extremes. Nevertheless, Figure 5.7 shows that the number of cold nights has been decreasing, although this trend is not significant. The number of hot days varies substantially from year to year. This may be partly explained by the equatorial location of Tarawa, which requires only small temperature increases for a day to be considered hot, i.e., in the top 10% of days compared to 1961–1990 (see Chapter 1 for details).

Figure 5.7:
Annual number of hot days and cold nights at Tarawa. The straight line indicates the linear trend. Criteria for statistical robustness were not met for determining a linear trend for hot days. Diamonds indicate years with insufficient data for one or both variables.

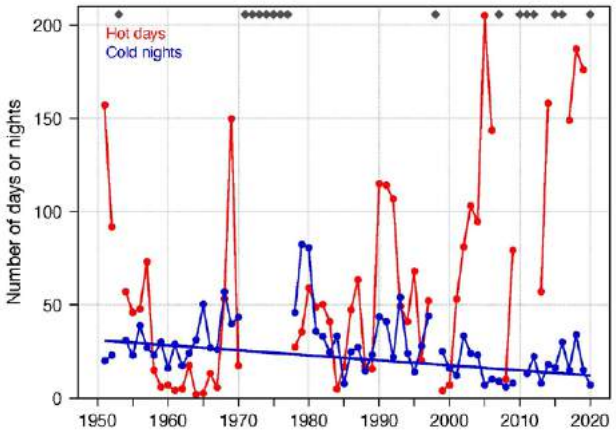

5.6 Tropical cyclones

5.6.1 Seasonal cycle

Tropical cyclones affect Kiribati during the southern hemisphere tropical cyclone season, which is from November to April, but the occurrence of cyclones is rare due to the country's geographic position near the equator. The tropical cyclone archive of the southern hemisphere indicates that between the 1969/70 and 2017/18 seasons, five tropical cyclones passed within the EEZ, with occurrences recorded in El Niño years 1977/78, 1982/83, 1991/92 and 1997/98 (Line Group), and 1987/88 (Phoenix Group) seasons. In addition, two tropical cyclones located in the Northwest Pacific basin passed near Tarawa in 1979 and 2015.

5.6.2 Trends

Trends in total number of tropical cyclones (<995 hPa) and severe tropical cyclones (<970hPa) are presented for the period 1981/82–2020/21 for the greater Southwest Pacific (135°E–120°W; 0–50°S). Trends are presented at a regional scale as the number of tropical cyclones occurring within Pacific Island EEZs is insufficient for reliable long-term trend analysis.

For the total number of tropical cyclones, the trend (and 95% confidence interval) is -0.92 (-1.85, 0.01) tropical cyclones/decade. There has been little change/marginal decline in the total number of tropical cyclones over the last 40 seasons. This trend is not statistically significant.

For the total number of severe tropical cyclones, the trend is -0.80 (-1.32, -0.29) tropical cyclones/decade. There is a negative trend in the number of severe tropical cyclones over the last 40 seasons. There has been little change/marginal decline in the proportion of tropical cyclones reaching severe status. The trend is -0.04 (-0.08, 0.00) tropical cyclones/decade. The negative trend is statistically significant.

Records of tropical cyclones exist from the late 1800s in some countries in the Southwest Pacific, but trends in tropical cyclones have only been presented from 1981/82. Satellite-based observations began in the Southwest Pacific in the early 1970s, but consistent coverage and reliable intensity estimates have only been available since the early 1980s. Confidence in tropical cyclone trends is moderate as the definition of a tropical cyclone has changed and satellite observation methods have continued to improve over the last 40 years.

5.7 Sea surface temperature

5.7.1 Seasonal cycle

Ocean temperature, as measured by the Tarawa tide-gauge, reaches on average a maximum of approximately 30 °C from June to October, but individual months can get as high as above 32 °C from September to November (Figure 5.8). Minimum average temperature is 29 °C in February.

Hourly temperatures can be up to 2.5 °C higher or lower than these hourly averages, although 50% of hourly observations fall within 1.5 °C of the average. Equatorial locations typically have little average variation but can drastically change in a given year depending on the ENSO cycle. The variability in temperatures between September and February is reflective of the peak months of ENSO.

Figure 5.8:
Annual temperatures measured at the Tarawa tide-gauge. Blue dots show the monthly average, and shaded boxes show the middle 50% of hourly observations. Lines show the top and bottom 25% of hourly observations

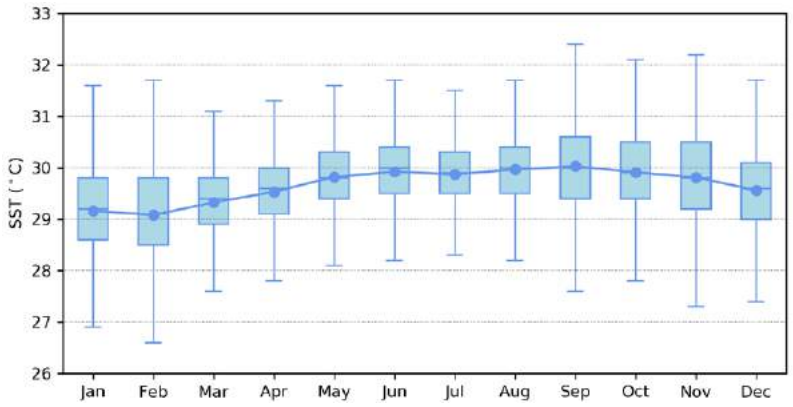

5.7.2 Trends

Figure 5.9 shows the 1981–2021 SST from satellite observations averaged over the EEZ regions. The data show a trend of 0.21 °C per decade with a 95% confidence interval of ±0.06 °C.

Figure 5.9:
Sea surface temperature from satellite observations averaged across Kiribati EEZ, shown as the orange line. The blue line shows the linear regression trend.

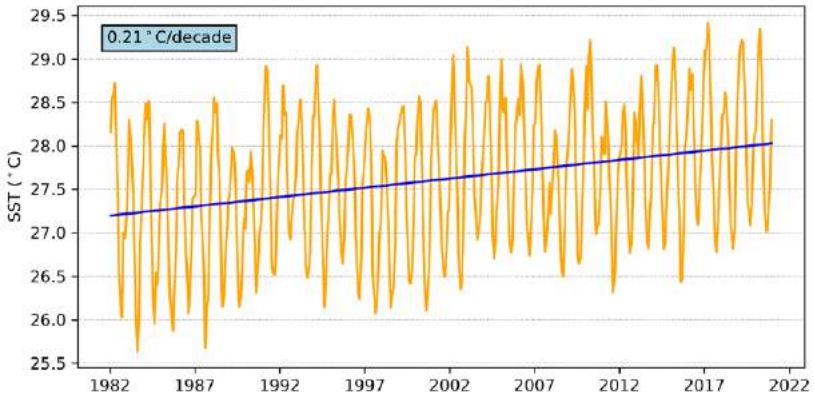

5.8 Sea level

5.8.1 Seasonal cycle

Kiribati experiences a semidiurnal tidal cycle, meaning two high and two low tides per day. The highest predicted tides of the year at Tarawa typically occur in August/September as well as December–February. For Kiritimati, highest predicted tides are around August, and also from November to January. Figure 5.10 shows the number of hours the 99th percentile (2.93 m) sea level threshold is exceeded per month across the entire sea level record at Tarawa. Peak sea levels typically occur from January to March but also in August/September. El Niño years typically have higher sea levels during February/March. Since approximately 2009, the number of hours that exceed the 99th percentile threshold has been increasing. This is due to a combination of sea-level rise and subsidence occurring at Kiribati (Brown et al. 2020).

Figure 5.10:
Number of hours exceeding 99th percentile sea level threshold per month from 1993 to 2020 at the Tarawa tide-gauge. Blue shading indicates the number of hours, and the final row provides a percentage summary of all the years.

Number of hours exceeding 2.93 m (Betio, Kiribati)

	Jan	Feb	Mar	Apr	May	Jun	Jul	Aug	Sep	Oct	Nov	Dec	Annual
1993	0	0	0	0	0	0	0	0	0	0	0	0	0
1994	0	0	0	0	0	0	0	0	0	0	0	3	3
1995	0	0	0	0	0	0	0	0	0	0	0	0	0
1996	1	0	0	0	0	0	0	0	0	0	0	0	1
1997	4	1	4	0	0	0	0	0	0	0	0	0	9
1998	0	0	0	0	0	0	0	0	0	0	0	0	0
1999	0	0	0	0	0	0	0	0	0	0	0	0	0
2000	0	0	0	0	0	0	0	0	0	0	0	0	0
2001	0	0	0	0	0	0	0	0	1	0	0	0	1
2002	0	0	0	0	0	0	0	1	2	0	0	0	3
2003	0	0	0	0	0	0	0	0	0	0	0	0	0
2004	0	0	0	0	0	0	0	0	0	0	0	0	0
2005	0	2	0	0	0	0	0	0	0	0	0	0	2
2006	0	2	2	0	0	0	0	0	2	1	1	0	8
2007	0	1	0	0	0	0	0	0	0	0	0	0	1
2008	0	0	0	0	0	0	0	0	0	0	0	0	0
2009	1	0	0	0	0	1	2	2	5	0	0	1	12
2010	3	2	2	0	0	0	0	0	0	0	0	0	7
2011	0	3	0	1	0	0	0	0	0	0	0	0	4
2012	0	0	0	1	0	0	0	0	0	0	0	0	1
2013	0	0	0	0	0	0	0	0	0	0	0	0	0
2014	0	6	6	0	0	0	1	3	1	0	0	0	17
2015	1	7	4	1	0	0	0	3	6	0	0	0	22
2016	0	0	0	0	0	0	0	0	0	0	0	0	0
2017	0	0	0	0	0	0	0	0	0	0	1	2	3
2018	2	0	0	0	0	0	0	1	2	0	0	0	5
2019	6	8	0	0	0	0	0	2	7	0	1	0	24
2020	0	4	1	0	0	0	0	0	0	0	2	0	7
Monthly Totals (%)	14	28	15	2	0	1	2	9	20	1	4	5	

5.8.2 Trends

Sea level across the three Kiribati island groups, measured by satellite altimeters (Figure 5.11) since 1993, has risen between 3 and 4 mm per year in the Gilbert and Phoenix Islands and far north/south of the Line Islands. Trends are between 4 and 4.5 mm per year in central Line Islands and far southern Phoenix Islands. This is larger than the global average of 3.1 ± 0.4 mm per year (von Schuckmann et al. 2021). The 95% confidence interval is between 0.6 and 1.0 mm for the Gilbert and Phoenix Islands, and up to 1.2 mm for central Line Islands. This rise is partly linked to a pattern related to climate variability from year to year and decade to decade.

Trend estimates at the Tarawa tide-gauge over a similar time span to the altimetry observations (December 1992 to July 2020) are provided in the PSLGM Monthly Data Report for July 2020 (http://www.bom.gov.au/ntc/IDO60101/IDO60101.202007.pdf). For Tarawa, the trend is reported as 4.4 mm per year, slightly higher than the altimetry trends shown in Figure 5.11 (tide-gauge indicated by star symbol). This difference is most likely attributed to subsidence occurring at Tarawa (Brown et al. 2020).

Figure 5.11:
Satellite altimetry annual trend for the Pacific from 1993 to 2020, with Kiribati EEZ highlighted. The star symbol indicates the location of the tide-gauge at Tarawa.

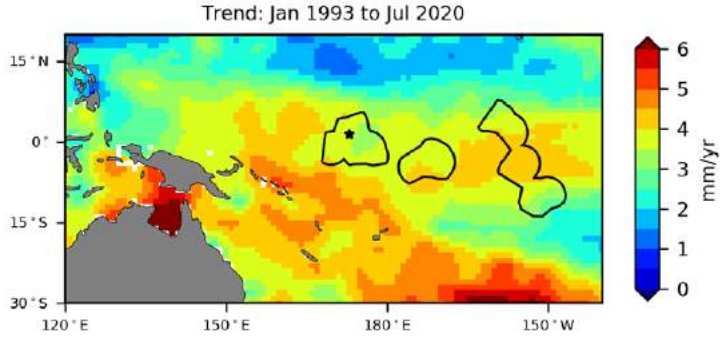

5.9 Waves

5.9.1 Seasonal cycle

The average wave climate at Betio is defined by the significant wave height, peak period and peak direction. The significant wave height is the mean wave height (from trough to crest) of the highest one third of waves and corresponds to the wave height that would be reported by an experienced observer. Peak period is the time interval between two waves of the dominant wave period. Peak direction is the direction from which the dominant waves are coming.

The average sea state is dominated by swells from the south. The annual mean wave height is 0.78 m, the annual mean wave direction is 209° and the annual mean wave period is 12.17 s. In the Pacific, waves often come from multiple directions and for different periods of time. In Betio, there are often more than seven different wave direction/period components with the majority coming from between south to southeast (Figure 5.12).

The significant wave height shows little change between the seasons at Betio. However, wave period is significantly higher from March to June (Figure 5.13). Wave height peaks in winter, and wave period peaks in May.

Figure 5.12:
Annual wave rose for Betio. Note that direction is where the wave is coming from.

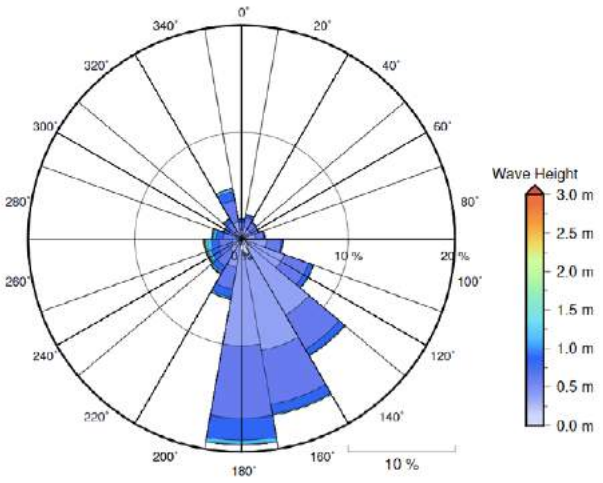

Figure 5.13:
Monthly wave height (black line), wave period (red line) and wave direction (arrows). The grey area represents the range of wave height between calm periods (10% of lowest wave height) and large wave events (10% of highest wave height).

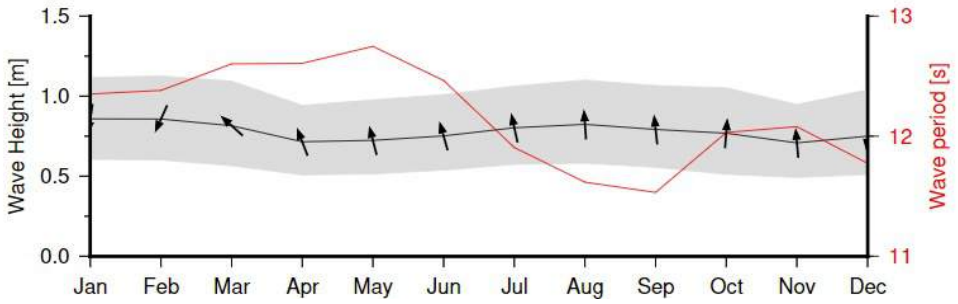

5.9.2 Trends

Waves change from month to month with the seasons and also from year to year with climate oscillations. Typically, these changes are smaller than the seasonal changes but can be important during phenomena such as ENSO. At Betio, the mean annual wave height has remained unchanged since 1979 (Figure 5.14). The mean annual wave height in Betio is not significantly correlated with the main climate indicators of the region.

Figure 5.14:
Annual wave height (black line), wave period (red line) and wave direction (arrows). The grey area represents the range of wave height between calm periods (10% of lowest wave height) and large wave events (10% of highest wave height).

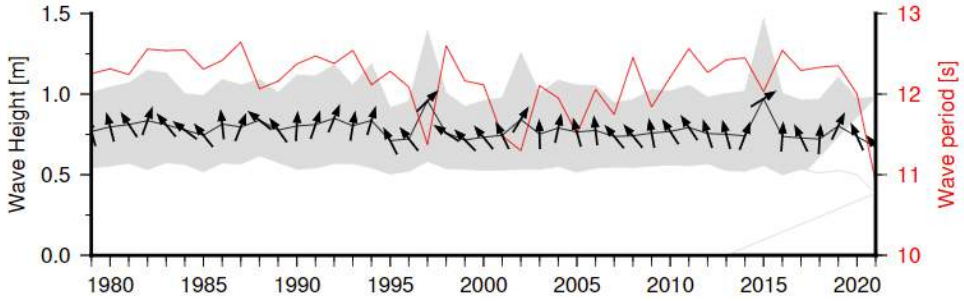

5.9.3 Extreme waves

Extreme wave analysis for Betio was done by defining a severe height threshold and fitting a generalized Pareto distribution (GPD). The optimum threshold selected was 1.41 m. In the 42-year wave hindcast, 163 wave events reached or exceeded this threshold, averaging 3.9 per year. The GPD was fitted to the largest wave height reached during each of these events (Figure 5.15, Table 5.14). Extreme wave analysis is a very useful tool but is not always accurate because the analysis is very sensitive to the data available, the type of distribution fitted and the threshold used. For example, this analysis does not accurately account for tropical cyclone waves. More in-depth analysis is required to obtain results appropriate for designing coastal infrastructure and coastal hazard planning.

Figure 5.15:
Extreme wave distribution for Betio. The crosses represent the wave events that have occurred since 1979. The solid line is the statistical distribution that best fits past wave events. The dashed lines show the upper and lower confidence limits of the fit. There is a 95% chance that the fitted distribution lies between the two dashed lines. Note that the annual return interval is in logarithmic scale.

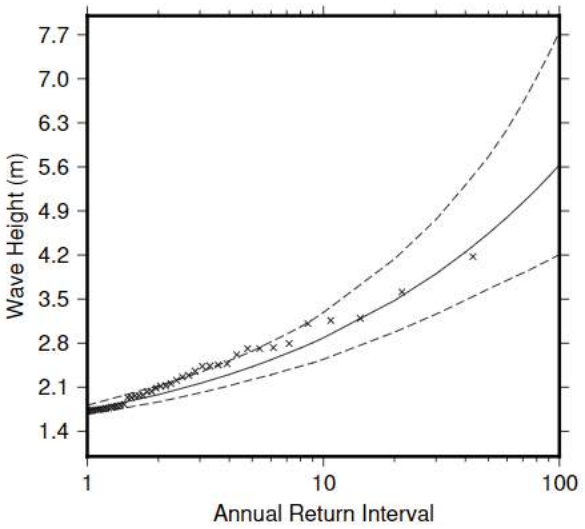

Table 5.3:
Summary of the results from extreme wave analysis in Betio

Large wave height (90th percentile)	1.26 m
Severe wave height (99th percentile)	1.74m
1-year ARI wave height	2.24 m
10-year ARI wave height	3.75 m
20-year ARI wave height	4.66 m
50-year ARI wave height	6.46 m
100-year ARI wave height	8.48 m

6 Marshall Islands

6.1 Summary

6.1.1 Climate

- Changes in air temperature from season to season are relatively small, with air temperatures strongly linked to changes in the surrounding ocean temperature. The Republic of Marshall Islands (RMI) has a wet season from May to November and a dry season from December to April.
- The seasonal cycle of rainfall is affected by the Intertropical Convergence Zone (ITCZ). In some years, the West Pacific Monsoon (WPM) also affects rainfall.
- Annual and seasonal air temperatures at Majuro and Kwajalein have increased since the 1950s. The number of warm nights has increased, and the number of cool days and cold nights has decreased at both sites. The energy required for cooling indoor environments has also increased at both sites.
- The longest run of days without rain has been decreasing at Majuro. All other annual, seasonal and extreme rainfall trends show little change at Majuro and Kwajalein.
- Tropical cyclones affect Marshall Islands year-round. Over the period 1969–2017, an average of 23 cyclones passed within the RMI exclusive economic zone (EEZ) per decade. Tropical cyclones were most frequent in El Niño years and least frequent in La Niña years. Year-to-year variability is large, ranging from no tropical cyclones in some years to 11 in 1972 and 1997.
- There has been little change in the number of severe tropical cyclones or the total number of tropical cyclones in the Northwest Pacific since 1981.

6.1.2 Ocean

- Highest sea levels typically occur from September to March.
- Sea-level rise within the EEZ, measured by satellite altimeters since 1993, is about 1.0 to 4.5 mm (0.04 to 0.18 in) per year.
- Monthly average ocean temperature, measured by the Majuro tide-gauge, ranges from 28 °C (82.4 °F) in February to 29.5 °C (85.1 °F) in September/October. However, monthly temperatures in any given year can be ±2 °C (±3.6 °F) of these averages.
- The sea surface temperature (SST) trend in the EEZ is 0.25 °C (0.45 °F) per decade.
- Dominant wave direction is from 54° (NE), with an average significant wave height of 1.56 m (5.12 ft) and average wave period of 9.7 s.
- Severe wave height was defined as 3.09 m (10.14 ft), with an average of 2.6 severe events per year.
- Peak average significant wave height occurs from November to March.

6.2 Country description

Located in the equatorial/tropical North Pacific Ocean, RMI is made up of 29 atolls and five individual islands between latitudes 3°N and 15°N, and longitudes 161°E and 173°E (Figure 6.1). The atolls and islands form two parallel chains running northwest to southeast: Ratak (sunrise) and Ralik (sunset). The largest atoll, with a land area of 16 km^2, is Kwajalein (Ralik chain). RMI has a total land area of 180 km^2 and an EEZ of 2.1 million km^2. The capital and largest city is Majuro, located on Majuro Atoll. The highest elevation is about 10 m (33 ft) above sea level on Likiep Atoll. RMI's population is approximately 59,100. About 52% of the population live on Majuro Atoll.

Figure 6.1:
Marshall Islands (RMI) and the locations of the climate stations used in this report

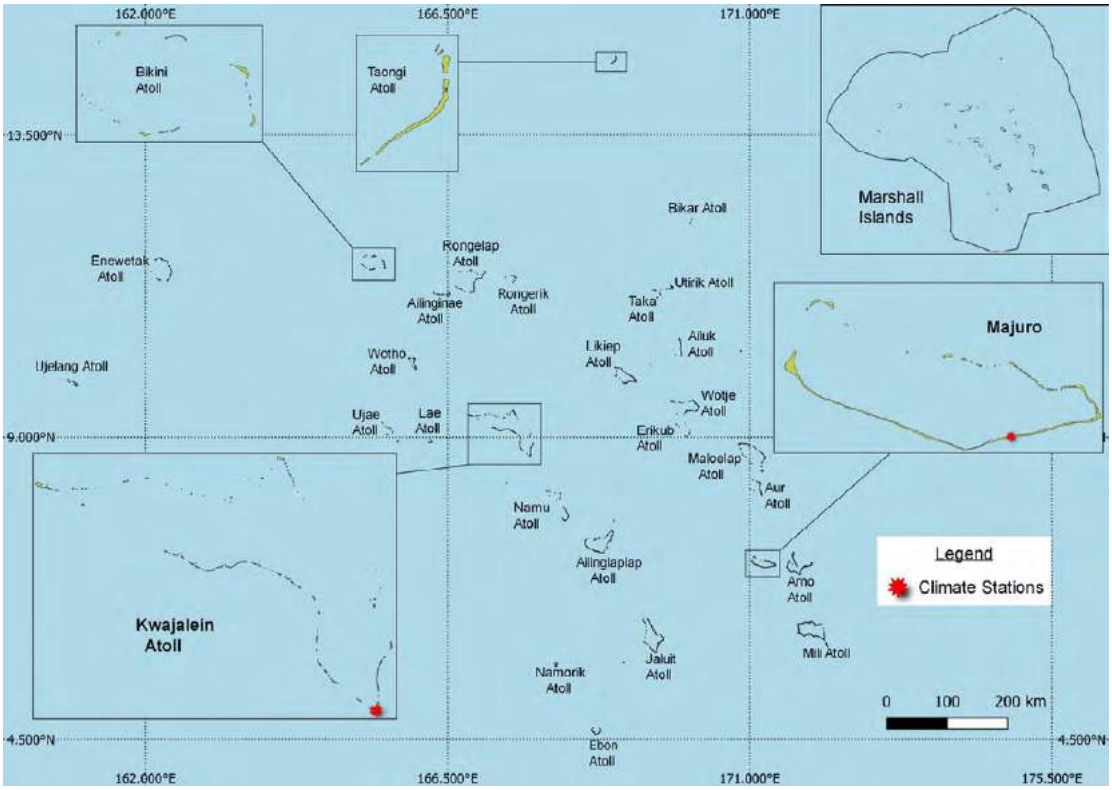

6.3 Data

Daily historical rainfall and air temperature records for Majuro and Kwajalein from 1951 were obtained from the United States National Oceanic and Atmospheric Administration Majuro Weather Service Office. These records have undergone data quality and homogeneity assessment. Where the maximum or minimum air temperature records were found to have discontinuities, these records have been adjusted to make them homogeneous (further information is provided in Chapter 1). Additional information on historical climate trends for RMI can be found in the Pacific Climate Change Data Portal http://www.bom.gov.au/climate/pccsp.

Tropical cyclone data and historical tracks starting from the 1969 season are available from the Western North Pacific Tropical Cyclone Data Portal http://www.bom.gov.au/cyclone/history/tracks/beta/?region=wnp.

SST covering the EEZ was obtained via the daily Optimum Interpolation SST version 2.1 (OISST v2.1) dataset from NOAA (Reynolds et al. 2007; Banzon et al. 2016). In situ ocean temperature data were obtained from the PSLGM Project tide-gauge located at Majuro, with data spanning from 1993 to 2021.

Wave data were obtained from the PACCSAP wave hindcast (Smith et al. 2021), available hourly from 1979 to 2021, with a grid resolution near RMI of 7 km (4.3 mi).

Regional sea level data were obtained from CSIRO satellite altimetry (updated by Benoit Legresy, Church and White 2011), with correction for seasonal signals, inverse barometer effect and glacial isostatic adjustment. Tide-gauge data were sourced from the Majuro tide-gauge station, spanning from 1993 to 2021 at hourly intervals.

6.4 Rainfall

6.4.1 Seasonal cycle

RMI is located in an area where the ITCZ produces high rainfall throughout the year (Figure 6.2). This band of heavy rainfall is caused by air rising over warm water where winds converge and is most intense and closest to RMI during the wet season months of May to November. Rainfall in some years is also influenced by the WPM, which brings wetter conditions when it is active over RMI.

Majuro receives 65% of the rainfall during the wet season, which averages 2197 mm (86.4 in) and 1187 mm (46.7 in) in the dry season. In Kwajalein, the average rainfall in the wet season is 1832 mm (71.2 in), which is 72% of the annual total. Kwajalein has a more distinct dry season, with the driest months (January–March) receiving about 100 mm (3.9 in) on average.

Figure 6.2:
Mean annual rainfall at Majuro and Kwajalein

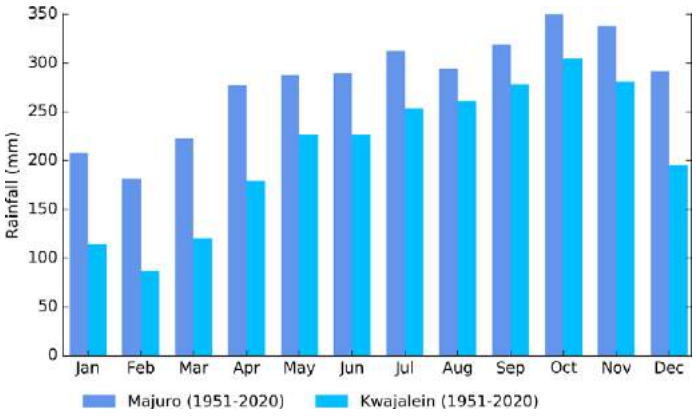

6.4.2 Trends

Trends in annual and seasonal rainfall are not statistically significant at Majuro and Kwajalein (Figure 6.3, Table 6.1). This means there has been little change in annual and seasonal rainfall at these sites.

Annual rainfall varies from approximately 2200 to 4500 mm (86.6 to 177.2 in) at Majuro and from approximately 1500 to 3700 mm (59.1 to 145.7 in) at Kwajalein. Approximately half of all days each year experience rain at Kwajalein and more than half of all days experience rain at Majuro (Figure 6.3).

Figure 6.3:
Annual rainfall (bar graph) and number of wet days (where rainfall is at least 1 mm, line graph) at Majuro (left) and Kwajalein (right). Straight lines indicate linear trends for annual rainfall (in black) and number of wet days (in blue). The magnitudes of the trends are presented in Table 6.1. Diamonds indicate years with insufficient data for one or both variables.

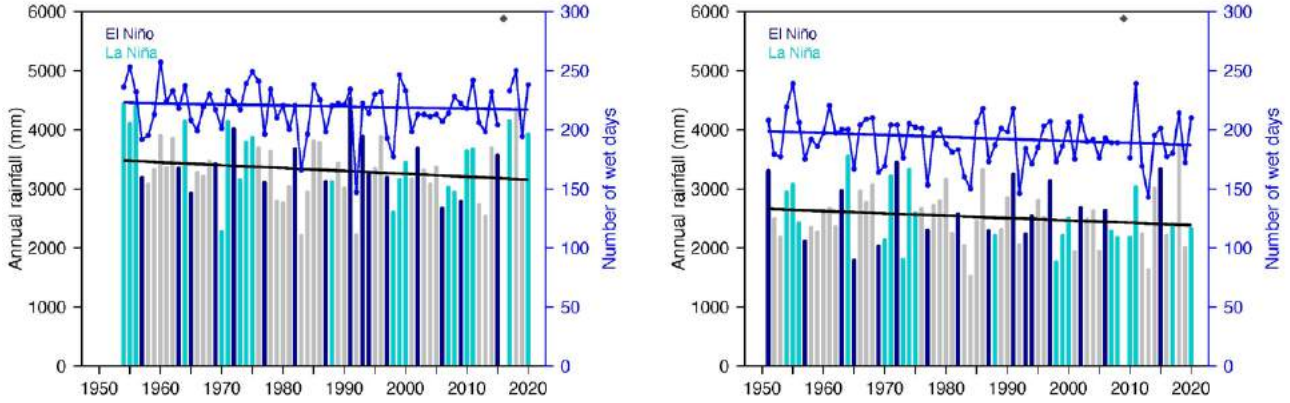

Table 6.1:
Trends in annual, seasonal and extreme rainfall at Majuro (left) and Kwajalein (right). The 95% confidence intervals are shown in parentheses, and trends significant at the 95% level are shown in bold. The contribution to total rainfall from extreme events and the standardised rainfall evapotranspiration index are measured relative to 1961–1990 (see Chapter 1 for details).

	Majuro	Kwajalein
	1954–2020	1951–2020
Annual rainfall (mm/decade)	-48.90 (-125.80, +16.97)	-39.95 (-99.17, +20.32)
November–April (mm/decade)	-5.76 (-64.37, +44.23)	+3.39 (-34.54, +41.16)
May–October (mm/decade)	-28.18 (-72.92, +23.73)	-29.88 (-65.78, +6.39)
Number of wet days (days/decade)	-0.91 (-3.66, +1.52)	-1.67 (-4.17, +0.93)
Contribution to total rainfall from extreme events (%/decade)	-0.79 (-1.75, +0.25)	+0.48 (-0.76, +1.66)
Consecutive dry days (days/decade)	**-0.48** (-0.91, 0.00)	0.00 (-0.57, +0.53)
Maximum one-day rainfall (mm/decade)	-0.97 (-6.33, +3.67)	+3.13 (-1.62, +7.88)
Standardised rainfall evapotranspiration index (November–April)	+0.01 (-0.15, +0.14)	+0.04 (-0.10, +0.18)
Standardised rainfall evapotranspiration index (May–October)	-0.08 (-0.24, +0.09)	-0.07 (-0.19, +0.05)

The longest run of days without rain each year has been decreasing at Majuro since 1954 (Figure 6.4). No significant trends in any other extreme rainfall indices were detected at either Majuro or Kwajalein (Table 6.1). An unusually high maximum daily rainfall at Majuro in 1972 was a result of tropical cyclone Violet.

Figure 6.4:
Annual longest run of consecutive dry days (bar graph) and maximum daily rainfall (line graph) at Majuro (left) and Kwajalein (right). Straight lines indicate linear trends for dry days (in black) and maximum daily rainfall (in blue). The magnitudes of the trends are presented in Table 6.1. Diamonds indicate years with insufficient data for one or both variables.

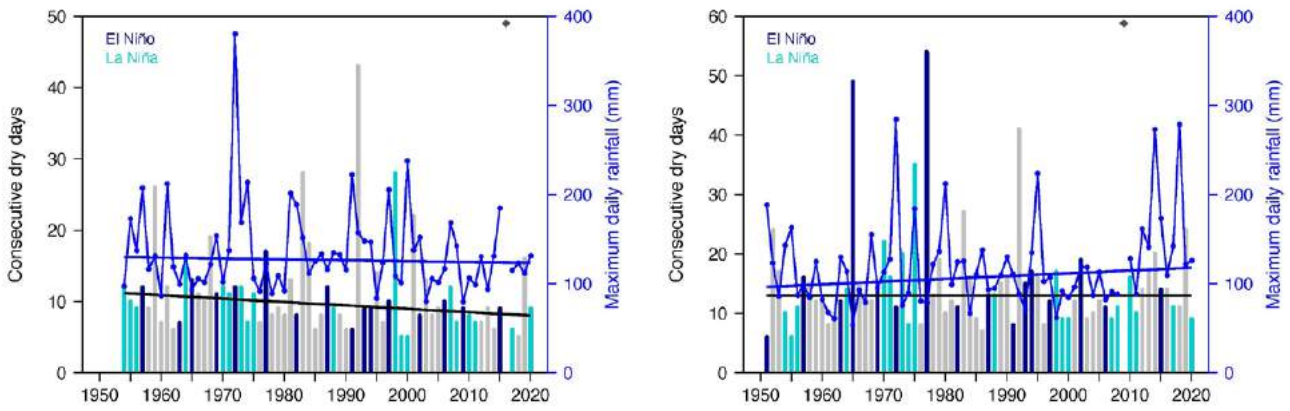

6.5 Air temperature

6.5.1 Seasonal cycle

The average air temperature across RMI is relatively constant year-round, with any changes in air temperatures strongly linked to changes in the surrounding ocean temperature (Figure 6.5). There has been a clear shift towards warmer average monthly temperatures between the climatology periods of 1961–1990 and 1991–2020, with warmer average temperatures occurring in all months throughout the year for both Majuro and Kwajalein, with the exception of average maximum temperatures at Kwajalein between October and April.

Figure 6.5:
Maximum and minimum air temperature seasonal cycle for Majuro (purple) and Kwajalein (green), and for the periods 1961–1990 (dotted lines) and 1991–2020 (solid lines)

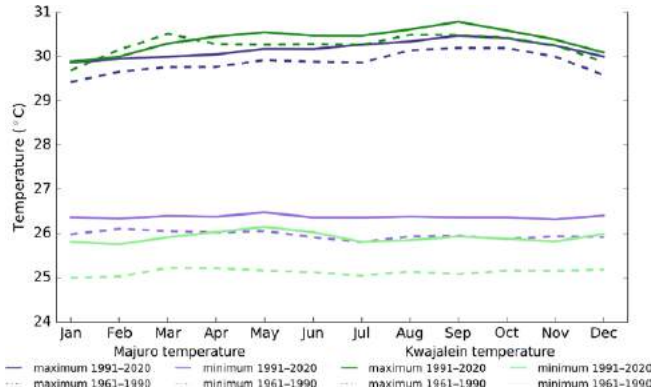

6.5.2 Trends

Average annual and seasonal temperatures have increased significantly at Majuro and Kwajalein (Figure 6.6, Table 6.2). Daily minimum temperatures are warming faster than daily maximum temperatures at Kwajalein. Variability consistent with the Interdecadal Pacific Oscillation is evident at Majuro, although this could be influenced by data quality issues in the mid-1970s.

Figure 6.6:
Annual, November–April and May–October average temperatures for Majuro (left) and Kwajalein (right). Straight lines indicate linear trends. The magnitudes of the trends are presented in Table 6.2. Diamonds indicate years with insufficient data for one or more variables.

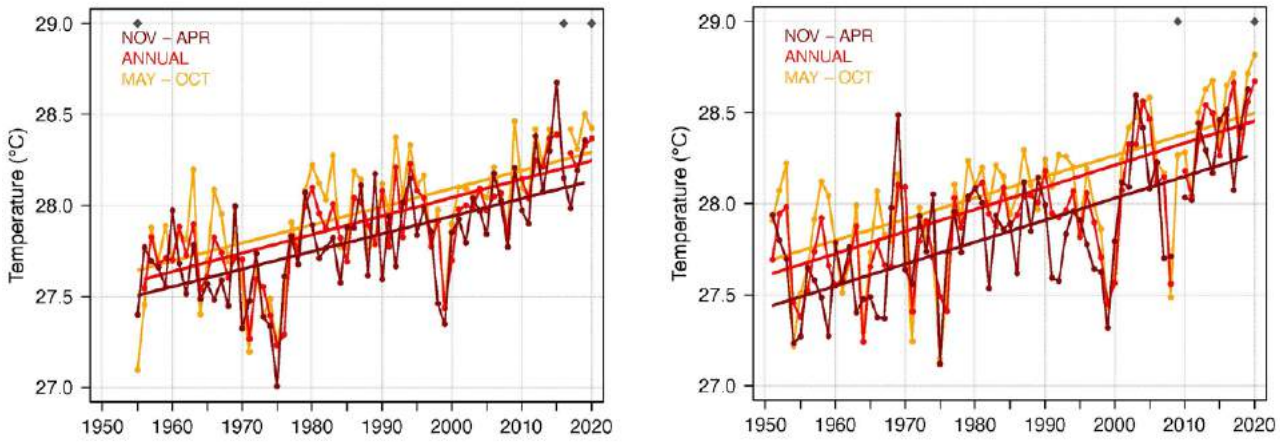

Table 6.2:
Trends in annual and seasonal air temperatures at Majuro (left) and Kwajalein (right). The 95% confidence intervals are shown in parentheses, and trends significant at the 95% level are shown in bold.

	Majuro Tmax (°C/decade)	Majuro Tmin (°C/decade)	Majuro Tmean (°C/decade)	Kwajalein Tmax (°C/10yrs)	Kwajalein Tmin (°C/10yrs)	Kwajalein Tmean (°C/10yrs)
	1955–2020			1951–2020		
Annual	**+0.09** (+0.02, +0.16)	**+0.12** (+0.08, +0.16)	**+0.10** (+0.07, +0.14)	**+0.09** (+0.01, +0.17)	**+0.14** (+0.08, +0.19)	**+0.12** (+0.08, +0.17)
November–April	**+0.10** (+0.04, +0.16)	**+0.10** (+0.07, +0.13)	**+0.10** (+0.06, +0.13)	**+0.11** (+0.03, +0.18)	**+0.14** (+0.09, +0.20)	**+0.12** (+0.08, +0.16)
May–October	+0.07 (0.00, +0.15)	**+0.12** (+0.09, +0.17)	**+0.10** (+0.05, +0.15)	**+0.09** (+0.01, +0.17)	**+0.14** (+0.10, +0.20)	**+0.12** (+0.08, +0.17)

The number of warm nights has increased at Majuro and Kwajalein, and the number of cool days and cold nights has decreased (Figure 6.7, Table 6.3). Decade-to-decade variability can be seen in the number of hot days at both sites.

The cooling degree days index provides a measure of the energy demand needed to cool a building down to 25 °C (77.0 °F), with the assumption that air conditioners are generally turned on at this temperature. There has been an increase in the cooling degree days index at both sites, suggesting the energy needed for cooling has increased significantly.

Table 6.3:
Trends in annual temperature extremes at Majuro (left) and Kwajalein (right). The 95% confidence intervals are shown in parentheses, and trends significant at the 95% level are shown in bold. Hot and cool days, and warm and cold nights are measured relative to 1961–1990 (see Chapter 1 for details).

	Majuro	Kwajalein
	1956–2020	1951–2020
Number of hot days (days/decade)	+4.70 (-3.40, +14.52)	+6.13 (-2.11, +13.81)
Number of warm nights (nights/decade)	**+13.48** (+4.41, +20.39)	**+14.96** (+8.96, +20.40)
Number of cool days (days/decade)	**-1.08** (-6.62, -4.03)	**-3.58** (-7.71, -0.32)
Number of cold nights (nights/decade)	**-3.31** (-6.26, -0.85)	**-5.77** (-8.08, -3.92)
Cooling degree days (degree days/decade)	**+32.03** (+7.41, +53.41)	**+41.09** (+25.35, +56.07)
Daily temperature range (°C/decade)	-0.08 (-0.22, +0.05)	-0.06 (-0.18, +0.04)

Figure 6.7:
Annual number of hot days and cold nights at Majuro (left) and Kwajalein (right). Straight lines indicate linear trends. The magnitudes of the trends are presented in Table 6.3. Diamonds indicate years with insufficient data for one or both variables.

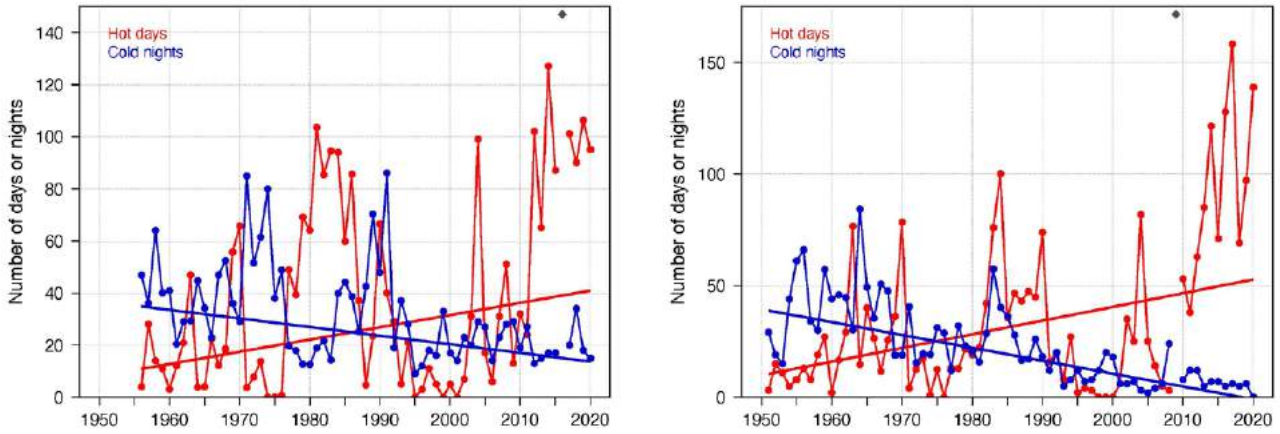

6.6 Tropical cyclones

6.6.1 Seasonal cycle

Tropical cyclones usually affect RMI year-round. The tropical cyclone archive of the western North Pacific indicates that between the 1969 and 2017 seasons, 111 tropical cyclones (Figure 6.8) passed within the EEZ. This represents an average of 23 cyclones per decade.

Tropical cyclones were most frequent in El Niño years (48 cyclones per decade), followed by neutral years (19 cyclones per decade) and least frequent in La Niña years (5 cyclones per decade).

Interannual variability in the number of tropical cyclones in the EEZ is large, ranging from zero in some seasons to 11 in 1972 and 1997 (Figure 6.8). High interannual variability and the small number of tropical cyclones occurring in the EEZ make reliable identification of long-term trends in frequency and intensity difficult.

Some tropical cyclone tracks analysed in this section include the tropical depression stage (sustained winds ≤34 knots) before and/or after tropical cyclone formation.

Figure 6.8:
Number of tropical cyclones passing within the EEZ per season. Each season is defined by the ENSO status, with light blue being an El Niño year, dark blue a La Niña year and grey showing a neutral ENSO year. The 11-year moving average is presented as a purple line and considers all years.

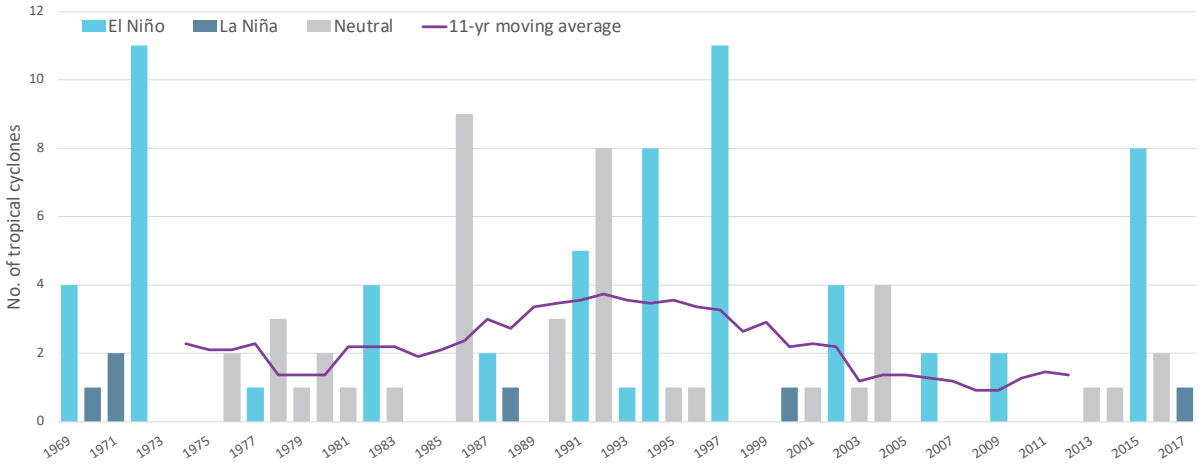

6.6.2 Trends

Trends in total number of tropical cyclones (<995 hPa) and severe tropical cyclones (<970 hPa) are presented for the period 1981–2021 for the Northwest Pacific (125°E–180°W; 0–20°N). Trends are presented at a regional scale as the number of tropical cyclones occurring within Pacific Island EEZs is insufficient for reliable long-term trend analysis.

For the total number of tropical cyclones, the trend (and 95% confidence interval) is -0.56 (-1.84, 0.72) tropical cyclones/decade. There has been little change in the total number of tropical cyclones over the last 41 seasons.

For the total number of severe tropical cyclones, the trend is -0.15 (-1.19, 0.89) tropical cyclones/decade. There has been little change in the number of severe tropical cyclones over the last 41 seasons. There has also been little change in the proportion of tropical cyclones reaching severe status. The trend is 0.01 (-0.04, 0.05) tropical cyclones/decade.

Records of tropical cyclones exist from the late 1800s in some countries in the Northwest Pacific, but trends in tropical cyclones have only been presented from 1981/82. Satellite-based observations began in the early 1970s, but consistent coverage and reliable intensity estimates have only been available since the early 1980s. Confidence in tropical cyclone trends is moderate as the definition of a tropical cyclone has changed and satellite observation methods have continued to improve over the last 41 years.

6.7 Sea surface temperature

6.7.1 Seasonal cycle

Ocean temperature, as measured by the Majuro tide-gauge from 1993 to 2021, reaches on average a maximum of 29.5 °C (85.1 °F) in September/October, but individual months can get as high as 31.0 °C (87.8 °F) between August and November (Figure 6.9). Minimum average temperature is 28.0 °C (82.4 °F) in February. Hourly temperatures can be up to 2 °C (3.6 °F) higher or lower than these monthly averages, although 50% of hourly observations fall within 1 °C (1.8 °F) of the monthly average between August and November, and within 0.5 °C (0.9 °F) in the remainder of the year.

Figure 6.9:
Annual temperatures measured at the Majuro tide-gauge. Blue dots show the monthly average, and shaded boxes show the middle 50% of hourly observations. Lines show the top and bottom 25% of hourly observations.

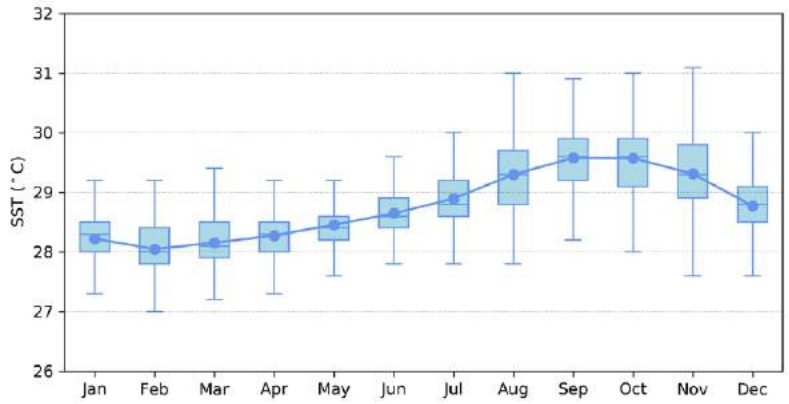

6.7.2 Trends

Figure 6.10 shows the 1981–2021 SST from satellite observations averaged over the EEZ. The data show a trend of 0.25 °C (0.45 °F) per decade with a 95% confidence interval of ±0.05 °C (0.09 °F).

Figure 6.10:
Sea surface temperature from satellite observations averaged across the RMI EEZ, shown as the orange line. The blue line shows the linear regression trend.

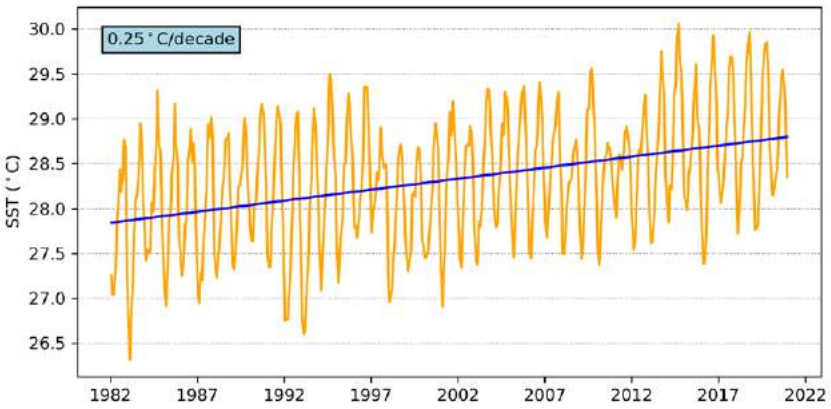

6.8 Sea level

6.8.1 Seasonal cycle

Majuro experiences a semidiurnal tidal cycle, meaning two high and two low tides per day. The highest predicted tides of the year typically occur from February to April as well as August/September. Figure 6.11 shows the number of hours the 99th percentile (2.2 m, 7.2 ft) sea level threshold is exceeded per month across the entire sea level record at Uliga, Majuro. Peak sea levels can occur between September and April but are primarily in February and September/October.

Since approximately 2005, more hours each year exceed the 99th percentile threshold. This is due to a combination of sea-level rise and subsidence occurring at RMI (Brown et al. 2020).

Figure 6.11:
Number of hours exceeding 99th percentile sea level threshold per month from 2001 to 2020 at the Majuro tide-gauge. Blue shading indicates the number of hours, and the final row provides a percentage summary of all the years.

Number of hours exceeding 2.2 m (Uliga, Marshall Islands)

	Jan	Feb	Mar	Apr	May	Jun	Jul	Aug	Sep	Oct	Nov	Dec	Annual
1993	0	0	0	0	0	0	0	0	0	0	0	0	0
1994	0	0	0	0	0	0	0	0	0	0	0	0	0
1995	0	0	0	0	0	0	0	0	0	0	0	0	0
1996	0	0	0	0	0	0	0	0	0	0	0	0	0
1997	0	0	1	0	0	0	0	0	0	0	0	0	1
1998	0	0	0	0	0	0	0	0	0	1	0	0	1
1999	0	0	0	0	0	0	0	0	0	0	0	0	0
2000	0	0	0	0	0	0	0	0	0	0	0	0	0
2001	0	4	0	0	0	0	0	0	0	0	0	0	4
2002	0	0	1	0	0	0	0	0	0	0	0	0	1
2003	0	0	0	1	0	0	0	0	0	0	0	0	1
2004	0	0	0	0	0	0	0	0	0	0	0	0	0
2005	0	0	0	0	0	0	0	0	0	0	0	0	0
2006	2	4	2	0	0	0	0	0	0	0	0	0	8
2007	0	1	0	3	0	0	0	0	10	2	0	0	16
2008	0	0	0	0	0	0	0	0	0	0	0	0	0
2009	0	1	0	0	0	0	0	0	0	0	0	0	1
2010	0	0	2	0	0	0	0	0	3	0	0	0	5
2011	0	8	1	0	0	0	0	0	3	1	0	0	13
2012	0	0	0	3	1	0	0	0	0	0	0	0	4
2013	0	0	0	0	0	0	0	0	0	0	0	0	0
2014	0	3	1	0	0	0	0	0	0	0	0	0	4
2015	0	1	0	0	0	0	0	0	0	0	0	0	1
2016	0	0	4	0	0	0	0	0	9	16	2	0	31
2017	0	0	3	0	0	0	0	0	0	0	6	3	12
2018	7	3	0	0	0	0	0	0	0	0	0	0	10
2019	1	2	1	0	0	0	0	2	13	2	0	0	21
2020	0	6	2	0	0	0	0	0	3	4	1	0	16
2021	0	1	0	0	0	0	0	0	0	12	4	2	19
Monthly Totals (%)	6	20	11	4	1	0	0	1	24	22	8	3	

6.8.2 Trends

Sea level at RMI, measured by satellite altimeters (Figure 6.12) since 1993, has risen between 1 mm (0.04 in) per year in the north and 4.5 mm (0.18 in) per year in the south, which is larger than the global average of 3.1 ± 0.4 mm (0.12 ± 0.02 in) per year (von Schuckmann et al. 2021). The 95% confidence interval ranges from ±0.6 mm (±0.02 in) in central to west regions and up to ±1.0 mm (±0.04 in) in the far west. This rise is partly linked to a pattern related to climate variability from year to year and decade to decade.

Trend estimates at the Majuro tide-gauge over a similar time span to the altimetry observations (May 1993 to July 2020) are provided in the PSLGM Monthly Data Report for July 2020 (http://www.bom.gov.au/ntc/IDO60101/IDO60101.202007.pdf). For Majuro, the trend is reported as 4.7 mm (0.2 in) per year, which is higher than the altimetry trends shown in Figure 6.12 (tide-gauge indicated by star symbol). This difference is most likely attributed to subsidence occurring at Pohnpei (Brown et al. 2020).

Figure 6.12:
Satellite altimetry annual trend for the Pacific from 1993 to 2020, with the RMI EEZ highlighted. The star symbol indicates the location of the tide-gauge at Majuro.

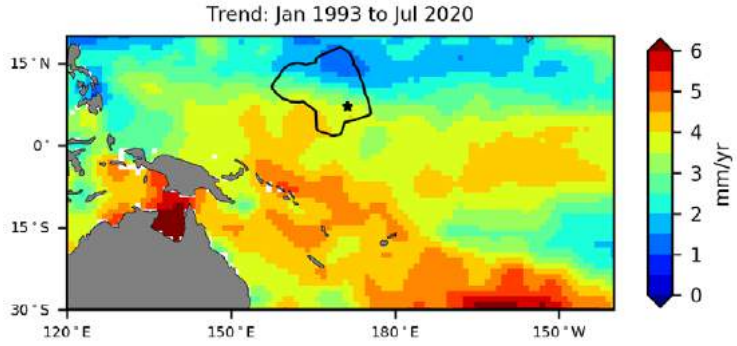

6.9 Waves

6.9.1 Seasonal cycle

The average wave climate in Majuro is defined by the significant wave height, peak period and peak direction. The significant wave height is the mean wave height (from trough to crest) of the highest one third of waves and corresponds to the wave height that would be reported by an experienced observer. Peak period is the time interval between two waves of the dominant wave period. Peak direction is the direction from which the dominant waves are coming.

The average sea state is dominated by wind seas from the northeast. The annual mean wave height is 1.56 m (4.99 ft), the annual mean wave direction is 54° and the annual mean wave period is 9.70 s. In the Pacific, waves often come from multiple directions and for different periods at a time. In Majuro, there are often more than three different wave direction/period components coming from the southeast to southwest (Figure 6.13).

Figure 6.13:
Annual wave rose for Majuro. Note that direction is where the wave is coming from.

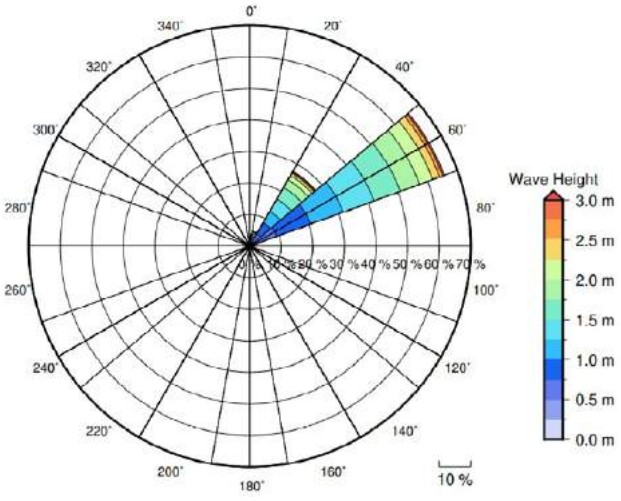

Seasonal wave activity peaks between November and March in terms of both wave height and period (Figure 6.14) due to North Pacific extra-tropical storm activity. Conversely, there is a distinct lull from May to July in terms of wave period and August to October in terms of wave height.

Figure 6.14:
Monthly wave height (black line), wave period (red line) and wave direction (arrows). The grey area represents the range of wave height between calm periods (10% of lowest wave height) and large wave events (10% of highest wave height).

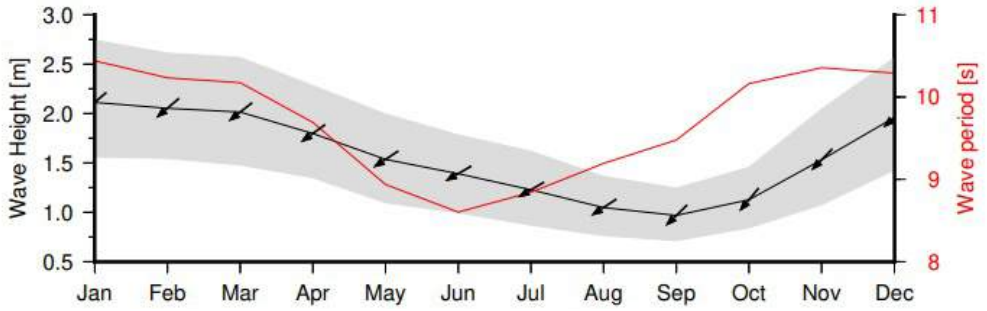

6.9.2 Trends

Waves change from month to month with the seasons, but they also change from year to year with climate oscillations. Typically, these changes are smaller than the seasonal changes but can be important during phenomena such as ENSO. In Majuro, the mean annual wave height has remained unchanged since 1979 (Figure 6.15). The mean annual wave height in Majuro is not significantly correlated with the main climate indicators of the region.

Figure 6.15:
Annual wave height (black line), wave period (red line) and wave direction (arrows). The grey area represents the range of wave height between calm periods (10% of lowest wave height) and large wave events (10% of highest wave height).

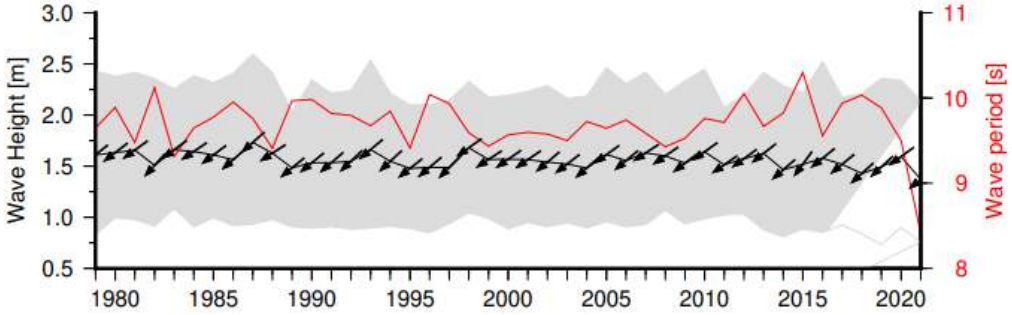

6.9.3 Extreme waves

Extreme wave analysis completed for Majuro was done by defining a severe height threshold and fitting a generalized Pareto distribution (GPD). The optimum threshold selected was 3.09 m (10.14 ft). In the 42-year wave hindcast, 110 wave events reached or exceeded this threshold, averaging 2.6 events per year. The GPD was fitted to the largest wave height reached during each of these events (Figure 6.16, Table 6.15). Extreme wave analysis is a very useful tool but is not always accurate because the analysis is very sensitive to the data available, the type of distribution fitted and the threshold used. For example, this analysis does not accurately account for tropical cyclone waves. More in-depth analysis is required to obtain results appropriate for designing coastal infrastructure and coastal hazard planning.

Figure 6.16:
Extreme wave distribution for Majuro. The crosses represent the wave events that have occurred since 1979. The solid line is the statistical distribution that best fits past wave events. The dashed lines show the upper and lower confidence limits of the fit. There is a 95% chance that the fitted distribution lies between the two dashed lines. Note that the annual return interval is in logarithmic scale.

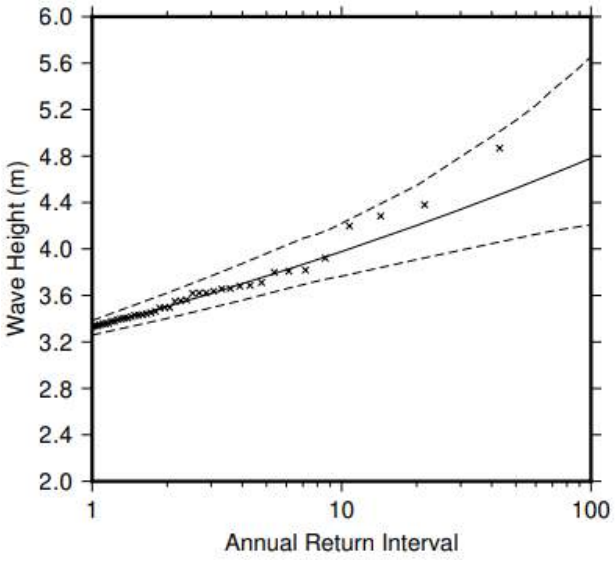

Table 6.4:
Summary of the results from extreme wave analysis in Majuro

Large wave height (90th percentile)	2.29 m (7.51 ft)
Severe wave height (99th percentile)	2.92 m (9.58 ft)
1-year ARI wave height	3.32 m (10.89 ft)
10-year ARI wave height	3.98 m (13.06 ft)
20-year ARI wave height	4.20 m (13.78 ft)
50-year ARI wave height	4.52 m (14.83 ft)
100-year ARI wave height	4.78 m (15.68 ft)

7 Nauru

7.1 Summary

7.1.1 Climate

- There is little change in the seasonal cycle of air temperature through the year, and changes are strongly linked to changes in the surrounding ocean temperature. The Republic of Nauru wet season is between December and April and the dry season between May to November.
- The seasonal cycle of rainfall is strongly affected by both the Intertropical Convergence Zone (ITCZ) and the South Pacific Convergence Zone (SPCZ) as Nauru is located between the usual position of both zones of convection.
- Warming trends are evident in annual and seasonal air temperatures over the period 1979–2021. The number of hot days and warm nights has increased, while the number of cool days and cold nights has decreased. The energy required for cooling indoor environments has also increased.
- Annual and seasonal rainfall trends show little change.
- As the Nauru is located within a few degrees of the equator, tropical cyclones rarely form within or pass through Nauru waters.

7.1.2 Ocean

- Highest sea levels typically occur in the months October–March.
- Sea-level rise at Nauru, measured by satellite altimeters from 1993 to mid-2020, ranges from 3.5 to 4.5 mm per year.
- Monthly average ocean temperature, as measured by the Nauru tide-gauge, ranges from 27.7 °C in February/March to 28.6 °C in July, with little difference between seasons. However, daily temperatures in any given year can be ±4 °C of these monthly averages due to variability from El Niño–Southern Oscillation (ENSO).
- The sea surface temperature (SST) trend across the Nauru exclusive economic zone (EEZ) is 0.22 °C per decade.
- Dominant wave direction is from 80° (east), with an average significant wave height of 1.31 m and average wave period of 10.54 s.
- Severe wave height was defined as 2.10 m, with an average of 3.4 severe events per year.
- Peak average wave activity in terms of significant wave height and period occurs from November to March.

7.2 Country description

Nauru is located in the equatorial Pacific Ocean, just south of the equator, between latitudes 0.5°S and 1°S, and longitudes 166.5°E and 167°E. Nauru is a single island country with a total land area of 21 km^2 and an EEZ of about 308,000 km^2. The capital of Nauru is Yaren, located on the west coast. The highest elevation is 65 m above sea level. Nauru has a population of approximately 10,000.

Figure 7.1:
Nauru and the location of the climate station used in this report

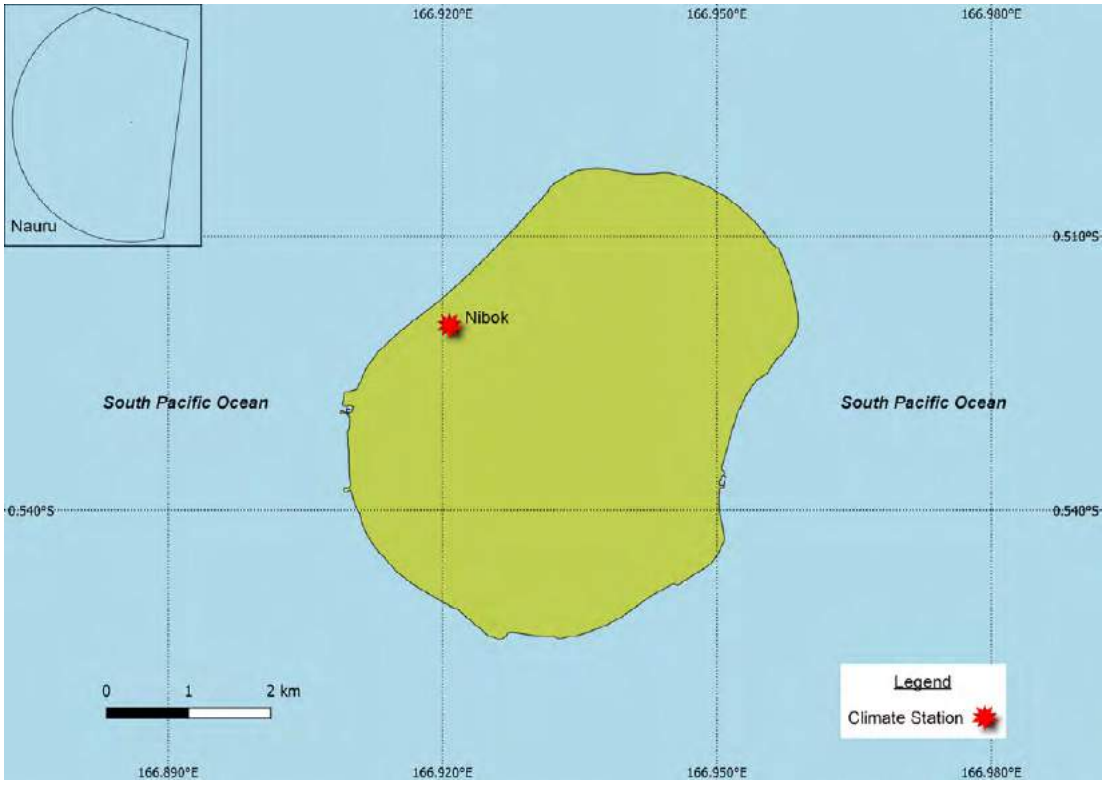

7.3 Data

Daily and monthly historical rainfall and air temperature records for Nauru from 1951 were obtained from The Bureau and Nauru Emergency Services Ministry. These records have undergone data quality and homogeneity assessment. While Nauru rainfall and temperature have been used to derive climatological information and rainfall trends in this report, there are insufficient maximum or minimum air temperature data to produce long-term trends. ERA5 reanalysis has been used to calculate temperature trends for 1979–2021 (further information is provided in Chapter 1). Additional information on historical climate trends for Nauru can be found in the Pacific Climate Change Data Portal http://www.bom.gov.au/climate/pccsp.

Tropical cyclone data and historical tracks starting from the 1969/70 season are available from the SHTC Data Portal http://www.bom.gov.au/cyclone/history/tracks/index.shtml.

SST covering the EEZ was obtained via the daily Optimum Interpolation SST version 2.1 (OISST v2.1) dataset from NOAA (Reynolds et al. 2007; Banzon et al. 2016). In situ ocean temperature data were obtained from the PSLGM Project tide-gauge located on Nauru, with data spanning from 1993 to 2021.

Wave data were obtained from the PACCSAP wave hindcast (Smith et al. 2021), available hourly from 1979 to present, with a grid resolution near Nauru of 7 km.

Regional sea level data were obtained from CSIRO satellite altimetry (updated by Benoit Legresy, Church and White 2011), with correction for seasonal signals, inverse barometer effect and glacial isostatic adjustment. Tide-gauge data were sourced from the Nauru tide-gauge station, spanning from 1993 to 2021 at hourly intervals.

7.4 Rainfall

7.4.1 Seasonal cycle

Nauru's location on the edge of the Pacific Warm Pool leads to an average annual rainfall total of over 2100 mm. There is a distinct wet season between December and April with average monthly rainfall above 200 mm per month, and 60% of the annual rainfall occurs during this season (Figure 7.2). The wettest month of the year is December, which averages rainfall of 270 mm. In contrast, the driest month of the year is September, which averages 130 mm.

The highest rainfall during the year occurs when the ITCZ is furthest south and also when the SPCZ is at its strongest. Nauru is located between these two convergence zones, and this leads to a marked increase in rainfall at the end of the year.

Figure 7.2:
Mean annual rainfall at Nauru

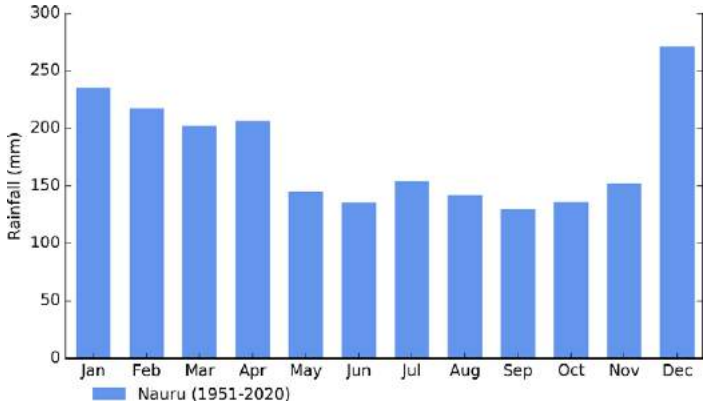

7.4.2 Trends

Trends in annual and seasonal rainfall since 1951 are not statistically significant at Nauru (Figure 7.3, Table 7.1). This means there has been little change in annual and seasonal rainfall at this location. Extremely large year-to-year variability associated with ENSO is evident, with El Niño years receiving significantly more rainfall than La Niña years. Annual rainfall since 1951 has varied from approximately 300 to 4400 mm. Limited daily precipitation is available for Nauru, so trends in rainfall extremes have not been calculated.

Figure 7.3:
Annual rainfall at Nauru. The straight line indicates the linear trend for annual rainfall (in black). The magnitude of this trend is presented in Table 7.1. Diamonds indicate years with insufficient data.

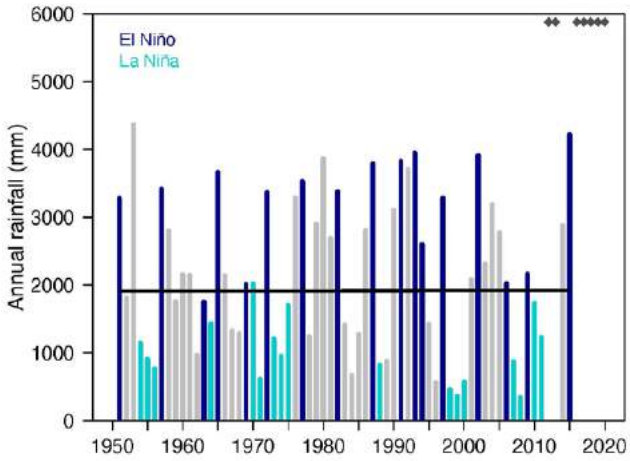

Table 7.1:
Trends in annual and seasonal rainfall at Nauru. The 95% confidence intervals are shown in parentheses, trends significant at the 95% level are shown in bold.

	Nauru
	1951–2015
Annual rainfall (mm/decade)	+1.52 (-198.67, +231.98)
November–April (mm/decade)	-58.33 (-179.30, +82.83)
May–October (mm/decade)	+19.81 (-36.57, +97.84)

7.5 Air temperature

7.5.1 Seasonal cycle

Nauru has a hot and humid climate with highly consistent air temperatures throughout the year (Figure 7.4). There is a slight peak in maximum temperatures during November at the onset of the wet season. The average monthly minimum and maximum temperature range is less than 1 °C, with air temperatures very closely related to the surrounding SST due to Nauru's small size and low topography.

Note there is a large amount of missing air temperature observations from 1978 onwards.

Figure 7.4:
Maximum and minimum air temperature seasonal cycle for Nauru for the period 1951–2020.

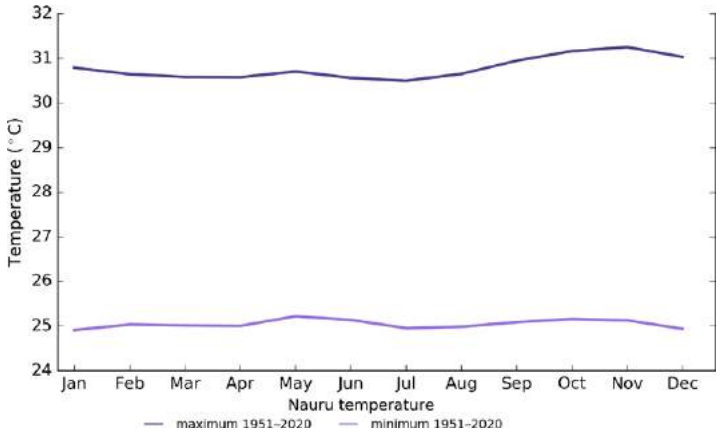

7.5.2 Trends

Limited station temperature data for trend analysis is available for Nauru. Therefore, reanalysis data have been used to calculate temperature trends. Average annual and seasonal temperatures have increased since 1979 (Table 7.2). All temperature trends are statistically significant and there is little difference between minimum and maximum temperature trends or between seasons due to Nauru's tropical location.

Table 7.2:
Trends in annual and seasonal air temperatures at Nauru from ERA5 reanalysis data. A reanalysis is a global weather simulation merged with observations and represents the most complete picture of historical climate, but shares the same limitations as climate models. The 95% confidence intervals are shown in parentheses, and trends significant at the 95% level are shown in bold.

	Nauru-ERA5 Tmax (°C/decade)	Nauru-ERA5 Tmin (°C/decade)	Nauru-ERA5 Tmean (°C/decade)
	1979–2021		
Annual	**+0.19** (+0.07, +0.29)	**+0.17** (+0.12, +0.22)	**+0.16** (+0.09, +0.23)
November–April	**+0.21** (+0.08, +0.32)	**+0.19** (+0.12, +0.24)	**+0.19** (+0.11, +0.28)
May–October	**+0.17** (+0.08, +0.25)	**+0.18** (+0.11, +0.24)	**+0.17** (+0.10, +0.23)

The number of hot days and warm nights are increasing, and the number of cool days and cold nights are decreasing at Nauru (Table 7.3). The cooling degree days index provides a measure of the energy demand needed to cool a building down to 25 °C, with the assumption that air conditioners are generally turned on at this temperature. There has been an increase in the cooling degree index, suggesting the energy needed for cooling has increased significantly since 1979.

Table 7.3:
Trends in annual temperature extremes at Nauru from ERA5 reanalysis data. A reanalysis is a global weather simulation merged with observations and represents the most complete picture of historical climate but shares the same limitations as climate models. The 95% confidence intervals are shown in parentheses, and trends significant at the 95% level are shown in bold. Hot and cool days, and warm and cold nights are measured relative to 1981–2010 (see Chapter 1 for details).

	Nauru - ERA5
	1979–2021
Number of hot days (days/decade)	**+21.99** (+9.26, +35.01)
Number of warm nights (nights/decade)	**+12.90** (+7.93, +23.54)
Number of cool days (days/decade)	**-7.64** (-16.09, -1.13)
Number of cold nights (nights/decade)	**-12.93** (-16.58, -7.69)
Cooling degree days (degree days/decade)	**+55.11** (+31.15, +81.55)
Daily temperature range (°C/decade)	-0.02 (-0.12, +0.05)

7.6 Tropical cyclones

7.6.1 Seasonal cycle

No tropical cyclones passed within the EEZ between the 1969/70 and 2017/18 seasons.

7.6.2 Trends

Trends in total number of tropical cyclones (<995 hPa) and severe tropical cyclones (<970 hPa) are presented for the period 1981/82–2020/21 for the greater Southwest Pacific (135°E–120°W; 0–50°S). Trends are presented at a regional scale as the number of tropical cyclones occurring within Pacific Island EEZs is insufficient for reliable long-term trend analysis.

For the total number of tropical cyclones, the trend (and 95% confidence interval) is -0.92 (-1.85, 0.01) tropical cyclones/decade. There has been little change/marginal decline in the total number of tropical cyclones over the last 40 seasons. This trend is not statistically significant.

For the total number of severe tropical cyclones, the trend is -0.80 (-1.32, -0.29) tropical cyclones/decade. There is a negative trend in the number of severe tropical cyclones over the last 40 seasons. There has been little change/marginal decline in the proportion of tropical cyclones reaching severe status. The trend is -0.04 (-0.08, 0.00) tropical cyclones/decade. The negative trend is statistically significant.

Records of tropical cyclones exist from the late 1800s in some countries in the Southwest Pacific, but trends in tropical cyclones have only been presented from 1981/82. Satellite-based observations began in the Southwest Pacific in the early 1970s, but consistent coverage and reliable intensity estimates have only been available since the early 1980s. Confidence in tropical cyclone trends is moderate as the definition of a tropical cyclone has changed and satellite observation methods have continued to improve over the last 40 years.

7.7 Sea surface temperature

7.7.1 Seasonal cycle

Ocean temperature, as measured by the Nauru tide-gauge, reaches on average a maximum of approximately 28.6 °C in July, but individual months can get as high as 31 °C (Figure 7.5). Minimum average temperature is 27.7 °C in February/March. Hourly temperatures can be up to 3 °C higher or 4 °C lower than these monthly averages, although 50% of hourly observations fall within 2 °C of the average. Equatorial locations typically have little average variation but can drastically change in a given year depending on the ENSO cycle. The variability in temperatures between October to March are reflective of peak months of ENSO.

Figure 7.5:
Annual temperatures measured at the Nauru tide-gauge. Blue dots show the monthly average, and shaded boxes show the middle 50% of hourly observations. Lines show the top and bottom 25% of hourly observations

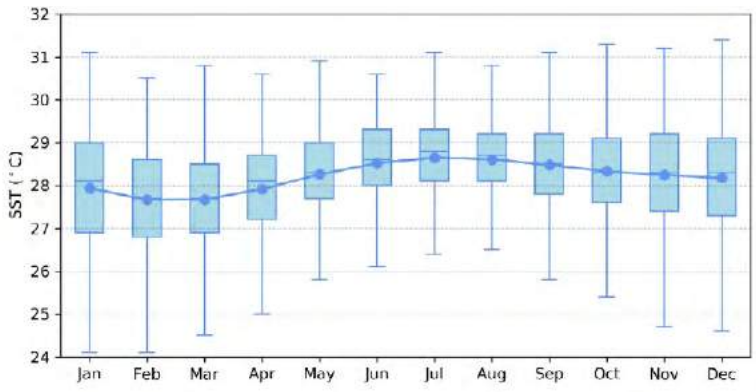

7.7.2 Trends

Figure 7.6 shows the 1981–2021 SST from satellite observations averaged over the Nauru EEZ. The data show a trend of 0.22 °C per decade with a 95% confidence interval of ±0.05 °C.

Figure 7.6:
Sea surface temperature from satellite observations averaged across the Nauru EEZ, shown as the orange line. The blue line shows the linear regression trend.

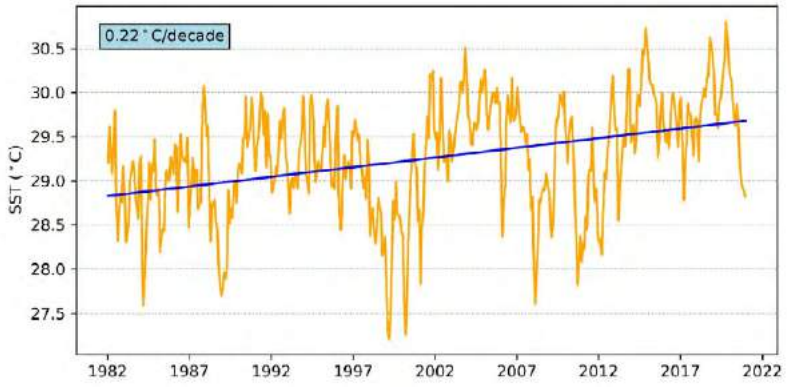

7.8 Sea level

7.8.1 Seasonal cycle

Nauru experiences a semidiurnal tidal cycle, meaning two high and two low tides per day. During the last quarter moon, there is little difference between the high and low tides. The highest predicted tides of the year typically occur from November to February. Figure 7.7 shows the number of hours the 99th percentile (2.72 m) sea level threshold is exceeded per month across the entire sea level record at Nauru. Peak sea levels typically occur between October and March.

Figure 7.7:
Number of hours exceeding 99th percentile sea level threshold per month from 1993 to 2021 at the Nauru tide-gauge. Blue shading indicates the number of hours, and the final row provides a summary of all the years.

Number of hours exceeding 2.72 m (Aiwo, Nauru)

	Jan	Feb	Mar	Apr	May	Jun	Jul	Aug	Sep	Oct	Nov	Dec	Annual
1993	0	0	0	0	0	0	0	0	0	0	0	0	0
1994	0	0	0	0	0	0	0	0	0	0	0	2	2
1995	0	0	0	0	0	0	0	0	0	0	0	0	0
1996	1	0	0	0	0	0	0	0	0	0	0	0	1
1997	0	3	5	0	0	0	0	0	0	0	0	0	8
1998	0	0	0	0	0	0	0	0	0	0	0	0	0
1999	0	0	0	0	0	0	0	0	0	0	0	0	0
2000	0	0	0	0	0	0	0	0	0	0	0	0	0
2001	0	0	0	0	0	0	0	0	0	0	0	11	11
2002	0	1	1	0	0	0	0	0	0	4	0	0	6
2003	0	0	0	0	0	0	0	0	0	1	5	0	6
2004	0	0	0	0	0	0	0	0	0	0	0	0	0
2005	0	2	2	0	0	0	0	0	0	0	0	0	4
2006	0	0	0	0	0	0	0	1	1	3	1	0	6
2007	0	0	0	0	0	0	0	0	0	0	0	0	0
2008	0	0	0	0	0	0	0	0	0	0	0	0	0
2009	0	0	0	0	0	0	0	0	0	0	0	0	0
2010	0	0	0	0	0	0	0	0	0	0	0	0	0
2011	0	0	0	0	0	0	0	0	0	0	0	0	0
2012	0	0	0	1	1	0	0	0	0	1	0	0	3
2013	0	0	0	0	0	0	0	0	0	0	0	0	0
2014	10	11	23	3	0	0	0	0	2	5	0	4	58
2015	4	2	6	0	0	0	4	0	0	0	0	2	18
2016	0	0	0	0	0	0	0	0	0	0	0	0	0
2017	0	0	0	0	0	0	0	0	0	0	0	1	1
2018	0	0	0	0	0	0	0	1	0	0	0	0	1
2019	2	1	0	0	0	0	0	3	3	0	6	0	15
2020	0	6	1	0	0	0	0	0	0	0	2	1	10
2021	0	1	0	2	0	0	0	0	0	0	2	2	7
Monthly Totals (%)	11	17	24	4	1	0	3	3	4	9	10	15	

7.8.2 Trends

Sea level at Nauru, measured by satellite altimeters (Figure 7.8) since 1993, has risen between 3.5 and 4.5 mm per year across the EEZ, with a confidence interval of ±0.6 to ±0.8 mm. These trend estimates are larger than the global average of 3.1 ± 0.4 mm per year (von Schuckmann et al. 2021). This rise is partly linked to a pattern related to climate variability from year to year and decade to decade.

Trend estimates at the Nauru tide-gauge over a similar time span to the altimetry observations (July 1993 to July 2020) are provided in the PSLGM Monthly Data Report for July 2020 (http://www.bom.gov.au/ntc/IDO60101/IDO60101.202007.pdf). For Nauru, the trend is reported as 5.5 mm per year, which is higher than the altimetry trends shown in Figure 7.8 (tide-gauge indicated by star symbol). This difference is most likely attributed to subsidence occurring at Nauru (Brown et al. 2020).

Figure 7.8:
Satellite altimetry annual trend for the Pacific from 1993 to 2020, with the Nauru EEZ highlighted. The star symbol indicates the location of the tide-gauge at Nauru.

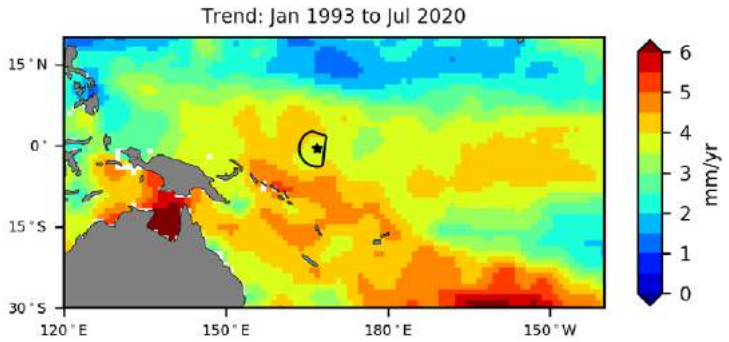

7.9 Waves

7.9.1 Seasonal cycle

The average wave climate at Nauru is defined by the significant wave height, peak period and peak direction. The significant wave height is the mean wave height (from trough to crest) of the highest one third of waves and corresponds to the wave height that would be reported by an experienced observer. Peak period is the time interval between two waves of the dominant wave period. Peak direction is the direction from which the dominant waves are coming.

The average sea state is dominated by wind seas from the east. The annual mean wave height is 1.31 m, the annual mean wave direction is 80° and the annual mean wave period is 10.54 s. In the Pacific, waves often come from multiple directions and for different periods at a time. In Nauru, there are often more than eight different wave direction/period components coming from the southeast to southwest (Figure 7.9).

Figure 7.9:
Annual wave rose for Nauru. Note that direction is where the wave is coming from.

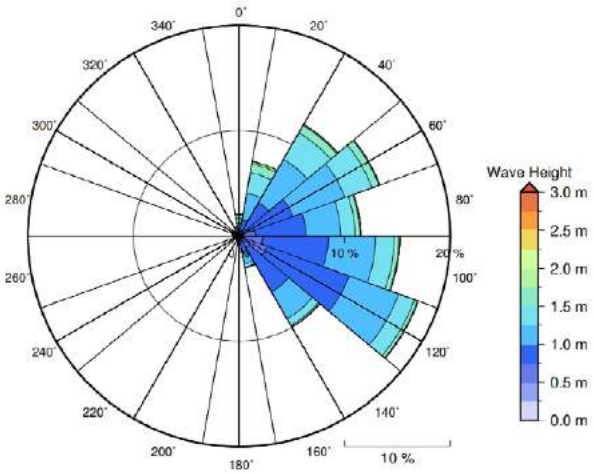

Seasonal wave activity peaks between November and March in terms of both wave height and period (Figure 7.10) due to North Pacific extra-tropical storm activity.

Figure 7.10:
Monthly wave height (black line), wave period (red line) and wave direction (arrows). The grey area represents the range of wave height between calm periods (10% of lowest wave height) and large wave events (10% of highest wave height).

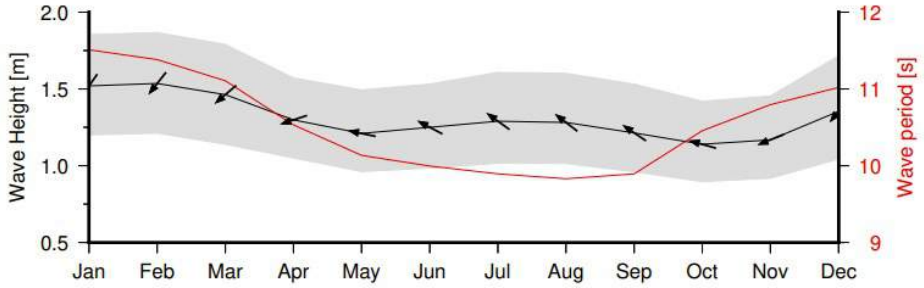

7.9.2 Trends

Waves change from month to month with the seasons, but they also change from year to year with climate oscillations. Typically, these changes are smaller than the seasonal changes but can be important during phenomena such as ENSO. At Nauru, the mean annual wave height has remained unchanged since 1979 (Figure 7.11). The mean annual wave height in Nauru is not significantly correlated with the main climate indicators of the region.

Figure 7.11:
Annual wave height (black line), wave period (red line) and wave direction (arrows). The grey area represents the range of wave height between calm periods (10% of lowest wave height) and large wave events (10% of highest wave height).

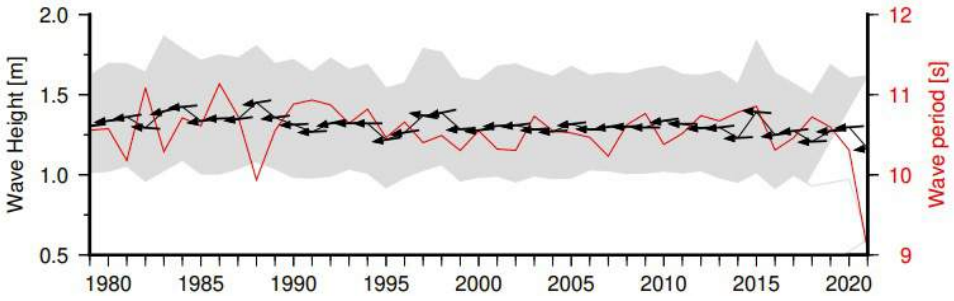

7.9.3 Extreme waves

Extreme wave analysis for Nauru was done by defining a severe height threshold and fitting a generalized Pareto distribution (GPD). The optimum threshold selected was 2.10 m. In the 42-year wave hindcast, 142 wave events reached or exceeded this threshold, averaging 3.4 per year. The GPD was fitted to the largest wave height reached during each of these events (Figure 7.12, Table 7.3). Extreme wave analysis is a very useful tool but is not always accurate because the analysis is very sensitive to the data available, the type of distribution fitted and the threshold used. For example, this analysis does not accurately account for tropical cyclone waves. More in-depth analysis is required to obtain results appropriate for designing coastal infrastructure and coastal hazard planning.

Figure 7.12:
Extreme wave distribution for Nauru. The crosses represent the wave events that have occurred since 1979. The solid line is the statistical distribution that best fits past wave events. The dashed lines show the upper and lower confidence limits of the fit. There is a 95% chance that the fitted distribution lies between the two dashed lines. Note that the annual return interval is in logarithmic scale.

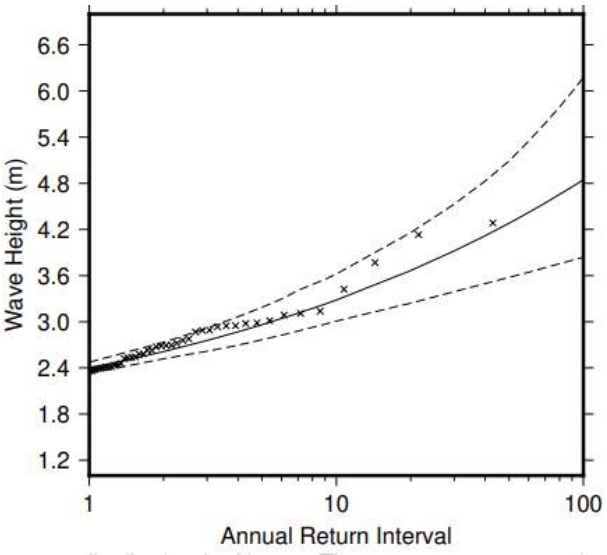

Table 7.3
Summary of the results from extreme wave analysis in Nauru

Large wave height (90th percentile)	1.67 m
Severe wave height (99th percentile)	2.12 m
1-year ARI wave height	2.39 m
10-year ARI wave height	3.28 m
20-year ARI wave height	3.66 m
50-year ARI wave height	4.28 m
100-year ARI wave height	4.85 m

8 Niue

8.1 Summary

8.1.1 Climate

- Changes in air temperature from season to season are relatively small and strongly linked to changes in the surrounding ocean temperature. Niue has two distinct seasons – a warm wet season from November to April and a cooler dry season from May to October.
- The seasonal cycle is strongly affected by the South Pacific Convergence Zone (SPCZ), which is most intense during the wet season.
- Annual and seasonal air temperatures at Alofi–Hanan Airport increased over the period 1951–2020.
- Annual and seasonal rainfall trends, as well as trends in rainfall extremes, show little change at Alofi–Hanan Airport.
- Tropical cyclones usually affect Niue between November and April. Over the period 1969–2018, an average of 16 cyclones passed within the Niue exclusive economic zone (EEZ) per decade. Tropical cyclones were most frequent in neutral or El Niño years and least frequent in La Niña years. Year-to-year variability is large, ranging from no tropical cyclones in some seasons to four.
- There has been little change in the total number of tropical cyclones in the Southwest Pacific since 1981/82. The number of severe tropical cyclones has declined over the same period/region.

8.1.2 Ocean

- Highest sea levels typically occur in the months November–February.
- Sea-level rise within the EEZ, measured by satellite altimeters since 1993, is about 3 to 5 mm per year.
- Monthly average ocean temperature, as measured by the Niue tide-gauge, ranges from 25.2 °C in August to 28.2 °C in March. However, monthly temperatures in any given year can be up to ±2 °C of these averages.
- The sea surface temperature (SST) trend, as per satellite observations, is 0.29 °C per decade, one of the highest trends in the Southwest Pacific.
- Dominant wave direction is from 212° (SSW), with an average significant wave height of 1.73 m and average wave period of 13.48 s.
- Severe wave height was defined as 3.65 m, with an average of 3.1 severe events per year.
- Peak average significant wave height occurs around July.

8.2 Country description

Niue is an island country located in the tropical western South Pacific Ocean between latitudes 18.5°S and 19.5°S, and longitudes 169°W and 170°W. It has a total land area of 261 km^2 and an EEZ of 127,000 km^2. Alofi, the capital is located on the west coast. The highest elevation is 68 m above sea level. Niue's population is approximately 1600.

Figure 8.1:
Niue and the location of the climate station used in this report

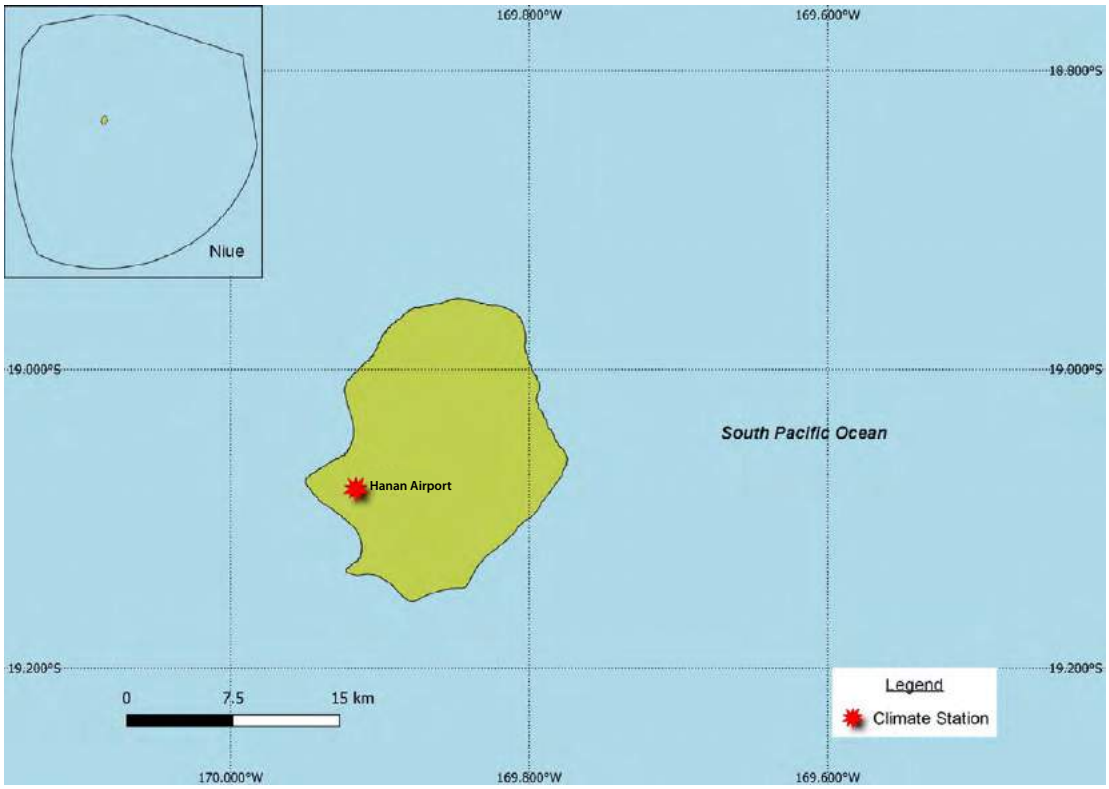

8.3 Data

Daily historical rainfall and air temperature records for an Alofi–Hanan Airport (Hanan Airport hereafter) station composite from 1951 were obtained from the Niue Meteorological Service. These records have undergone data quality and homogeneity assessment. Where the maximum or minimum air temperature records were found to have discontinuities, these records have been adjusted to make them homogeneous (further information is provided in Chapter 1). Additional information on historical climate trends for Niue can be found in the Pacific Climate Change Data Portal http://www.bom.gov.au/climate/pccsp.

Tropical cyclone data and historical tracks starting from the 1969/70 season are available from the SHTC Data Portal http://www.bom.gov.au/cyclone/history/tracks/index.shtml.

SST covering the EEZ was obtained via the daily Optimum Interpolation SST version 2.1 (OISST v2.1) dataset from NOAA (Reynolds et al. 2007; Banzon et al. 2016). In situ ocean temperature data were obtained from the PSLGM Project tide-gauge located at Alofi, with data spanning from 2015 to 2019.

Wave data were obtained from the PACCSAP wave hindcast (Smith et al. 2021), available hourly from 1979 to present, with a grid resolution near Niue of 7 km.

Regional sea level data were obtained from CSIRO satellite altimetry (updated by Benoit Legresy, Church and White 2011), with correction for seasonal signals, inverse barometer effect and glacial isostatic adjustment. Tide-gauge data were sourced from the Alofi tide-gauge station, spanning from 1993 to 2021 at hourly intervals.

8.4 Rainfall

8.4.1 Seasonal cycle

During the wetter/warmer half of the year from November to April, the trade winds weaken and the SPCZ is most active, leading to almost two thirds of Hanan Airport's rain to fall during this period (Figure 8.2). This reflects the importance of the SPCZ on rainfall, which is most active during the wet season months and positioned closest to Niue, compared to the dry season where the SPCZ is further to the northeast and less active.

Niue's climate is also influenced by subtropical high-pressure systems and the trade winds, which blow mainly from the southeast.

Figure 8.2:
Mean annual rainfall at Hanan Airport

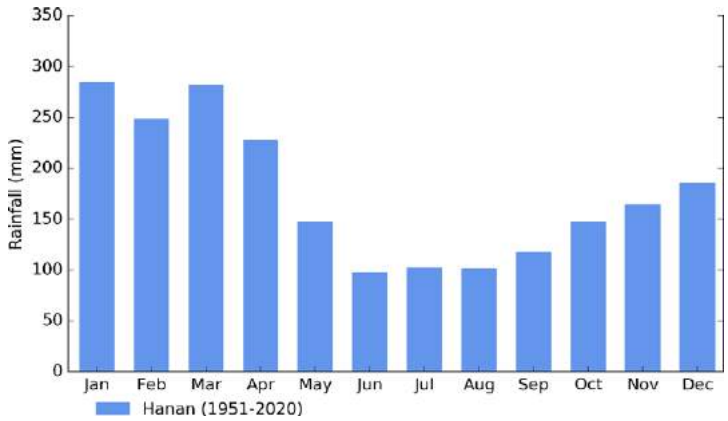

8.4.2 Trends

Trends in annual and seasonal rainfall since 1951 are not statistically significant at Hanan Airport (Figure 8.3, Table 8.1). This means there has been little change in annual and seasonal rainfall at this location. Variability associated with El Niño–Southern Oscillation (ENSO) is evident, with La Niña years generally experiencing higher rainfall than El Niño years. Annual rainfall at Hanan Airport varies from approximately 800 to 3900 mm.

Figure 8.3:
Annual rainfall (bar graph) and number of wet days (where rainfall is at least 1 mm; line graph) at Hanan Airport. Straight lines indicate linear trends for annual rainfall (in black) and number of wet days (in blue). The magnitudes of the trends are presented in Table 8.1.

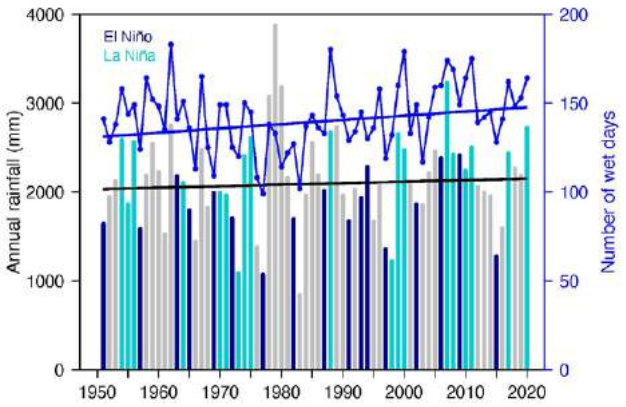

Table 8.1:
Trends in annual, seasonal and extreme rainfall at Hanan Airport. The 95% confidence intervals are shown in parentheses. The contribution to total rainfall from extreme events and the standardised rainfall evapotranspiration index are measured relative to 1961–1990 (see Chapter 1 for details).

	Hanan Airport
	1951–2020
Annual rainfall (mm/decade)	+17.09 (-63.13, +101.24)
November–April (mm/decade)	+5.18 (-46.02, +50.09)
May–October (mm/decade)	+19.60 (-22.56, +60.44)
Number of wet days (days/decade)	+2.39 (-0.40, +5.27)
Contribution to total rainfall from extreme events (%/decade)	-0.41 (-1.73, +0.92)
Consecutive dry days (days/decade)	0.00 (-0.49, +0.41)
Maximum one-day rainfall (mm/decade)	-0.21 (-5.60, +5.52)
Standardised rainfall evapotranspiration index (November–April)	-0.01 (-0.12, +0.09)
Standardised rainfall evapotranspiration index (May–October)	+0.06 (-0.04, +0.17)

Similar to annual and seasonal rainfall, no significant trends in extreme rainfall indices, including the standardised rainfall evapotranspiration drought index, were detected (Table 8.1). Figure 8.4 shows low interannual variability in consecutive dry days and most years do not experience more than three weeks without rain.

Figure 8.4:
Annual longest run of consecutive dry days (bar graph) and maximum daily rainfall (line graph) at Hanan Airport. Straight lines indicate linear trends for dry days (in black) and maximum daily rainfall (in blue). The magnitudes of the trends are presented in Table 8.1.

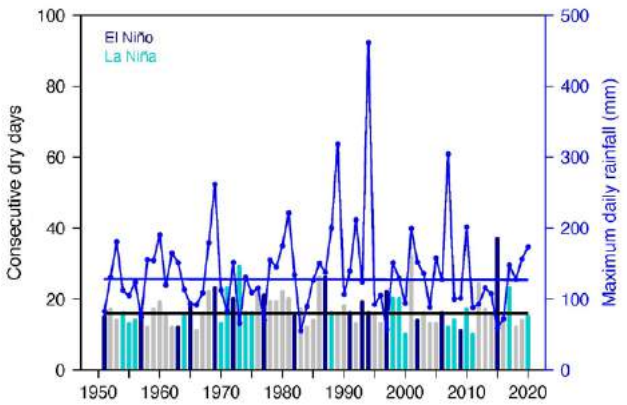

8.5 Air temperature

8.5.1 Seasonal cycle

The range in average monthly maximum and minimum temperatures throughout the year at Hanan Airport is 4 ºC for the 1961–1990 climatology period and 3.7 ºC for the 1991–2020 period. There has been a clear shift towards warmer average monthly temperatures between the climatology periods of 1961–1990 and 1991–2020 (Figure 8.5), with warmer average temperatures occurring in all months throughout the year, with the exception of May average minimum temperatures. The largest increase in average minimum temperatures occurs during July and August, with almost 1 ºC of warming, while average maximum temperatures have seen the largest warming between July and December.

Figure 8.5:
Maximum and minimum air temperature seasonal cycle for Hanan Airport for the periods 1961–1990 (dotted lines) and 1991–2020 (solid lines)

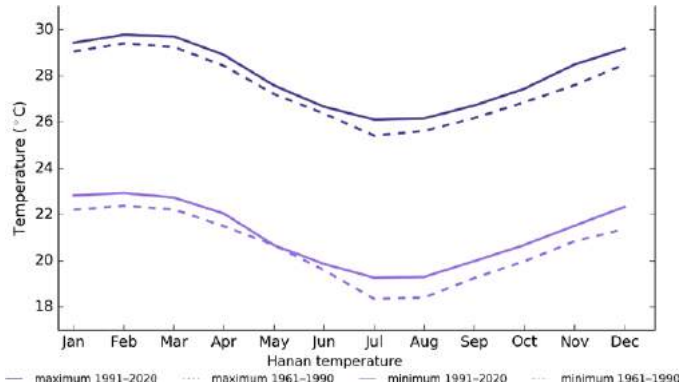

8.5.2 Trends

Average annual and seasonal temperatures have increased significantly at Hanan Airport (Figure 8.6). November–April temperatures are warming at approximately the same rate as May–October temperatures (Table 8.2).

Figure 8.6:
Average annual, November–April and May–October temperatures for Hanan Airport. Straight lines indicate linear trends. The magnitudes of the trends are presented in Table 8.2. Diamonds indicate years with insufficient data for one or more variables.

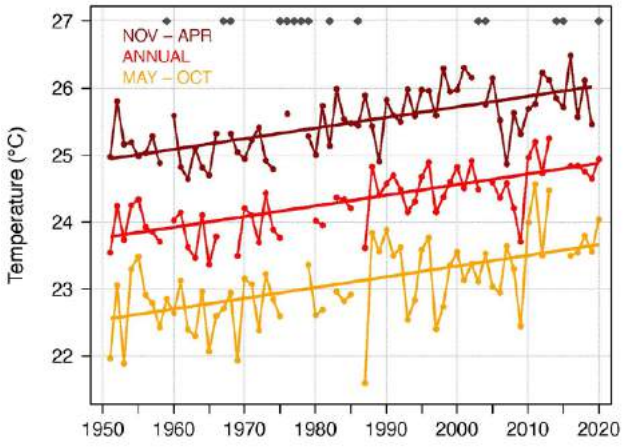

Table 8.2:
Trends in annual and seasonal air temperatures at Hanan Airport. The 95% confidence intervals are shown in parentheses, and trends significant at the 95% level are shown in bold.

	Hanan Airport Tmax (°C/decade)	Hanan Airport Tmin (°C/decade)	Hanan Airport Tmean (°C/decade)
	1951–2020		
Annual	**+0.16** (+0.12, +0.21)	**+0.15** (+0.09, +0.20)	**+0.16** (+0.11, +0.21)
November–April	**+0.19** (+0.13, +0.24)	**+0.13** (+0.05, +0.20)	**+0.16** (+0.11, +0.22)
May–October	**+0.17** (+0.08, +0.24)	**+0.16** (+0.10, +0.23)	**+0.16** (+0.10, +0.23)

Numerous gaps exist in the daily temperature record for Hanan Airport, which prevents the robust calculation of trends for most temperature extremes. However, Figure 8.7 shows that most years since 2010 have experienced over twice as many hot days compared with the beginning of the record. This is consistent with the increases in annual and seasonal temperatures (Figure 8.6) as well as trends in temperature extremes in neighbouring Pacific Island countries.

Figure 8.7:
Annual number of hot days and cold nights at Hanan Airport. The straight line indicates a linear trend for cold nights. Criteria for statistical robustness were not met for determining a linear trend for hot days. Diamonds indicate years with insufficient data for one or both variables.

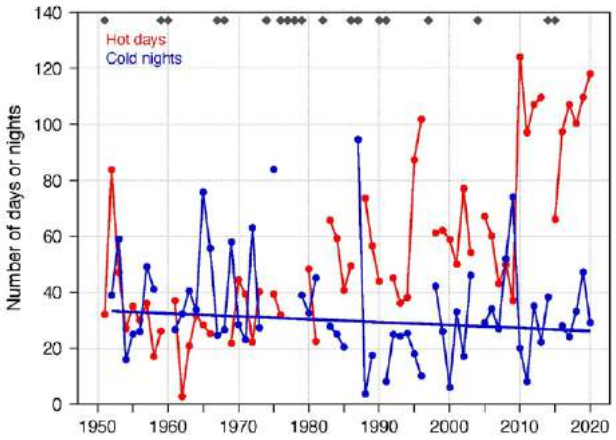

8.6 Tropical cyclones

8.6.1 Seasonal cycle

Tropical cyclones usually affect Niue during the southern hemisphere tropical cyclone season, which is from November to April, but also occasionally occur outside the tropical cyclone season. The Southern Hemisphere Tropical Cyclone Archive indicates that between the 1969/70 and 2017/18 seasons, 51 tropical cyclones (Figure 8.8) passed within the EEZ. This represents an average of 10 cyclones per decade. Tropical cyclones were most frequent in neutral or El Niño years (12 cyclones per decade) and least frequent in La Niña years (7 cyclones per decade).

Interannual variability in the number of tropical cyclones in the EEZ is large, ranging from zero in some seasons to four in 1979/80, 2002/03 and 2015/16 (Figure 8.8). High interannual variability and the small number of tropical cyclones occurring in the EEZ make reliable identification of long-term trends in frequency and intensity difficult.

Some tropical cyclone tracks analysed in this section include the tropical depression stage (sustained winds ≤34 knots) before and/or after tropical cyclone formation.

Figure 8.8:
Number of tropical cyclones passing within the Niue EEZ per season. Each season is defined by the ENSO status, with light blue being an El Niño year, dark blue a La Niña year and grey showing a neutral ENSO year. The 11-year moving average is presented as a purple line and considers all years.

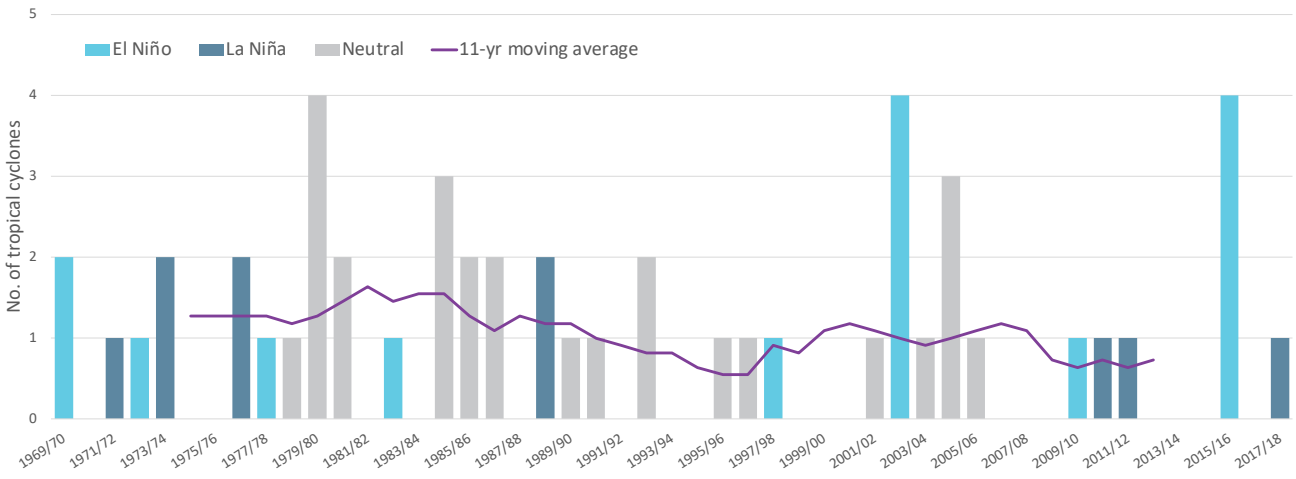

8.6.2 Trends

Trends in total number of tropical cyclones (<995 hPa) and severe tropical cyclones (<970 hPa) are presented for the period 1981/82–2020/21 for the greater Southwest Pacific (135°E–120°W; 0–50°S). Trends are presented at a regional scale as the number of tropical cyclones occurring within Pacific Island EEZs is insufficient for reliable long-term trend analysis.

For the total number of tropical cyclones, the trend (and 95% confidence interval) is -0.92(-1.85, 0.01) tropical cyclones/decade. There has been little change/marginal decline in the total number of tropical cyclones over the last 40 seasons. This trend is not statistically significant.

For the total number of severe tropical cyclones, the trend is -0.80 (-1.32, -0.29) tropical cyclones/decade. There is a negative trend in the number of severe tropical cyclones over the last 40 seasons. There has been little change/marginal decline in the proportion of tropical cyclones reaching severe status. The trend is -0.04 (-0.08, 0.00) tropical cyclones/decade. The negative trend is statistically significant.

Records of tropical cyclones exist from the late 1800s in some countries in the Southwest Pacific, but trends in tropical cyclones have only been presented from 1981/82. Satellite-based observations began in the Southwest Pacific in the early 1970s, but consistent coverage and reliable intensity estimates have only been available since the early 1980s. Confidence in tropical cyclone trends is moderate as the definition of a tropical cyclone has changed and satellite observation methods have continued to improve over the last 40 years.

8.7 Sea surface temperature

8.7.1 Seasonal cycle

Ocean temperature, as measured by satellite observations near Alofi from 1982 to 2021, reaches on average a maximum of 28.2 °C in March, but individual months can get as high as 29.5 °C. Minimum average temperatures reach a low of 25.2 °C in August. Daily temperatures can be up to 2 °C higher or lower than these monthly averages, although 50% of daily observations fall within 1.5 °C of the average.

Figure 8.9:
Annual sea surface temperatures near Alofi. Blue dots show the monthly average, and shaded boxes show the middle 50% of daily observations. Lines show the top and bottom 25% of daily observations.

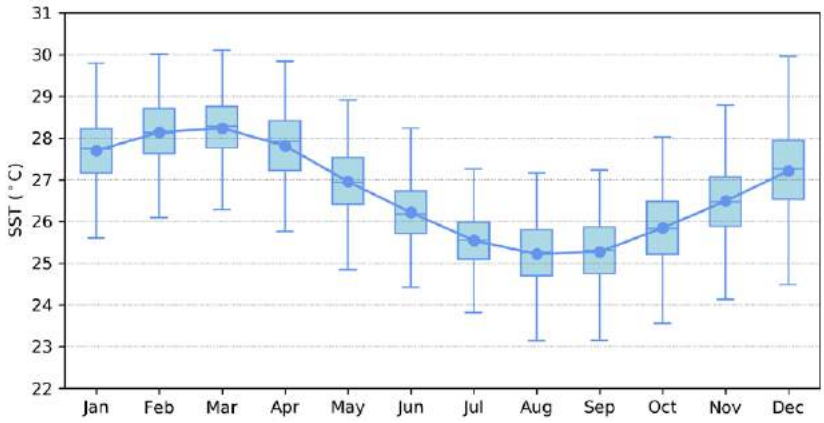

8.7.2 Trends

Figure 8.10 shows the 1981–2021 SST from satellite observations averaged over the Niue EEZ. The data show a trend of 0.29 °C per decade with a 95% confidence interval of ±0.10 °C.

Figure 8.10:
Sea surface temperature from satellite observations averaged across the Niue EEZ, shown as the orange line. The blue line shows the linear regression trend.

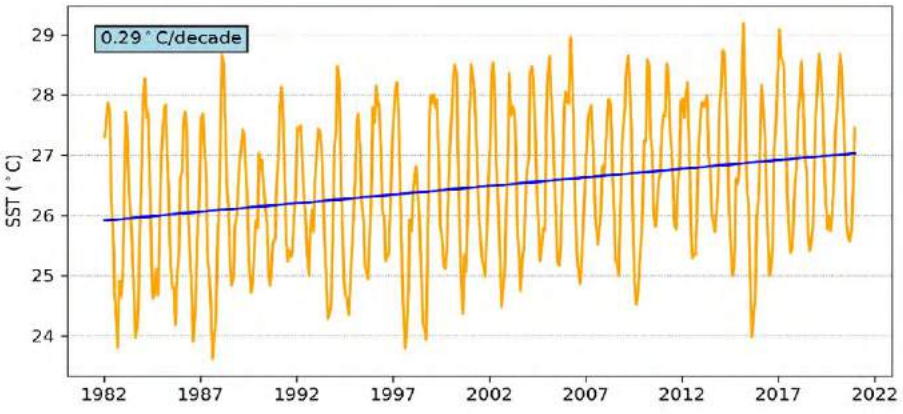

8.8 Sea level

8.8.1 Seasonal cycle

Niue experiences a semidiurnal tidal cycle, meaning two high and two low tides per day. The highest predicted tides of the year typically occur during the wet season months of December to February. Figure 8.11 shows the number of hours the 99th percentile (1.53 m) sea level threshold is exceeded per month across the entire sea level record at Niue. Peak sea levels typically occur in November–February.

Figure 8.11:
Number of hours exceeding 99th percentile sea level threshold per month from 2015 to 2019 at the Niue tide-gauge. Blue shading indicates the number of hours, and the final row provides a percentage summary of all the years.

Number of hours exceeding 1.53 m (Alofi Wharf, Niue)

	Jan	Feb	Mar	Apr	May	Jun	Jul	Aug	Sep	Oct	Nov	Dec	Annual
2015	0	0	0	0	0	0	0	0	0	0	2	0	2
2016	2	0	0	0	0	0	0	0	0	0	0	0	2
2017	0	4	0	0	0	0	0	0	0	0	1	10	15
2018	0	0	0	0	0	0	0	3	0	0	0	0	3
2019	0	4	0	0	0	0	0	0	0	0	0	4	8
Monthly Totals (%)	7	27	0	0	0	0	0	10	0	0	10	47	

8.8.2 Trends

Sea level at Niue, measured by satellite altimeters (Figure 8.12) since 1993, has risen between 3 and 5 mm per year across the EEZ (the highest in the south), with a 95% confidence interval of ±0.4 to ±0.6 mm. This rise is partly linked to a pattern related to climate variability from year to year and decade to decade. Most of the EEZ has a higher sea level trend than the global average of 3.1 ± 0.4 mm per year (von Schuckmann et al. 2021).

Figure 8.12:
Satellite altimetry annual trend for the Pacific from 1993 to 2020, with Niue EEZ highlighted. The star symbol indicates the location of the tide-gauge.

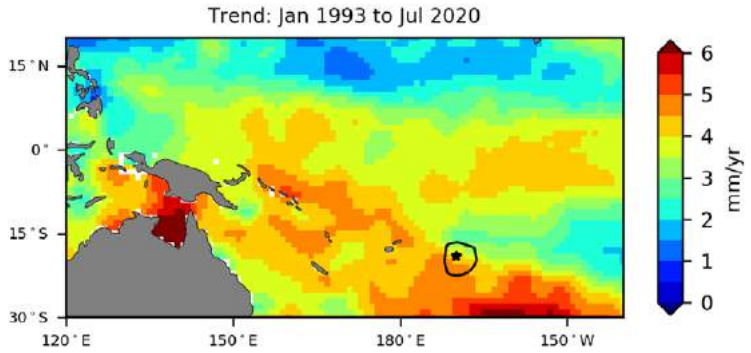

8.9 Waves

8.9.1 Seasonal cycle

The average wave climate in Niue is defined by the significant wave height, peak period and peak direction. The significant wave height is the mean wave height (from trough to crest) of the highest one third of waves and corresponds to the wave height that would be reported by an experienced observer. Peak period is the time interval between two waves of the dominant wave period. Peak direction is the direction from which the dominant waves are coming.

The average sea state is dominated by swells from the south. The annual mean wave height is 1.73 m, the annual mean wave direction is 212° and the annual mean wave period is 13.48 s. In the Pacific, waves often come from multiple directions and for different periods at a time. In Niue, there are often more than four different wave direction/period components coming from the southeast to southwest (Figure 8.13).

Figure 8.13:
Annual wave rose for Niue. Note that direction is where the wave is coming from Seasonal wave height peaks in July, whereas the seasonal wave period peaks in September/October (Figure 8.14). This is related to the intensification of the Southern Ocean storm track during winter (June–August). Conversely, there is slightly reduced wave activity during the summer (December–February) months.

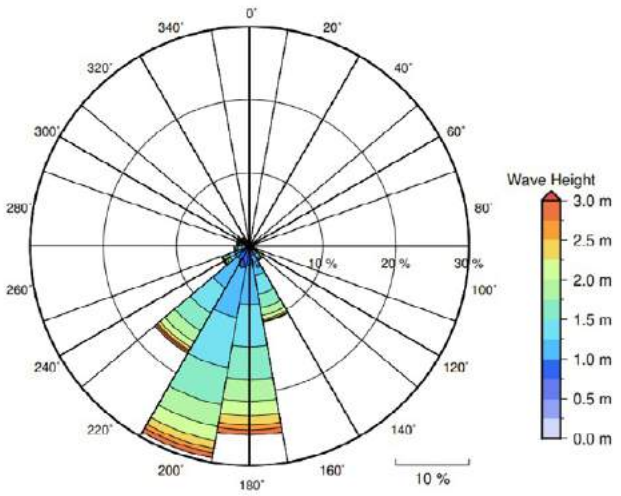

Figure 8.14:
Monthly wave height (black line), wave period (red line) and wave direction (arrows). The grey area represents the range of wave height between calm periods (10% of lowest wave height) and large wave events (10% of highest wave height).

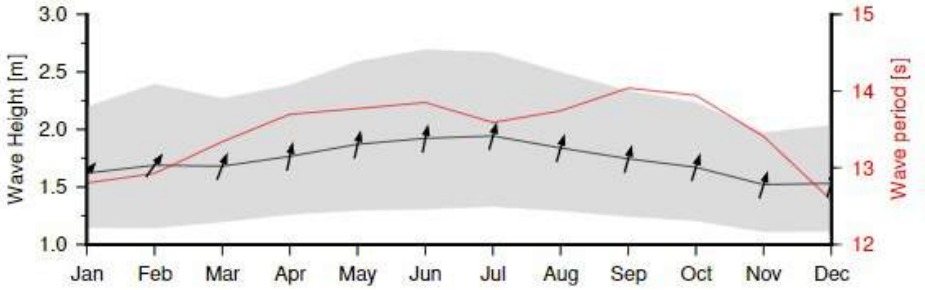

8.9.2 Trends

Waves change from month to month with the seasons, but they also change from year to year with climate oscillations. Typically, these changes are smaller than the seasonal changes but can be important during phenomena such as ENSO. In Niue, the mean annual wave height has remained unchanged since 1979 (Figure 8.15). The mean annual wave height in Niue is not significantly correlated with the main climate indicators of the region.

Figure 8.15:
Annual wave height (black line), wave period (red line) and wave direction (arrows). The grey area represents the range of wave height between calm periods (10% of lowest wave height) and large wave events (10% of highest wave height).

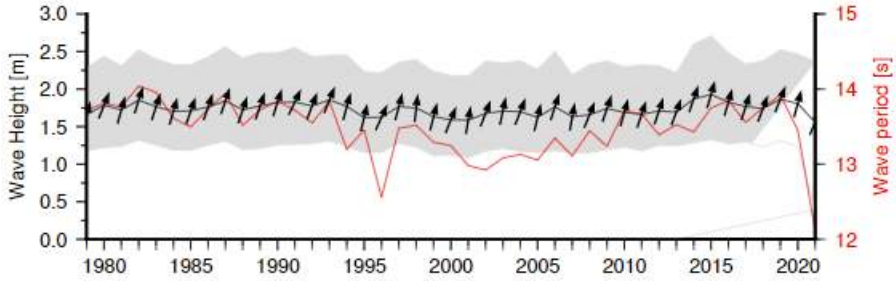

8.9.3 Extreme waves

Extreme wave analysis completed for Niue was done by defining a severe height threshold and fitting a generalized Pareto distribution (GPD). The optimum threshold selected was 3.65 m. In the 42-year wave hindcast, 131 wave events reached or exceeded this threshold, averaging 3.1 per year. The GPD was fitted to the largest wave height reached during each of these events (Figure 8.16, Table 8.4). Extreme wave analysis is a very useful tool but is not always accurate because the analysis is very sensitive to the data available, the type of distribution fitted and the threshold used. For example, this analysis does not accurately account for tropical cyclone waves. More in-depth analysis is required to obtain results appropriate for designing coastal infrastructure and coastal hazard planning.

Figure 8.16:
Extreme wave distribution for Niue. The crosses represent the wave events that have occurred since 1979. The solid line is the statistical distribution that best fits past wave events. The dashed lines show the upper and lower confidence limits of the fit. There is a 95% chance that the fitted distribution lies between the two dashed lines. Note that the annual return interval is in logarithmic scale.

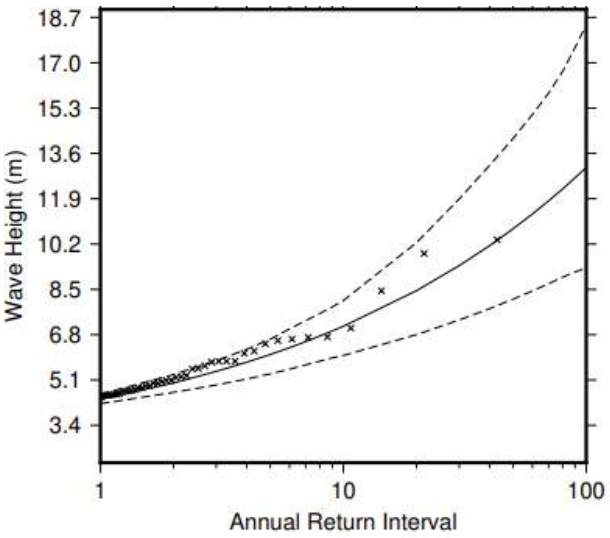

Table 8.4: Summary of the results from extreme wave analysis in Niue

Large wave height (90th percentile)	2.38 m
Severe wave height (99th percentile)	3.41 m
1-year ARI wave height	4.37 m
10-year ARI wave height	7.12 m
20-year ARI wave height	8.45 m
50-year ARI wave height	10.77 m
100-year ARI wave height	13.07 m

9 Palau

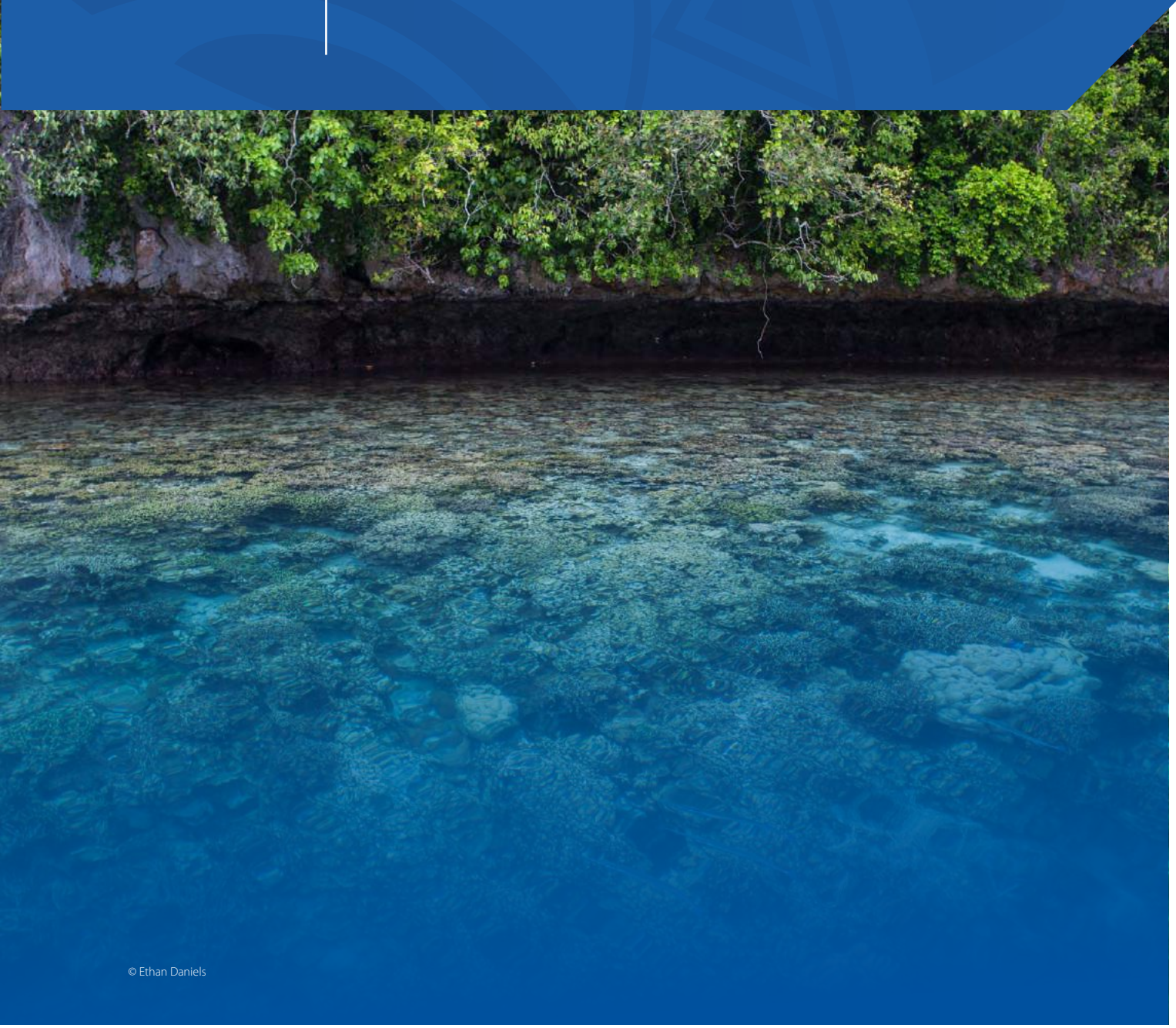

9.1 Summary

9.1.1 Climate

- There is little seasonal variation in air temperature, which is strongly linked to changes in the surrounding ocean temperature. Palau's wet season is from May to October.
- There is a year-round impact on rainfall from the Intertropical Convergence Zone (ITCZ) and Palau's location near the Pacific Warm Pool, which leads to relatively high rainfall through the year.
- Annual and seasonal air temperatures at Koror increased over the period 1952–2017. The annual number of hot days and warm nights has increased, while the number of cool days and cold nights has decreased. The energy required for cooling indoor environments has also increased.
- There has been little change in annual, seasonal and extreme rainfall at Koror.
- Tropical cyclones can affect Palau year-round. Over the period 1969–2017, an average of 31 cyclones passed within Palau's exclusive economic zone (EEZ) per decade. Tropical cyclones were most frequent in neutral El Niño–Southern Oscillation (ENSO) years and least frequent in El Niño years. Year-to-year variability is large, ranging from no tropical cyclones in some years to nine in 1971.
- There has been little change in the number of severe tropical cyclones or the total number of tropical cyclones in the Northwest Pacific since 1981.

9.1.2 Ocean

- Highest sea levels typically occur in the months June–September.
- Sea-level rise at the EEZ, measured by satellite altimeters from 1993 to mid-2020, ranges from about 2 to 3.5 mm (0.08 to 0.14 in) per year.
- Monthly average sea surface temperature (SST) near Koror, as measured by satellite, ranges from approximately 28 °C (82.4 °F) in February to 29.4 °C (84.9 °F) in June. Daily temperatures in any given year can be up to ±2 °C (± 3.6 °F) of these monthly averages.
- The SST trend in the EEZ is 0.24 °C (0.43 °F) per decade.
- Dominant wave direction is from 80° (south), with an average significant wave height of 0.71 m (2.33 ft) and average wave period of 9.19 s.
- Severe wave height was defined as 1.61 m (5.28 ft), with an average of 3.7 severe events per year.
- Peak average significant wave height occurs between November and March.

9.2 Country description

The Republic of Palau is an archipelago located in the equatorial/tropical North Pacific Ocean (Figure 9.1). The nation has approximately 340 islands located between latitudes 3°N and 8°N, and longitudes 131°E and 135°E. Palau has a total land area of 466 km^2 and an EEZ of 0.6 million km^2. Babeldaob, the largest island at 331 km^2, includes the capital, Ngerulmud. The highest elevation is 242 m (794 ft) above sea level on Babeldaob. Palau's population is approximately 18,000. About two thirds of the population live on Koror.

Figure 9.1:
Palau and the location of the climate station used in this report

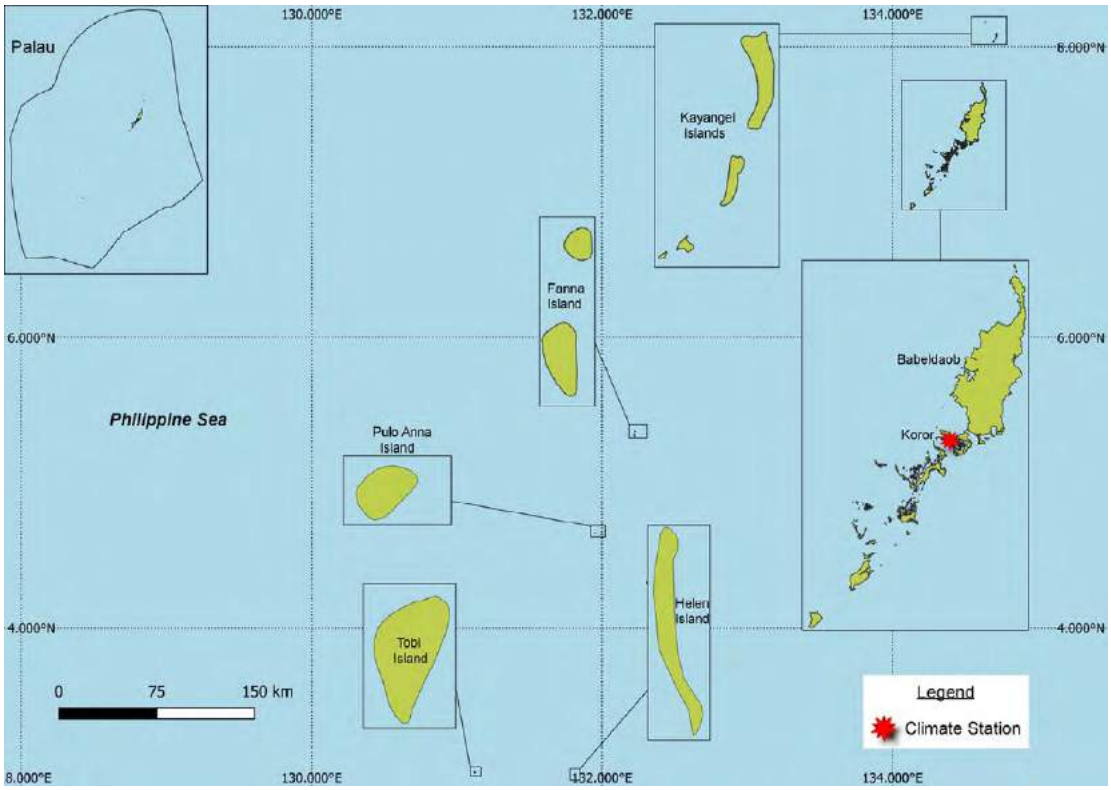

9.3 Data

Daily historical rainfall and air temperature records for Koror Weather Service Office from 1951 were obtained from the United States National Oceanic and Atmospheric Administration Palau Weather Service Office. These records have undergone data quality and homogeneity assessment. Where the maximum or minimum air temperature records were found to have discontinuities, these records have been adjusted to make them homogeneous (further information is provided in Chapter 1). Additional information on historical climate trends for Palau can be found in the Pacific Climate Change Data Portal http://www.bom.gov.au/climate/pccsp.

Tropical cyclone data and historical tracks starting from the 1969 season are available from the Western Northern Hemisphere Tropical Cyclone Data Portal http://www.bom.gov.au/cyclone/history/tracks/beta/?region=wnp.

SST covering the EEZ for Palau was obtained via the daily Optimum Interpolation SST version 2.1 (OISST v2.1) dataset from NOAA (Reynolds et al. 2007; Banzon et al. 2016).

Wave data were obtained from the PACCSAP wave hindcast (Smith et al. 2021), available hourly from 1979 to 2021, with a grid resolution near Palau of 7 km (4.3 mi).

Regional sea level data were obtained from CSIRO satellite altimetry (updated by Benoit Legresy, Church and White 2011), with correction for seasonal signals, inverse barometer effect and glacial isostatic adjustment. Tide-gauge data were sourced from the University of Hawaii Sea Level Center data archive for the Malakal tide-gauge station, spanning from 1990 to 2018 at hourly intervals.

9.4 Rainfall

9.4.1 Seasonal cycle

Palau's location on the edge of the Pacific Warm Pool and the year-long influence of the ITCZ lead to a relatively high average monthly rainfall. Koror's wet season is from May to October, which averages over 2100 mm (82.7 in) of rainfall or 58% or Koror's annual rainfall (Figure 9.2). The WPM is usually most active and brings heavy rainfall during these wet season months. March, the driest month, still averages 207 mm (8.1 in) of rainfall.

Winds are generally moderate, and the northeasterly trades prevail from December through to March. During April, the frequency of trade winds decreases, and there is an increase in the frequency of easterly winds. In May, the winds are predominantly from southeast to northeast.

Figure 9.2:
Mean annual rainfall at Koror

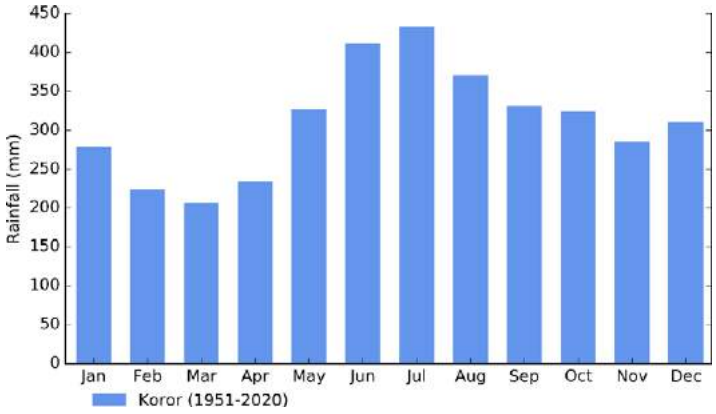

9.4.2 Trends

Trends in annual and seasonal rainfall since 1952 are not statistically significant at Koror (Figure 9.3, Table 9.1). This means there has been little change in annual and seasonal rainfall at this location. Annual rainfall has varied from approximately 2500 to 5500 mm (98.4 to 216.5 in).

Figure 9.3:
Annual rainfall (bar graph) and number of wet days (where rainfall is at least 1 mm; line graph) at Koror. Straight lines indicate linear trends for annual rainfall (in black) and number of wet days (in blue). The magnitudes of the trends are presented in Table 9.1. Diamonds indicate years with insufficient data for one or both variables.

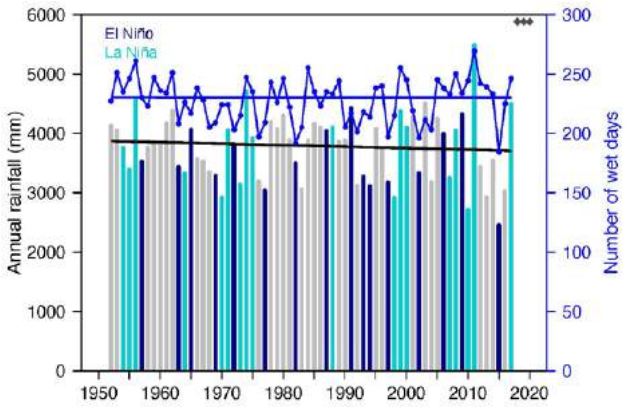

Table 9.1:
Trends in annual, seasonal and extreme rainfall at Koror. The 95% confidence intervals are shown in parentheses. The contribution to total rainfall from extreme events and the standardised rainfall evapotranspiration index are measured relative to 1961–1990 (see Chapter 1 for details).

	Koror
	1952–2017
Annual rainfall (mm/decade)	-24.92 (-103.73, +52.52)
November–April (mm/decade)	-1.43 (-51.70, +54.03)
May–October (mm/decade)	-33.22 (-83.83, +15.96)
Number of wet days (days/decade)	-0.01 (-3.52, +3.34)
Contribution to total rainfall from extreme events (%/decade)	-0.56 (-1.76, +0.63)
Consecutive dry days (days/decade)	0.00 (-0.21, +0.62)
Maximum one-day rainfall (mm/decade)	-4.73 (-10.67, +1.84)
Standardised rainfall evapotranspiration index (November–April)	0.00 (-0.17, +0.16)
Standardised rainfall evapotranspiration index (May–October)	-0.11 (-0.27, +0.07)

Similar to annual and seasonal rainfall, no significant trends in extreme rainfall indices, including the standardised rainfall evapotranspiration drought index, were detected (Table 9.1). Figure 9.4 shows change and variability in the longest run of days without rain and maximum daily rainfall at Koror. Some decade-to-decade variability in maximum daily rainfall is evident, and dry days rarely persist for longer than two weeks, consistent with Koror's tropical location.

Figure 9.4:
Annual longest run of consecutive dry days (bar graph) and maximum daily rainfall (line graph) at Koror. Straight lines indicate linear trends for dry days (in black) and maximum daily rainfall (in blue). The magnitudes of the trends are presented in Table 9.1. Diamonds indicate years with insufficient data for one or both variables.

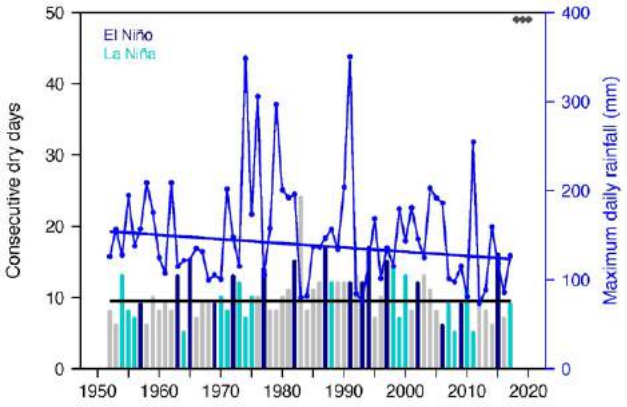

9.5 Air temperature

9.5.1 Seasonal cycle

Air temperatures in Koror have very little seasonal variation throughout the year and are strongly linked to changes in the surrounding ocean temperature. The maximum average temperature for Koror is around 32 °C (89.6 °F), with a minimum average temperature of approximately 25 °C (77.0 °F) and an average difference between the warmest and coolest months of less than 1 °C for both maximum and minimum temperatures (Figure 9.5). There has been a shift towards warmer average monthly temperatures for both maximum and minimum temperatures between the climatology periods of 1961–1990 and 1991–2020. Warmer average temperatures occurred in all months at Koror for the most recent climatology period. The largest increase in average maximum monthly temperatures occurred during the warmer/drier season (November–April).

Figure 9.5:
Maximum and minimum air temperature seasonal cycle for Koror (purple), and for the periods 1961–1990 (dotted lines) and 1991–2020 (solid lines).

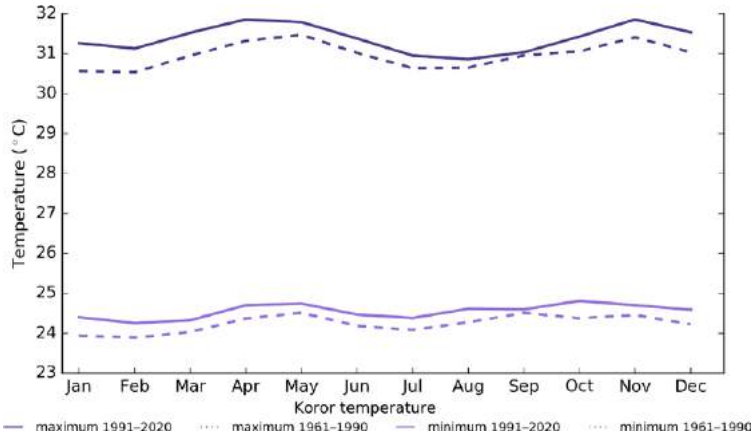

9.5.2 Trends

Average annual and seasonal temperatures have increased significantly at Koror (Figure 9.6, Table 9.2). November–April temperatures have increased faster than May–October temperatures. Year-to-year fluctuations in temperature are typically small and can be attributed to Koror's tropical location.

Figure 9.6:
Average annual, November–April and May–October temperatures for Koror. Straight lines indicate linear trends. The magnitudes of the trends are presented in Table 9.2. Diamonds indicate years with insufficient data for one or more variables.

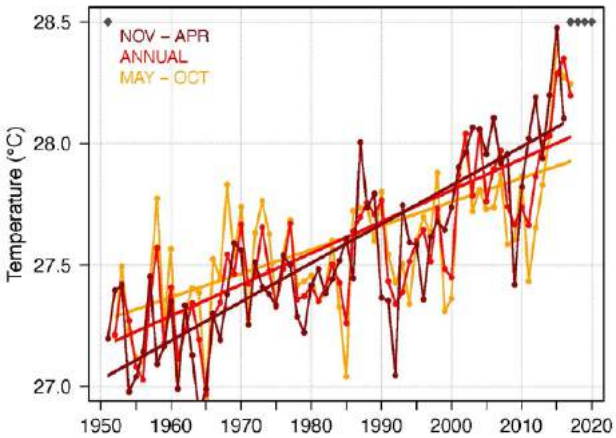

Table 9.2:
Trends in annual and seasonal air temperatures at Koror. The 95% confidence intervals are shown in parentheses, and trends significant at the 95% level are shown in bold.

	Koror Tmax (°C/decade)	Koror Tmin (°C/decade)	Koror Tmean (°C/decade)
	1952–2017		
Annual	**+0.13** (+0.09, +0.18)	**+0.10** (+0.03, +0.17)	**+0.13** (+0.08, +0.17)
November–April	**+0.18** (+0.13, +0.23)	**+0.13** (+0.07, +0.18)	**+0.16** (+0.12, +0.20)
May–October	**+0.08** (+0.04, +0.12)	**+0.10** (+0.03, +0.17)	**+0.10** (+0.05, +0.14)

The number of hot days and warm nights has increased, and the number of cool days and cold nights has decreased at Koror (Table 9.3, Figure 9.7). The number of hot days exhibits large decadal variability. This may be partly due to Koror's tropical location, which requires only small temperature changes for a day to be considered hot, i.e., in the top 10% of days compared to 1961–1990 (see Chapter 1 for details).

The cooling degree days index provides a measure of the energy demand needed to cool a building down to 25 °C (77.0 °F), with the assumption that air conditioners are generally turned on at this temperature. There has been a strong increase in the cooling degree index, suggesting the energy needed for cooling has increased significantly since 1952.

Table 9.3:
Trends in annual temperature extremes at Koror. The 95% confidence intervals are shown in parentheses, and trends significant at the 95% level are shown in bold. Hot and cool days, and warm and cold nights are measured relative to 1961–1990 (see Chapter 1 for details).

	Koror
	1952–2017
Number of hot days (days/decade)	**+13.69** (+7.99, +20.84)
Number of warm nights (nights/decade)	**+9.19** (+3.73, +14.51)
Number of cool days (days/decade)	**-4.30** (-5.92, -2.92)
Number of cold nights (nights/decade)	**-2.75** (-4.79, -0.69)
Cooling degree days (degree days/decade)	**+46.45** (+30.41, +61.43)
Daily temperature range (°C/decade)	+0.03 (-0.05, +0.13)

Figure 9.7:
Annual number of hot days and cold nights at Koror. Straight lines indicate linear trends. The magnitudes of the trends are presented in Table 9.3. Diamonds indicate years with insufficient data for one or both variables.

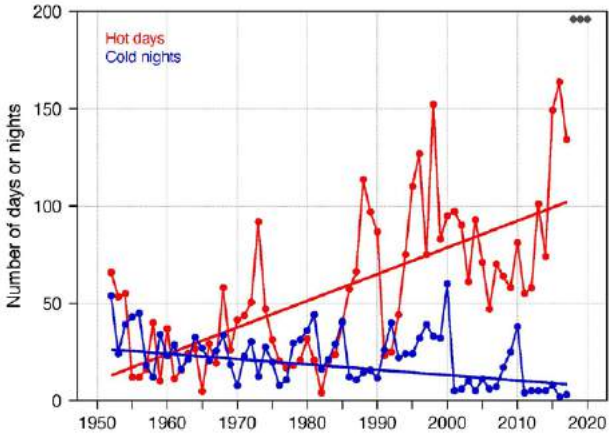

9.6 Tropical cyclones

9.6.1 Seasonal cycle

Tropical cyclones usually affect Palau year-round. The tropical cyclone archive of the western North Pacific indicates that between the 1969 and 2017 seasons, 153 tropical cyclones (Figure 9.8) passed within the EEZ. This represents an average of 31 cyclones per decade. Tropical cyclones were most frequent in neutral years (33 cyclones per decade), followed by La Niña years (31 cyclones per decade) and least frequent in El Niño years (29 cyclones per decade).

Interannual variability in the number of tropical cyclones in the EEZ is large, ranging from zero in some seasons to nine in 1971 (Figure 9.8). High interannual variability and the small number of tropical cyclones occurring in the EEZ make reliable identification of long-term trends in frequency and intensity difficult.

Some tropical cyclone tracks analysed in this section include the tropical depression stage (sustained winds ≤34 knots) before and/or after tropical cyclone formation.

Figure 9.8:
Number of tropical cyclones passing within the Palau EEZ per season. Each season is defined by the ENSO status, with light blue being an El Niño year, dark blue a La Niña year and grey showing a neutral ENSO year. The 11-year moving average is presented as a purple line and considers all years.

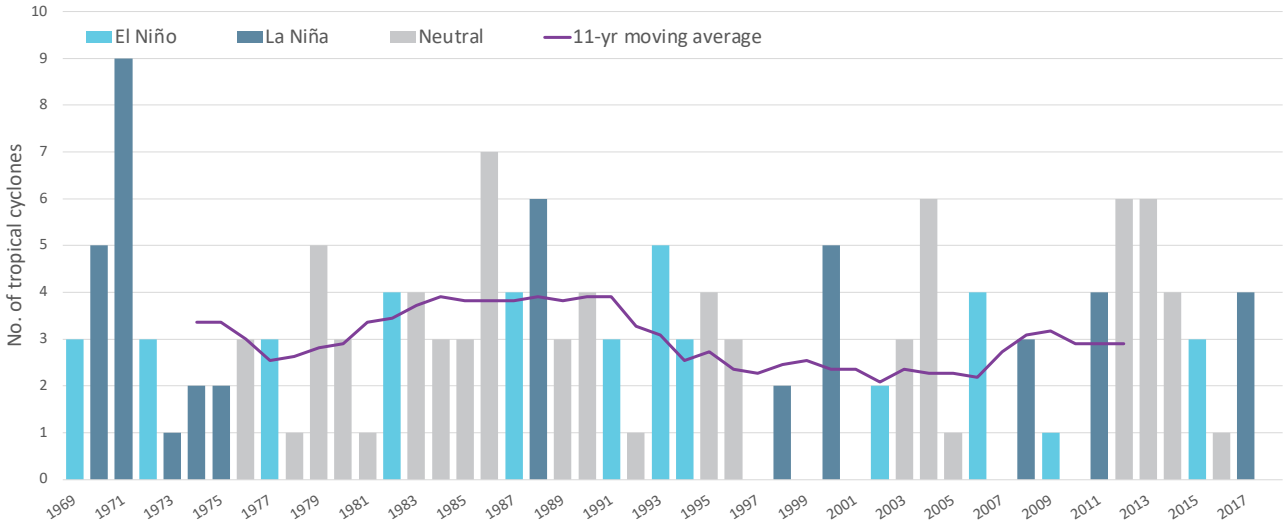

9.6.2 Trends

Trends in total number of tropical cyclones (<995 hPa) and severe tropical cyclones (<970 hPa) are presented for the period 1981–2021 for the Northwest Pacific (125°E–180°W; 0–20°N). Trends are presented at a regional scale as the number of tropical cyclones occurring within Pacific Island EEZs is insufficient for reliable long-term trend analysis.

For the total number of tropical cyclones, the trend (and 95% confidence interval) is -0.56 (-1.84, 0.72) tropical cyclones/decade. There has been little change in the total number of tropical cyclones over the last 41 seasons.

For the total number of severe tropical cyclones, the trend is -0.15 (-1.19, 0.89) tropical cyclones/decade. There has been little change in the number of severe tropical cyclones over the last 41 seasons.

There has also been little change in the proportion of tropical cyclones reaching severe status. The trend is 0.01 (-0.04, 0.05) tropical cyclones/decade.

Records of tropical cyclones exist from the late 1800s in some countries in the Northwest Pacific, but trends in tropical cyclones have only been presented from 1981/82. Satellite-based observations began in the early 1970s, but consistent coverage and reliable intensity estimates have only been available since the early 1980s. Confidence in tropical cyclone trends is moderate as the definition of a tropical cyclone has changed and satellite observation methods have continued to improve over the last 41 years.

9.7 Sea surface temperature

9.7.1 Seasonal cycle

Sea surface temperature, as measured by satellite observations near Koror from 1982 to 2021, reaches on average a maximum of 29.4°C (84.9 °F) in June and then reaches a secondary peak of 29.3 °C (84.7 °F) in November but can get as high as 30.6 °C (87.1 °F) in September (Figure 9.9). Minimum average temperature drops to almost 28 °C (82.4 °F) in February. Daily temperatures can be up to 2 °C (3.6 °F) higher or lower than these monthly averages, although 50% of daily observations fall within 1.0 °C (1.8 °F) of the average.

Figure 9.9:
Annual temperatures near Koror from satellite observations. Blue dots show the monthly average, and shaded boxes show the middle 50% of daily observations. Lines show the top and bottom 25% of daily observations.

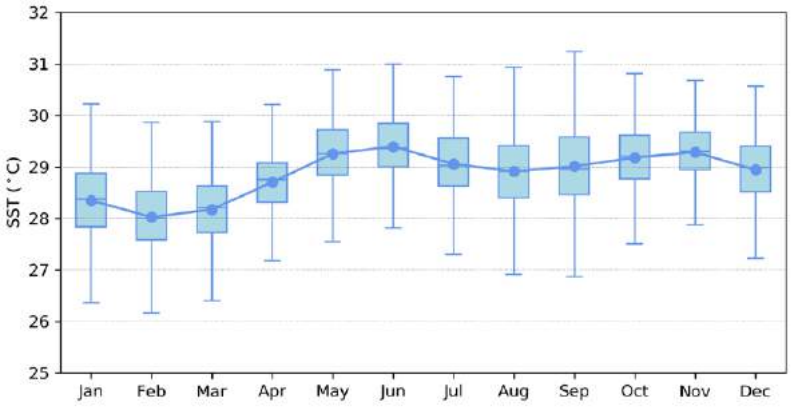

9.7.2 Trends

Figure 9.10 shows the 1981–2021 SST from satellite observations averaged over the Palau EEZ. The data show a trend of 0.24 °C (0.43 °F) per decade with a 95% confidence interval of ±0.05 °C (±0.09 °F).

Figure 9.10:
Sea surface temperature from satellite observations averaged across the Palau EEZ, shown as the orange line. The blue line shows the linear regression trend.

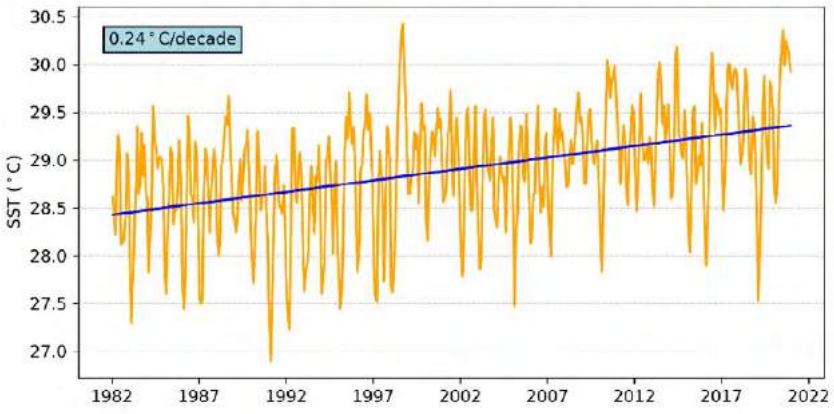

9.8 Sea level

9.8.1 Seasonal cycle

Palau experiences a semidiurnal tidal cycle, meaning two high and two low tides per day. The highest predicted tides of the year typically occur between July and October. Figure 9.11 shows the number of hours the 99th percentile (1.82 m, 5.97 ft) sea level threshold is exceeded per month across the entire sea level record at Malakal Island, Koror. Peak sea levels typically occur between June and September.

Figure 9.11:
Number of hours exceeding 99th percentile sea level threshold per month from 1990 to 2017 at the Malakal Island tide-gauge. Blue shading indicates the number of hours, and the final row provides a percentage summary of all the years.

Number of hours exceeding 1.82 m (Koror, Palau)

	Jan	Feb	Mar	Apr	May	Jun	Jul	Aug	Sep	Oct	Nov	Dec	Annual
1990	0	0	0	0	0	0	0	0	0	0	0	0	0
1991	0	0	0	0	0	0	0	0	0	0	0	0	0
1992	0	0	0	0	0	0	0	0	0	0	0	0	0
1993	0	0	0	0	0	0	0	0	0	0	0	0	0
1994	0	0	0	0	0	0	0	0	0	0	0	0	0
1995	0	0	0	0	0	0	0	0	0	0	0	0	0
1996	0	0	0	0	0	0	0	0	0	0	0	0	0
1997	0	0	0	0	0	0	0	0	0	0	0	0	0
1998	0	0	0	1	1	0	2	1	4	0	1	0	10
1999	0	0	0	0	0	0	8	0	0	0	0	1	9
2000	0	0	0	0	0	0	0	11	0	0	0	0	11
2001	2	2	1	2	1	0	0	0	0	0	0	0	8
2002	0	0	0	0	0	0	0	0	0	0	0	0	0
2003	0	0	0	0	0	0	0	0	0	0	0	0	0
2004	0	0	0	0	0	0	0	0	0	0	0	0	0
2005	0	0	0	0	0	0	0	0	0	0	0	0	0
2006	0	0	0	0	0	0	0	0	0	0	0	0	0
2007	0	0	0	0	0	0	0	0	0	0	0	0	0
2008	0	3	0	0	0	0	1	1	0	1	1	1	8
2009	0	0	0	0	0	0	0	0	0	0	0	0	0
2010	0	0	0	0	0	0	3	0	0	0	0	0	3
2011	0	0	5	0	0	0	0	0	1	0	0	0	6
2012	0	0	0	0	0	0	2	0	0	0	0	0	2
2013	0	0	0	0	0	16	15	0	9	2	2	2	46
2014	0	0	0	0	0	0	0	0	0	0	0	0	0
2015	0	0	0	0	0	0	0	0	0	0	0	0	0
2016	0	0	0	0	0	0	0	0	0	3	0	0	3
2017	0	0	0	0	0	0	0	0	0	0	0	0	0
Monthly Totals (%)	2	5	6	3	2	15	29	12	13	6	4	4	

9.8.2 Trends

Sea level at Palau, measured by satellite altimeters (Figure 9.12) since 1993, has risen between 2 and 3.5 mm (0.08 and 0.14 in) per year, with a 95% confidence interval between ±1 mm (±0.04 in) and ±1.8 mm (±0.07 in). Palau falls in the region with the highest uncertainty in trend estimates in the southern and western/central Pacific.

Figure 9.12:
The satellite altimetry annual trend for the Pacific from 1993 to 2020, with the Palau EEZ highlighted. The star symbol indicates the location of the tide-gauge at Koror.

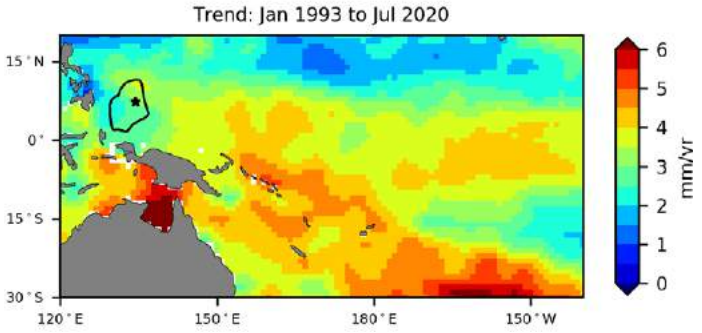

The Malakal Island tide-gauge has sea level data spanning from May 1969 to December 2018. A trend analysis of the data shows a rising trend of 2.31 mm (0.09 in) per year with a confidence interval of ±1.33 mm (±0.05 in), which is very similar to the altimeter trend shown at the location of the star symbol in Figure 9.12. An additional trend analysis was undertaken on the tide-gauge data to match as best as possible the time span of the altimetry, from January 1993 to December 2018. Over this shorter period, the trend becomes 4.89 mm (0.19 in) per year with a confidence interval of ±1.9 mm (±0.07 in), which is higher than the altimetry estimates, suggesting that subsidence has been occurring at Palau in recent decades.

9.9 Waves

9.9.1 Seasonal cycle

The average wave climate in Koror is defined by the significant wave height, peak period and peak direction. The significant wave height is the mean wave height (from trough to crest) of the highest one third of waves and corresponds to the wave height that would be reported by an experienced observer. Peak period is the time interval between two waves of the dominant wave period. Peak direction is the direction from which the dominant waves are coming.

The average sea state is dominated by wind seas from the east. The annual mean wave height is 0.71 m (2.32 ft), the annual mean wave direction is 80° and the annual mean wave period is 9.19 s. In the Pacific, waves often come from multiple directions and for different periods at a time. In Koror, there are often more than three different wave direction/period components coming from the southeast to southwest (Figure 9.13).

Figure 9.13:
Annual wave rose for Koror. Note that direction is where the wave is coming from.

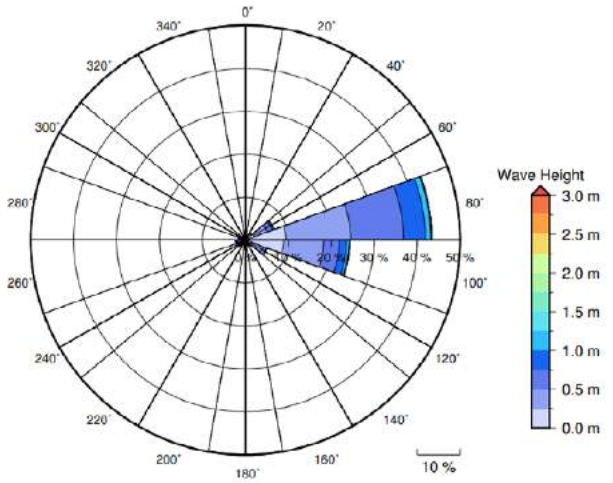

Seasonal wave activity peaks between December and March in terms of both wave height and period (Figure 9.14) due to North Pacific extra-tropical storm activity. Conversely, there is a distinct lull between May and October in wave activity.

Figure 9.14:
Monthly wave height (black line), wave period (red line) and wave direction (arrows). The grey area represents the range of wave height between calm periods (10% of lowest wave height) and large wave events (10% of highest wave height).

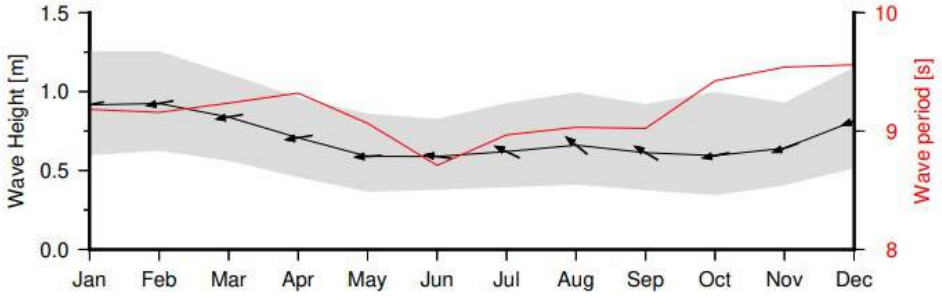

9.9.2 Trends

Waves change from month to month with the seasons, but they also change from year to year with climate oscillations. Typically, these changes are smaller than the seasonal changes but can be important during phenomena such as ENSO. In Koror, the mean annual wave height has remained unchanged since 1979 (Figure 9.15). The mean annual wave height in Koror is not significantly correlated with the main climate indicators of the region.

Figure 9.15:
Annual wave height (black line), wave period (red line) and wave direction (arrows). The grey area represents the range of wave height between calm periods (10% of lowest wave height) and large wave events (10% of highest wave height).

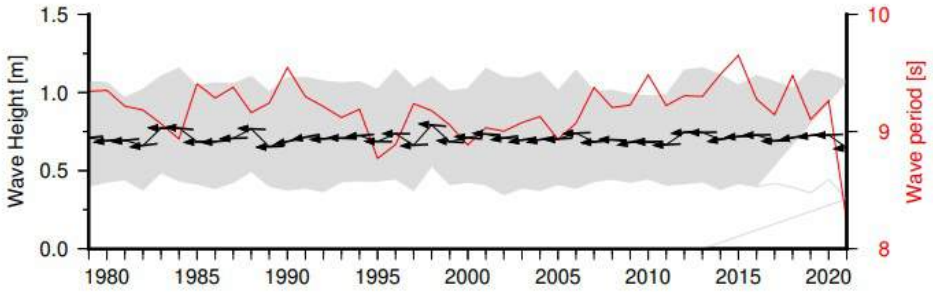

9.9.3 Extreme waves

Extreme wave analysis completed for Koror was done by defining a severe height threshold and fitting a generalized Pareto distribution (GPD). The optimum threshold selected was 1.61 m (5.28 ft). In the 42-year wave hindcast, 155 wave events reached or exceeded this threshold, averaging 3.7 per year. The GPD was fitted to the largest wave height reached during each of these events (Figure 9.16, Table 9.4). Extreme wave analysis is a very useful tool but is not always accurate because the analysis is very sensitive to the data available, the type of distribution fitted and the threshold used. For example, this analysis does not accurately account for tropical cyclone waves. More in-depth analysis is required to obtain results appropriate for designing coastal infrastructure and coastal hazard planning.

Figure 9.16:
Extreme wave distribution for Koror. The crosses represent the wave events that have occurred since 1979. The solid line is the statistical distribution that best fits past wave events. The dashed lines show the upper and lower confidence limits of the fit. There is a 95% chance that the fitted distribution lies between the two dashed lines. Note that the annual return interval is in logarithmic scale.

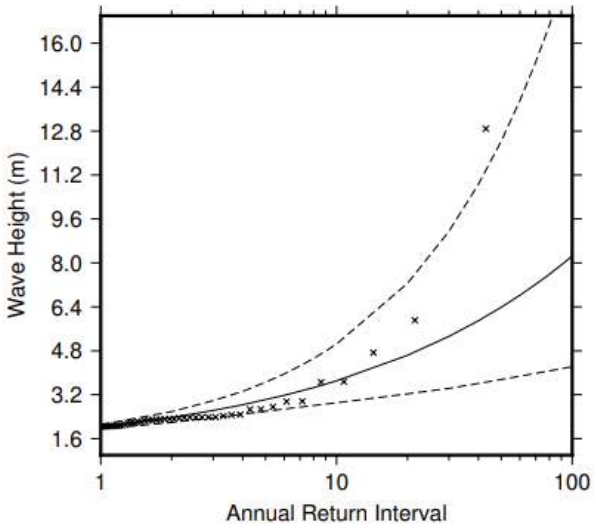

Table 9.4:
Summary of the results from extreme wave analysis in Koror

Large wave height (90th percentile)	1.07 m (3.51 ft)
Severe wave height (99th percentile)	1.54 m (5.05 ft)
1-year ARI wave height	2.03 m (6.66 ft)
10-year ARI wave height	3.70 m (12.14 ft)
20-year ARI wave height	4.64 m (15.22 ft)
50-year ARI wave height	6.38 m (20.93 ft)
100-year ARI wave height	8.25 m (27.07 ft)

10 Papua New Guinea

10.1 Summary

10.1.1 Climate

- Changes in air temperature from season to season for Papua New Guinea (PNG) island locations and along the coast of the mainland are relatively small and strongly linked to changes in the surrounding ocean temperature.
- Port Moresby has a wet season from December to April influenced by the West Pacific Monsoon (WPM), while Momote Airport (Manus Island), further north, has more consistent rainfall through the year influenced by the Intertropical Convergence Zone (ITCZ).
- Annual and seasonal air temperatures at Port Moresby increased over the period 1951–2019. The annual number of hot days and warm nights has increased, while the number of cool days and cold nights has decreased. The energy required for cooling indoor environments has increased and the difference between daytime and night-time temperatures has decreased.
- There has been little change in annual, seasonal and extreme rainfall at Port Moresby and Momote.
- Tropical cyclones usually affect PNG between November and April. Over the period 1969–2018, an average of 16 cyclones passed within the PNG exclusive economic zone (EEZ) per decade. Tropical cyclones were most frequent in neutral El Niño–Southern Oscillation (ENSO) years and least frequent in La Niña years. Year-to-year variability is large, ranging from no tropical cyclones in some seasons to six in the 1971/72 season.
- There has been little change in the total number of tropical cyclones in the Southwest Pacific since 1981/82. The number of severe tropical cyclones has declined over the same period/region.

10.1.2 Ocean

- Highest sea levels typically occur in the months November–February, with the majority in December/January. La Niña brings noticeably higher sea levels in December and January, with the year 2021 representing almost half of the exceedance hours in the 27-year record.
- Sea-level rise within the EEZ, measured by satellite altimeters from 1993 to mid-2020, ranges from about 2.5 to 5.0 mm per year, with highest estimates in the east and southwest.
- Monthly average ocean temperature, as measured by the Lombrum (Manus Island) tide-gauge, ranges from approximately 30 °C in February to 32.7 °C in November and 30.7 °C in May. However, monthly temperatures in any given year can be up to ±2 °C of these averages.
- The sea surface temperature (SST) trend in the EEZ is 0.23 °C per decade.
- Dominant wave direction is from 55° (NE), with an average significant wave height of 0.47 m and average wave period of 9.08 s.
- Severe wave height was defined as 1.23 m, with an average of 2.4 severe events per year.
- Peak average significant wave height occurs between July and September, driven predominantly by strong local winds.

10.2 Country description

The Independent State of Papua New Guinea is located in the equatorial/tropical South Pacific Ocean between latitudes 1°S and 11°S, and longitudes 141°E and 157°E (Figure 10.1). PNG is the world's third-largest island country. The mainland is the eastern half of New Guinea island. Other major islands include New Ireland, New Britain, Manus and Bougainville. There are over 600 lesser islets and atolls to the north and east. PNG has a total land area of 462,840 km^2 and an EEZ of 2.4 million km^2. The highest elevation is 4509 m at Mt Wilhelm. There are several major rivers, including the Sepik River, which runs through lowland swamp plains to the north coast, and the Fly River, which flows to the south coast.

PNG's population is estimated to be just over 9 million. About 87% of the population live in rural areas, with 40% in highlands. PNG's capital, located along its southeast coast, is Port Moresby (population approximately 400,000).

Figure 10.1:
Papua New Guinea and the locations of the climate stations used in this report

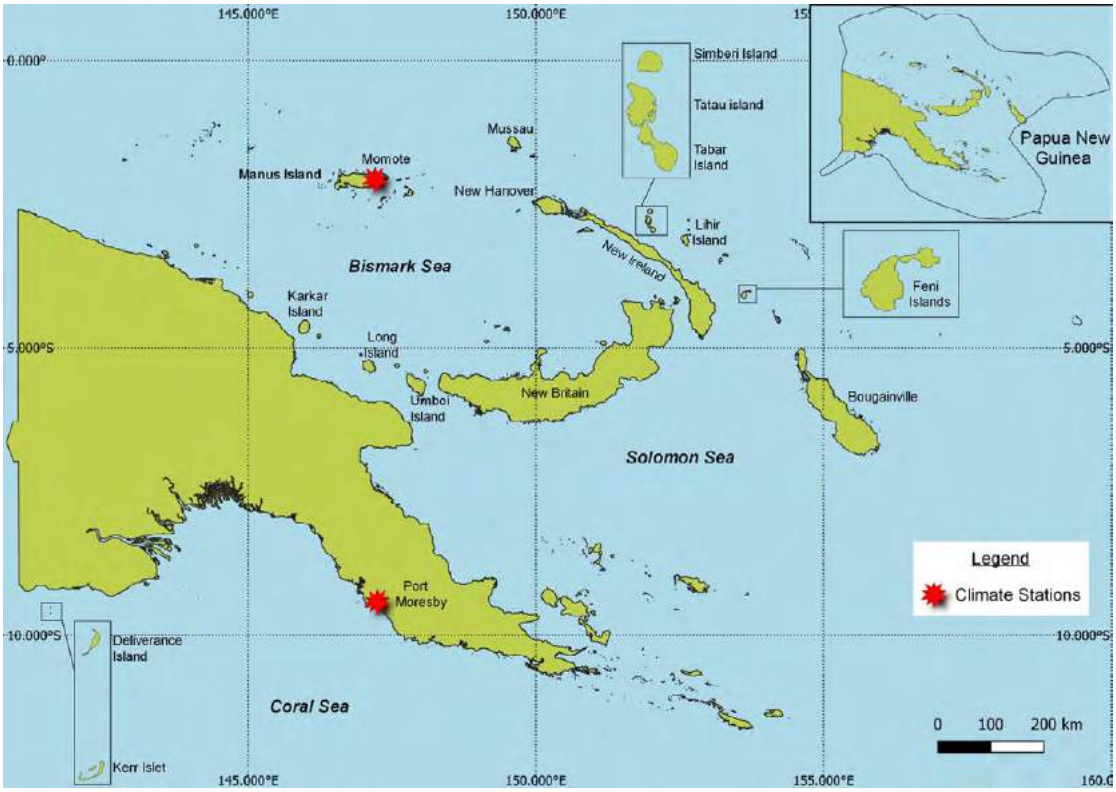

10.3 Data

Daily historical rainfall and air temperature records for Port Moresby and Momote (Manus Island) from 1951 were obtained from the PNG National Weather Service. These records have undergone data quality and homogeneity assessment. Where the maximum or minimum air temperature records were found to have discontinuities, these records have been adjusted to make them homogeneous (further information is provided in Chapter 1). Additional information on historical climate trends for PNG can be found in the Pacific Climate Change Data Portal http://www.bom.gov.au/climate/pccsp.

Tropical cyclone data and historical tracks starting from the 1969/70 season are available from the SHTC Data Portal http://www.bom.gov.au/cyclone/history/tracks/index.shtml.

SST covering the EEZ was obtained via the daily Optimum Interpolation SST version 2.1 (OISST v2.1) dataset from NOAA (Reynolds et al. 2007; Banzon et al. 2016). In situ ocean temperature data were obtained from the PSLGM Project tide-gauge located at Lombrum (Manus Island), with data spanning from 1994 to 2021.

Wave data were obtained from the PACCSAP wave hindcast (Smith et al. 2021), available hourly from 1979 to 2021, with a grid resolution near PNG of 7 km.

Regional sea level data were obtained from CSIRO satellite altimetry (updated by Benoit Legresy, Church and White 2011), with correction for seasonal signals, inverse barometer effect and glacial isostatic adjustment. Tide-gauge data were sourced from the Lombrum tide-gauge station, spanning from 1994 to 2021 at hourly intervals.

10.4 Rainfall

10.4.1 Seasonal cycle

Port Moresby has a wet season between December and April, with 80% of the annual rainfall occurring during these months (Figure 10.2). The WPM is responsible for most of the rainfall in Port Moresby early in the year. During May–October, dry south-easterly winds are more dominant, leading to reduced rainfall.

Momote has more consistent rainfall throughout the year and with an annual total of over 3300 mm, it receives almost three times the amount of rainfall as Port Moresby. The peak rainfall month is July with an average of 383 mm. Due to its location, Momote is strongly influenced by the ITCZ and the Pacific Warm Pool, which act to bring high rainfall throughout the year.

Figure 10.2:
Mean annual rainfall at Port Moresby and Momote

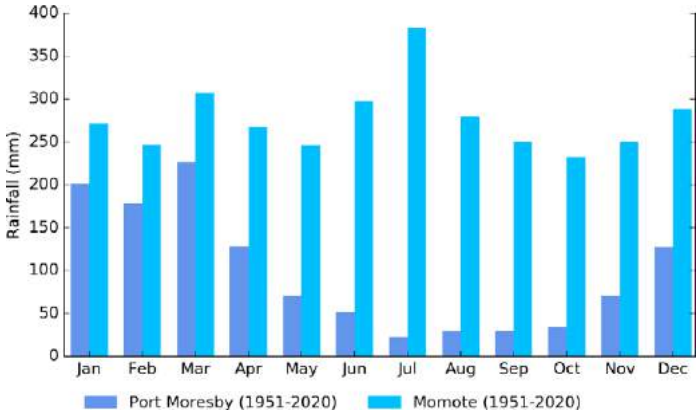

10.4.2 Trends

Trends in annual and seasonal rainfall are not statistically significant at Port Moresby and Momote (Figure 10.3, Table 10.1). This means there has been little change in annual and seasonal rainfall at these sites. Annual rainfall has varied from approximately 600 to 1600 mm at Port Moresby and from approximately 1600 to 4700 mm at Momote.

Figure 10.3:
Annual rainfall (bar graph) and number of wet days (where rainfall is at least 1 mm; line graph) at Port Moresby (left) and Momote (right). Straight lines indicate linear trends for annual rainfall (in black) and number of wet days (in blue). The magnitudes of the trends are presented in Table 10.1. Diamonds indicate years with insufficient data for one or both variables.

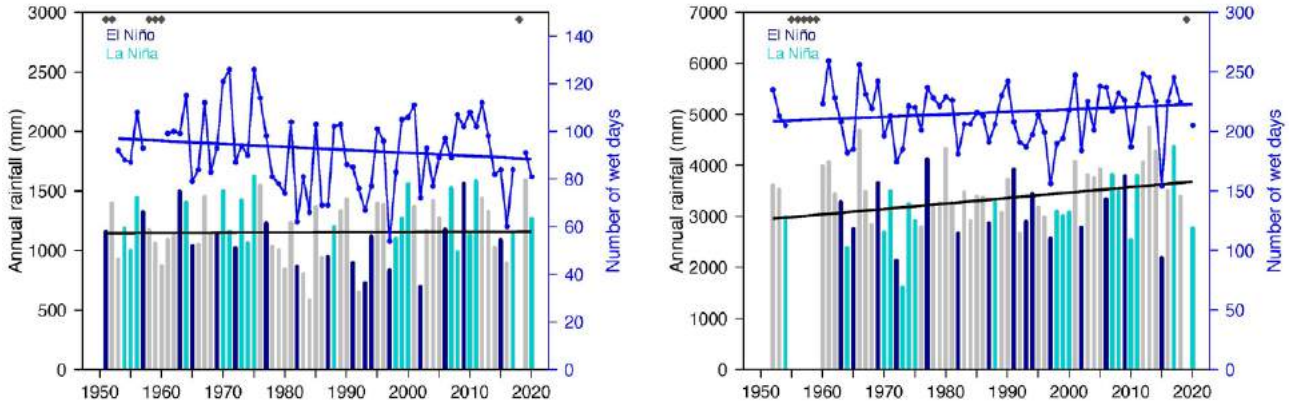

Table 10.1:
Trends in annual, seasonal and extreme rainfall at Port Moresby (left) and Momote (right). The 95% confidence intervals are shown in parentheses. The contribution to total rainfall from extreme events and the standardised rainfall evapotranspiration index are measured relative to 1961–1990 (see Chapter 1 for details). The standardised rainfall evapotranspiration index is not available for Momote due to the lack of daily temperature observations at this site.

	Port Moresby	Momote
	1951–2020	1952–2020
Annual rainfall (mm/decade)	+1.98 (-43.98, +40.46)	+107.02 (-6.69, +201.38)
November–April (mm/decade)	-3.57 (-35.50, +26.04)	+15.86 (-25.30, +57.64)
May–October (mm/decade)	+8.00 (-7.11, +21.33)	+76.60 (-2.28, +142.43)
Number of wet days (days/decade)	-1.27 (-4.54, +1.81)	+2.05 (-2.72, +6.22)
Contribution to total rainfall from extreme events (%/decade)	+1.16 (-0.42, +2.62)	+0.59 (-0.37, +1.54)
Consecutive dry days (days/decade)	+0.25 (-2.14, +2.61)	0.00 (-0.31, +0.64)
Maximum one-day rainfall (mm/decade)	+5.12 (-0.69, +10.61)	+2.25 (-2.16, +6.87)
Standardised rainfall evapotranspiration index (November–April)	0.00 (-0.20, +0.16)	-
Standardised rainfall evapotranspiration index (May–October)	+0.14 (-0.03, +0.29)	-

Similar to annual and seasonal rainfall, no significant trends in extreme rainfall indices, including the standardised rainfall evapotranspiration drought index, were detected (Table 10.1). Figure 10.4 shows change and variability in the longest run of days without rain and maximum daily rainfall at Port Moresby and Momote. Substantial variability associated with ENSO is evident at both sites, with El Niño years typically experiencing longer dry spells than La Niña years.

Figure 10.4:
Annual longest run of consecutive dry days (bar graph) and maximum daily rainfall (line graph) at Port Moresby (left) and Momote (right). Straight lines indicate linear trends for dry days (in black) and maximum daily rainfall (in blue). The magnitudes of the trends are presented in Table 10.1. Diamonds indicate years with insufficient data for one or both variables.

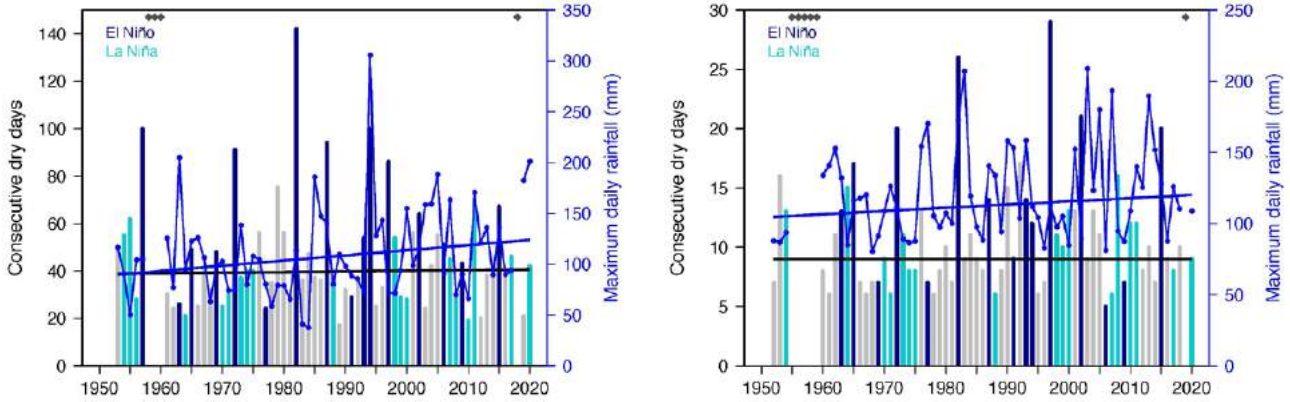

10.5 Air temperature

10.5.1 Seasonal cycle

Coastal locations on the PNG mainland and offshore islands experience small seasonal variations in temperature (Figure 10.5), the largest of which is a maximum temperature range of 1.3 °C at Port Moresby for the 1961–1990 climatology period and 1.2 °C for the 1991–2020 period. There is a peak in maximum temperature during the wet season and a minimum during the dry season months of June–August. The seasonal range in temperature is less than 1 °C for minimum temperature and for both daytime and night-time temperatures at Momote station on Manus Island, which is more strongly influenced by the surrounding sea surface temperature.

There has been a clear shift towards warmer average minimum monthly temperatures between the climatology periods of 1961–1990 and 1991–2020 (Figure 10.5) at Port Moresby and Momote. For maximum temperatures at Port Moresby, temperatures are warmer during the first few months of the year for the most recent climatology period but similar between the earlier and later climatology period for the remainder of the year.

Figure 10.5:
Maximum and minimum air temperature seasonal cycle for Port Moresby (purple) and Momote (green), and for the periods 1961–1990 (dotted lines) and 1991–2020 (solid lines)

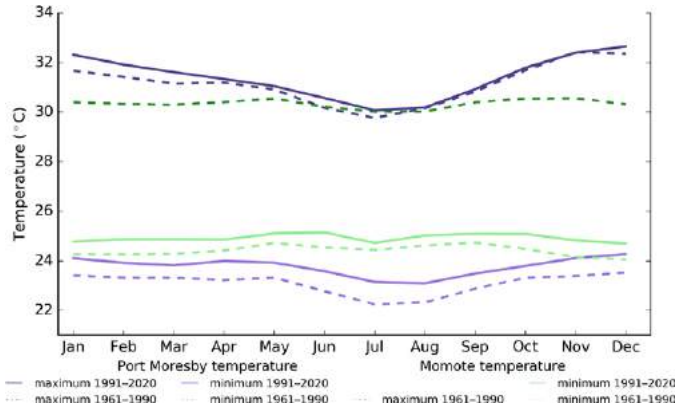

10.5.2 Trends

Average annual and seasonal temperatures have increased significantly at Port Moresby (Figure 10.6). Daily minimum temperatures are warming faster than daily maximum temperatures (Table 10.2). The small year-to-year fluctuations in temperature can be attributed to Port Moresby's tropical location.

Figure 10.6:
Average annual, November–April and May–October temperatures for Port Moresby. Straight lines indicate linear trends. The magnitudes of the trends are presented in Table 10.2. Diamonds indicate years with insufficient data for one or more variables.

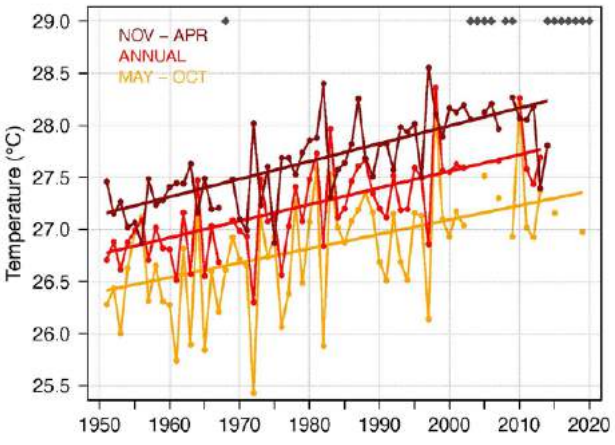

Table 10.2:
Trends in annual and seasonal air temperatures at Port Moresby. The 95% confidence intervals are shown in parentheses, and trends significant at the 95% level are shown in bold.

	Port Moresby Tmax (°C/decade)	Port Moresby Tmin (°C/decade)	Port Moresby Tmean (°C/decade)
	1951–2019		
Annual	**+0.11** (+0.05, +0.16)	**+0.21** (+0.17, +0.25)	**+0.16** (+0.13, +0.19)
November–April	**+0.12** (+0.07, +0.16)	**+0.23** (+0.18, +0.27)	**+0.17** (+0.14, +0.20)
May–October	**+0.08** (+0.01, +0.17)	**+0.22** (+0.17, +0.27)	**+0.14** (+0.08, +0.20)

The number of hot days and warm nights has increased, and the number of cool days and cold nights has decreased at Port Moresby (Table 10.3, Figure 10.7). The high year-to-year variability in the number of hot days and cold nights may be related to Port Moresby's tropical location, which requires only small temperature increases for a day to be considered hot or a night to be considered cold, i.e., to be in the hottest or coldest 10% of days or nights compared to 1961–1990 (see Chapter 1 for details).

The cooling degree days index provides a measure of the energy demand needed to cool a building down to 25 °C, with the assumption that air conditioners are generally turned on at this temperature. There has been a strong increase in the cooling degree index, suggesting the energy needed for cooling has increased significantly since 1951. The difference between daytime and night-time temperatures has also been decreasing (Table 10.3).

Table 10.3:
Trends in annual temperature extremes at Port Moresby. The 95% confidence intervals are shown in parentheses, and trends significant at the 95% level are shown in bold. Hot and cool days, and warm and cold nights are measured relative to 1961–1990 (see Chapter 1 for details).

	Port Moresby
	1951–2020
Number of hot days (days/decade)	**+4.81** (+2.23, +7.97)
Number of warm nights (nights/decade)	**+8.47** (+5.46, +11.23)
Number of cool days (days/decade)	**-4.55** (-7.56, -2.00)
Number of cold nights (nights/decade)	**-7.09** (-9.56, -5.41)
Cooling degree days (degree days/decade)	**+49.96** (+36.72, +65.84)
Daily temperature range (°C/decade)	**-0.13** (-0.25, -0.02)

Figure 10.7:
Annual number of hot days and cold nights at Port Moresby. Straight lines indicate linear trends. The magnitudes of the trends are presented in Table 10.3. Diamonds indicate years with insufficient data for one or both variables.

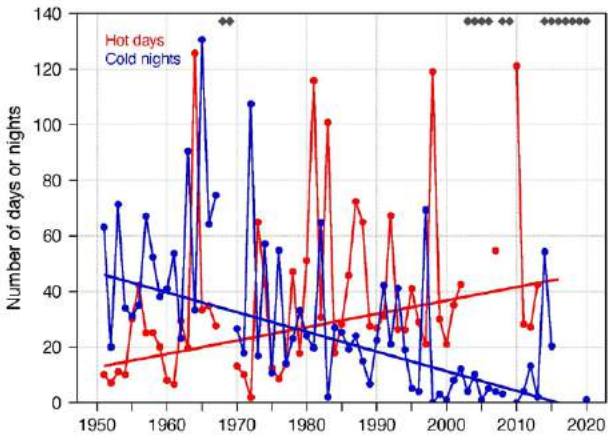

10.6 Tropical cyclones

10.6.1 Seasonal cycle

Tropical cyclones usually affect PNG during the southern hemisphere tropical cyclone season, which is from November to April, but also occasionally occur outside the tropical cyclone season. The Southern Hemisphere Tropical Cyclone Archive indicates that between the 1969/70 and 2017/18 seasons, 80 tropical cyclones (Figure 10.8) passed within the EEZ. This represents an average of 16 cyclones per decade. Tropical cyclones were most frequent in neutral years (18 cyclones per decade), followed by La Niña years (16 cyclones per decade) and least frequent in El Niño years (14 cyclones per decade).

Interannual variability in the number of tropical cyclones in the EEZ is large, ranging from zero in some seasons to six in 1971/72 and five in 2013/14 (Figure 10.8). High interannual variability and the small number of tropical cyclones occurring in the EEZ make reliable identification of long-term trends in frequency and intensity difficult.

Some tropical cyclone tracks analysed in this section include the tropical depression stage (sustained winds ≤34 knots) before and/or after tropical cyclone formation.

Figure 10.8:
Number of tropical cyclones passing within the PNG EEZ per season. Each season is defined by the ENSO status, with light blue being an El Niño year, dark blue a La Niña year and grey showing a neutral ENSO year. The 11-year moving average is presented as a purple line and considers all years.

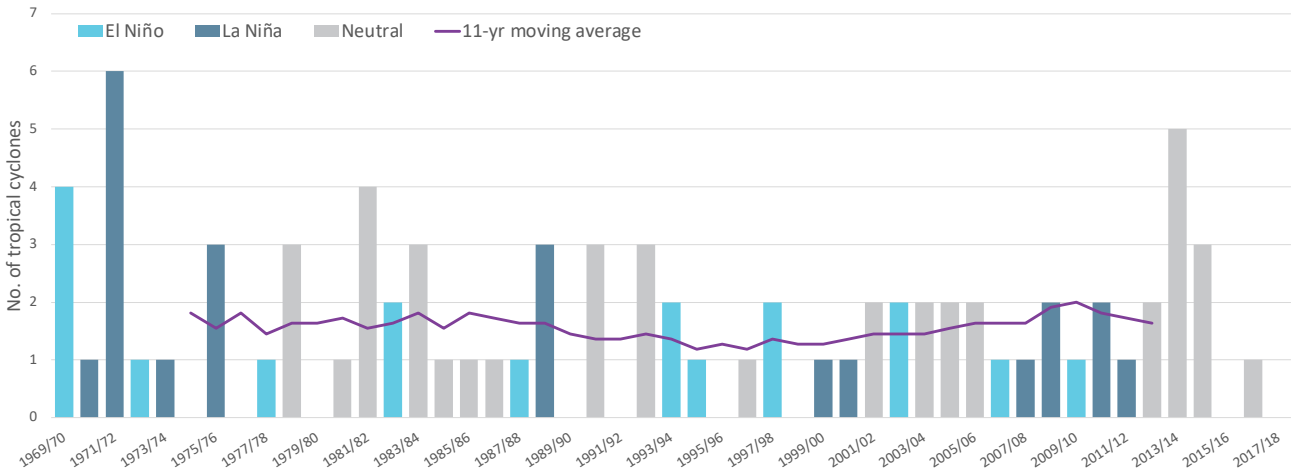

10.6.2 Trends

Trends in total number of tropical cyclones (<995 hPa) and severe tropical cyclones (<970 hPa) are presented for the period 1981/82–2020/21 for the greater Southwest Pacific (135°E–120°W; 0–50°S). Trends are presented at a regional scale as the number of tropical cyclones occurring within Pacific Island EEZs is insufficient for reliable long-term trend analysis.

For the total number of tropical cyclones, the trend (and 95% confidence interval) is -0.92 (-1.85, 0.01) tropical cyclones/decade. There has been little change/marginal decline in the total number of tropical cyclones over the last 40 seasons. This trend is not statistically significant.

For the total number of severe tropical cyclones, the trend is -0.80 (-1.32, -0.29) tropical cyclones/decade. There is a negative trend in the number of severe tropical cyclones over the last 40 seasons. There has been little change/marginal decline in the proportion of tropical cyclones reaching severe status. The trend is -0.04 (-0.08, 0.00) tropical cyclones/decade. The negative trend is statistically significant.

Records of tropical cyclones exist from the late 1800s in some countries in the Southwest Pacific, but trends in tropical cyclones have only been presented from 1981/82. Satellite-based observations began in the Southwest Pacific in the early 1970s, but consistent coverage and reliable intensity estimates have only been available since the early 1980s. Confidence in tropical cyclone trends is moderate as the definition of a tropical cyclone has changed and satellite observation methods have continued to improve over the last 40 years.

10.7 Sea surface temperature

10.7.1 Seasonal cycle

Ocean temperature, as measured by the Lombrum tide-gauge from 1994 to 2021, reaches on average a maximum of approximately 31 °C in November with a secondary peak of 30.7 °C in May but can get as high as 32.7 °C in December (Figure 10.9). Minimum average temperature reaches almost 30 °C in February. There is little seasonal variation in the averages. However, hourly temperatures can be up to 2.0 °C higher or lower than these monthly averages, although 50% of hourly observations fall within 1.0 °C of the average.

Figure 10.9:
Annual temperatures measured at the Lombrum tide gauge. Blue dots show the monthly average, and shaded boxes show the middle 50% of hourly observations. Lines show the top and bottom 25% of hourly observations.

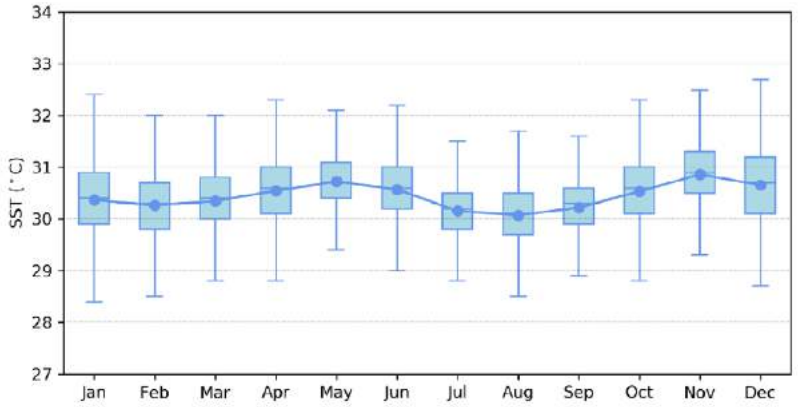

10.7.2 Trends

Figure 10.10 shows the 1981–2021 sea surface temperature (SST) from satellite observations averaged over the EEZ. The data show a trend of 0.23 °C per decade with a 95% confidence interval of ±0.05 °C.

Figure 10.10:
Sea surface temperature from satellite observations averaged across the PNG EEZ, shown as the orange line. The blue line shows the linear regression trend.

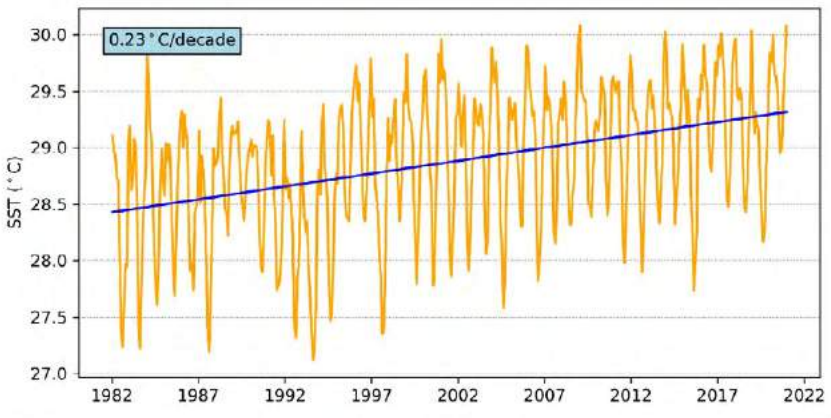

10.8 Sea level

10.8.1 Seasonal cycle

Tidal analysis of Lombrum sea level data shows that it experiences a diurnal tide, meaning only one high and one low tide per day. The highest predicted tides of the year typically occur mostly in December and January. Figure 10.11 shows the number of hours the 99th percentile (1.29 m) sea level threshold is exceeded per month across the entire sea level record at Lombrum. Peak sea levels typically occur between November and February, but they are mostly confined to December/January. La Niña years typically have higher sea levels in December and January. The year 2021 alone accounts for almost half of all exceedance hours in the record.

Figure 10.11:
Number of hours exceeding 99th percentile sea level threshold per month from 1994 to 2021 at the Lombrum tide-gauge. Blue shading indicates the number of hours, and the final row provides a percentage summary of all the years.

Number of hours exceeding 1.29 m (Lombrum, Papua New Guinea)

	Jan	Feb	Mar	Apr	May	Jun	Jul	Aug	Sep	Oct	Nov	Dec	Annual
1994	0	0	0	0	0	0	0	0	0	0	0	0	0
1995	0	0	0	0	0	0	0	0	0	0	0	0	0
1996	0	0	0	0	0	0	0	0	0	0	0	0	0
1997	0	0	0	0	0	0	0	0	0	0	0	0	0
1998	0	0	0	0	0	0	0	0	0	0	0	0	0
1999	0	0	0	0	0	0	0	0	0	0	0	0	0
2000	0	0	0	0	0	0	0	0	0	0	0	0	0
2001	0	2	0	0	0	0	0	0	0	0	0	0	2
2002	0	0	0	0	0	0	0	0	0	0	0	0	0
2003	0	0	0	0	0	0	0	0	0	0	0	0	0
2004	0	0	0	0	0	0	0	0	0	0	0	0	0
2005	0	0	0	0	0	0	0	0	0	0	0	1	1
2006	10	0	0	0	0	0	0	0	0	0	0	0	10
2007	0	0	0	0	0	0	0	0	0	0	4	2	6
2008	0	2	0	0	0	0	0	0	0	0	0	4	6
2009	13	3	0	0	0	0	0	0	0	0	0	0	16
2010	0	0	0	0	0	0	0	0	0	0	3	5	8
2011	5	1	0	0	2	0	0	0	0	0	0	8	16
2012	6	0	0	0	0	0	0	0	0	0	0	0	6
2013	5	0	0	0	0	0	0	0	0	0	0	0	5
2014	7	0	0	0	0	0	0	0	0	0	0	0	7
2015	0	0	0	0	0	0	0	0	0	0	0	0	0
2016	0	0	0	0	0	0	0	0	0	0	0	0	0
2017	0	0	0	0	0	0	0	0	0	0	0	1	1
2018	17	0	0	1	0	0	4	0	0	4	0	2	28
2019	0	0	0	0	0	0	0	0	0	0	0	0	0
2020	0	0	0	0	0	0	0	0	0	1	0	13	14
2021	34	10	0	0	0	0	4	0	0	0	8	50	106
Monthly Totals (%)	42	8	0	0	1	0	3	0	0	2	6	37	

10.8.2 Trends

Sea level at PNG, measured by satellite altimeters (Figure 10.12) since 1993, has risen between 2.5 and 5.0 mm per year, with highest estimates in the east and southwest (around Torres Strait and the Gulf of Papua). For most of the Papua New Guinea EEZ, sea-level rise is larger than the global average of 3.1 ± 0.4 mm per year (von Schuckmann et al. 2021). The 95% confidence interval ranges from ±0.6 to ±1.2 mm. This rise is partly linked to a pattern related to climate variability from year to year and decade to decade.

Trend estimates at the Lombrum tide-gauge over a shorter time span than the altimetry observations (September 1994 to July 2020) are provided in the PSLGM Monthly Data Report for July 2020 (http://www.bom.gov.au/ntc/IDO60101/IDO60101.202007.pdf). For Lombrum, the trend is reported as 5.1 mm per year, a higher trend than the altimetry trends shown in Figure 10.12 (tide-gauge indicated by star symbol). This difference is most likely attributed to subsidence occurring at Lombrum (Brown et al. 2020).

Figure 10.12:
The satellite altimetry annual trend for the Pacific from 1993 to 2020, with the PNG EEZ highlighted. The star symbol indicates the location of the tide-gauge at Lombrum, Manus Island.

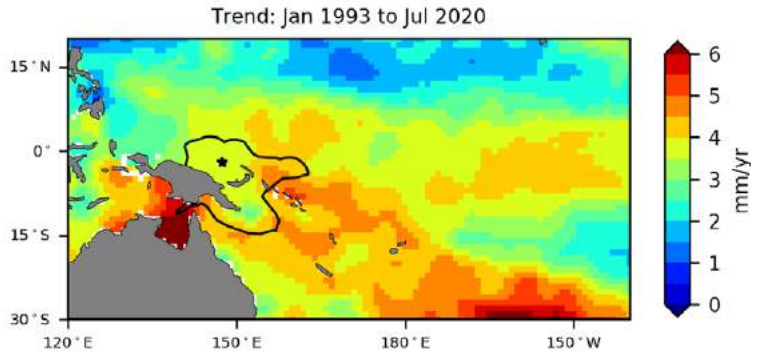

10.9 Waves

10.9.1 Seasonal cycle

The average wave climate in Madang (south of Karkar Island in the Bismarck Sea) is defined by the significant wave height, peak period and peak direction. The significant wave height is the mean wave height (from trough to crest) of the highest one third of waves and corresponds to the wave height that would be reported by an experienced observer. Peak period is the time interval between two waves of the dominant wave period. Peak direction is the direction from which the dominant waves are coming.

The average sea state is dominated by wind seas from the northeast. The annual mean wave height is 0.47 m, the annual mean wave direction is 55° and the annual mean wave period is 9.08 s. In the Pacific, waves often come from multiple directions and for different periods at a time. In Madang, there are often more than four different wave direction/period components coming from the southeast to southwest (Figure 10.13).

Figure 10.13:
Annual wave rose for Madang. Note that direction is where the wave is coming from.

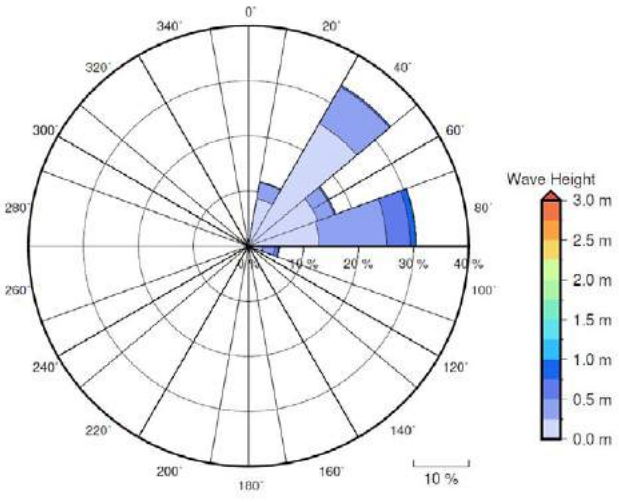

The significant wave height peaks around August. However, the period peaks between November and March, and is significantly less between June and September (Figure 10.14), showing that waves at PNG are predominantly driven by strong easterly local winds between July and September.

Figure 10.14:
Monthly wave height (black line), wave period (red line) and wave direction (arrows). The grey area represents the range of wave height between calm periods (10% of lowest wave height) and large wave events (10% of highest wave height).

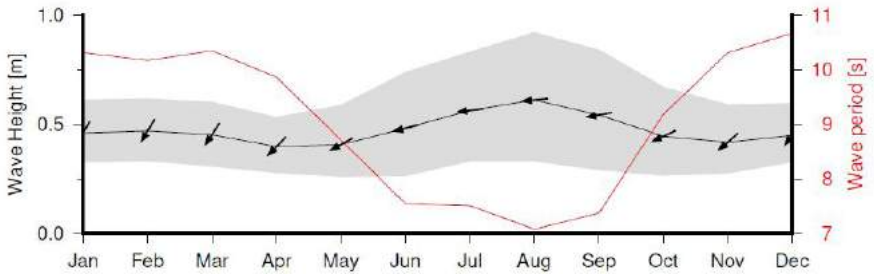

10.9.2 Trends

Waves change from month to month with the seasons, but they also change from year to year with climate oscillations. Typically, these changes are smaller than the seasonal changes but can be important during phenomena such as ENSO. At Madang, the mean annual wave height has remained unchanged since 1979 (Figure 10.15). The mean annual wave height in Madang is not significantly correlated with the main climate indicators of the region.

Figure 10.15:
Annual wave height (black line), wave period (red line) and wave direction (arrows). The grey area represents the range of wave height between calm periods (10% of lowest wave height) and large wave events (10% of highest wave height).

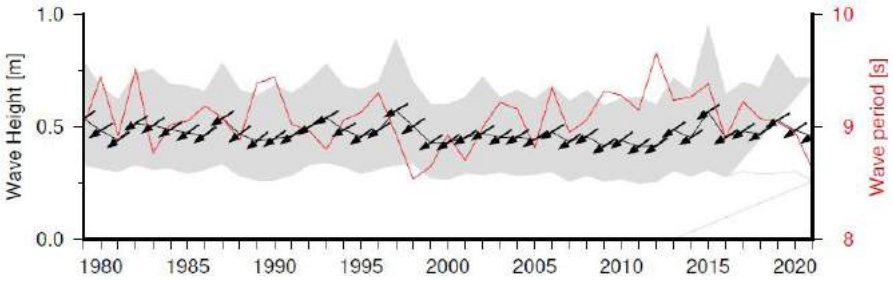

10.9.3 Extreme waves

Extreme wave analysis completed for Madang was done by defining a severe height threshold and fitting a generalized Pareto distribution (GPD). The optimum threshold selected was 1.23 m. In the 42-year wave hindcast, 102 wave events reached or exceeded this threshold, averaging 2.4 events per year. The GPD was fitted to the largest wave height reached during each of these events (Figure 10.16, Table 10.4). Extreme wave analysis is a very useful tool but is not always accurate because the analysis is very sensitive to the data available, the type of distribution fitted and the threshold used. For example, this analysis does not accurately account for tropical cyclone waves. More in-depth analysis is required to obtain results appropriate for designing coastal infrastructure and coastal hazard planning.

Figure 10.16:
Extreme wave distribution for Madang. The crosses represent the wave events that have occurred since 1979. The solid line is the statistical distribution that best fits past wave events. The dashed lines show the upper and lower confidence limits of the fit. There is a 95% chance that the fitted distribution lies between the two dashed lines. Note that the annual return interval is in logarithmic scale.

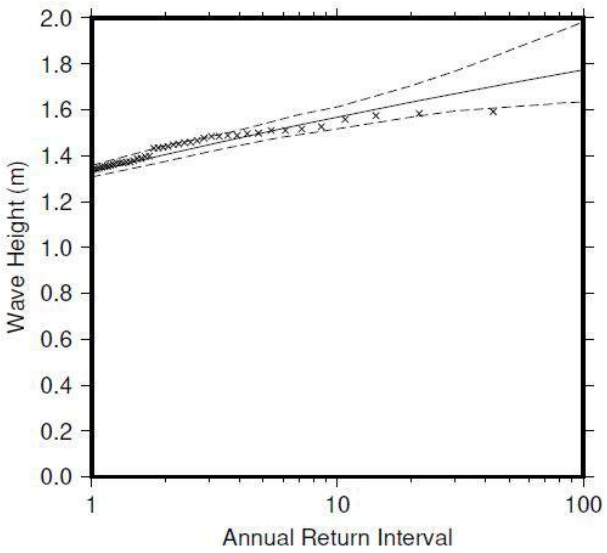

Table 10.4:
Summary of the results from extreme wave analysis in Madang

Large wave height (90th percentile)	0.69 m
Severe wave height (99th percentile)	0.99 m
1-year ARI wave height	1.33 m
10-year ARI wave height	1.57 m
20-year ARI wave height	1.63 m
50-year ARI wave height	1.71 m
100-year ARI wave height	1.77 m

11 Samoa

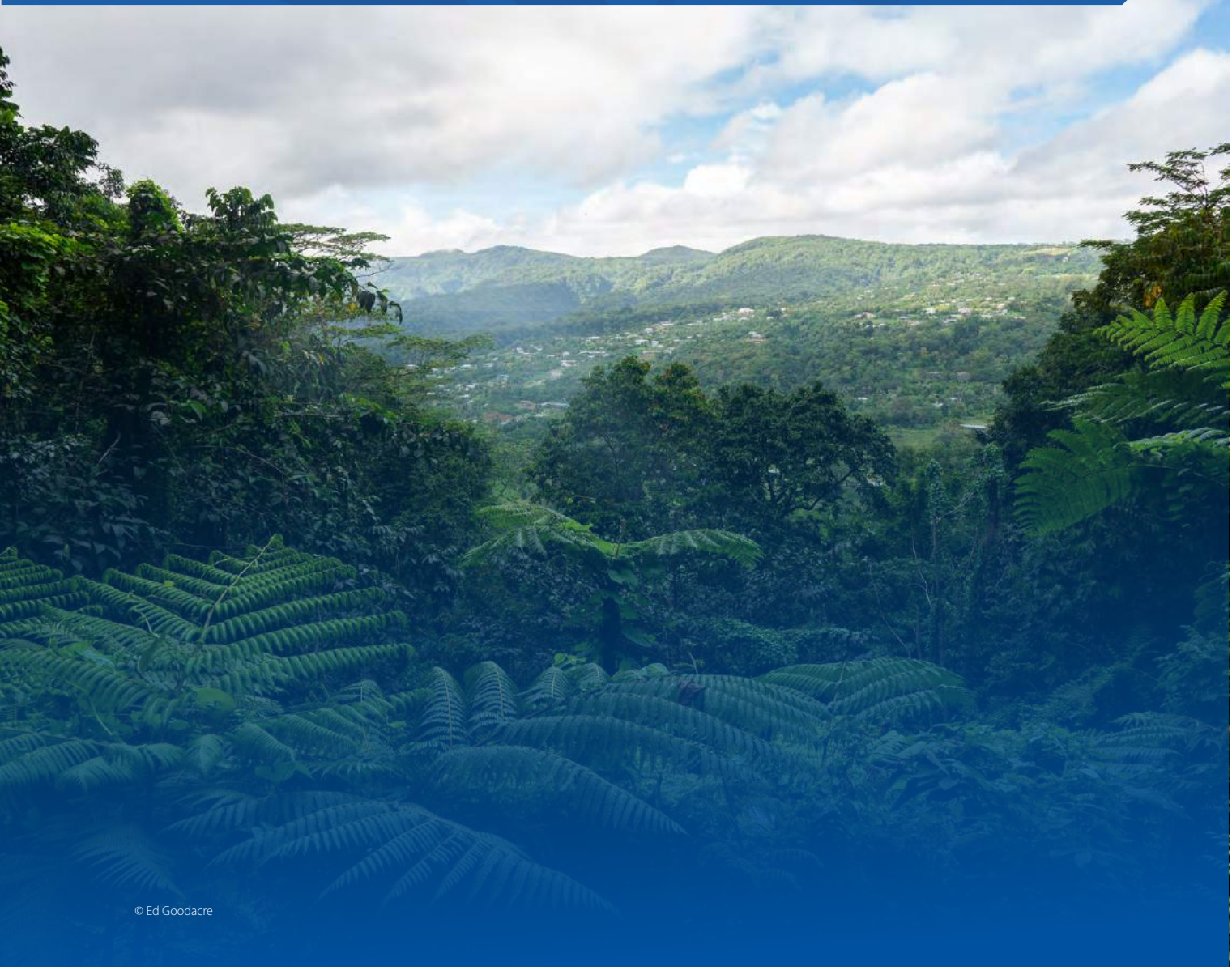

© Ed Goodacre

11.1 Summary

11.1.1 Climate

- Changes in air temperature from season to season are relatively small and strongly linked to changes in the surrounding ocean temperature. Samoa has two distinct seasons – a warm wet season from November to April and a slightly cooler dry season from May to October.
- The seasonal cycle is strongly affected by the South Pacific Convergence Zone (SPCZ), which is most intense during the wet season.
- Annual and seasonal air temperatures at Apia increased over the period 1979–2021. The number of hot days and warm nights also increased, while the number of cool days decreased. The energy required for cooling indoor environments has also increased.
- Annual maximum daily rainfall has increased at Apia, along with the contribution of extreme of extreme rainfall events to the total annual rainfall amount.
- Tropical cyclones usually affect Samoa between November and April. Over the period 1969–2018, an average of eight cyclones passed within the Samoa exclusive economic zone (EEZ) per decade. Tropical cyclones were most frequent in El Niño years and least frequent in La Niña years. Year-to-year variability is large, ranging from no tropical cyclones in some seasons to four in 2009/10.
- There has been little change in the total number of tropical cyclones in the Southwest Pacific since 1981/82. The number of severe tropical cyclones has declined over the same period/region.

11.1.2 Ocean

- Highest sea levels typically occur in the months December–May.
- Sea-level rise within the EEZ, measured by satellite altimeters since 1993, is about 3.5 to 4 mm per year.
- Monthly average ocean temperature, as measured by the Apia tide-gauge, ranges from 28.2 °C in August to almost 30 °C in April. However, monthly temperatures in any given year can be ±2 °C of these averages.
- The sea surface temperature (SST) trend from satellite observations is 0.31 °C per decade, one of the highest trends in the Southwest Pacific.
- Dominant wave direction is from 35° (NE), with an average significant wave height of 1.26 m and average wave period of 10.54 s.
- Severe wave height was defined as 2.29 m, with an average of 3.9 severe events per year.
- Peak average significant wave height occurs between December and March.

11.2 Country description

The Independent State of Samoa is located in the tropical western South Pacific Ocean between latitudes 13°S and 14.5°S, and longitudes 171°W and 174°W (Figure 11.1). Samoa consists of two main islands (Savai'i and Upolu), two smaller inhabited islands and several small uninhabited islands. It has a total land area of 2842 km^2 and an EEZ of about 128,000 km^2. The main islands account for 99% of the total land area. The capital Apia is located on Upolu. The highest elevation is 1858 m above sea level on Savai'i. Samoa's population is approximately 194,000. About 75% live on the main island of Upolu.

Figure 11.1:
Samoa and the location of the climate station used in this report

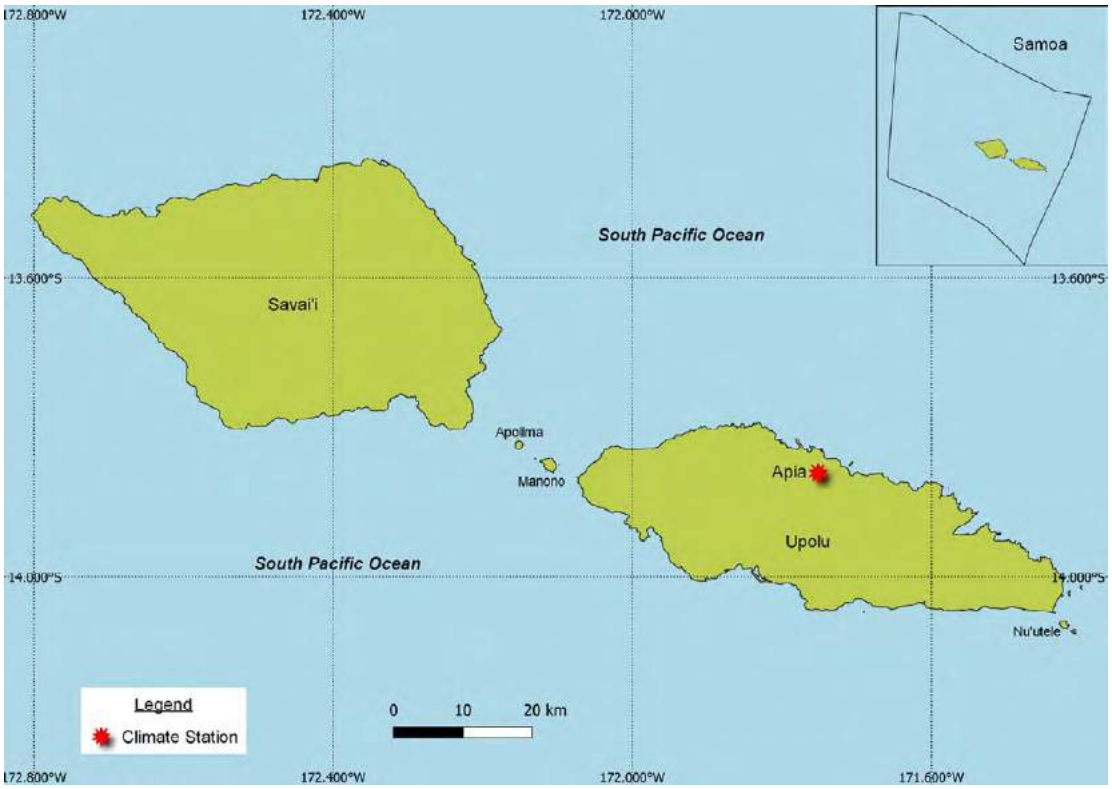

11.3 Data

Daily historical rainfall and air temperature records for Apia from 1951 were obtained from the Samoa Meteorological Division. These records have undergone data quality and homogeneity assessment. While Apia rainfall and temperature data have been used to derive climatological information and rainfall trends in this report, there are insufficient maximum or minimum air temperature data to produce long-term trends. ERA5 reanalysis has been used to calculate temperature trends from 1979 to 2021 (further information is provided in Chapter 1). Additional information on historical climate trends for Samoa can be found in the Pacific Climate Change Data Portal http://www.bom.gov.au/climate/pccsp.

Tropical cyclone data and historical tracks starting from the 1969/70 season are available from the SHTC Data Portal http://www.bom.gov.au/cyclone/history/tracks/index.shtml.

SST covering the EEZ was obtained via the daily Optimum Interpolation SST version 2.1 (OISST v2.1) dataset from NOAA (Reynolds et al. 2007; Banzon et al. 2016). In situ ocean temperature data were obtained from the PSLGM Project tide-gauge located at Apia, with data spanning from 1993 to 2021.

Wave data were obtained from the PACCSAP wave hindcast (Smith et al. 2021), available hourly from 1979 to present, with a grid resolution near Samoa of 7 km.

Regional sea level data were obtained from CSIRO satellite altimetry (updated by Benoit Legresy, Church and White 2011), with correction for seasonal signals, inverse barometer effect and glacial isostatic adjustment. Tide-gauge data were sourced from the Apia tide-gauge station, spanning from 1993 to 2021 at hourly intervals.

11.4 Rainfall

11.4.1 Seasonal cycle

Rainfall is Samoa is greatly influenced by the position and strength of the SPCZ. This band of heavy rainfall is caused by air rising over warm water where winds converge, resulting in thunderstorm activity. It extends across the South Pacific Ocean from the Solomon Islands to the Cook Islands and typically lies between Samoa and Fiji during the wet season. The wet season months of November–April receive 68%, or 2021 mm, of the annual rainfall with the peak month in January with 440 mm (Figure 11.2). The dry season averages 960 mm rainfall, with lowest average recorded rainfall of 119 mm in August.

Figure 11.2:
Mean annual rainfall at Apia

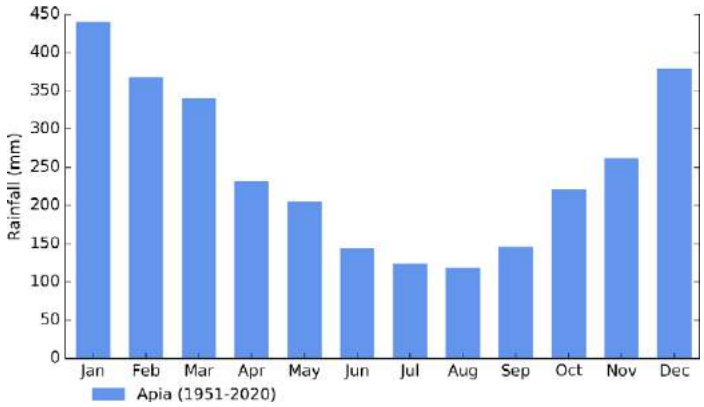

11.4.2 Trends

Trends in annual and seasonal rainfall since 1951 are not statistically significant at Apia (Figure 11.3, Table 11.1). This means there has been little change in annual and seasonal rainfall at this location. Notable year-to-year variability associated with El Niño–Southern Oscillation (ENSO) is present, with higher rainfall typically occurring during La Niña years compared to El Niño years (Figure 11.3). Annual rainfall since 1951 has varied from approximately 1700 to 4200 mm, and approximately half of the year experiences rain.

Figure 11.3:
Annual rainfall (bar graph) and number of wet days (where rainfall is at least 1 mm; line graph) at Apia. Straight lines indicate linear trends for annual rainfall (in black) and number of wet days (in blue). The magnitudes of the trends are presented in Table 11.1. Diamonds indicate years with insufficient data for one or both variables.

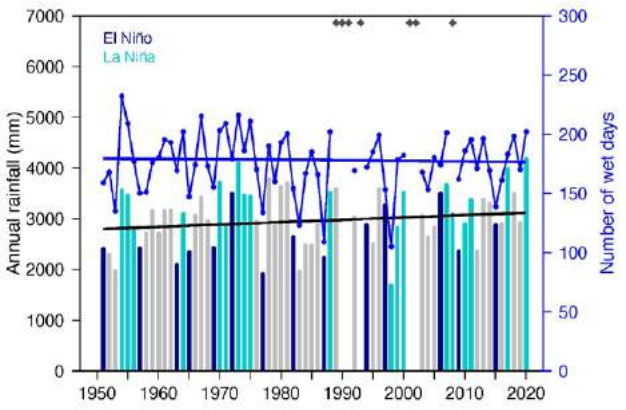

Table 11.1:
Trends in annual, seasonal and extreme rainfall at Apia. The 95% confidence intervals are shown in parentheses, and trends significant at the 95% level are shown in bold. The contribution from very wet days and the standardised rainfall evapotranspiration index are measured relative to 1961–1990 (see Chapter 1 for details).

	Apia
	1951–2020
Annual rainfall (mm/decade)	+46.42 (-26.08, +129.79)
November–April (mm/decade)	+30.27 (-25.36, +83.41)
May–October (mm/decade)	+8.41 (-30.88, +53.83)
Wet days (days/decade)	-0.41 (-4.11, +3.20)
Contribution from very wet days (%/decade)	**+1.65** (+0.75, +2.38)
Consecutive dry days (days/decade)	-0.19 (-0.95, +0.36)
Maximum one-day rainfall (mm/decade)	**+7.71** (+1.55, +13.65)
Standardised rainfall evapotranspiration index (November–April)	+0.02 (-0.11, +0.17)
Standardised rainfall evapotranspiration index (May–October)	-0.08 (-0.24, +0.08)

Maximum daily rainfall, as well as the contribution to annual rainfall from extreme events, has increased significantly since 1951 at Apia (Figure 11.4, Table 11.1). All other extreme rainfall indices, including the standardised rainfall evapotranspiration drought index, have not changed significantly. Variability associated with ENSO is evident, with El Niño years experiencing substantially longer dry spells than La Niña years (Figure 11.4).

Figure 11.4:
Annual longest run of consecutive dry days (bar graph) and maximum daily rainfall (line graph) at Apia. Straight lines indicate linear trends for dry days (in black) and maximum daily rainfall (in blue). The magnitudes of the trends are presented in Table 11.1. Diamonds indicate years with insufficient data for one or both variables.

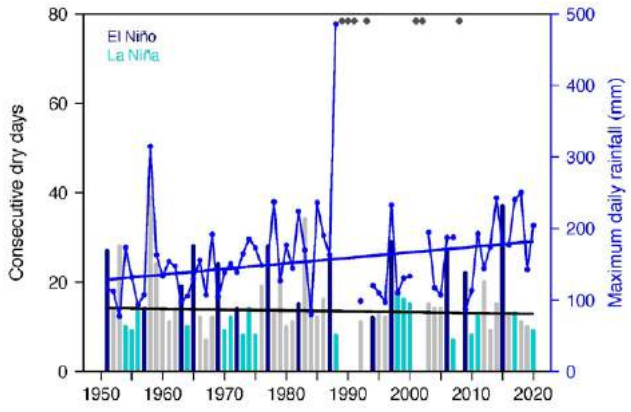

11.5 Air temperature

11.5.1 Seasonal cycle

In Samoa, air temperatures are generally consistent throughout the year, with only very small seasonal differences (Figure 11.5) as temperatures are strongly linked to the surrounding ocean temperatures. The average maximum and minimum temperatures are coldest in August and warmest in April.

The maximum temperature seasonal cycle range for the 1991–2020 period is 1.3 °C, and for minimum temperature it is 1.1 °C. All average maximum temperature months warmed in the 1991–2020 period when compared to the earlier 1961–1990 period, with the strongest difference occurring in April (0.4 °C). For average minimum temperatures, there was marginal warming from June to August.

Figure 11.5:
Maximum and minimum air temperature seasonal cycle for Apia (purple), and for the periods 1961–1990 (dotted lines) and 1991–2020 (solid lines)

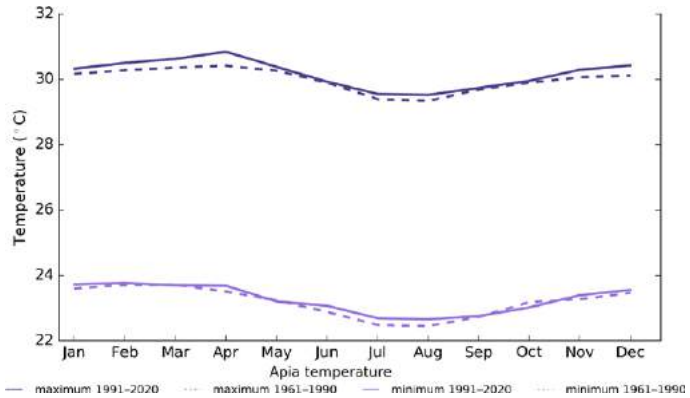

11.5.2 Trends

Due to quality and completeness issues in the daily temperature record from Apia, reanalysis data have been used to calculate temperature trends. Average annual and seasonal temperatures have increased at Apia since 1979 (Table 11.2).

Table 11.2:
Trends in annual and seasonal air temperatures at Apia from ERA5 reanalysis data (station temperatures have quality and completeness issues). A reanalysis is a global weather simulation merged with observations and represents the most complete picture of historical climate, but shares the same limitations as climate models. The 95% confidence intervals are shown in parentheses, and trends significant at the 95% level are shown in bold.

	Apia-ERA5 Tmax (°C/decade)	Apia-ERA5 Tmin (°C/decade)	Apia-ERA5 Tmean (°C/decade)
	1979–2021		
Annual	**+0.13** (+0.06, +0.20)	**+0.13** (+0.06, +0.18)	**+0.13** (+0.06, +0.19)
November–April	**+0.13** (+0.03, +0.21)	**+0.14** (+0.04, +0.21)	**+0.13** (+0.03, +0.21)
May–October	**+0.15** (+0.08, +0.22)	**+0.15** (+0.08, +0.21)	**+0.15** (+0.08, +0.22)

The number of hot days and warm nights has increased, and the number of cool days has decreased at Apia (Table 11.3). The cooling degree days index provides a measure of the energy demand needed to cool a building down to 25 °C, with the assumption that air conditioners are generally turned on at this temperature. There has been a strong increase in the cooling degree index, suggesting the energy needed for cooling has increased significantly since 1979.

Table 11.3:
Trends in annual temperature extremes at Apia from ERA5 reanalysis data (station temperatures have quality and completeness issues). A reanalysis is a global weather simulation merged with observations and represents the most complete picture of historical climate but shares the same limitations as climate models. The 95% confidence intervals are shown in parentheses, and trends significant at the 95% level are shown in bold. Hot and cool days, and warm and cold nights are measured relative to 1981–2010 (see Chapter 1 for details).

	Apia–ERA5
	1979–2021
Number of hot days (days/decade)	**+17.27** (+9.70, +27.00)
Number of warm nights (nights/decade)	**+14.75** (+9.90, +20.92)
Number of cool days (days/decade)	**-9.08** (-14.45, -3.24)
Number of cold nights (nights/decade)	-7.77 (-14.33, +0.04)
Cooling degree days (degree days/decade)	**+45.27** (+22.40, +67.32)
Daily temperature range (°C/decade)	0.00 (-0.01, +0.02)

11.6 Tropical cyclones

11.6.1 Seasonal cycle

Tropical cyclones usually affect Samoa during the southern hemisphere tropical cyclone season, which is from November to April, but also occasionally occur outside the tropical cyclone season. The Southern Hemisphere Tropical Cyclone Archive indicates that between the 1969/70 and 2017/18 seasons, 38 tropical cyclones (Figure 11.6) passed within the EEZ. This represents an average of eight cyclones per decade. Tropical cyclones were most frequent in El Niño years (10 cyclones per decade), followed by neutral years (9 cyclones per decade) and least frequent in La Niña years (4 cyclones per decade).

Interannual variability in the number of tropical cyclones in the EEZ is large, ranging from zero in some seasons to three in 1980/81 and four in 2009/10 (Figure 11.6). High interannual variability and the small number of tropical cyclones occurring in the EEZ make reliable identification of long-term trends in frequency and intensity difficult.

Some tropical cyclone tracks analysed in this section include the tropical depression stage (sustained winds ≤34 knots) before and/or after tropical cyclone formation.

Figure 11.6:
Number of tropical cyclones passing within the Samoa EEZ per season. Each season is defined by the ENSO status, with light blue being an El Niño year, dark blue a La Niña year and grey showing a neutral ENSO year. The 11-year moving average is presented as a purple line and considers all years.

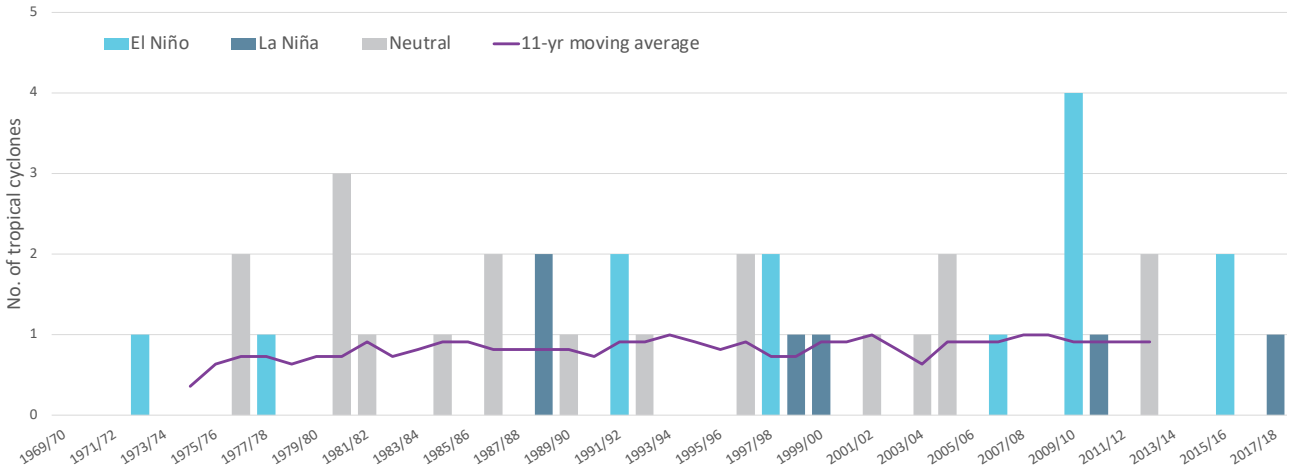

11.6.2 Trends

Trends in total number of tropical cyclones (<995 hPa) and severe tropical cyclones (<970 hPa) are presented for the period 1981/82–2020/21 for the greater Southwest Pacific (135°E–120°W; 0–50°S). Trends are presented at a regional scale as the number of tropical cyclones occurring within Pacific Island EEZs is insufficient for reliable long-term trend analysis.

For the total number of tropical cyclones, the trend (and 95% confidence interval) is -0.92 (-1.85, 0.01) tropical cyclones/decade. There has been little change/marginal decline in the total number of tropical cyclones over the last 40 seasons. This trend is not statistically significant.

For the total number of severe tropical cyclones, the trend is -0.80 (-1.32, -0.29) tropical cyclones/decade. There is a negative trend in the number of severe tropical cyclones over the last 40 seasons. There has been little change/marginal decline in the proportion of tropical cyclones reaching severe status. The trend is -0.04 (-0.08, 0.00) tropical cyclones/decade. The negative trend is statistically significant.

Records of tropical cyclones exist from the late 1800s in some countries in the Southwest Pacific, but trends in tropical cyclones have only been presented from 1981/82. Satellite-based observations began in the Southwest Pacific in the early 1970s, but consistent coverage and reliable intensity estimates have only been available since the early 1980s. Confidence in tropical cyclone trends is moderate as the definition of a tropical cyclone has changed and satellite observation methods have continued to improve over the last 40 years.

11.7 Sea surface temperature

11.7.1 Seasonal cycle

Ocean temperature, as measured by the Apia tide-gauge from 1993 to 2021, reaches on average a maximum of almost 30 °C in April, but individual months can get as high as 31.4 °C (Figure 11.7). Minimum average temperature is 28.2 °C in August. Hourly temperatures can be up to 2 °C higher or lower than these monthly averages, although 50% of hourly observations fall within 1 °C of the average.

Figure 11.7:
Annual temperatures measured at the Apia tide-gauge. Blue dots show the monthly average, and shaded boxes show the middle 50% of hourly observations. Lines show the top and bottom 25% of hourly observations..

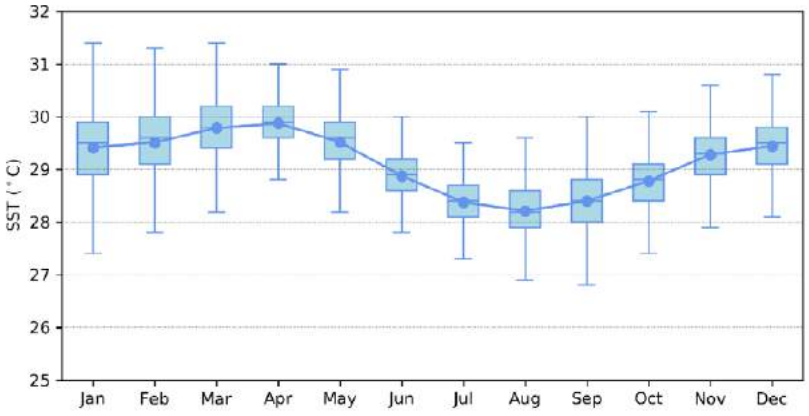

11.7.2 Trends

Figure 11.8 shows the 1981–2021 SST from satellite observations averaged over the EEZ. The data show a trend of 0.31 °C per decade with a 95% confidence interval of ±0.05 °C. This SST trend estimate is one of the highest trends among Southwest Pacific countries.

Figure 11.8:
Sea surface temperature from satellite observations averaged across the Samoa EEZ, shown as the orange line. The blue line shows the linear regression trend.

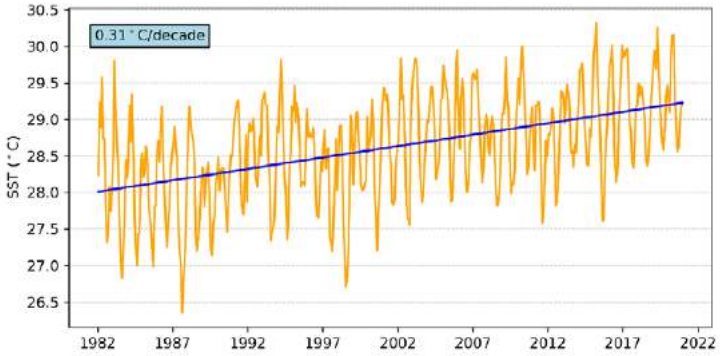

11.8 Sea level

11.8.1 Seasonal cycle

Samoa experiences a semidiurnal tidal cycle, meaning two high and two low tides per day. The highest predicted tides of the year typically occur from December to February and also July to September. Figure 11.9 shows the number of hours the 99th percentile (1.66 m) sea level threshold is exceeded per month across the entire sea level record at Apia. Peak sea levels typically occur between December and May. Since approximately 2010, increasingly more hours each year exceed the 99th percentile threshold. This is due to a combination of sea-level rise and subsidence occurring at Samoa (Brown et al. 2020).

Figure 11.9:
Number of hours exceeding 99th percentile sea level threshold per month from 1993 to 2021 at the Apia tide-gauge. Blue shading indicates the number of hours, and the final row provides a percentage summary of all the years.

Number of hours exceeding 1.66 m (Apia, Samoa)

	Jan	Feb	Mar	Apr	May	Jun	Jul	Aug	Sep	Oct	Nov	Dec	Annual
1993	0	0	0	0	0	0	0	0	0	0	0	0	0
1994	0	0	0	0	0	0	0	0	0	0	0	0	0
1995	0	0	0	0	0	0	0	0	0	0	0	0	0
1996	0	0	0	0	0	0	0	0	0	0	0	0	0
1997	0	0	0	0	0	0	0	0	0	0	0	0	0
1998	0	0	0	0	0	0	0	0	0	0	0	0	0
1999	0	0	0	0	0	0	0	0	0	0	0	0	0
2000	0	0	0	0	0	0	0	0	0	0	0	0	0
2001	0	0	0	0	0	0	0	0	0	0	0	0	0
2002	0	0	0	0	0	0	0	0	0	0	0	0	0
2003	0	0	0	0	0	0	0	0	0	0	0	0	0
2004	0	0	0	0	0	0	0	0	0	0	0	0	0
2005	0	0	0	0	0	0	0	0	0	0	0	0	0
2006	0	0	0	0	0	0	0	0	0	0	0	0	0
2007	0	0	0	0	0	0	0	0	0	0	0	0	0
2008	0	0	0	0	0	0	0	0	0	0	0	0	0
2009	0	0	0	0	0	0	0	0	0	0	0	0	0
2010	0	0	0	0	0	0	0	0	0	0	0	0	0
2011	0	1	0	4	0	0	0	0	0	0	0	0	5
2012	0	0	0	0	0	0	0	0	0	0	0	2	2
2013	0	0	0	0	0	0	1	0	0	0	0	0	1
2014	0	0	0	0	0	0	0	0	2	0	0	0	2
2015	0	1	0	0	0	0	0	0	2	0	0	0	3
2016	0	0	0	0	0	0	0	0	0	2	1	4	7
2017	5	1	0	0	0	0	0	0	0	0	0	1	7
2018	2	2	0	0	0	2	1	0	2	0	0	1	10
2019	8	21	11	10	0	0	0	9	7	8	2	0	76
2020	0	0	1	14	8	2	0	0	0	3	0	1	29
2021	5	5	21	12	8	0	0	0	0	1	0	6	58
Monthly Totals (%)	10	16	16	20	8	2	1	4	6	7	2	8	

11.8.2 Trends

Sea level at Samoa, measured by satellite altimeters (Figure 11.10) since 1993, has risen between 3.5 and 4.0 mm per year across the EEZ, with a 95% confidence interval of ±0.6 to ±1.0 mm. This rise is partly linked to a pattern related to climate variability from year to year and decade to decade, and is a higher trend than the global average of 3.1 ± 0.4 mm per year (von Schuckmann et al. 2021).

Trend estimates at the Apia tide-gauge over a similar time span to the altimetry observations (February 1993 to July 2020) are provided in the PSLGM Monthly Data Report for July 2020 (http://www.bom.gov.au/ntc/IDO60101/IDO60101.202007.pdf). For Apia, the trend is reported as 9.8 mm per year, more than double the altimetry trends shown in Figure 11.10 (tide-gauge indicated by star symbol). This difference is largely attributed to subsidence occurring at Samoa (Brown et al. 2020).

Figure 11.10:
Satellite altimetry annual trend for the Pacific from 1993 to 2020, with the Samoa and American Samoa EEZ highlighted. The star symbol represents the location of the tide-gauge.

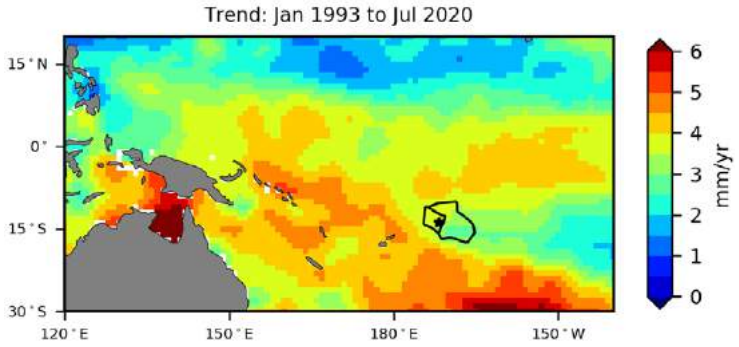

11.9 Waves

11.9.1 Seasonal cycle

The average wave climate in Apia is defined by the significant wave height, peak period and peak direction. The significant wave height is the mean wave height (from trough to crest) of the highest one third of waves and corresponds to the wave height that would be reported by an experienced observer. Peak period is the time interval between two waves of the dominant wave period. Peak direction is the direction from which the dominant waves are coming.

The average sea state is dominated by wind seas from the northeast. The annual mean wave height is 1.26 m, the annual mean wave direction is 35° and the annual mean wave period is 10.54 s. In the Pacific, waves often come from multiple directions and for different periods at a time. In Apia, there are often more than four different wave direction/period components coming from the southeast to southwest (Figure 11.11).

Figure 11.11:
Annual wave rose for Apia. Note that direction is where the wave is coming from.

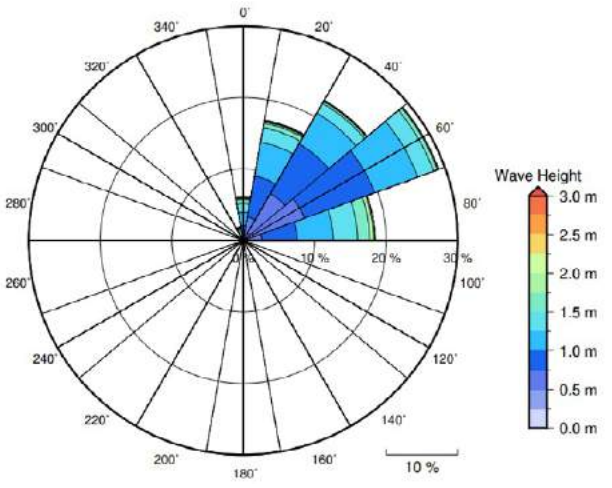

The significant wave height and wave period peak is from November to March. However, there is a secondary wave height peak from June to September, which is accompanied by lower wave periods (Figure 11.12). This shows that waves at Samoa are predominantly driven by strong easterly local and trade winds from May to September.

Figure 11.12:
Monthly wave height (black line), wave period (red line) and wave direction (arrows). The grey area represents the range of wave height between calm periods (10% of lowest wave height) and large wave events (10% of highest wave height).

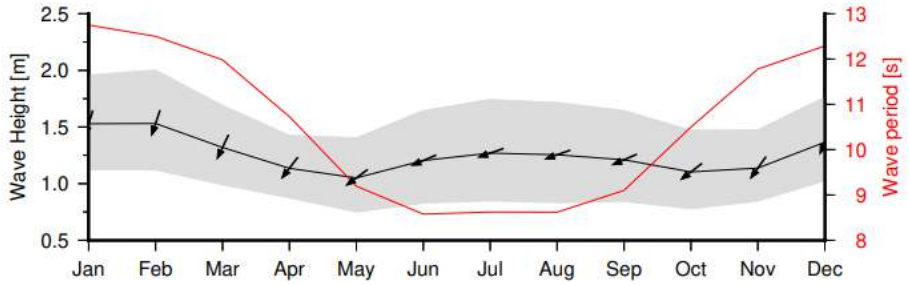

11.9.2 Trends

Waves change from month to month with the seasons, but they also change from year to year with climate oscillations. Typically, these changes are smaller than the seasonal changes but can be important during phenomena such as ENSO. In Apia, the mean annual wave height has remained unchanged since 1979 (Figure 11.13). The mean annual wave height in Apia is not significantly correlated with the main climate indicators of the region.

Figure 11.13:
Annual wave height (black line), wave period (red line) and wave direction (arrows). The grey area represents the range of wave height between calm periods (10% of lowest wave height) and large wave events (10% of highest wave height).

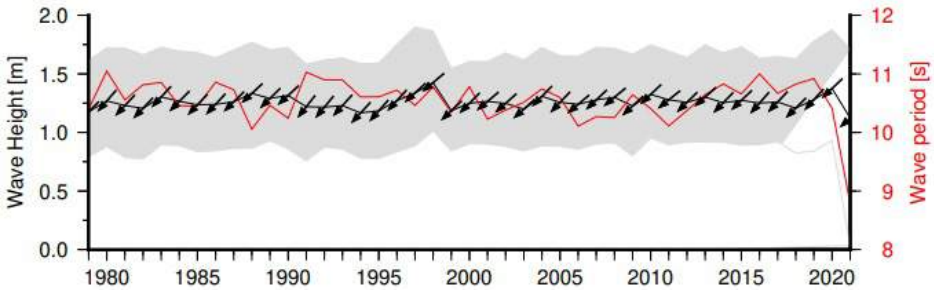

11.9.3 Extreme waves

Extreme wave analysis completed for Apia was done by defining a severe height threshold and fitting a generalized Pareto distribution (GPD). The optimum threshold selected was 2.29 m. In the 42-year wave hindcast, 163 wave events reached or exceeded this threshold, averaging 3.9 events per year. The GPD was fitted to the largest wave height reached during each of these events (Figure 11.14, Table 11.4). Extreme wave analysis is a very useful tool but is not always accurate because the analysis is very sensitive to the data available, the type of distribution fitted and the threshold used. For example, this analysis does not accurately account for tropical cyclone waves. More in-depth analysis is required to obtain results appropriate for designing coastal infrastructure and coastal hazard planning.

Figure 11.14:
Extreme wave distribution for Apia. The crosses represent the wave events that have occurred since 1979. The solid line is the statistical distribution that best fits past wave events. The dashed lines show the upper and lower confidence limits of the fit. There is a 95% chance that the fitted distribution lies between the two dashed lines. Note that the annual return interval is in logarithmic scale.

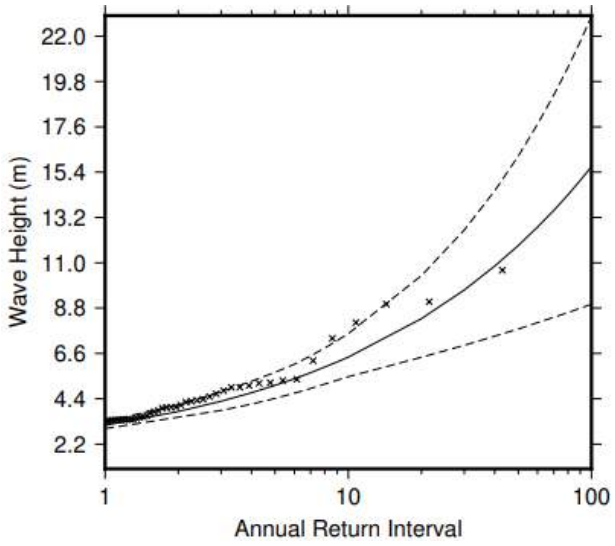

Table 11.4:
Summary of the results from extreme wave analysis in Apia

Large wave height (90th percentile)	1.69 m
Severe wave height (99th percentile)	2.54 m
1-year ARI wave height	3.11 m
10-year ARI wave height	6.42 m
20-year ARI wave height	8.29 m
50-year ARI wave height	11.84 m
100-year ARI wave height	15.66 m

12 Solomon Islands

12.1 Summary

12.1.1 Climate

- Changes in air temperature from season to season are relatively small and strongly linked to changes in the surrounding ocean temperature. The Solomon Islands have two distinct seasons – a warm wet season from November to April and a cooler dry season from May to October.
- The seasonal cycle of rainfall is affected by the South Pacific Convergence Zone (SPCZ) and the West Pacific Monsoon (WPM) during the wet season months, with additional influence from the Intertropical Convergence Zone (ITCZ) over the northern islands throughout the year.
- Annual and seasonal air temperatures at Honiara increased over the period 1951–2020. The number of cold nights has decreased.
- Annual maximum daily rainfall has increased at Honiara and Munda (New Georgia). Conversely, the number of rainy days each year has decreased at Honiara.
- Tropical cyclones usually affect the Solomon Islands between November and April. Over the period 1969–2018, an average of 28 cyclones passed within the Solomon Islands exclusive economic zone (EEZ) per decade. Tropical cyclones were most frequent in El Niño years and least frequent in La Niña years. Year-to-year variability is large, ranging from no tropical cyclones in some seasons to eight in 1997/98.
- There has been little change in the total number of tropical cyclones in the Southwest Pacific since 1981/82. The number of severe tropical cyclones has declined over the same period/region.

12.1.2 Ocean

- Highest sea levels typically occur in the months November–January and March/April.
- Sea-level rise within the EEZ, measured by satellite altimeters from 1993 to mid-2020, ranges from about 3.5 and 5.5 mm per year.
- Monthly average ocean temperature, as measured by the Honiara tide-gauge, ranges from 28.7 °C in August to approximately 30 °C in the months December/January and again in April, exhibiting a bimodal peak. Monthly temperatures in any given year can be ±2 °C of these averages.
- The sea surface temperature (SST) trend in the EEZ is 0.26 °C per decade from 1981 to 2021.
- Dominant wave direction is from 17° (NNE), with an average significant wave height of 0.11 m and average wave period of 9.86 s.
- Severe wave height was defined as 1.00 m, with an average of 1.7 severe events every two years.
- Peak average significant wave height occurs in January–March, with associated high wave periods driven by swell from the north.

12.2 Country description

The Solomon Islands are located in the tropical South Pacific Ocean between latitudes 5°S and 13°S, and longitudes 155°E and 169°E (Figure 12.1). The nation consists of six major islands and over 900 smaller islands. The Solomon Islands have a total land area of 28,896 km^2 and an EEZ of 1.6 million km^2. The archipelago includes Choiseul, the Shortland Islands, the New Georgia Islands, Santa Isabel, the Russell Islands, the Florida Islands, Tulagi, Malaita, Maramasike, Ulawa, Owaraha (Santa Ana), Makira (San Cristobal) and the main island of Guadalcanal. The highest elevation is 2330 m, at Mt Popomanaseu.

The population is approximately 653,000. About 24% live on Guadalcanal, which includes the capital Honiara. Guadalcanal is the second-most populous island in the country after Malaita (approximately 25%).

Figure 12.1:
Solomon Islands and the location of the climate station used in this report

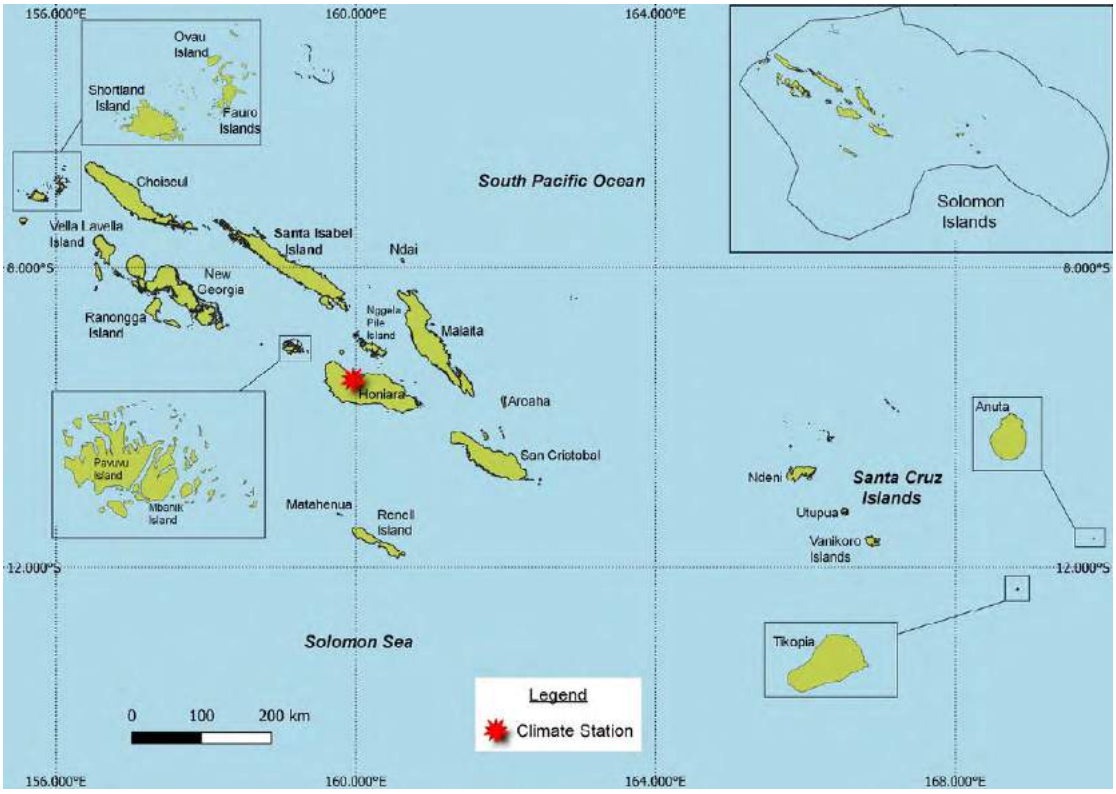

12.3 Data

Daily historical rainfall and air temperature records for a Honiara–Henderson Airport composite and Munda (New Georgia) from 1951 were obtained from the Solomon Islands Meteorological Service. These records have undergone data quality and homogeneity assessment. Where the maximum or minimum air temperature records were found to have discontinuities, these records have been adjusted to make them homogeneous (further information is provided in Chapter 1). Additional information on historical climate trends for the Solomon Islands can be found in the Pacific Climate Change Data Portal http://www.bom.gov.au/climate/pccsp.

Tropical cyclone data and historical tracks starting from the 1969/70 season are available from the SHTC Data Portal http://www.bom.gov.au/cyclone/history/tracks/index.shtml.

SST covering the EEZ was obtained via the daily Optimum Interpolation SST version 2.1 (OISST v2.1) dataset from NOAA (Reynolds et al. 2007; Banzon et al. 2016). In situ ocean temperature data were obtained from the PSLGM Project tide-gauge located at Honiara, with data spanning from 1994 to 2021.

Wave data were obtained from the PACCSAP wave hindcast (Smith et al. 2021), available hourly from 1979 to 2021, with a grid resolution near the Solomon Islands of 7 km.

Regional sea level data were obtained from CSIRO satellite altimetry (updated by Benoit Legresy, Church and White 2011), with correction for seasonal signals, inverse barometer effect and glacial isostatic adjustment. Tide-gauge data were sourced from the Honiara tide-gauge station, spanning from 1994 to 2021 at hourly intervals.

12.4 Rainfall

12.4.1 Seasonal cycle

Rainfall in the Solomon Islands is strongly affected by the SPCZ. The SPCZ contributes to the high rainfall during the wet season from December to April at both Honiara and Munda. The wet season at Honiara is more pronounced than at Munda, with 69% of the annual rainfall during this time and a peak in March of 310 mm on average (Figure 12.2). The highest rainfall months at Honiara are during January–March when the WPM is most active in the region. This feeds moisture into the SPCZ, which is strongest in the wet season.

Munda has a more even distribution of rainfall during the year, with the wettest months being January–March and a second peak in rainfall in July. Located closer to the western Warm Pool and the normal location of the SPCZ, Munda averages between 410 mm of rainfall in January and 260 mm in June.

Figure 12.2:
Mean annual rainfall at Honiara and Munda

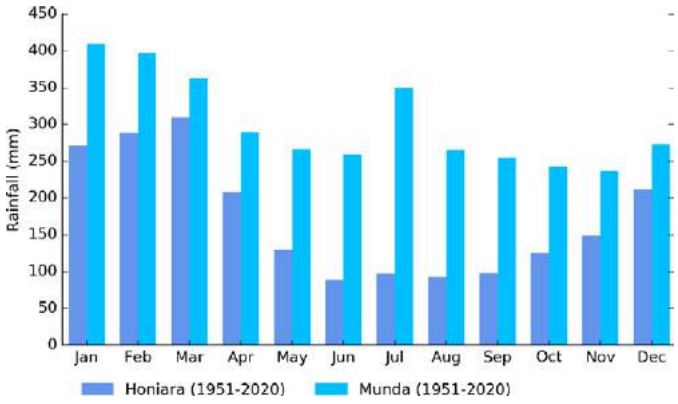

12.4.2 Trends

Trends in annual and seasonal rainfall are not statistically significant at Honiara and Munda (Figure 12.3, Table 12.1). This means there has been little change in annual and seasonal rainfall at these sites. However, the number of wet days has been decreasing at Honiara. Annual rainfall varies from approximately 1300 to 3000 mm at Honiara and from approximately 2600 to 4400 mm at Munda.

Figure 12.3:
Annual rainfall (bar graph) and number of wet days (where rainfall is at least 1 mm; line graph) at Honiara (left) and Munda (right). Straight lines indicate linear trends for annual rainfall (in black) and number of wet days (in blue). The magnitudes of the trends are presented in Table 12.1. Diamonds indicate years with insufficient data for one or both variables.

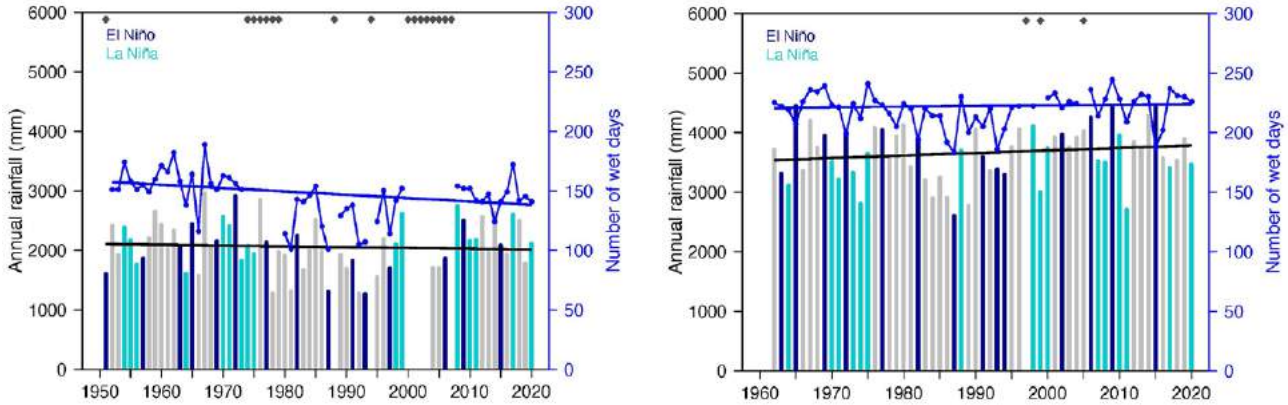

Table 12.1:
Trends in annual, seasonal and extreme rainfall at Honiara (left) and Munda (right). The 95% confidence intervals are shown in parentheses, and trends significant at the 95% level are shown in bold. The contribution to total rainfall from extreme events and the standardised rainfall evapotranspiration index are measured relative to 1961–1990 (see Chapter 1 for details). The standardised rainfall evapotranspiration index is not available for Munda due to the lack of daily temperature observations at this site.

	Honiara	Munda
	1951–2020	1962–2020
Annual rainfall (mm/decade)	-13.59 (-78.68, +38.86)	+42.63 (-44.52, +114.27)
November–April (mm/decade)	+0.72 (-46.92, +56.00)	+14.79 (-49.29, +73.05)
May–October (mm/decade)	-11.03 (-32.39, +12.25)	+29.69 (-31.02, +86.96)
Number of wet days (days/decade)	**-2.82** (-5.37, -0.49)	+0.59 (-2.42, +3.20)
Contribution to total rainfall from extreme events (%/decade)	+0.72 (-0.56, +2.08)	+1.42 (-0.04, +2.57)
Consecutive dry days (days/decade)	+0.17 (-0.22, +0.79)	+0.18 (-0.43, +0.77)
Maximum one-day rainfall (mm/decade)	**+6.08** (0.00, +12.16)	**+7.08** (+1.17, +13.13)
Standardised rainfall evapotranspiration index (November–April)	-0.03 (-0.15, +0.11)	-
Standardised rainfall evapotranspiration index (May–October)	-0.08 (-0.20, +0.05)	-

There has been a significant increase in maximum daily rainfall at Honiara and Munda (Table 12.1, Figure 12.4). The longest run of days without any rain has not been changing and rarely exceeds three weeks at Honiara and two weeks at Munda (Figure 12.4). At Honiara, variability associated with ENSO is evident, with El Niño years generally experiencing longer dry spells. In 2010, a maximum daily rainfall of over 500 mm at Munda was associated with a tropical depression that brought heavy flooding to several islands.

Figure 12.4:
Annual longest run of consecutive dry days (bar graph) and maximum daily rainfall (line graph) at Honiara (left) and Munda (right). Straight lines indicate linear trends for dry days (in black) and maximum daily rainfall (in blue). The magnitudes of the trends are presented in Table 12.1. Diamonds indicate years with insufficient data for one or both variables.

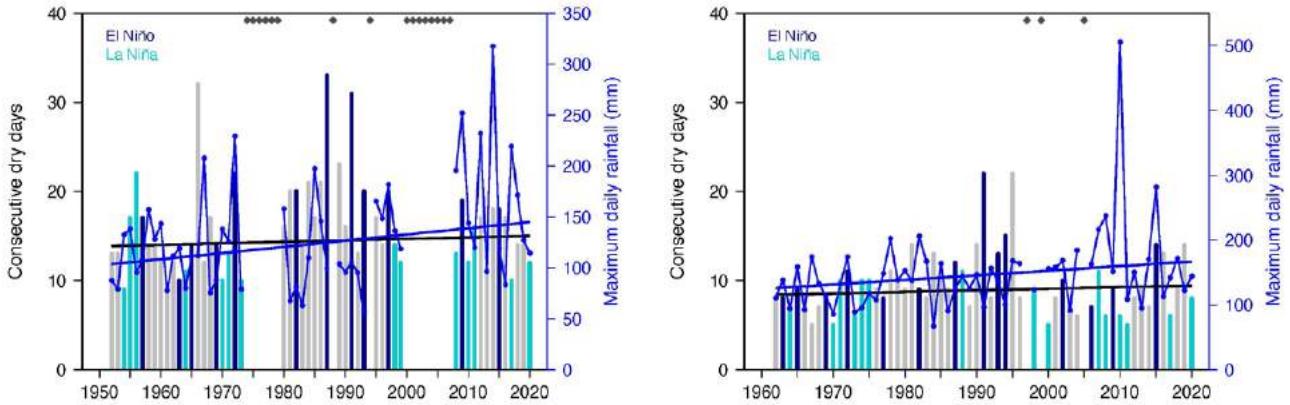

12.5 Air temperature

12.5.1 Seasonal cycle

Air temperatures throughout the year show only small seasonal variations (Figure 12.5) as they are strongly linked to the surrounding ocean temperatures. The most significant variation in air temperatures is in July and August, when cooler air blows in from the south. This change is most evident in the average minimum temperatures at Munda, which has a minimum temperature range of 1.6 °C for the 1961–1990 climatology period. Honiara has a maximum and minimum temperature range of less than 1 °C.

Both Honiara and Munda display a clear warming of average minimum temperatures between the 1991–2020 climatology period and the 1961–1990 period for all months throughout the year. Honiara also warms across all months for maximum temperature (maximum temperature data for Munda for the 1991–2020 period is not available).

Figure 12.5:
Maximum and minimum air temperature seasonal cycle for Honiara (purple) and Munda (green), and for the periods 1961–1990 (dotted lines) and 1991–2020 (solid lines)

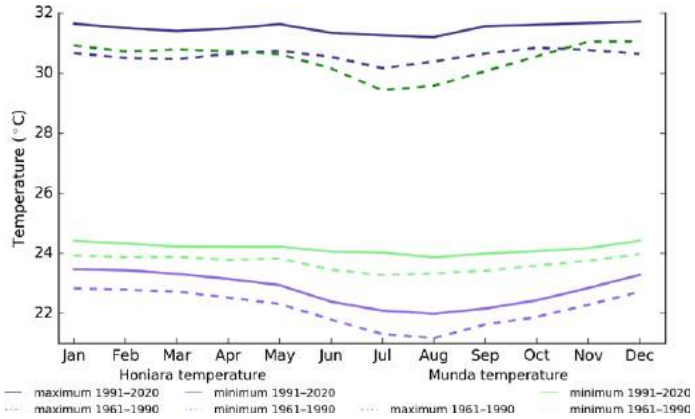

12.5.2 Trends

Average annual and seasonal temperatures have increased significantly at Honiara (Figure 12.6, Table 12.2). The relatively small year-to-year fluctuations in temperature can be attributed to Honiara's tropical location.

Figure 12.6:
Average annual, November–April and May–October temperatures for Honiara. Straight line indicates linear trend. The magnitudes of the trends are presented in Table 12.2. Diamonds indicate years with insufficient data for one or more variables.

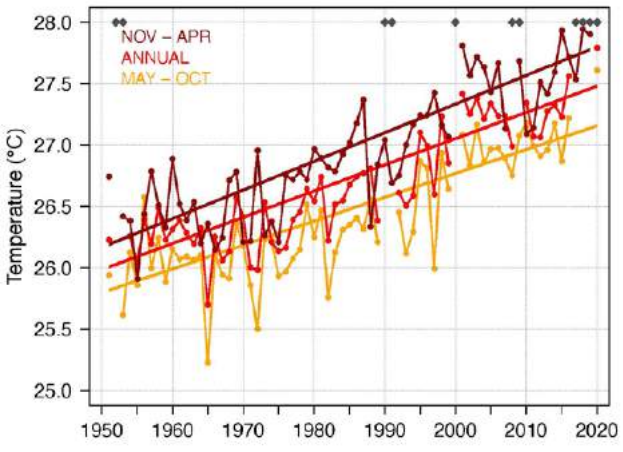

Table 12.2:
Trends in annual and seasonal air temperatures at Honiara. The 95% confidence intervals are shown in parentheses, and trends significant at the 95% level are shown in bold.

	Honiara Tmax (°C/decade)	Honiara Tmin (°C/decade)	Honiara Tmean (°C/decade)
	1951–2020		
Annual	**+0.23** (+0.17, +0.28)	**+0.19** (+0.14, +0.24)	**+0.21** (+0.17, +0.25)
November–April	**+0.26** (+0.19, +0.31)	**+0.20** (+0.15, +0.27)	**+0.23** (+0.19, +0.27)
May–October	**+0.22** (+0.16, +0.27)	**+0.18** (+0.13, +0.22)	**+0.19** (+0.16, +0.23)

Numerous gaps exist in the daily temperature record at Honiara, which prevents the robust calculation of trends in many temperature extremes. Despite this, the number of cold nights has decreased significantly and available data suggest Honiara now experiences more than three times as many hot days compared to the 1950s (Figure 12.7). However, it is possible that some of this warming trend is due to increased urban density at Honiara or unresolved data homogeneity issues in the Honiara–Henderson Airport composite.

Figure 12.7:
Annual number of hot days and cold nights at Honiara. The straight line indicates the linear trend. Criteria for statistical robustness were not met for determining a linear trend for hot days. Diamonds indicate years with insufficient data for one or both variables.

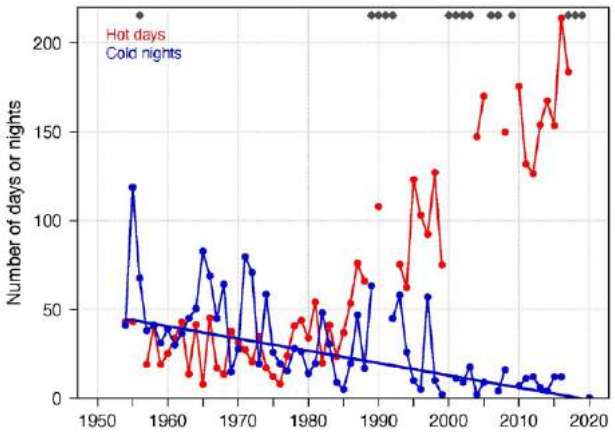

12.6 Tropical cyclones

16.6.1 Seasonal cycle

Tropical cyclones usually affect Solomon Islands during the southern hemisphere tropical cyclone season, which is from November to April, but also occasionally occur outside the tropical cyclone season. The Southern Hemisphere Tropical Cyclone Archive indicates that between the 1969/70 and 2017/18 seasons, 138 tropical cyclones (Figure 12.8) passed within the EEZ. This represents an average of 28 cyclones per decade. Tropical cyclones were most frequent in El Niño years (42 cyclones per decade), followed by neutral years (25 cyclones per decade) and least frequent in La Niña years (20 cyclones per decade).

Interannual variability in the number of tropical cyclones in the EEZ is large, ranging from zero in some seasons to eight in 1997/98 and six in 1971/72, 1996/97 and 2002/03 (Figure 12.8). High interannual variability and the small number of tropical cyclones occurring in the EEZ make reliable identification of long-term trends in frequency and intensity difficult.

Some tropical cyclone tracks analysed in this section include the tropical depression stage (sustained winds ≤34 knots) before and/or after tropical cyclone formation.

Figure 12.8:
Number of tropical cyclones passing within the Solomon Islands EEZ per season. Each season is defined by the ENSO status, with light blue being an El Niño year, dark blue a La Niña year and grey showing a neutral ENSO year. The 11-year moving average is presented as a purple line and considers all years.

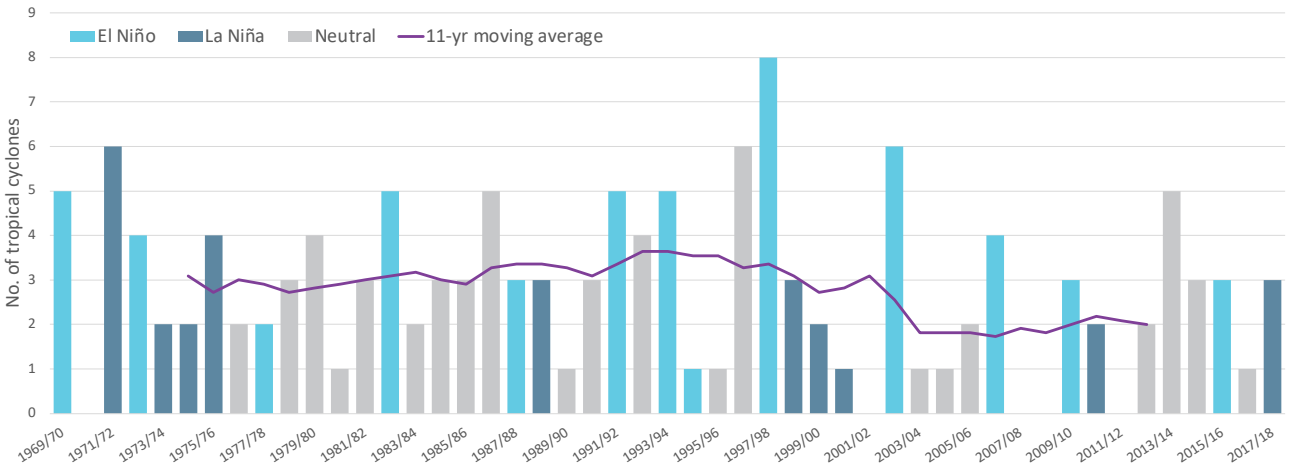

12.6.2 Trends

Trends in total number of tropical cyclones (<995 hPa) and severe tropical cyclones (<970 hPa) are presented for the period 1981/82–2020/21 for the greater Southwest Pacific (135°E–120°W; 0–50°S). Trends are presented at a regional scale as the number of tropical cyclones occurring within Pacific Island EEZs is insufficient for reliable long-term trend analysis.

For the total number of tropical cyclones, the trend (and 95% confidence interval) is -0.92 (-1.85, 0.01) tropical cyclones/decade. There has been little change/marginal decline in the total number of tropical cyclones over the last 40 seasons. This trend is not statistically significant.

For the total number of severe tropical cyclones, the trend is -0.80 (-1.32, -0.29) tropical cyclones/decade. There is a negative trend in the number of severe tropical cyclones over the last 40 seasons. There has been little change/marginal decline in the proportion of tropical cyclones reaching severe status. The trend is -0.04(-0.08, 0.00) tropical cyclones/decade. The negative trend is statistically significant.

Records of tropical cyclones exist from the late 1800s in some countries in the Southwest Pacific, but trends in tropical cyclones have only been presented from 1981/82. Satellite-based observations began in the Southwest Pacific in the early 1970s, but consistent coverage and reliable intensity estimates have only been available since the early 1980s. Confidence in tropical cyclone trends is moderate as the definition of a tropical cyclone has changed and satellite observation methods have continued to improve over the last 40 years.

12.7 Sea surface temperature

12.7.1 Seasonal cycle

Ocean temperature, as measured by the Honiara tide-gauge from 1994 to 2021, reaches on average a maximum of almost 30 °C in December/January and again in April, exhibiting a unique bimodal peak during the wet season (Figure 12.9). However, maximum temperatures in individual months can get as high as 31.5 °C in January. Minimum average temperature is 28.7 °C in August. Hourly temperatures can be up to 2 °C higher or lower than these monthly averages although 50% of hourly observations fall within 1 °C of the average.

Figure 12.9:
Annual temperatures measured at the Honiara tide-gauge. Blue dots show the monthly average, and shaded boxes show the middle 50% of hourly observations. Lines show the top and bottom 25% of hourly observations.

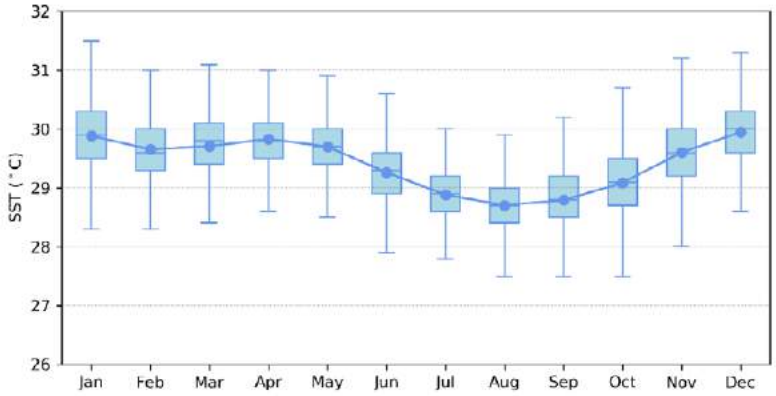

12.7.2 Trends

Figure 12.10 shows the 1981–2021 SST from satellite observations averaged over the EEZ. The data show a trend of 0.26 °C per decade, with a 95% confidence interval of ±0.05 °C.

Figure 12.10:
Sea surface temperature from satellite observations averaged across the Solomon Islands EEZ, shown as the orange line. The blue line shows the linear regression trend.

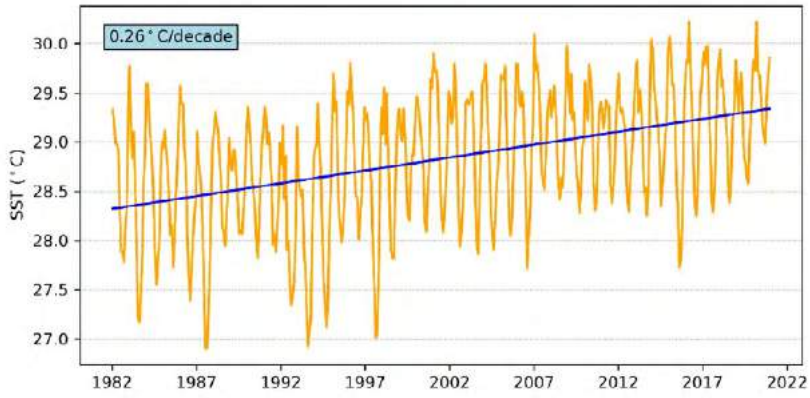

12.8 Sea level

12.8.1 Seasonal cycle

Honiara experiences a mixed tidal cycle, meaning it can be both diurnal and semidiurnal depending on the time of month. Sometimes there are two high and two low tides a day, and sometimes there is only one high and one low tide per day. The highest predicted tides of the year typically occur during the wet season months of November–January and also April/May. Figure 12.11 shows the number of hours the 99th percentile (1.27 m) sea level threshold is exceeded per month across the entire sea level record at Honiara. Blue shading indicates the number of hours, and the final row provides a summary of all the years. Peak sea levels typically occur in November to January and March/April.

Figure 12.11: Number of hours exceeding 99th percentile sea level threshold per month from 1994 to 2021 at the Honiara tide-gauge. Blue shading indicates the number of hours, and the final row provides a percentage summary of all the years.

Number of hours exceeding 1.27 m (Honiara, Solomon Islands)

	Jan	Feb	Mar	Apr	May	Jun	Jul	Aug	Sep	Oct	Nov	Dec	Annual
1994	0	0	0	0	0	0	0	0	0	0	0	0	0
1995	0	0	0	0	0	0	0	0	0	0	0	0	0
1996	0	0	0	0	0	0	0	0	0	0	0	0	0
1997	0	0	0	0	0	0	0	0	0	0	0	0	0
1998	0	0	0	0	0	0	0	0	0	0	0	0	0
1999	0	0	0	0	0	0	0	0	0	0	0	0	0
2000	0	0	0	0	0	0	0	0	0	0	0	0	0
2001	0	0	0	1	0	0	0	0	0	0	0	0	1
2002	0	0	0	0	0	0	0	0	0	0	0	0	0
2003	0	0	0	0	0	0	0	0	0	0	0	0	0
2004	0	0	0	0	0	0	0	0	0	0	0	0	0
2005	0	0	0	0	0	0	0	0	0	0	0	0	0
2006	0	0	4	5	0	0	0	0	0	0	0	0	9
2007	0	0	0	0	0	0	0	0	0	0	18	8	26
2008	0	0	15	15	11	0	0	0	0	0	0	1	42
2009	2	0	5	2	0	0	0	0	0	0	0	0	9
2010	0	0	0	0	0	0	0	0	0	0	0	6	6
2011	0	0	0	0	0	0	0	0	0	0	0	6	6
2012	0	2	9	0	0	0	0	0	0	0	0	0	11
2013	0	0	0	0	0	0	0	0	0	0	0	0	0
2014	0	0	0	0	0	0	0	0	0	0	0	0	0
2015	0	0	0	0	0	0	0	0	0	0	0	0	0
2016	0	0	0	0	0	0	0	0	0	0	0	0	0
2017	0	0	1	1	0	0	0	0	0	0	0	0	2
2018	0	0	0	0	0	0	0	0	0	0	0	0	0
2019	0	0	0	0	0	0	0	0	0	0	0	0	0
2020	0	0	0	3	0	0	0	0	0	0	0	6	9
2021	25	0	0	12	1	0	0	0	0	0	17	35	90
Monthly Totals (%)	13	1	16	18	6	0	0	0	0	0	17	29	

12.8.2 Trends

Sea level within the EEZ, measured by satellite altimeters (Figure 12.12) since 1993, has risen between 3.5 and 5.5 mm per year, with a confidence interval of up to ±1.2 mm across the islands. This rise is partly linked to a pattern related to climate variability from year to year and decade to decade. Although these trend estimates are larger than the global average of 3.1 ± 0.4 mm per year (von Schuckmann et al. 2021), the high uncertainty estimate means the trend could be as low as 2.3 mm/year or as high as 6.7 mm/year.

Trend estimates at the Honiara tide-gauge over a shorter time span than the altimetry observations (July 1994 to July 2020) are provided in the PSLGM Monthly Data Report for July 2020 (http://www.bom.gov.au/ntc/IDO60101/IDO60101.202007.pdf). For Honiara, the trend is reported as 3.7 mm per year, which is similar to the altimetry trends seen near Honiara (3.5 to 4.0 mm/year) shown in Figure 12.12 (tide-gauge indicated by star symbol).

Figure 12.12:
Satellite altimetry annual trend for the Pacific from 1993 to 2020, with the Solomon Islands EEZ highlighted. The star symbol indicates the location of the tide-gauge at Honiara.

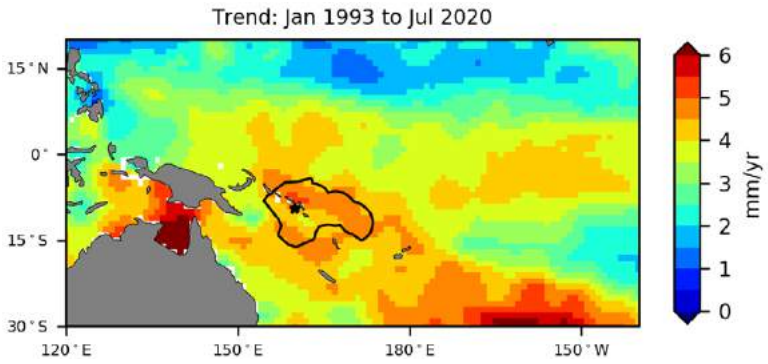

12.9 Waves

12.9.1 Seasonal cycle

The average wave climate in Honiara is defined by the significant wave height, peak period and peak direction. The significant wave height is the mean wave height (from trough to crest) of the highest one third of waves and corresponds to the wave height that would be reported by an experienced observer. Peak period is the time interval between two waves of the dominant wave period. Peak direction is the direction from which the dominant waves are coming.

The average sea state is dominated by wind seas from the northeast. The annual mean wave height is 0.11 m, the annual mean wave direction is 17° and the annual mean wave period is 9.86 s. In the Pacific, waves often come from multiple directions and for different periods at a time. In Honiara, there are often more than one different wave direction/period components coming from the southeast to southwest (Figure 12.13).

Figure 12.13:
Annual wave rose for Honiara. Note that direction is where the wave is coming from.

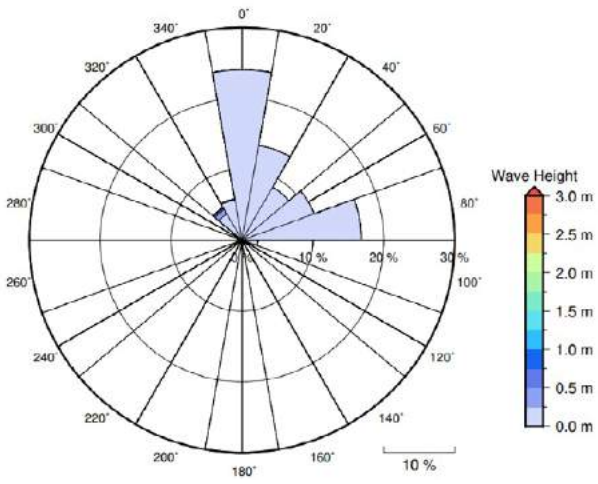

The significant wave height peaks around February, with the period also highest between October and April, but is significantly less in July/August (Figure 12.14) This shows that waves at Solomon Islands are predominantly driven by easterly local winds from June to September, which changes to a dominant northerly swell over the remainder of the year.

Figure 12.14:
Monthly wave height (black line), wave period (red line) and wave direction (arrows). The grey area represents the range of wave height between calm periods (10% of lowest wave height) and large wave events (10% of highest wave height).

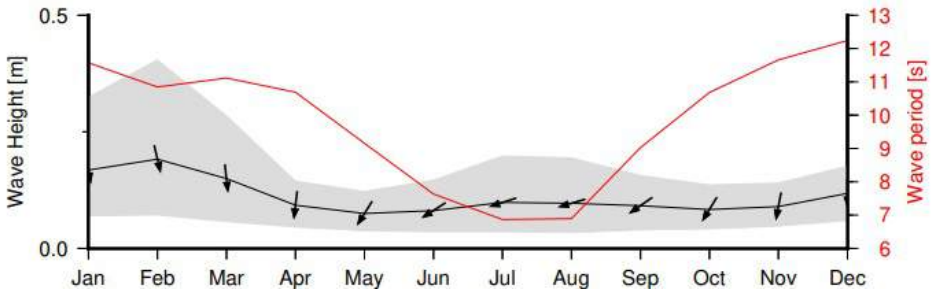

12.9.2 Trends

Waves change from month to month with the seasons, but they also change from year to year with climate oscillations. Typically, these changes are smaller than the seasonal changes but can be important during phenomena such as ENSO. In Honiara, the mean annual wave height has remained unchanged since 1979 (Figure 12.15). The mean annual wave height in Honiara is not significantly correlated with the main climate indicators of the region.

Figure 12.15.
Annual wave height (black line), wave period (red line) and wave direction (arrows). The grey area represents the range of wave height between calm periods (10% of lowest wave height) and large wave events (10% of highest wave height).

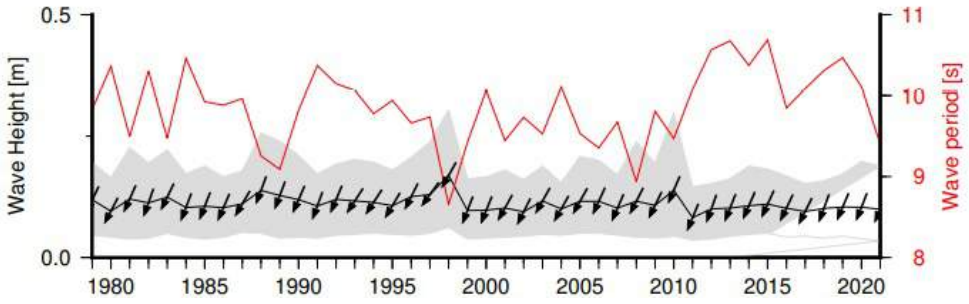

12.9.3 Extreme waves

Extreme wave analysis completed for Honiara was done by defining a severe height threshold and fitting a generalized Pareto distribution (GPD). The optimum threshold selected was 1.00 m. In the 42-year wave hindcast, 35 wave events reached or exceeded this threshold, averaging 1.7 events every two years. The GPD was fitted to the largest wave height reached during each of these events (Figure 12.16, Table 12.4). Extreme wave analysis is a very useful tool but is not always accurate because the analysis is very sensitive to the data available, the type of distribution fitted and the threshold used. For example, this analysis does not accurately account for tropical cyclone waves. More in-depth analysis is required to obtain results appropriate for designing coastal infrastructure and coastal hazard planning.

Figure 12.16:
Extreme wave distribution for Honiara. The crosses represent the wave events that have occurred since 1979. The solid line is the statistical distribution that best fits past wave events. The dashed lines show the upper and lower confidence limits of the fit. There is a 95% chance that the fitted distribution lies between the two dashed lines. Note that the annual return interval is in logarithmic scale.

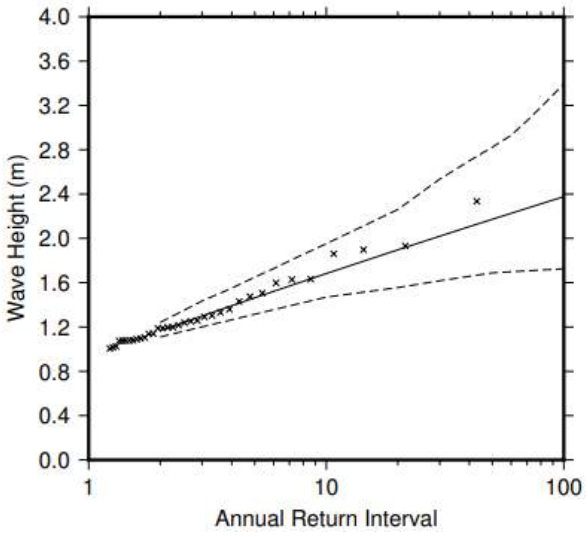

Table 12.4:
Summary of the results from extreme wave analysis in Honiara

Large wave height (90th percentile)	0.19 m
Severe wave height (99th percentile)	0.56 m
1-year ARI wave height	1.0 m
10-year ARI wave height	1.68 m
20-year ARI wave height	1.90 m
50-year ARI wave height	2.17 m
100-year ARI wave height	2.38 m

13 Tokelau

© credit

13.1 Summary

13.1.1 Climate

- Tokelau has a year-round hot and humid climate. Changes in air temperature from season to season are relatively small and strongly linked to changes in the surrounding ocean temperature. Tokelau has a wet season from October to March and a drier season from April to September.
- The seasonal cycle is strongly affected by the South Pacific Convergence Zone (SPCZ), which is most intense during the wet season.
- Annual and seasonal air temperatures at Nukunonu increased over the period 1979–2021. The annual number of hot days and warm nights has increased, and the number of cool days has decreased. The energy required for cooling indoor environments has also increased.
- No recent data exist to inform current rainfall trends.
- Tropical cyclones usually affect Tokelau between November and April. Over the period 1969–2018, an average of three cyclones passed within the Tokelau exclusive economic zone (EEZ) per decade. Tropical cyclones were equally likely in El Niño and neutral years and least frequent in La Niña years. Year-to-year variability is large, ranging from no tropical cyclones in some seasons to three in 2009/10.
- There has been little change in the total number of tropical cyclones in the Southwest Pacific since 1981/82. The number of severe tropical cyclones has declined over the same period/region.

13.1.2 Ocean

- Highest sea levels typically occur in the months January–May.
- Sea-level rise within the EEZ, measured by satellite altimeters since 1993, is about 3.5 to 4.5 mm per year.
- Monthly average sea surface temperature (SST) near Nukunonu, as measured by satellite, ranges from 28.6 °C in August to 29.5 °C in April. However, daily temperatures in any given year can be ±2 °C of these monthly averages.
- The SST trend, as per satellite observations, is 0.2 °C per decade.
- Dominant wave direction is from 151° (SE), with an average significant wave height of 1.54 m and average wave period of 11.82 s.
- Severe wave height was defined as 2.78 m, with an average of three severe events per year.
- Peak average significant wave height occurs between June and September.

13.2 Country description

Tokelau, a dependent territory of New Zealand is located in the tropical western South Pacific Ocean between latitudes 8°S and 10°S, and longitudes 171°W and 173°W (Figure 13.1). Tokelau is made up three coral atolls: Atafu, Nukunonu and Fakaofo.

The total land area is 10 km^2, and Tokelau has an EEZ of about 319,000 km^2. The capital rotates among the three atolls. The highest elevation is 5 m above sea level on Nukunonu. Tokelau has a population of approximately 1500.

Figure 13.1:
Tokelau and the location of the climate station used in this report

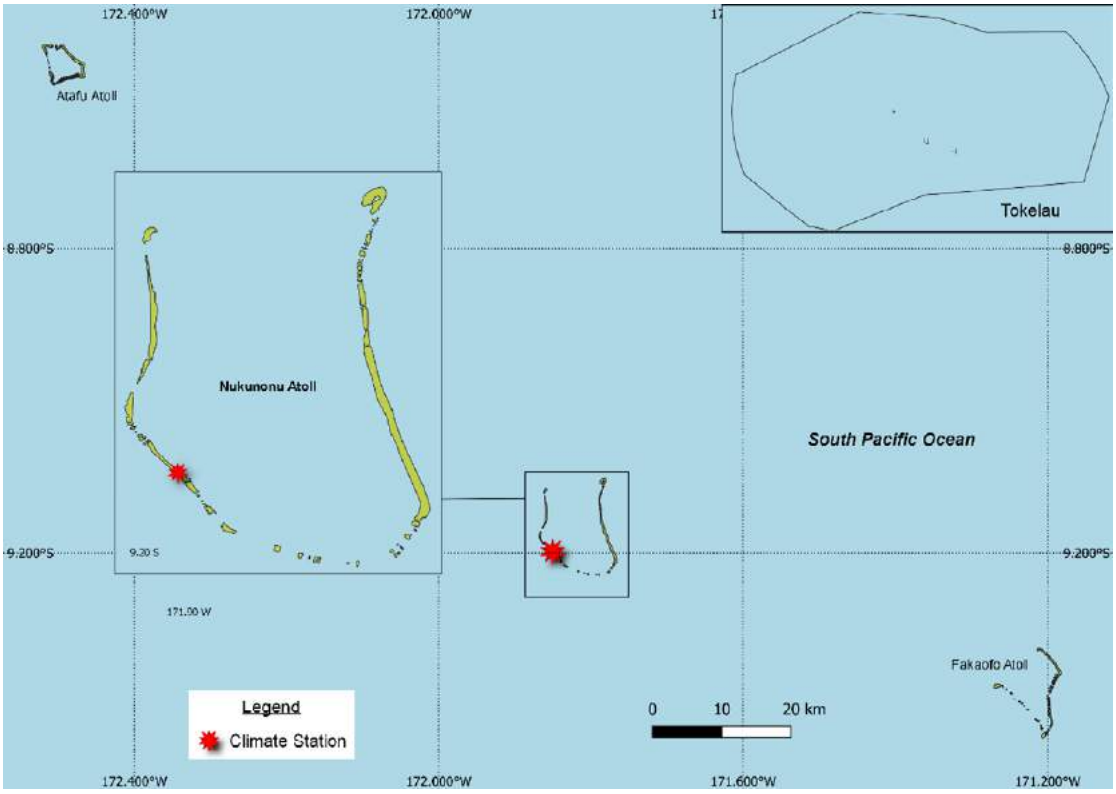

13.3 Data

Daily historical rainfall and air temperature records for Nukunonu from 1946 to 1996 were obtained from New Zealand's National Institute for Water and Atmosphere. Recent Automatic Weather Station data are available for Nukunonu, but the completeness of this data record is low and data were not available at the time data analysis was conducted. Nukunonu data have undergone data quality and homogeneity assessment. While Nukunonu rainfall and temperature have been used to derive climatological information and rainfall trends in this report, there are insufficient maximum or minimum air temperature data to produce long-term trends. ERA5 reanalysis has been used to calculate temperature trends from 1979 to 2021 (further information is provided in Chapter 1). Additional information on historical climate trends for Tokelau can be found in the Pacific Climate Change Data Portal http://www.bom.gov.au/climate/pccsp.

Tropical cyclone data and historical tracks starting from the 1969/70 season are available from the SHTC Data Portal http://www.bom.gov.au/cyclone/history/tracks/index.shtml.

SST covering the EEZ was obtained via the daily Optimum Interpolation SST version 2.1 (OISST2.1) dataset from NOAA (Reynolds et al. 2007; Banzon et al. 2016).

Wave data were obtained from the PACCSAP wave hindcast (Smith et al. 2021), available hourly from 1979 to present, with a grid resolution near Tokelau of 7 km.

Regional sea level data were obtained from CSIRO satellite altimetry (updated by Benoit Legresy, Church and White 2011), with correction for seasonal signals, inverse barometer effect and glacial isostatic adjustment.

13.4 Rainfall

13.4.1 Seasonal cycle

Rainfall is dominated by the SPCZ, which is typically located to the southwest of Tokelau during the wet season when the SPCZ is most active, contributing to rainfall averages in excess of 300 mm (Figure 13.2). The wettest months at Nukunonu fall between October and March, with 60% of the rainfall during these months and a peak in January with an average of 352 mm.

During the middle months of the year, the SPCZ moves closer to Tokelau, and despite being weaker and often inactive, its location during the drier season between April and September contributes to relatively high rainfall averages compared to neighbouring islands, with the driest month of May averaging 170 mm of rainfall.

Figure 13.2:
Mean annual rainfall at Nukunonu

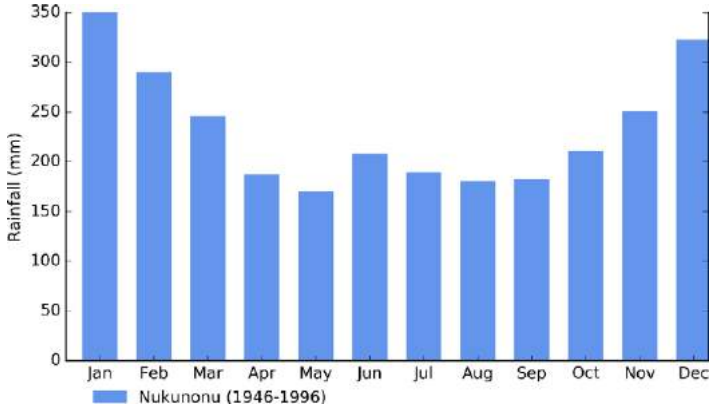

13.4.2 Trends

Annual and daily rainfall records at Nukunonu are short and end in 1993 (Figure 13.3). Due to the lack of data since this time, no trends are shown. Annual rainfall has varied from approximately 1400 to 3800 mm and approximately half of all days each year experience some rain (Figure 13.3).

Figure 13.4 shows variability in the longest run of days without rain and maximum daily rainfall at Nukunonu. Maximum daily rainfall has varied from 50 mm to almost 250 mm. Nukunonu rarely experiences more than 15 days without rain. Due to substantial gaps in the daily rainfall record and the lack of any recent data, trends in these two variables are not shown.

Figure 13.3:
Annual rainfall (bar graph) and number of wet days (where rainfall is at least 1 mm; line graph) at Nukunonu. Diamonds indicate years with insufficient data for one or both variables.

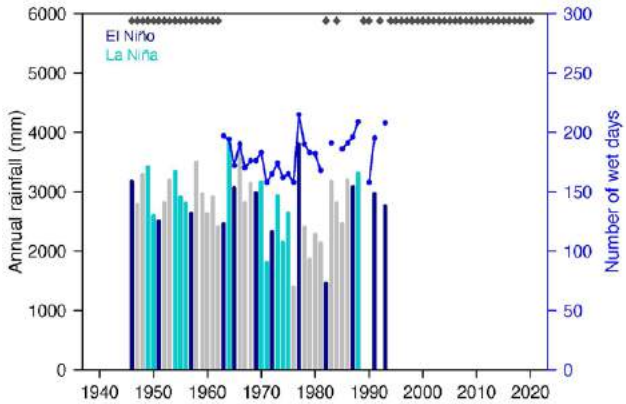

Figure 13.4:
Annual longest run of consecutive dry days (bar graph) and maximum daily rainfall (line graph) at Nukunonu. Diamonds indicate years with insufficient data for one or both variables.

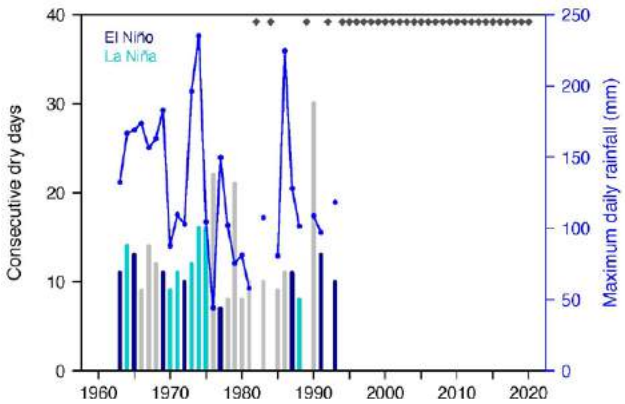

13.5 Air temperature

13.5.1 Seasonal cycle

Air temperatures have a small seasonal cycle over Tokelau (Figure 13.5). Being a small atoll, air temperatures over Tokelau are strongly linked to the surrounding sea surface temperatures. There is a 1.1 °C difference from the coolest average maximum temperature in January to the warmest in April. The coolest average minimum temperatures occur during July and August at a time when the cool, dry southeast trade winds are strongest.

Figure 13.5:
Maximum (dark purple) and minimum (purple) air temperature seasonal cycle for Nukunonu for the period 1961–1990

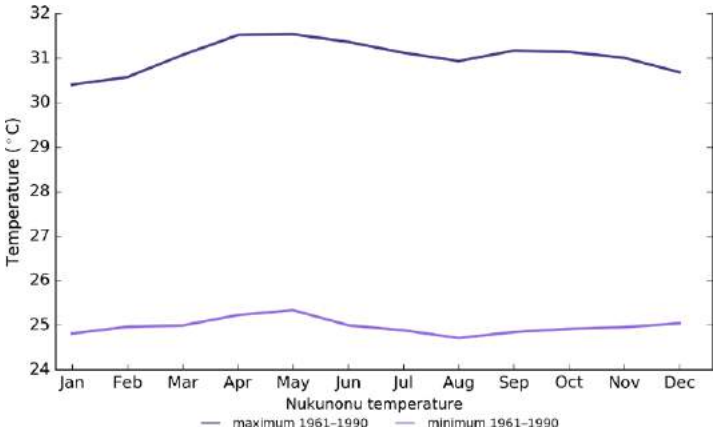

13.5.2 Trends

Due to quality and completeness issues with daily temperature records at Nukunonu, reanalysis data have been used to calculate temperature trends. Average annual and seasonal temperatures have increased at Nukunonu since 1979 (Table 13.1). All temperature trends are statistically significant, and November–April temperatures are increasing faster than May–October temperatures.

Table 13.1:
Trends in annual and seasonal air temperatures at Nukunonu from ERA5 reanalysis data (station temperatures have quality and completeness issues). A reanalysis is a global weather simulation merged with observations and represents the most complete picture of historical climate, but shares the same limitations as climate models. The 95% confidence intervals are shown in parentheses, and trends significant at the 95% level are shown in bold.

	Nukunonu–ERA5 Tmax (°C/decade)	Nukunonu–ERA5 Tmin (°C/decade)	Nukunonu–ERA5 Tmean (°C/decade)
	1979–2021		
Annual	**+0.13** (+0.04, +0.21)	**+0.10** (+0.03, +0.18)	**+0.12** (+0.04, +0.19)
November–April	**+0.16** (+0.06, +0.25)	**+0.14** (+0.04, +0.22)	**+0.15** (+0.05, +0.24)
May–October	**+0.11** (+0.05, +0.18)	**+0.09** (+0.03, +0.14)	**+0.10** (+0.05, +0.16)

The number of hot days and warm nights has increased and the number of cool days has decreased at Nukunonu (Table 13.2). The cooling degree days index provides a measure of the energy demand needed to cool a building down to 25 °C, with the assumption that air conditioners are generally turned on at this temperature. There has been a strong increase in the cooling degree index, suggesting the energy needed for cooling has increased significantly since 1979.

Table 13.2:
Trends in annual temperature extremes at Nukunonu from ERA5 reanalysis data (station temperatures have quality and completeness issues). A reanalysis is a global weather simulation merged with observations and represents the most complete picture of historical climate but shares the same limitations as climate models. The 95% confidence intervals are shown in parentheses, and trends significant at the 95% level are shown in bold. Hot and cool days, and warm and cold nights are measured relative to 1981–2010 (see Chapter 1 for details).

	Nukunonu–ERA5
	1979–2021
Number of hot days (days/decade)	**+22.91** (+9.99, +33.92)
Number of warm nights (nights/decade)	**+13.25** (+6.86, +18.75)
Number of cool days (days/decade)	**-7.76** (-17.23, -0.31)
Number of cold nights (nights/decade)	-4.12 (-11.73, +2.96)
Cooling degree days (degree days/decade)	**+44.07** (+12.44, +69.85)
Daily temperature range (°C/decade)	+0.02 (-0.01, +0.04)

13.6 Tropical cyclones

13.6.1 Seasonal cycle

Tropical cyclones usually affect Tokelau during the southern hemisphere tropical cyclone season, which occurs from November to April. The Southern Hemisphere Tropical Cyclone Archive indicates that between the 1969/70 and 2017/18 seasons, 15 tropical cyclones (Figure 13.6) passed within the EEZ. This represents an average of three cyclones per decade. Tropical cyclones are equally likely in El Niño and neutral years (3.2 cyclones per decade), and less frequent during La Niña years (2.0 cyclones per decade).

Interannual variability in the number of tropical cyclones in the EEZ is large, ranging from zero in many seasons to three in 2009/10 and two in 1997/98 and 2007/08 (Figure 13.6). High interannual variability and the small number of tropical cyclones occurring in the EEZ make reliable identification of long-term trends in frequency and intensity difficult.

Some tropical cyclone tracks analysed in this section include the tropical depression stage (sustained winds ≤34 knots) before and/or after tropical cyclone formation.

Figure 13.6:
Number of tropical cyclones passing within the Tokelau EEZ per season. Each season is defined by the ENSO status, with light blue being an El Niño year, dark blue a La Niña year and grey showing a neutral ENSO year.

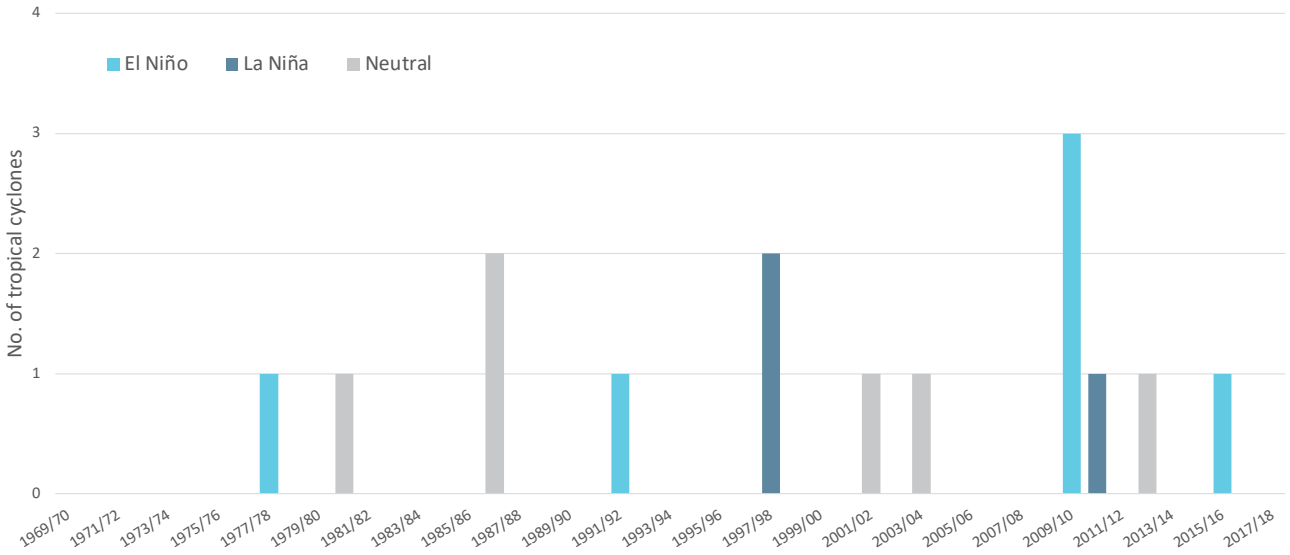

13.6.2 Trends

Trends in total number of tropical cyclones (<995 hPa) and severe tropical cyclones (<970 hPa) are presented for the period 1981/82–2020/21 for the greater Southwest Pacific (135°E–120°W; 0–50°S). Trends are presented at a regional scale as the number of tropical cyclones occurring within Pacific Island EEZs is insufficient for reliable long-term trend analysis.

For the total number of tropical cyclones, the trend (and 95% confidence interval) is -0.92 (-1.85, 0.01) tropical cyclones/decade. There has been little change/marginal decline in the total number of tropical cyclones over the last 40 seasons. This trend is not statistically significant.

For the total number of severe tropical cyclones, the trend is -0.80 (-1.32, -0.29) tropical cyclones/decade. There is a negative trend in the number of severe tropical cyclones over the last 40 seasons. There has been little change/marginal decline in the proportion of tropical cyclones reaching severe status. The trend is -0.04 (-0.08, 0.00) tropical cyclones/decade. The negative trend is statistically significant.

Records of tropical cyclones exist from the late 1800s in some countries in the Southwest Pacific, but trends in tropical cyclones have only been presented from 1981/82. Satellite-based observations began in the Southwest Pacific in the early 1970s, but consistent coverage and reliable intensity estimates have only been available since the early 1980s. Confidence in tropical cyclone trends is moderate as the definition of a tropical cyclone has changed and satellite observation methods have continued to improve over the last 40 years.

13.7 Sea surface temperature

13.7.1 Seasonal cycle

Sea surface temperature, as measured by satellite observations near Nukunonu from 1982 to 2021, reaches on average a maximum of just above 29.5°C in April but can get as high as 30.5 °C (Figure 13.7). Minimum average temperature is 28.6 °C in August. Daily temperatures can be up to 2°C higher or lower than these monthly averages,, although 50% of daily observations fall within 1°C of the average.

Figure 13.7:
Annual sea surface temperatures near Nukunonu. Blue dots show the monthly average, and shaded boxes show the middle 50% of daily observations Lines show the top and bottom 25% of daily observations

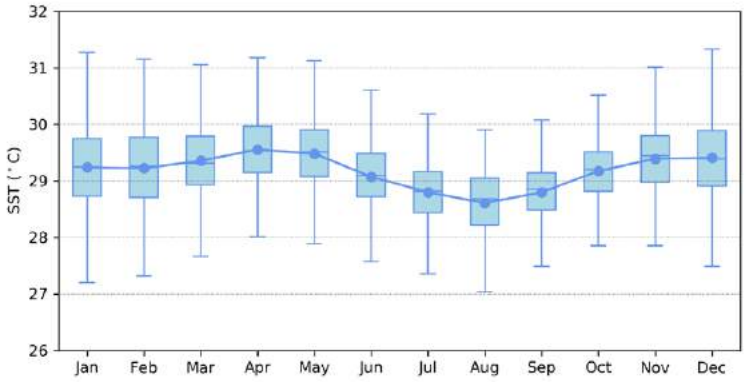

13.7.2 Trends

Figure 13.8 shows the 1981–2021 SST from satellite observations averaged over the EEZ. The data show a trend of 0.20 °C per decade with a 95% confidence interval of ±0.04 °C.

Figure 13.8:
Sea surface temperature from satellite observations averaged across the Tokelau EEZ, shown as the orange line. The blue line shows the linear regression trend.

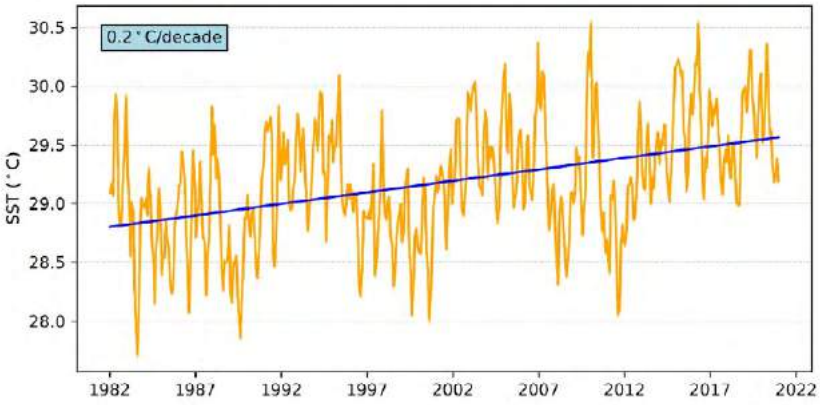

13.8 Sea level

13.8.1 Seasonal cycle

Tokelau experiences a semidiurnal tidal cycle, meaning two high and two low tides per day. Figure 13.9 shows the monthly percentage where the 99th percentile sea level threshold is exceeded near Nukunonu. Peak sea levels typically occur January to May.

Figure 13.9:
Percentage of monthly occurrence where the 99th percentiles is exceeded from January 1993 to July 2020 near Nukunonu. The row provides a percentage summary of all the years.

	Number of months exceeding 90th percentile											
	Jan	Feb	Mar	Apr	May	Jun	Jul	Aug	Sep	Oct	Nov	Dec
Monthly Totals (%)	13	22	28	16	13	3	0	0	0	0	3	3

13.8.2 Trends

Sea level at Tokelau, measured by satellite altimeters (Figure 13.10) since 1993, is between 3.5 and 4.5 mm per year across the EEZ, with a 95% confidence interval of ±0.6 to ±0.8 mm. This rise is partly linked to a pattern related to climate variability from year to year and decade to decade, and is a higher trend than the global average of 3.1 ± 0.4 mm per year (von Schuckmann et al. 2021).

Figure 13.10:
Satellite altimetry annual trend for the Pacific from 1993 to 2020, with the Tokelau EEZ highlighted. The star symbol indicates the location of seasonal SST and sea level analysis.

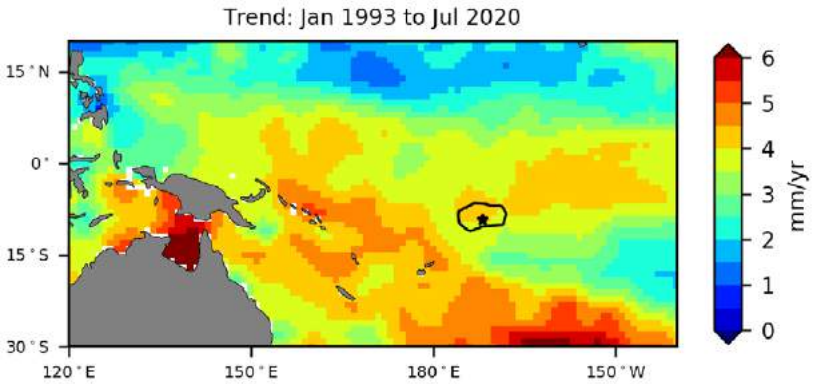

13.9 Waves

13.9.1 Seasonal cycle

The average wave climate in Nukunonu is defined by the significant wave height, peak period and peak direction. The significant wave height is the mean wave height (from trough to crest) of the highest one third of waves and corresponds to the wave height that would be reported by an experienced observer. Peak period is the time interval between two waves of the dominant wave period. Peak direction is the direction from which the dominant waves are coming.

The average sea state is dominated by swells from the southeast. The annual mean wave height is 1.54 m, the annual mean wave direction is 151° and the annual mean wave period is 11.82 s. In the Pacific, waves often come from multiple directions and for different periods at a time. In Nukunonu, there are often more than eight different wave direction/period components coming from the southeast to southwest (Figure 13.11).

The seasonal average significant wave height peaks between June and September, whereas the wave period peaks between January and March (Figure 13.12). Average wave direction is also from the southeast when the storm activity in the Southern Ocean is at its highest (May–October).

Figure 13.11:
Annual wave rose for Nukunonu. Note that direction is where the wave is coming from.

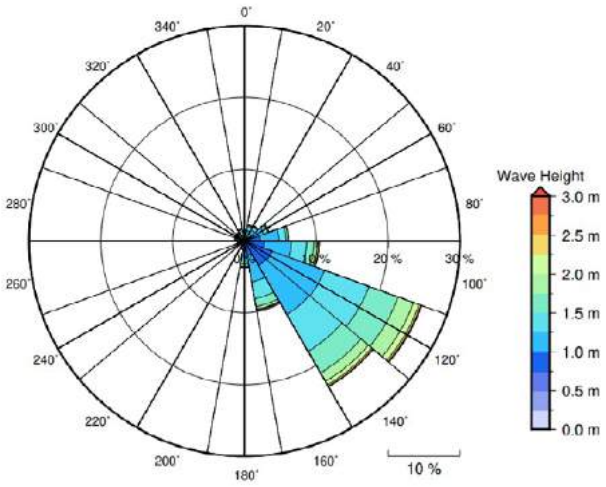

Figure 13.12:
Monthly wave height (black line), wave period (red line) and wave direction (arrows). The grey area represents the range of wave height between calm periods (10% of lowest wave height) and large wave events (10% of highest wave height).

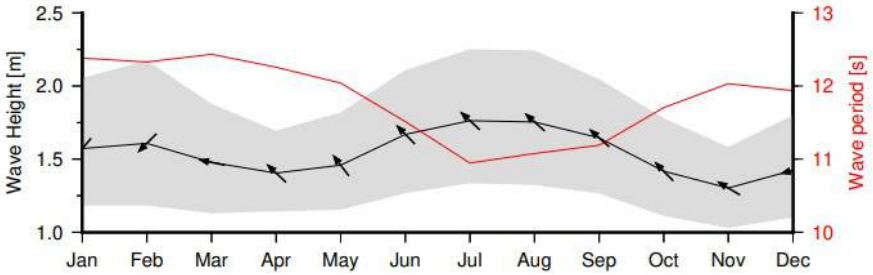

13.9.2 Trends

Waves change from month to month with the seasons, but they also change from year to year with climate oscillations. Typically, these changes are smaller than the seasonal changes but can be important during phenomena such as ENSO. In Nukunonu, the mean annual wave height has remained unchanged since 1979. The mean annual wave height in Nukunonu is not significantly correlated with the main climate indicators of the region.

Figure 13.13:
Annual wave height (black line), wave period (red line) and wave direction (arrows). The grey area represents the range of wave height between calm periods (10% of lowest wave height) and large wave events (10% of highest wave height).

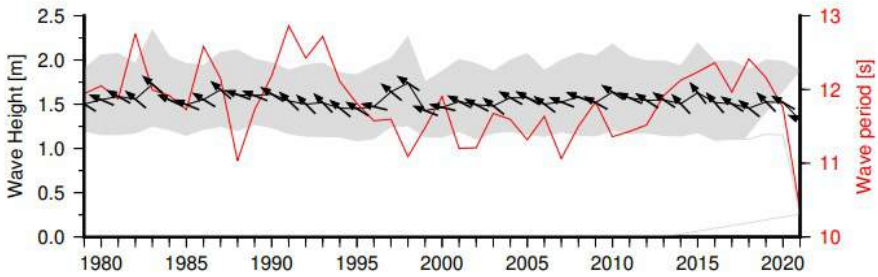

13.9.3 Extreme waves

Extreme wave analysis completed for Nukunonu was done by defining a severe height threshold and fitting a generalized Pareto distribution (GPD). The optimum threshold selected was 2.78 m. In the 42-year wave hindcast, 128 wave events reached or exceeded this threshold, averaging three per year. The GPD was fitted to the largest wave height reached during each of these events (Figure 13.14, Table 17.4). Extreme wave analysis is a very useful tool but is not always accurate because the analysis is very sensitive to the data available, the type of distribution fitted and the threshold used. For example, this analysis does not accurately account for tropical cyclone waves. More in-depth analysis is required to obtain results appropriate for designing coastal infrastructure and coastal hazard planning.

Figure 13.14:
Extreme wave distribution for Nukunonu. The crosses represent the wave events that have occurred since 1979. The solid line is the statistical distribution that best fits past wave events. The dashed lines show the upper and lower confidence limits of the fit. There is a 95% chance that the fitted distribution lies between the two dashed lines. Note that the annual return interval is in logarithmic scale.

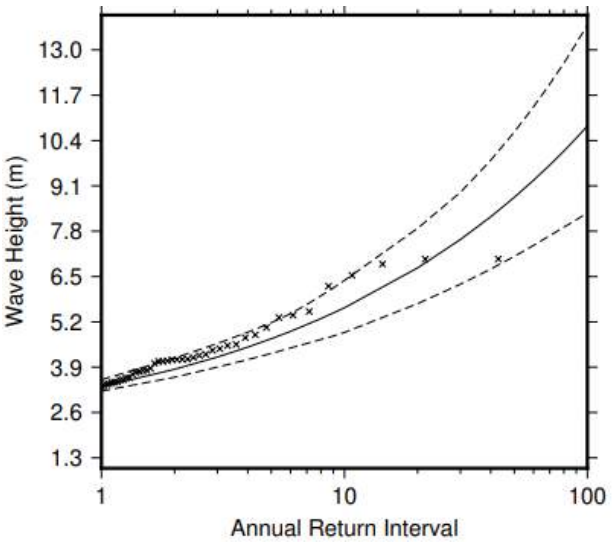

Table 13.4:
Summary of the results from extreme wave analysis in Nukunonu

Large wave height (90th percentile)	1.99 m
Severe wave height (99th percentile)	2.87 m
1-year ARI wave height	3.34 m
10-year ARI wave height	5.60 m
20-year ARI wave height	6.75 m
50-year ARI wave height	8.77 m
100-year ARI wave height	10.82 m

14 Tonga

14.1 Summary

14.1.1 Climate

- Changes in air temperature from season to season are relatively small and strongly linked to changes in the surrounding ocean temperature. Tonga has two distinct seasons – a warm wet season from November to April and a cooler dry season from May to October.
- The seasonal cycle is strongly affected by the South Pacific Convergence Zone (SPCZ), which is most intense during the wet season.
- Annual and seasonal air temperatures at Nuku'alofa increased over the period 1951–2020.
- At Lupepau'u, May to October rainfall has increased along with the proportion of total rain that falls during extreme events.
- Tropical cyclones usually affect Tonga between November and April. Over the period 1969–2018, an average of 21 cyclones passed within the Tonga exclusive economic zone (EEZ) per decade. Tropical cyclones were most frequent in El Niño years and least frequent in La Niña years. Year-to-year variability is large, ranging from no tropical cyclones in some seasons to six in 2015/16.
- There has been little change in the total number of tropical cyclones in the Southwest Pacific since 1981/82. The number of severe tropical cyclones has declined over the same period/region.

14.1.2 Ocean

- Highest sea levels typically occur in the months December–April.
- Sea-level rise within the EEZ, measured by satellite altimeters since 1993, is about 3.5 to 5 mm per year.
- Monthly average ocean temperature, as measured by the Nukualofa tide-gauge, ranges from 23 °C in August to 27.5 °C in the months February/March. However, monthly temperatures in any given year can be ±3 °C of these averages.
- The sea surface temperature (SST) trend, as per satellite observations, is 0.27 °C per decade.
- Dominant wave direction is from 60° (NE), with an average significant wave height of 1.30 m and average wave period of 13.48 s.
- Severe wave height was defined as 3.65 m, with an average of 3.1 severe events per year.
- Peak average significant wave height occurs around July.

14.2 Country description

The Kingdom of Tonga is located in the tropical western South Pacific Ocean between latitudes 15°S and 22°S, and longitudes 173°W and 176°W (Figure 14.1). Tonga is an archipelago of 169 islands of which 36 are inhabited and divided into three main groups, Vava'u, Ha'apai and Tongatapu, which extend over 800 km from north to south. Tonga has a total land area of 750 km^2 and an EEZ of 0.7 million km^2. The largest island Tongatapu, on which the capital Nuku'alofa is located, covers about 260 km^2. The highest elevation is 1078 m above sea level on Kao Island in the Ha'apai Group. Tonga's population is approximately 104,000. About 70% live on the main island of Tongatapu.

Figure 14.1:
Tonga and the locations of the climate stations used in this report

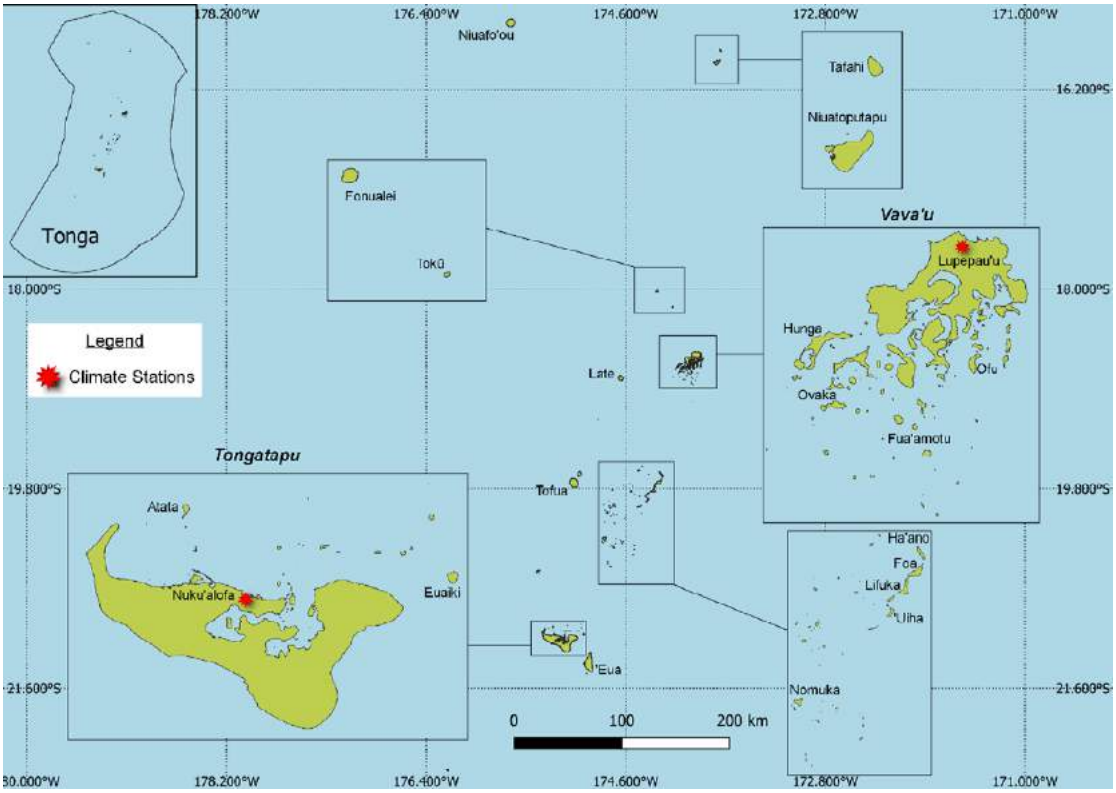

14.3 Data

Daily and monthly historical rainfall and air temperature records for Nuku'alofa and Vava'u–Lupepau'u from 1951 were obtained from the Tonga Meteorological Service. These records have undergone data quality and homogeneity assessment. Where the maximum or minimum air temperature records were found to have discontinuities, these records have been adjusted to make them homogeneous (further information is provided in Chapter 1). Additional information on historical climate trends for Tonga can be found in the Pacific Climate Change Data Portal http://www.bom.gov.au/climate/pccsp.

Tropical cyclone data and historical tracks starting from the 1969/70 season are available from the SHTC Data Portal http://www.bom.gov.au/cyclone/history/tracks/index.shtml.

SST covering the EEZ was obtained via the daily Optimum Interpolation SST version 2.1 (OISST v2.1) dataset from NOAA (Reynolds et al. 2007; Banzon et al. 2016). In situ ocean temperature data were obtained from the PSLGM Project tide-gauge located at Nuku'alofa, with data spanning from 1992 to present.

Wave data were obtained from the PACCSAP wave hindcast (Smith et al. 2021), available hourly from 1979 to present, with a grid resolution near Tonga of 7 km.

Regional sea level data were obtained from CSIRO satellite altimetry (updated by Benoit Legresy, Church and White 2011), with correction for seasonal signals, inverse barometer effect and glacial isostatic adjustment. Tide-gauge data were sourced from the Nuku'alofa tide-gauge station, which dates back to 1988 at hourly intervals.

14.4 Rainfall

14.4.1 Seasonal cycle

The seasonal cycle of rainfall over Tonga is dominated by the SPCZ, which is most active and closest to Tonga during the wet season, resulting in average rainfall above 200 mm during January–March (Figure 14.2). Wet season rainfall between November and April accounts for 63% of Nuku'alofa's annual rainfall and 65% of Vavau–Lupepau'u's. Active phases of the Madden–Julian Oscillation (MJO) near Tonga can be associated with significant rainfall for several days in the wet season.

In the cooler/drier half of the year (May–October), less energy is received from the sun and subtropical high pressure systems move north, bringing cooler, drier conditions to Nuku'alofa and Vavau–Lupepau'u.

Figure 14.2:
Mean annual rainfall at Nuku'alofa and Vavau–Lupepau'u

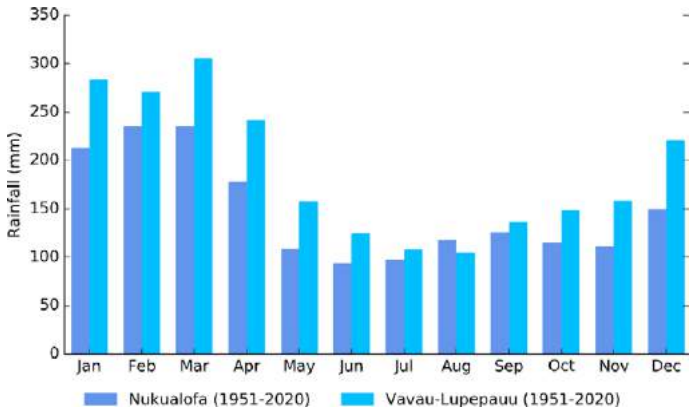

14.4.2 Trends

May–October rainfall has increased significantly at Lupepau'u. All other trends in annual and seasonal rainfall at Nuku'alofa and Lupepau'u are not significant (Figure 14.2, Table 14.1). Notable year-to-year variability associated with El Niño–Southern Oscillation (ENSO) is evident at both sites, with La Niña years generally receiving more rainfall than El Niño years (Figure 14.2). Annual rainfall has varied from approximately 800 to 2700 mm at Nuku'alofa and approximately 1100 to 3300 mm at Lupepau'u.

Figure 14.3:
Annual rainfall (bar graph) and number of wet days (where rainfall is at least 1 mm; line graph) at Nuku'alofa (left) and Lupepau'u (right). Straight lines indicate linear trends for annual rainfall (in black) and number of wet days (in blue). Criteria for statistical robustness were not met for determining a linear trend for wet days at Nuku'alofa. The magnitudes of the trends are presented in Table 14.1. Diamonds indicate years with insufficient data for one or both variables.

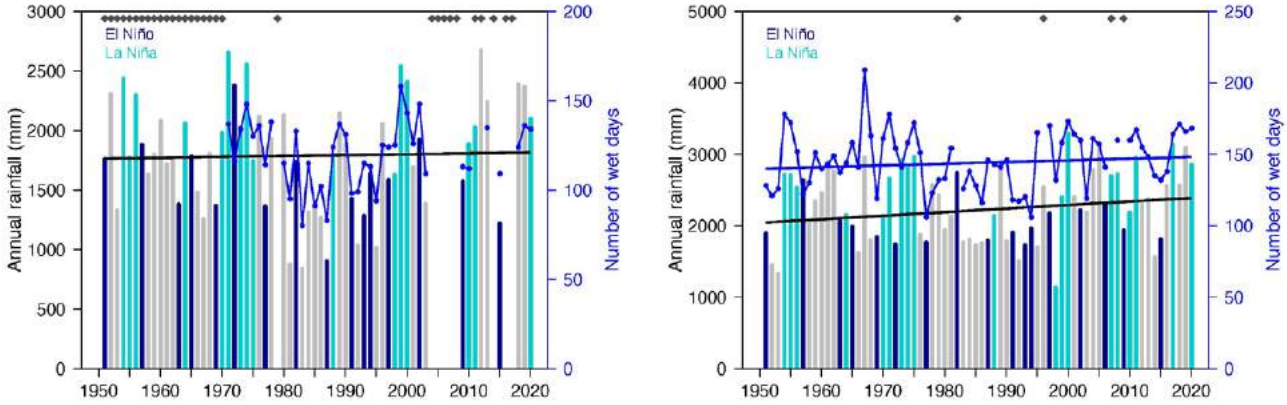

Table 14.1:
Trends in annual, seasonal and extreme rainfall at Nuku'alofa (left) and Lupepau'u (right). The 95% confidence intervals are shown in parentheses, and trends significant at the 95% level are shown in bold. The contribution to total rainfall from extreme events and the standardised rainfall evapotranspiration index are measured relative to 1961–1990 (see Chapter 1 for details). Criteria for statistical robustness were not met for determining linear trends for some rainfall extremes at Nuku'alofa. The standardised rainfall evapotranspiration index is not available for Lupepau'u due to the lack of daily temperature observations at this site.

	Nuku'alofa	Lupepau'u
	1951–2020	1951–2020
Annual rainfall (mm/decade)	+7.33 (-89.86, +100.78)	+49.62 (-37.24, +134.86)
November–April (mm/decade)	+4.34 (-63.35, +68.85)	-4.58 (-57.70, +50.92)
May–October (mm/decade)	+9.59 (-19.38, +36.86)	**+33.5** (+1.60, +61.41)
	1971–2020	1951–2020
Number of wet days (days/decade)	-	+1.20 (-2.41, +4.85)
Contribution to total rainfall from extreme events (%/decade)	-	**+1.47** (+0.04, +3.22)
Consecutive dry days (days/decade)	-	-0.16 (-1.12, +0.80)
Maximum one-day rainfall (mm/decade)	+6.50 (-6.00, +18.00)	+3.14 (-4.40, +10.69)
Standardised rainfall evapotranspiration index (November–April)	+0.36 (-0.04, +0.79)	-
Standardised rainfall evapotranspiration index (May–October)	+0.10 (-0.13, +0.30)	-

Numerous gaps exist in the daily rainfall record for Nuku'alofa, which prevents the robust calculation of trends for some rainfall extremes (Table 14.2). However, the proportion of total rain falling during extreme events has been increasing significantly at Lupepau'u. Maximum daily rainfall since 1971 has increased at Nuku'alofa, although this trend is not statistically significant (Figure 14.4).

Figure 14.4:
Annual longest run of consecutive dry days (bar graph) and maximum daily rainfall (line graph) at Nukuʻalofa (left) and Lupepauʻu (right). Straight lines indicate linear trends for dry days (in black) and maximum daily rainfall (in blue). Criteria for statistical robustness were not met for determining a linear trend for consecutive dry days at Nukuʻalofa. The magnitudes of the trends are presented in Table 14.1. Diamonds indicate years with insufficient data for one or both variables.

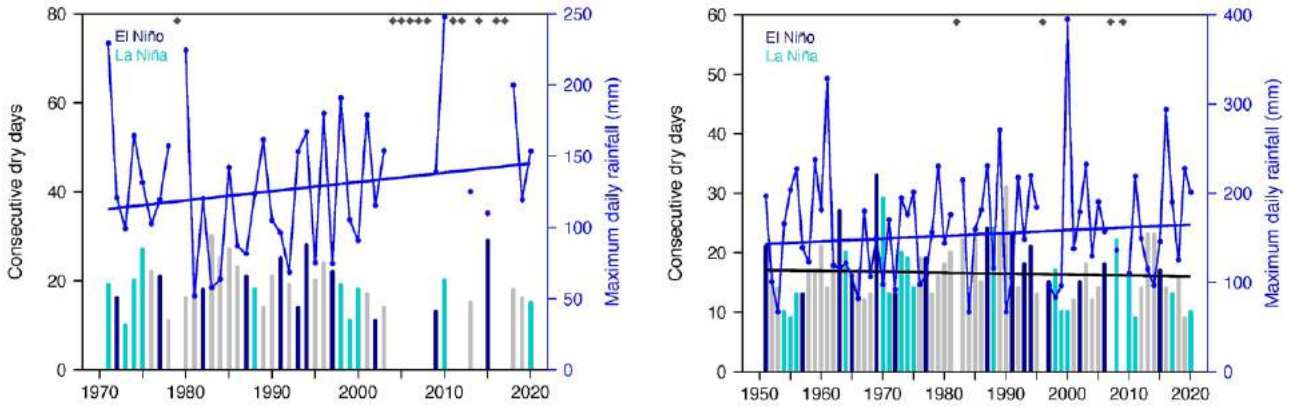

14.5 Air temperature

14.5.1 Seasonal cycle

Air temperatures at Tonga are driven by surrounding ocean temperatures, and during the dry season from May to October are also affected by subtropical high-pressure systems that direct cooler air from the south. Seasonal variations in maximum and minimum air temperatures at Nukuʻalofa are in excess of 5 °C (Figure 14.5). Vavau–Lupepauʻu has less pronounced seasonal changes in air temperatures, with variations for air temperatures across the year less than 4 °C. Air temperatures are generally much warmer in the middle months of the year at Vavau–Lupepauʻu compared to Nukuʻalofa, which is further to the south and close to the subtropics.

There has been warming across all months at Nukuʻalofa for both maximum and minimum air temperatures between the 1991–2020 and 1961–1990 climatology periods. The largest difference between the climatology periods is 0.9 °C for maximum temperature during November and December.

Figure 14.5:
Maximum and minimum air temperature seasonal cycle for Nukuʻalofa (purple) and Vavau – Lupepauʻu (green), and for the periods 1961–1990 (dotted lines) and 1991–2020 (solid lines)

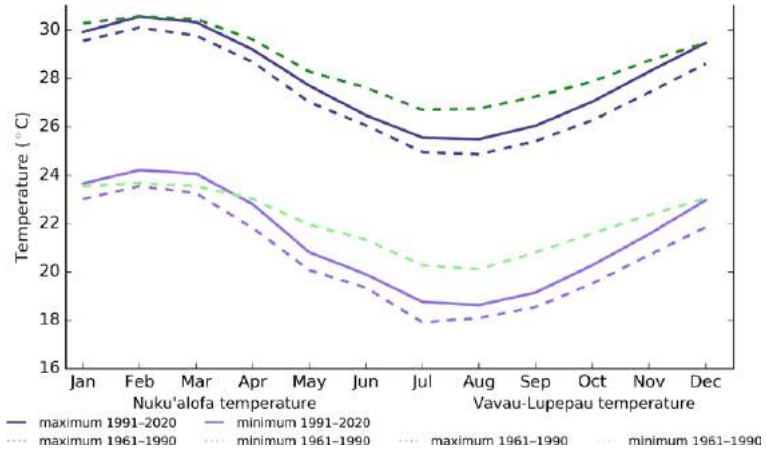

14.5.2 Trends

Average annual and seasonal temperatures have increased significantly at Nuku'alofa (Figure 14.6). Daily minimum temperatures are increasing faster than daily maximum temperatures and November–April temperatures are increasing faster than May–October temperatures (Table 14.2).

Figure 14.6:
Average annual, November–April and May–October temperatures for Nuku'alofa. Straight lines indicate linear trends. The magnitudes of the trends are presented in Table 14.2. Diamonds indicate years with insufficient data for one or more variables.

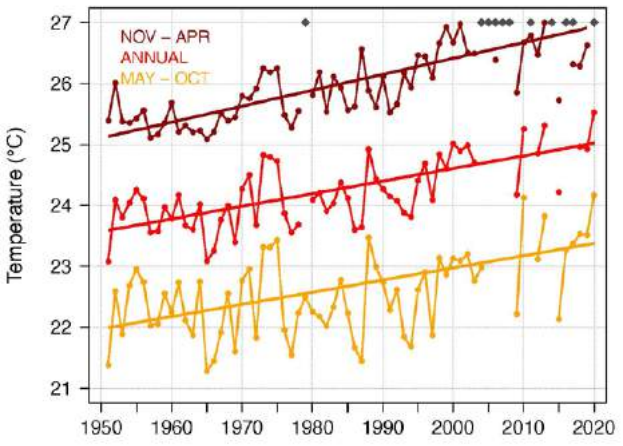

Table 14.2:
Trends in annual and seasonal air temperatures at Nuku'alofa. The 95% confidence intervals are shown in parentheses, and trends significant at the 95% level are shown in bold.

	Nuku'alofa Tmax (°C/decade)	Nuku'alofa Tmin (°C/decade)	Nuku'alofa Tmean (°C/decade)
	1951–2020		
Annual	**+0.18** (+0.09, +0.26)	**+0.23** (+0.13, +0.34)	**+0.21** (+0.11, +0.30)
November–April	**+0.21** (+0.16, +0.27)	**+0.29** (+0.18, +0.39)	**+0.26** (+0.18, +0.34)
May–October	**+0.16** (+0.07, +0.27)	**+0.22** (+0.09, +0.32)	**+0.20** (+0.08, +0.29)

Numerous gaps exist in the daily temperature record for Nuku'alofa, which prevents the robust calculation of trends in temperature extremes. Nevertheless, Figure 14.7 shows that several years since 2010 experienced more than three times as many hot days compared to the beginning of the record. This is consistent with the increases in average temperatures (Figure 14.6) and trends in temperature extremes in neighbouring Pacific Island countries.

Figure 14.7:
Annual number of hot days and cold nights at Nuku'alofa. Diamonds indicate years with insufficient data for one or both variables.

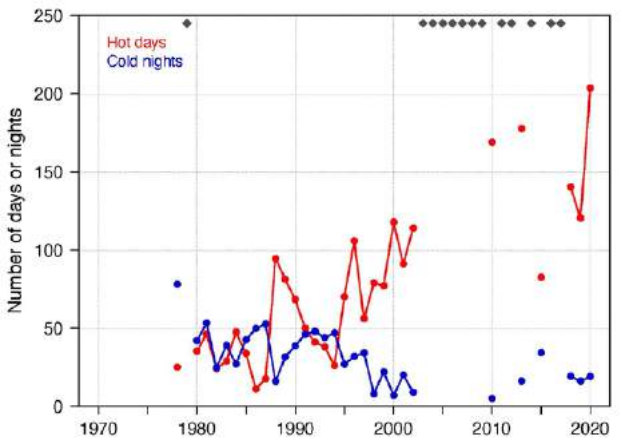

14.6 Tropical cyclones

14.6.1 Seasonal cycle

Tropical cyclones usually affect Tonga during the southern hemisphere tropical cyclone season, which is from November to April, but also occasionally occur outside the tropical cyclone season. The Southern Hemisphere Tropical Cyclone Archive indicates that between the 1969/70 and 2017/18 seasons, 101 tropical cyclones (Figure 14.8) passed within the EEZ. This represents an average of 21 cyclones per decade. Tropical cyclones were most frequent in neutral years (23 cyclones per decade), followed by El Niño years (20 cyclones per decade) and least frequent in La Niña years (17 cyclones per decade).

Interannual variability in the number of tropical cyclones in the EEZ is large, ranging from zero in some seasons to six in 2015/16 and five in 1979/80, 1992/93 and 2002/03 (Figure 14.8). High interannual variability and the small number of tropical cyclones occurring in the EEZ make reliable identification of long-term trends in frequency and intensity difficult.

Some tropical cyclone tracks analysed in this section include the tropical depression stage (sustained winds ≤34 knots) before and/or after tropical cyclone formation.

Figure 14.8:
Number of tropical cyclones passing within the Tonga EEZ per season. Each season is defined by the ENSO status, with light blue being an El Niño year, dark blue a La Niña year and grey showing a neutral ENSO year. The 11-year moving average is presented as a purple line and considers all years.

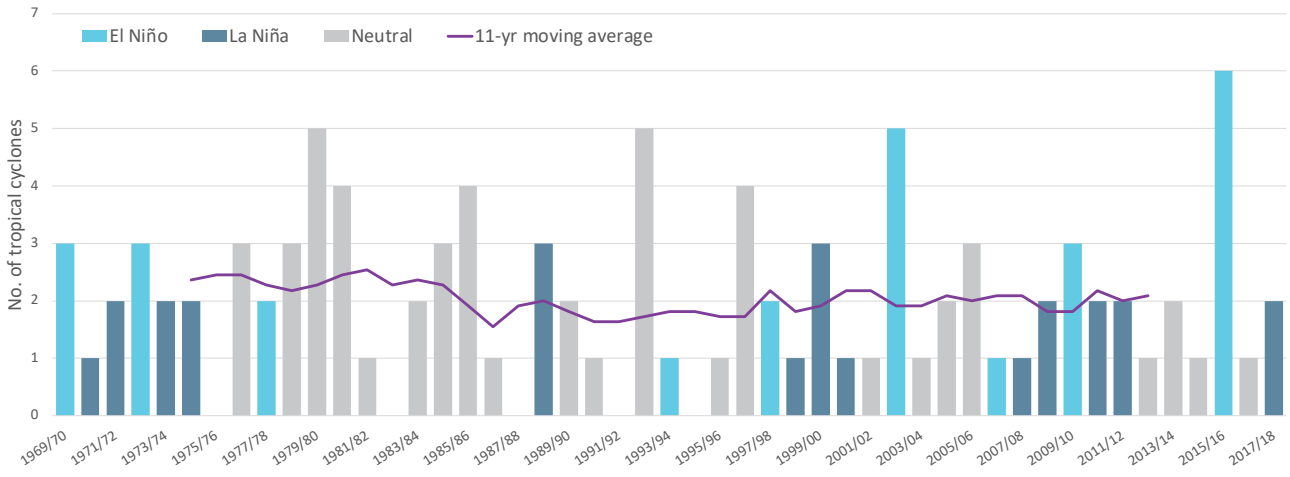

14.6.2 Trends

Trends in total number of tropical cyclones (<995 hPa) and severe tropical cyclones (<970 hPa) are presented for the period 1981/82–2020/21 for the greater Southwest Pacific (135°E–120°W; 0–50°S). Trends are presented at a regional scale as the number of tropical cyclones occurring within Pacific Island EEZs is insufficient for reliable long-term trend analysis.

For the total number of tropical cyclones, the trend (and 95% confidence interval) is -0.92 (-1.85, 0.01) tropical cyclones/decade. There has been little change/marginal decline in the total number of tropical cyclones over the last 40 seasons. This trend is not statistically significant.

For the total number of severe tropical cyclones, the trend is -0.80 (-1.32, -0.29) tropical cyclones/decade. There is a negative trend in the number of severe tropical cyclones over the last 40 seasons. There has been little change/marginal decline in the proportion of tropical cyclones reaching severe status. The trend is -0.04 (-0.08, 0.00) tropical cyclones/decade. The negative trend is statistically significant.

Records of tropical cyclones exist from the late 1800s in some countries in the Southwest Pacific, but trends in tropical cyclones have only been presented from 1981/82. Satellite-based observations began in the Southwest Pacific in the early 1970s, but consistent coverage and reliable intensity estimates have only been available since the early 1980s. Confidence in tropical cyclone trends is moderate as the definition of a tropical cyclone has changed and satellite observation methods have continued to improve over the last 40 years.

14.7 Sea surface temperature

14.7.1 Seasonal cycle

Ocean temperature, as measured by the Nuku'alofa tide-gauge from 1992 to 2021, reaches on average a maximum of 27.5 °C in February/March, but individual months in January to March can get as high as almost 30 °C (Figure 14.9). Minimum average temperature is approximately 23 °C in August. Hourly temperatures can be up to 3 °C higher or lower than these monthly averages, although 50% of hourly observations fall within 1.5 °C of the average.

Figure 14.9:
Annual temperatures measured at the Nuku'alofa tide-gauge. Blue dots show the monthly average, and shaded boxes show the middle 50% of hourly observations. Lines show the top and bottom 25% of hourly observations.

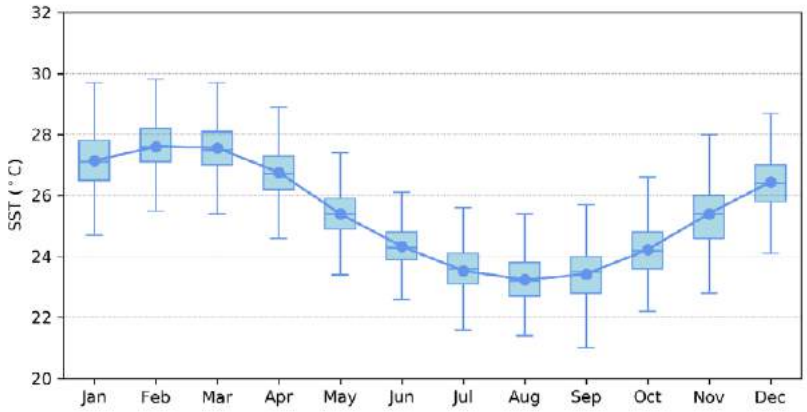

14.7.2 Trends

Figure 14.10 shows the 1981–2021 SST from satellite observations averaged over the EEZ. The satellite data show a trend of 0.27 °C per decade with a 95% confidence interval of ±0.11 °C.

Figure 14.10:
Sea surface temperature from satellite observations averaged across the Tonga EEZ, shown as the orange line. The blue line shows the linear regression trend.

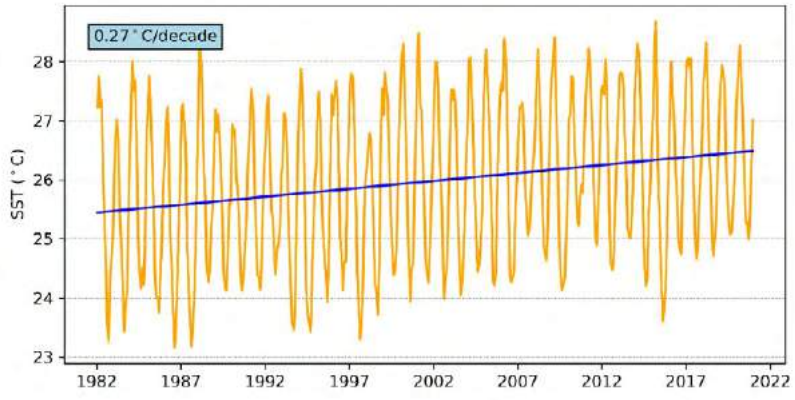

14.8 Sea level

14.8.1 Seasonal cycle

Tonga experiences a semidiurnal tidal cycle, meaning two high and two low tides per day. The highest predicted tides of the year typically occur during the wet season months of December–February. Figure 14.11 shows the number of hours the 99th percentile (1.91 m) sea level threshold is exceeded per month across the entire sea level record at Nuku'alofa. Peak sea levels typically occur over a significant portion of the year, ranging from December to April. Since approximately 2008, increasingly more hours each year exceed the 99th percentile threshold. This is due to a combination of sea-level rise and subsidence occurring at Tonga (Brown et al. 2020).

Figure 14.11:
Number of hours exceeding 99th percentile sea level threshold per month from 1993 to 2021 at the Nuku'alofa tide-gauge. Blue shading indicates the number of hours, and the final row provides a percentage summary of all the years.

Number of hours exceeding 1.91 m (Nuku'Alofa, Tonga)

	Jan	Feb	Mar	Apr	May	Jun	Jul	Aug	Sep	Oct	Nov	Dec	Annual
1993	0	0	0	0	0	0	0	0	0	0	0	0	0
1994	0	0	0	0	0	0	0	0	0	0	0	0	0
1995	0	0	0	0	0	0	0	0	0	0	0	0	0
1996	0	0	0	0	0	0	0	0	0	0	0	0	0
1997	0	0	12	0	0	0	0	0	0	0	0	0	12
1998	0	0	0	0	0	0	0	0	0	0	0	2	2
1999	0	0	0	0	0	0	0	0	0	0	0	1	1
2000	9	0	2	0	0	0	0	0	0	0	0	0	11
2001	0	0	0	0	0	0	0	0	0	0	0	0	0
2002	0	0	3	0	0	0	0	0	0	0	0	0	3
2003	0	0	0	0	0	0	0	0	0	0	0	0	0
2004	0	0	0	0	0	0	0	0	0	0	0	0	0
2005	0	0	0	0	0	0	0	0	0	0	0	0	0
2006	0	0	0	0	0	0	0	0	0	0	0	0	0
2007	0	0	0	0	0	0	0	0	0	1	2	0	3
2008	0	0	0	0	0	0	0	0	0	0	0	4	4
2009	14	0	0	0	0	0	0	0	0	0	0	0	14
2010	1	3	0	0	0	0	0	0	0	0	0	0	4
2011	0	0	0	2	0	0	0	0	1	0	0	0	3
2012	0	3	0	6	0	0	0	0	0	0	0	3	12
2013	3	0	0	0	0	0	1	0	0	0	0	0	4
2014	8	5	14	0	0	0	1	0	0	0	0	0	28
2015	0	0	2	0	0	0	0	0	0	0	0	0	2
2016	0	0	0	0	0	0	0	0	0	0	0	0	0
2017	0	0	0	0	0	0	0	0	0	0	0	5	5
2018	5	1	0	0	0	0	0	1	0	0	0	0	7
2019	4	3	4	0	0	0	0	0	1	0	0	0	12
2020	3	3	7	7	0	0	0	0	0	7	6	11	44
2021	0	1	0	3	1	0	0	0	0	0	0	7	12
Monthly Totals (%)	26	10	24	10	1	0	1	1	1	4	4	18	

14.8.2 Trends

Sea level at Tonga, measured by satellite altimeters (Figure 14.12) since 1993, has risen between 3.5 and 5 mm per year across most of the EEZ region, with a confidence interval between ±0.4 mm and ±0.6 mm. Sea-level rise for the EEZ is larger than the global average of 3.1 ± 0.4 mm per year (von Schuckmann et al. 2021), with higher estimates in the south. This rise is partly linked to a pattern related to climate variability from year to year and decade to decade.

Trend estimates at the Nuku'alofa tide-gauge over a similar time span to the altimetry observations (January 1993 to July 2020) are provided in the PSLGM Monthly Data Report for July 2020 (http://www.bom.gov.au/ntc/IDO60101/IDO60101.202007.pdf). For Nuku'alofa, the trend is reported as 6.6 mm per year, significantly higher than altimetry trends shown in Figure 14.12 (tide-gauge indicated by star symbol). This difference is largely attributed to subsidence occurring at Nuku'alofa, Tonga (Brown et al. 2020).

Figure 14.12:
Satellite altimetry annual trend for the Pacific from 1993 to 2020, with the Tonga EEZ highlighted. The star symbol indicates the location of the tide-gauge.

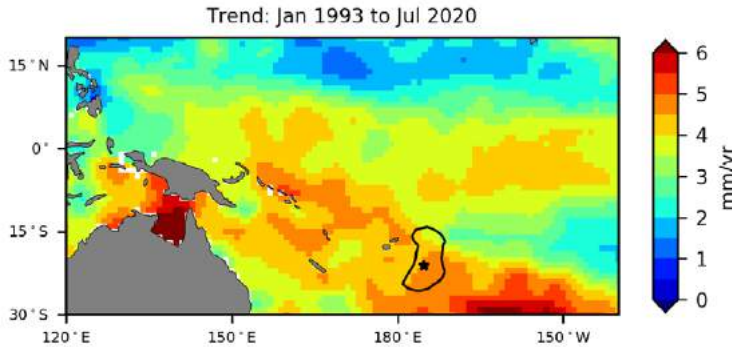

14.9 Waves

14.9.1 Seasonal cycle

The average wave climate in Nuku'alofa is defined by the significant wave height, peak period and peak direction. The significant wave height is the mean wave height (from trough to crest) of the highest one third of waves and corresponds to the wave height that would be reported by an experienced observer. Peak period is the time interval between two waves of the dominant wave period. Peak direction is the direction from which the dominant waves are coming.

The average sea state is dominated by wind seas from the east. The annual mean wave height is 1.30 m, the annual mean wave direction is 60° and the annual mean wave period is 10.33 s. In the Pacific, waves often come from multiple directions and for different periods of time. In Nuku'alofa, there are often more than six different wave direction/period components coming from the southeast to southwest (Figure 14.13).

Figure 14.13:
Annual wave rose for Nuku'alofa. Note that direction is where the wave is coming from.

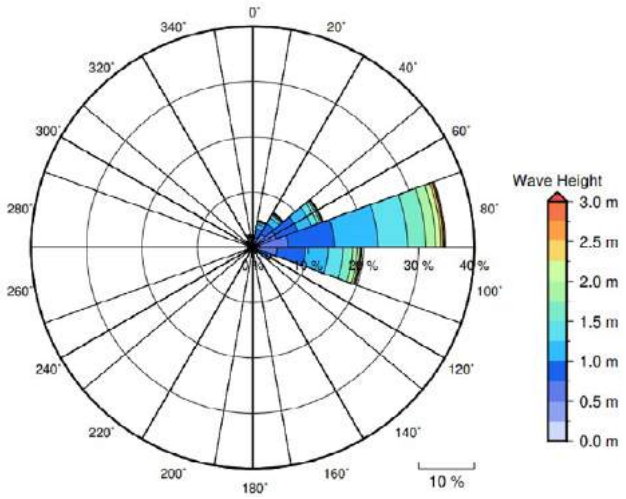

Seasonal wave height and period peaks between November and March due to North Pacific extra-tropical storm activity (Figure 14.14). Due to Tonga's location in the Southwest Pacific, swell waves from the North Pacific have weakened significantly before reaching Tonga and therefore do not show much of an effect on the wave height seasonal peak. Nuku'alofa's location on the northern shoreline of Tongatapu means there is little influence from Southern Ocean waves, with prevailing easterly waves from regional winds driving wave activity in May–October.

Figure 14.14:
Monthly wave height (black line), wave period (red line) and wave direction (arrows). The grey area represents the range of wave height between calm periods (10% of lowest wave height) and large wave events (10% of highest wave height).

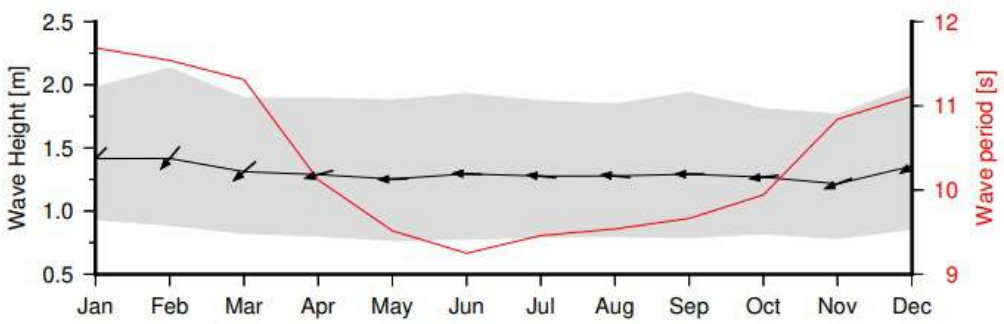

14.9.2 Trends

Waves change from month to month with the seasons, but they also change from year to year with climate oscillations. Typically, these changes are smaller than the seasonal changes but can be important during phenomena such as ENSO. In Nuku'alofa, the mean annual wave height has remained unchanged since 1979 (Figure 14.15). The mean annual wave height in Nuku'alofa is not significantly correlated with the main climate indicators of the region.

Figure 14.15:
Annual wave height (black line), wave period (red line) and wave direction (arrows). The grey area represents the range of wave height between calm periods (10% of lowest wave height) and large wave events (10% of highest wave height).

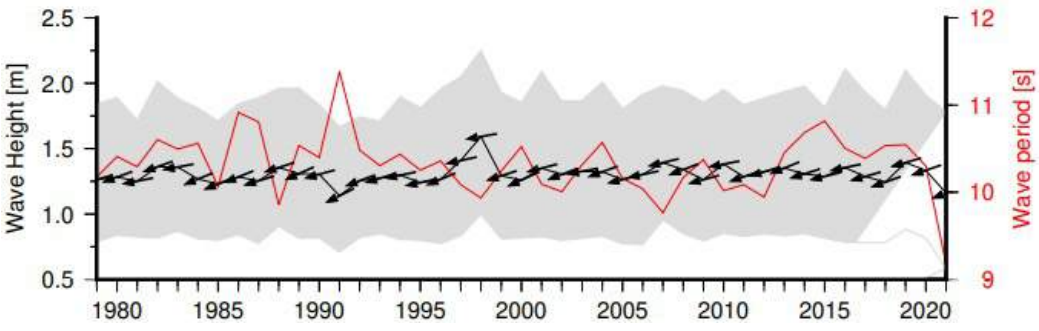

14.9.3 Extreme waves

Extreme wave analysis completed for Nuku'alofa was done by defining a severe height threshold and fitting a generalized Pareto distribution (GPD). The optimum threshold selected was 2.95 m. In the 42-year wave hindcast, 169 wave events reached or exceeded this threshold, averaging four waves per year. The GPD was fitted to the largest wave height reached during each of these events (Figure 14.16, Table 14.4). Extreme wave analysis is a very useful tool but is not always accurate because the analysis is very sensitive to the data available, the type of distribution fitted and the threshold used. For example, this analysis does not accurately account for tropical cyclone waves. More in-depth analysis is required to obtain results appropriate for designing coastal infrastructure and coastal hazard planning.

Figure 14.16:
Extreme wave distribution for Nuku'alofa. The crosses represent the wave events that have occurred since 1979. The solid line is the statistical distribution that best fits past wave events. The dashed lines show the upper and lower confidence limits of the fit. There is a 95% chance that the fitted distribution lies between the two dashed lines. Note that the annual return interval is in logarithmic scale.

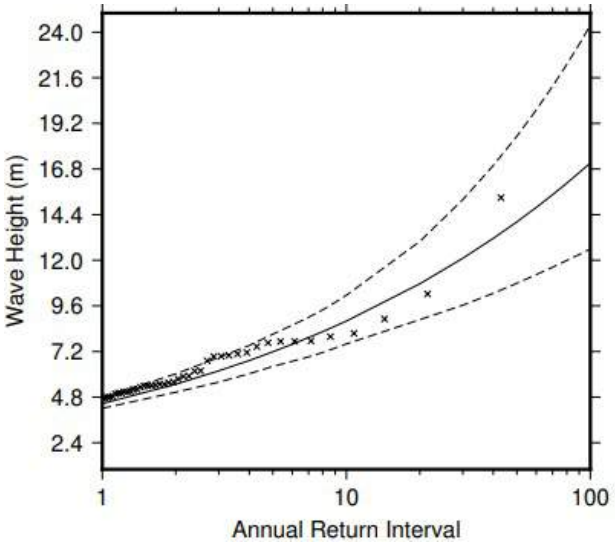

Table 14.4:
Summary of the results from extreme wave analysis in Nuku'alofa

Large wave height (90th percentile)	1.90 m
Severe wave height (99th percentile)	2.97 m
1-year ARI wave height	4.46 m
10-year ARI wave height	8.80 m
20-year ARI wave height	10.76 m
50-year ARI wave height	14.02 m
100-year ARI wave height	17.11 m

15 Tuvalu

15.1 Summary

15.1.1 Climate

- Changes in air temperature from season to season are relatively small and strongly linked to changes in the surrounding ocean temperature. Tuvalu has two distinct rainfall seasons – a wet season from December to March and a dry season from April to November.
- The seasonal cycle is strongly affected by the South Pacific Convergence Zone (SPCZ), which is most intense during the wet season.
- Annual and seasonal air temperatures at Funafuti increased over the period 1951–2020. The annual number of hot days and warm nights has increased, while the number of cool days and cold nights has decreased. The energy required for cooling indoor environments has also increased.
- The longest stretch of days without rain each year at Funafuti has increased since 1951. Otherwise, trends in annual, seasonal and extreme rainfall show little change.
- Tropical cyclones usually affect Tuvalu between November and April. Over the period 1969–2018, an average of nine cyclones passed within the Tuvalu exclusive economic zone (EEZ) per decade. Tropical cyclones were most frequent in El Niño years and least frequent in La Niña years. Year-to-year variability is large, ranging from no tropical cyclones in some seasons to four in 2004/05 and 2015/16.
- There has been little change in the total number of tropical cyclones in the Southwest Pacific since 1981/82. The number of severe tropical cyclones has declined over the same period/region.

15.1.2 Ocean

- Highest sea levels typically occur in the months January–April.
- Sea-level rise within the EEZ, measured by satellite altimeters from 1993 to mid-2020, ranges from 3.5 to 4.5 mm per year.
- Monthly average ocean temperature, as measured by the Funafuti tide-gauge, ranges from 29 °C in August to 30 °C in the months November/December and April/May, exhibiting a bimodal peak during the wet season. Monthly temperatures in any given year can be ±2 °C of these averages.
- The sea surface temperature (SST) trend in the EEZ is 0.22 °C per decade.
- Highest waves at Tuvalu occur in June–September, with a distinct lull during November–April.
- Dominant wave direction is from 117° (ESE), with an average significant wave height of 1.29 m and average wave period of 11.37 s.
- Severe wave height was defined as 2.26 m, with an average of 2.8 severe events per year.

15.2 Country description

Located in the tropical western South Pacific Ocean, Tuvalu is composed of three reef islands and six atolls between latitudes 5°S and 10°S, and longitudes 176°E and 180° (Figure 15.1). Tuvalu has a total land area of 26 km^2 and an EEZ of 0.9 million km^2. Funafuti, the largest atoll at 2.4 km^2, includes the capital of the same name. The highest elevation is 4.6 m above sea level on Niulakita. Tuvalu's population is approximately 12,000. About 60% live on Funafuti.

Figure 15.1:
Tuvalu and the locations of the climate stations used in this report

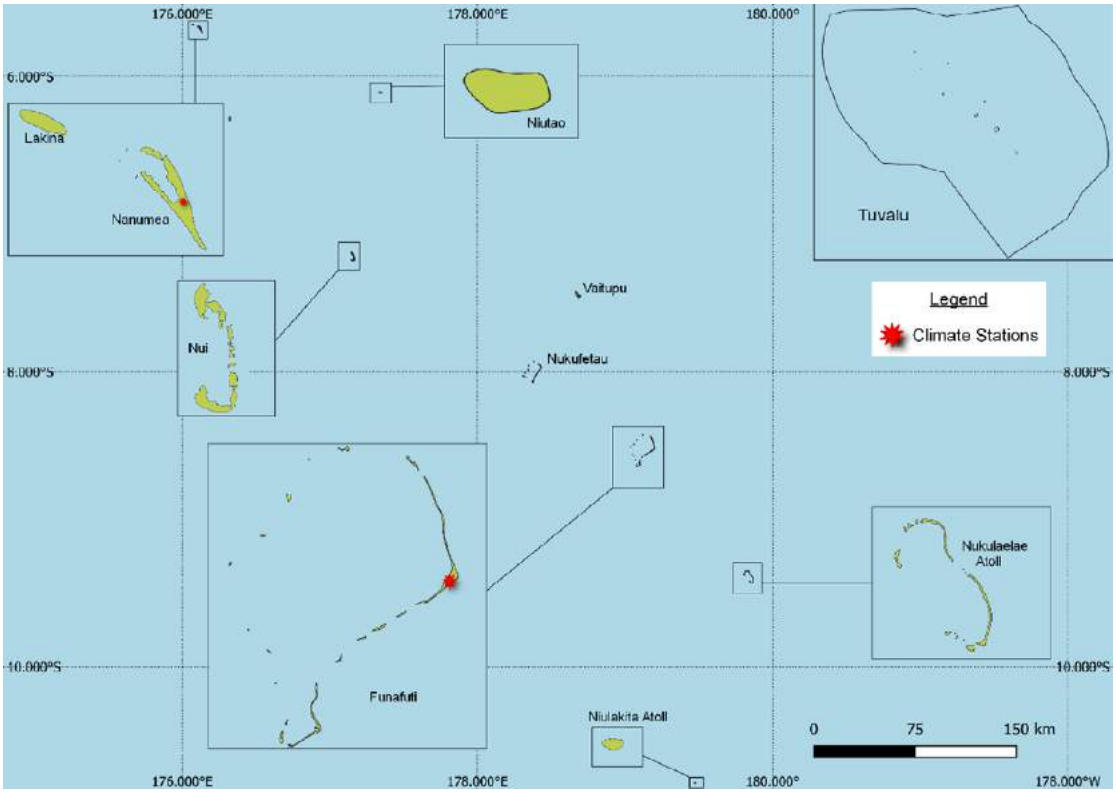

15.3 Data

Daily historical rainfall and air temperature records for Funafuti and Nanumea from 1951 were obtained from the Tuvalu Meteorological Service. These records have undergone data quality and homogeneity assessment. Where the maximum or minimum air temperature records were found to have discontinuities, these records have been adjusted to make them homogeneous (further information is provided in Chapter 1). Additional information on historical climate trends for Tuvalu can be found in the Pacific Climate Change Data Portal http://www.bom.gov.au/climate/pccsp.

Tropical cyclone data and historical tracks starting from the 1969/70 season are available are the SHTC Data Portal http://www.bom.gov.au/cyclone/history/tracks/index.shtml.

SST covering the EEZ was obtained via the daily Optimum Interpolation SST version 2.1 (OISST v2.1) dataset from NOAA (Reynolds et al. 2007; Banzon et al. 2016). In situ ocean temperature data were obtained from the PSLGM Project tide-gauge located at Funafuti, with data spanning from 1993 to 2021.

Wave data were obtained from the PACCSAP wave hindcast (Smith et al. 2021), available hourly from 1979 to 2021, with a grid resolution near Tuvalu of 7 km.

Regional sea level data were obtained from CSIRO satellite altimetry (updated by Benoit Legresy, Church and White 2011), with correction for seasonal signals, inverse barometer effect and glacial isostatic adjustment. Tide-gauge data were sourced from the Funafuti tide-gauge station, spanning from 1993 to 2021 at hourly intervals.

15.4 Rainfall

15.4.1 Seasonal cycle

Tuvalu is characterised by a distinct wet season from December to March (Figure 15.2), driven by the strength of the SPCZ, which is most active during the wet season months. The WPM can also bring high rainfall to Tuvalu during these months.

The percentage of rainfall received at Funafuti and Nanumea during the wet season months of December–March is 43%. Funafuti receives an average of 411 mm in January. The driest months at Nanumea are September–November, with average rainfall during September of 159 mm.

Figure 15.2:
Mean annual rainfall at Funafuti and Nanumea

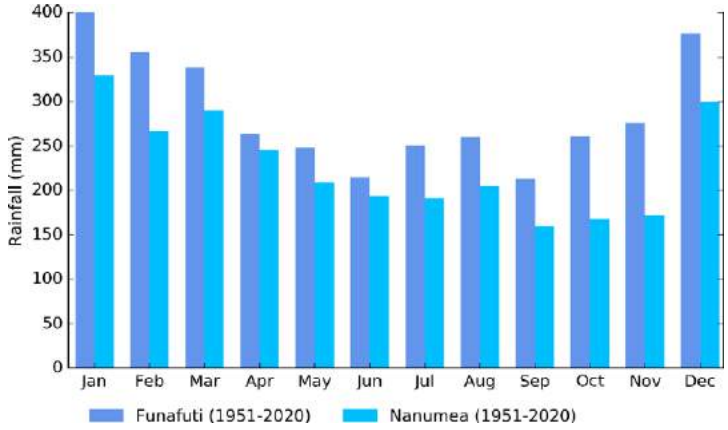

15.4.2 Trends

Trends in annual and seasonal rainfall since 1951 are not statistically significant at Funafuti (Figure 15.3, Table 15.1). This means there has been little change in annual and seasonal rainfall at this location. Annual rainfall since 1951 has varied from approximately 2000 to 4800 mm, and on average, over half of the days each year experience rain.

Figure 15.3:
Annual rainfall (bar graph) and number of wet days (where rainfall is at least 1 mm; line graph) at Funafuti. Straight lines indicate linear trends for annual rainfall (in black) and number of wet days (in blue). The magnitudes of the trends are presented in Table 15.1. Diamonds indicate years with insufficient data for one or both variables.

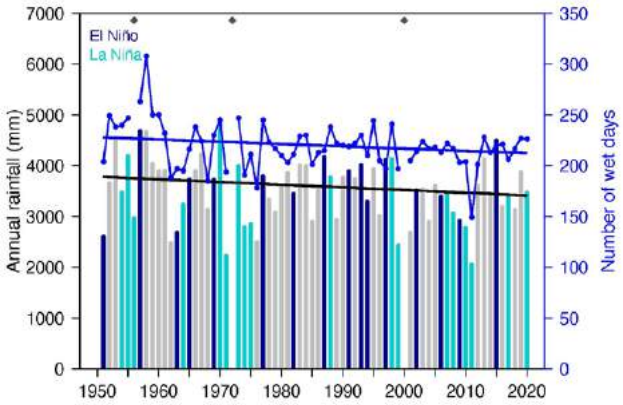

Table 15.1:
Trends in annual, seasonal and extreme rainfall at Funafuti. The 95% confidence intervals are shown in parentheses and trends significant at the 95% level are shown in bold. The contribution to total rainfall from extreme events and the standardised rainfall evapotranspiration index are measured relative to 1961–1990 (see Chapter 1 for details).

	Funafuti
	1951–2020
Annual rainfall (mm/decade)	-53.19 (-129.16, +32.61)
November–April (mm/decade)	-4.87 (-49.71, +43.10)
May–October (mm/decade)	-16.56 (-72.24, +36.81)
Number of wet days (days/decade)	-2.24 (-5.09, +0.97)
Contribution to total rainfall from extreme events (%/decade)	-0.29 (-1.10, +0.72)
Consecutive dry days (days/decade)	**+0.36** (+0.01, +0.63)
Maximum one-day rainfall (mm/decade)	-1.00 (-5.39, +3.17)
Standardised rainfall evapotranspiration index (November–April)	-0.01 (-0.15, +0.12)
Standardised rainfall evapotranspiration index (May–October)	-0.05 (-0.20, +0.09)

The longest run of days without rain each year has increased since 1951 (Table 15.1, Figure 15.4). Trends in all other extreme rainfall indices, including the standardised rainfall evapotranspiration drought index, are not statistically significant.

Figure 15.4:
Annual longest run of consecutive dry days (bar graph) and maximum daily rainfall (line graph) at Funafuti. Straight lines indicate linear trends for dry days (in black) and maximum daily rainfall (in blue). The magnitudes of the trends are presented in Table 15.1. Diamonds indicate years with insufficient data for one or both variables.

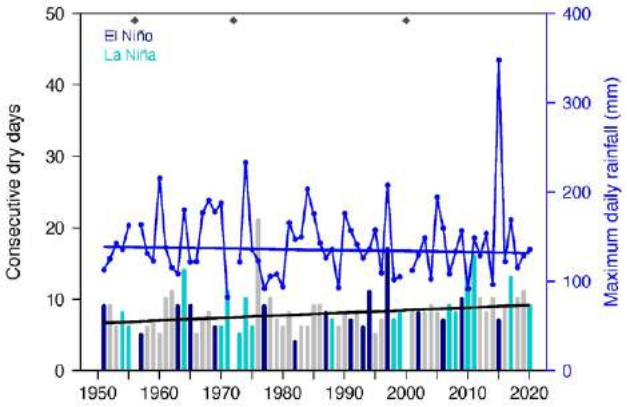

15.5 Air temperature

15.5.1 Seasonal cycle

Air temperatures have a small seasonal cycle at Funafuti and Nanumea, with less than 1 °C change in average monthly maximum and minimum temperatures during the year (Figure 15.5). Being small atoll islands, air temperatures over Tuvalu are strongly linked to the surrounding sea surface temperatures. In El Niño years, minimum air temperatures are typically higher, and conversely, minimum temperatures are typically lower during La Niña years, similarly for maximum air temperatures during the wet season.

There has been a clear shift towards warmer average monthly temperatures between the climatology periods of 1961–1990 and 1991–2020 (Figure 15.5), with warmer average temperatures occurring in all months throughout the year for both Funafuti and Nanumea, with the exception of average minimum temperatures at Nanumea for April and June.

Figure 15.5:
Maximum and minimum air temperature seasonal cycle for Funafuti (purple) and Nanumea (green), and for the periods 1961–1990 (dotted lines) and 1991–2020 (solid lines)

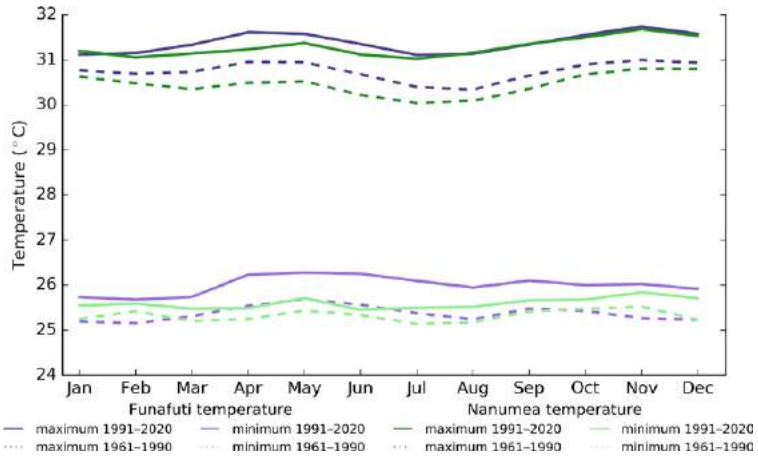

15.5.2 Trends

Average annual and seasonal temperatures have increased significantly at Funafuti (Figure 15.6). May–October temperatures are warming faster than November–April temperatures (Table 15.2). Daily minimum temperatures are warming faster than daily maximum temperatures. The relatively small year-to-year fluctuations in temperature can be attributed to Funafuti's tropical location.

Figure 15.6:
Annual, November–April and May–October average temperatures for Funafuti. Straight lines indicate linear trends. The magnitudes of the trends are presented in Table 15.2. Diamonds indicate years with insufficient data for one or more variables.

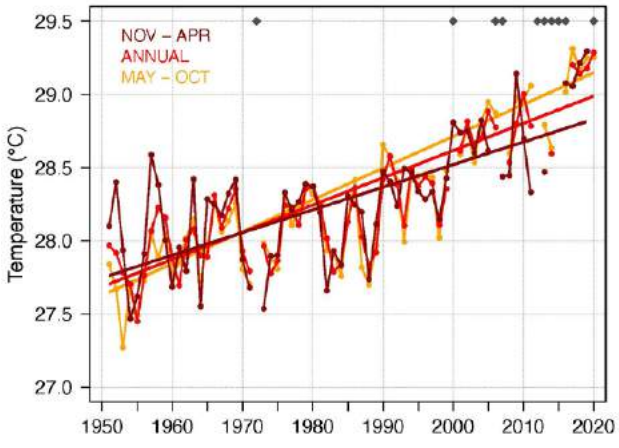

Table 15.2:
Trends in annual and seasonal air temperatures at Funafuti. The 95% confidence intervals are shown in parentheses, and trends significant at the 95% level are shown in bold.

	Funafuti Tmax (°C/decade)	Funafuti Tmin (°C/decade)	Funafuti Tmean (°C/decade)
	1951–2020		
Annual	**+0.17** (+0.07, +0.28)	**+0.21** (+0.17, +0.25)	**+0.19** (+0.12, +0.26)
November–April	**+0.12** (+0.03, +0.2)	**+0.20** (+0.15, +0.25)	**+0.15** (+0.09, +0.21)
May–October	**+0.20** (+0.12, +0.28)	**+0.24** (+0.19, +0.28)	**+0.22** (+0.16, +0.28)

The number of hot days and warm nights has increased, and the number of cool days and cold nights has decreased at Funafuti (Table 15.3). Since 2015, over half of all days each year were considered hot (Figure 15.7). This warming is consistent with increases in annual and seasonal temperatures at Funafuti (Figure 15.6) as well as global climate change. However, the rapid rate of this warming can also be attributed to Funafuti's tropical location, where only small temperature increases are necessary for a day to be considered hot (i.e., in the hottest 10% of days compared to 1961–1990, see Chapter 1 for details).

The cooling degree days index provides a measure of the energy demand needed to cool a building down to 25 °C, with the assumption that air conditioners are generally turned on at this temperature. There has been a very strong increase in the cooling degree index at Funafuti, suggesting the energy needed for cooling has increased significantly since 1951.

Table 15.3:
Trends in annual temperature extremes at Funafuti. The 95% confidence intervals are shown in parentheses, and trends significant at the 95% level are shown in bold. Hot and cool days, and warm and cold nights are measured relative to 1961–1990 (see Chapter 1 for details).

	Funafuti
	1951–2020
Number of hot days (days/decade)	**+28.92** (+11.15, +44.58)
Number of warm nights (nights/decade)	**+14.16** (+10.27, +18.09)
Number of cool days (days/decade)	**-4.93** (-7.87, -1.65)
Number of cold nights (nights/decade)	**-8.51** (-10.94, -5.84)
Cooling degree days (degree days/decade)	**+71.37** (+52.82, +98.60)
Daily temperature range (°C/decade)	-0.07 (-0.14, 0.00)

Figure 15.7:
Annual number of hot days and cold nights at Funafuti. Straight lines indicate linear trends. The magnitudes of the trends are presented in Table 15.3. Diamonds indicate years with insufficient data for one or both variables.

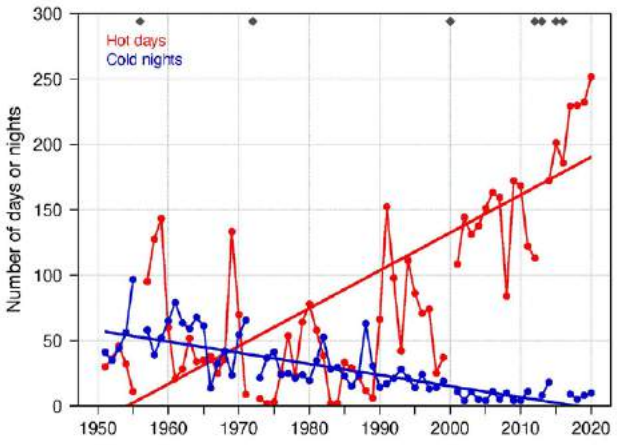

15.6 Tropical cyclones

15.6.1 Seasonal cycle

Tropical cyclones usually affect Tuvalu during the southern hemisphere tropical cyclone season, which is from November to April, but also occasionally occur outside the tropical cyclone season. The Southern Hemisphere Tropical Cyclone Archive indicates that between the 1969/70 and 2017/18 seasons, 43 tropical cyclones (Figure 15.8) passed within the EEZ. This represents an average of nine cyclones per decade. Tropical cyclones were most frequent in El Niño years (12 cyclones per decade), followed by neutral years (10 cyclones per decade) and least frequent in La Niña years (3 cyclones per decade).

Interannual variability in the number of tropical cyclones in the EEZ is large, ranging from zero in some seasons to four in 2004/05 and 2015/16 (Figure 15.8). High interannual variability and the small number of tropical cyclones occurring in the EEZ make reliable identification of long-term trends in frequency and intensity difficult.

Some tropical cyclone tracks analysed in this section include the tropical depression stage (sustained winds ≤34 knots) before and/or after tropical cyclone formation.

Figure 15.8:
Number of tropical cyclones passing within the Tuvalu EEZ per season. Each season is defined by the ENSO status, with light blue being an El Niño year, dark blue a La Niña year and grey showing a neutral ENSO year. The 11-year moving average is presented as a purple line and considers all years.

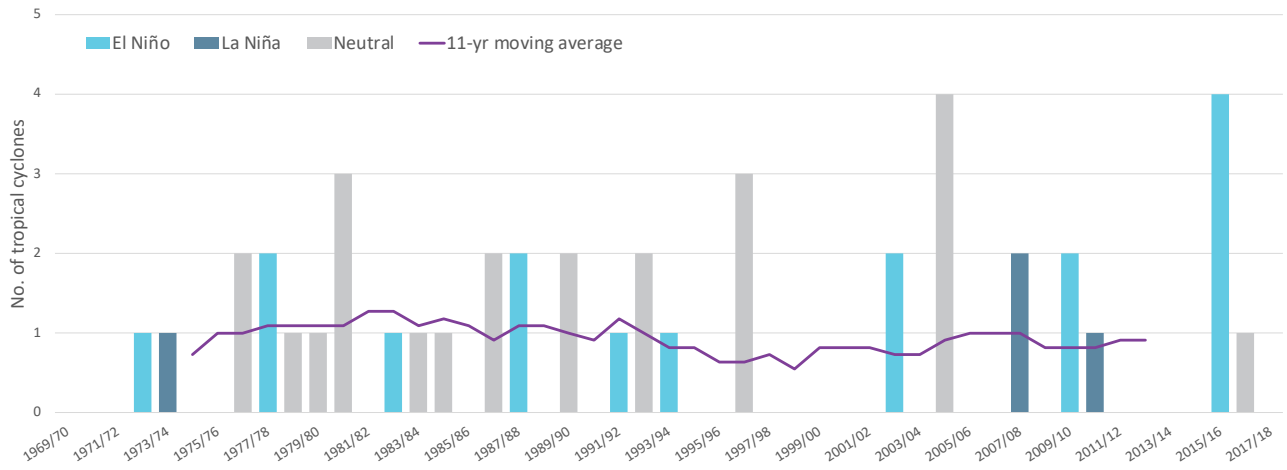

15.6.2 Trends

Trends in total number of tropical cyclones (<995 hPa) and severe tropical cyclones (<970 hPa) are presented for the period 1981/82–2020/21 for the greater Southwest Pacific (135°E–120°W; 0–50°S). Trends are presented at a regional scale as the number of tropical cyclones occurring within Pacific Island EEZs is insufficient for reliable long-term trend analysis.

For the total number of tropical cyclones, the trend (and 95% confidence interval) is -0.92 (-1.85, 0.01) tropical cyclones/decade. There has been little change/marginal decline in the total number of tropical cyclones over the last 40 seasons. This trend is not statistically significant.

For the total number of severe tropical cyclones, the trend is -0.80 (-1.32, -0.29) tropical cyclones/decade. There is a negative trend in the number of severe tropical cyclones over the last 40 seasons. There has been little change/marginal decline in the proportion of tropical cyclones reaching severe status. The trend is -0.04 (-0.08, 0.00) tropical cyclones/decade. The negative trend is statistically significant.

Records of tropical cyclones exist from the late 1800s in some countries in the Southwest Pacific, but trends in tropical cyclones have only been presented from 1981/82. Satellite-based observations began in the Southwest Pacific in the early 1970s, but consistent coverage and reliable intensity estimates have only been available since the early 1980s. Confidence in tropical cyclone trends is moderate as the definition of a tropical cyclone has changed, and satellite observation methods have continued to improve over the last 40 years.

15.7 Sea surface temperature

15.7.1 Seasonal cycle

Ocean temperature, as measured by the Tuvalu tide-gauge from 1993 to 2021, reaches on average a maximum of almost 30 °C in November/December and then again around April/May, exhibiting a unique bimodal wet season peak (Figure 15.9). Individual monthly temperatures can reach has high as 31.5 °C. Minimum average temperature only dips down to 29 °C in August. The average seasonal cycle only changes by approximately 1 °C. Hourly temperatures can be up to 2 °C higher or lower than these monthly averages, although 50% of hourly observations fall within 1 °C of the average.

Figure 15.9:
Annual temperatures measured at the Funafuti tide-gauge. Blue dots show the monthly average, and shaded boxes show the middle 50% of hourly observations. Lines show the top and bottom 25% of hourly observations.

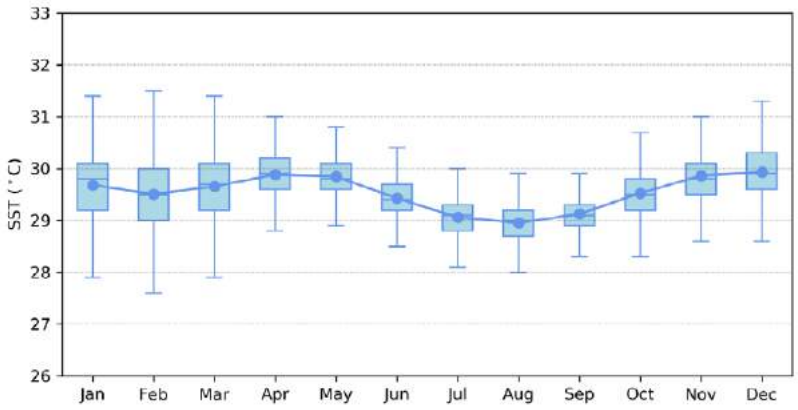

15.7.2 Trends

Figure 15.10 shows the 1981–2021 SST from satellite observations averaged over the EEZ. The data show a trend of 0.22 °C per decade with a 95% confidence interval of ±0.03 °C.

Figure 15.10:
Sea surface temperature from satellite observations averaged across the Tuvalu EEZ, shown as the orange line. The blue line shows the linear regression trend.

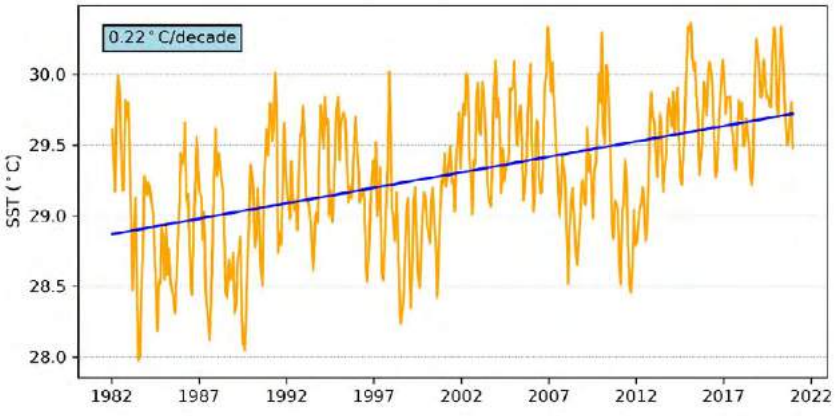

15.8 Sea level

15.8.1 Seasonal cycle

Tuvalu experiences a semidiurnal tidal cycle, meaning two high and two low tides per day. The highest predicted tides of the year typically occur during the wet season months of December–March. Figure 15.11 shows the number of hours the 99th percentile (3.22 m) sea level threshold is exceeded per month across the entire sea level record at Funafuti. Peak sea levels typically occur between January and April.

Figure 15.11:
Number of hours exceeding 99th percentile sea level threshold per month from 1993 to 2021 at the Funafuti tide-gauge. Blue shading indicates the number of hours, and the final row provides a percentage summary of all the years.

Number of hours exceeding 3.22 m (Fongafale, Tuvalu)

	Jan	Feb	Mar	Apr	May	Jun	Jul	Aug	Sep	Oct	Nov	Dec	Annual
1993	0	0	0	0	0	0	0	0	0	0	0	0	0
1994	0	2	0	0	0	0	0	0	0	0	0	0	2
1995	0	0	0	0	0	0	0	0	0	0	0	0	0
1996	2	5	0	0	0	0	0	0	0	0	0	0	7
1997	0	2	6	0	0	0	0	0	0	0	0	0	8
1998	0	0	0	0	0	0	0	0	0	0	0	0	0
1999	0	0	0	0	0	0	0	0	0	0	0	0	0
2000	2	0	0	0	0	0	0	0	0	0	0	0	2
2001	0	4	5	0	0	0	0	0	0	0	0	0	9
2002	1	2	7	0	0	0	0	0	0	0	0	0	10
2003	0	0	0	2	4	0	0	0	0	0	0	0	6
2004	0	0	0	0	0	0	0	0	0	0	0	0	0
2005	0	0	0	0	0	0	0	0	0	0	0	0	0
2006	5	6	5	0	0	0	0	0	0	0	0	0	16
2007	0	0	2	1	0	0	0	0	0	0	0	0	3
2008	0	0	0	0	0	0	0	0	0	0	0	0	0
2009	2	3	0	0	0	0	0	0	0	0	0	0	5
2010	0	0	0	0	0	0	0	0	0	1	0	0	1
2011	4	1	0	0	0	0	0	0	0	0	0	0	5
2012	0	0	0	0	0	0	0	0	0	0	0	0	0
2013	3	0	0	0	0	0	0	0	0	0	0	0	3
2014	1	2	3	0	0	0	0	0	0	0	0	0	6
2015	0	7	6	0	0	0	0	0	0	0	0	0	13
2016	0	0	0	0	0	0	0	0	0	0	0	0	0
2017	0	0	0	0	0	0	0	0	0	0	0	5	5
2018	4	5	4	0	0	1	0	0	0	0	0	0	14
2019	1	1	0	0	0	0	0	0	0	0	0	0	2
2020	0	3	5	11	2	0	0	0	1	1	1	0	24
Monthly Totals (%)	18	30	30	10	4	1	0	0	1	1	1	4	

15.8.2 Trends

Sea level at Tuvalu, measured by satellite altimeters (Figure 15.12) since 1993, has risen 3.5 and 4.5 mm per year across the EEZ, with a confidence interval of ±1.0 mm in the south and up to ±0.4 mm in the north. This places most of the EEZ trend higher than the global average of 3.1 ± 0.4 mm per year (von Schuckmann et al. 2021). This rise is partly linked to a pattern related to climate variability from year to year and decade to decade.

Trend estimates at the Funafuti tide-gauge over a similar time span to the altimetry observations (March 1993 to July 2020) are provided in the PSLGM Monthly Data Report for July 2020 (http://www.bom.gov.au/ntc/IDO60101/IDO60101.202007.pdf). For Funafuti, the trend is reported as 4.5 mm per year, which is very similar to the altimetry trends shown in Figure 15.12 (tide-gauge indicated by star symbol).

Figure 15.12:
The satellite altimetry annual trend for the Pacific from 1993 to 2020, with the Tuvalu EEZ highlighted. The star symbol indicates the location of the tide-gauge at Funafuti.

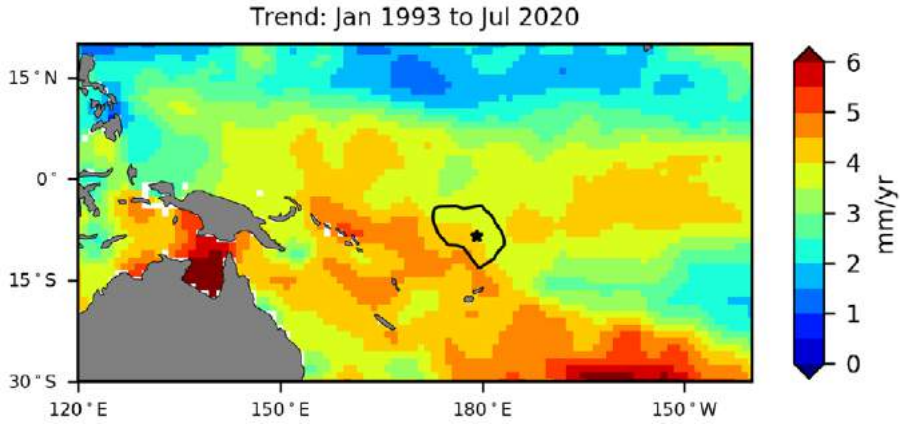

15.9 Waves

15.9.1 Seasonal cycle

The average wave climate in Funafuti is defined by the significant wave height, peak period and peak direction. The significant wave height is the mean wave height (from trough to crest) of the highest one third of waves and corresponds to the wave height that would be reported by an experienced observer. Peak period is the time interval between two waves of the dominant wave period. Peak direction is the direction from which the dominant waves are coming.

The average sea state is dominated by swells from the east. The annual mean wave height is 1.29 m, the annual mean wave direction is 117° and the annual mean wave period is 11.37 s. In the Pacific, waves often come from multiple directions and for different periods at a time. In Funafuti, there are often more than four different wave direction/period components coming from the southeast to southwest (Figure 15.13).

Seasonal wave height peaks between June and September with dominant waves coming from the southeast (Figure 15.14). Wave period is lower during these months. However, waves are still classified as swell-dominated (period > 8 seconds).

Figure 15.13:
Annual wave rose for Funafuti. Note that direction is where the wave is coming from.

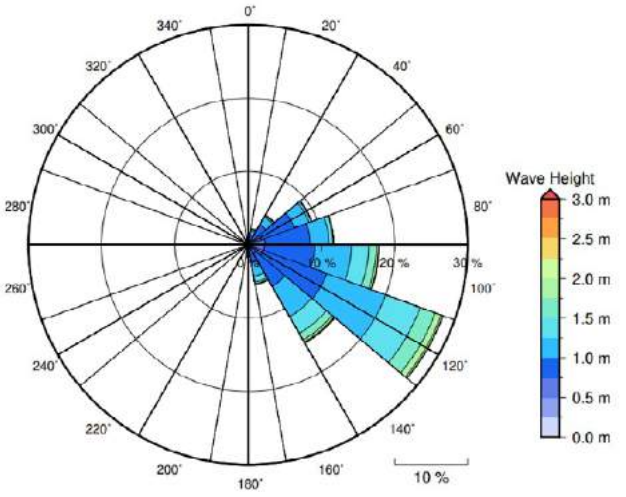

Figure 15.14:
Monthly wave height (black line), wave period (red line) and wave direction (arrows). The grey area represents the range of wave height between calm periods (10% of lowest wave height) and large wave events (10% of highest wave height).

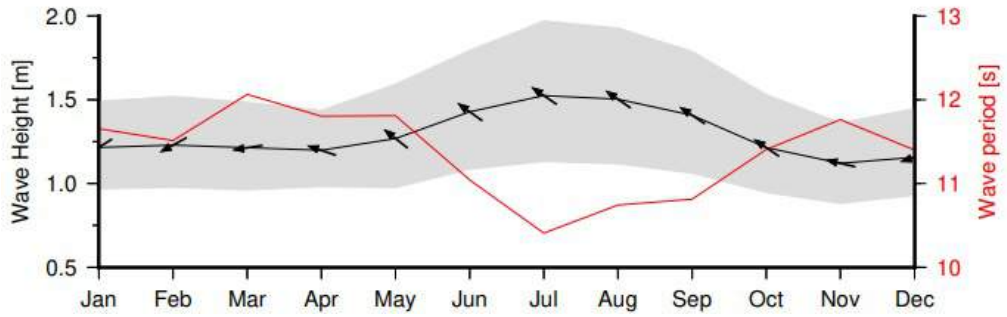

15.9.2 Trends

Waves change from month to month with the seasons, but they also change from year to year with climate oscillations. Typically, these changes are smaller than the seasonal changes but can be important during phenomena such as ENSO. In Funafuti, the mean annual wave height has remained unchanged since 1979 (Figure 15.15). The mean annual wave height in Funafuti is not significantly correlated with the main climate indicators of the region.

Figure 15.15:
Annual wave height (black line), wave period (red line) and wave direction (arrows). The grey area represents the range of wave height between calm periods (10% of lowest wave height) and large wave events (10% of highest wave height).

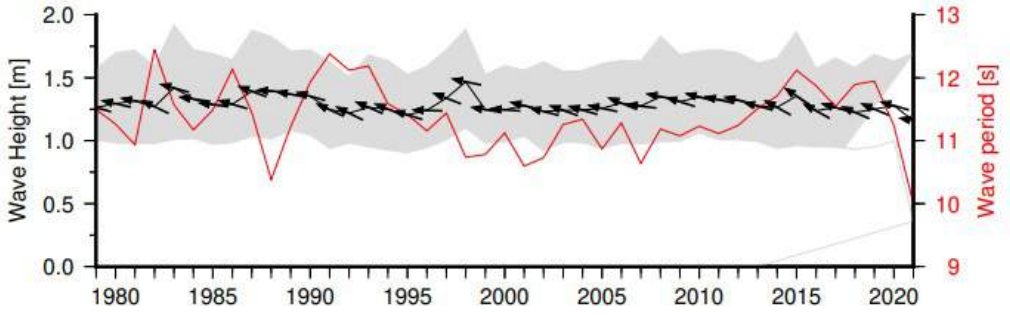

15.9.3 Extreme waves

Extreme wave analysis completed for Funafuti wave buoy was done by defining a severe height threshold and fitting a generalized Pareto distribution (GPD). The optimum threshold selected was 2.26 m. In the 42-year wave hindcast, 117 wave events reached or exceeded this threshold, averaging 2.8 events per year. The GPD was fitted to the largest wave height reached during each of these events (Figure 15.16, Table 15.4). Extreme wave analysis is a very useful tool but is not always accurate because the analysis is very sensitive to the data available, the type of distribution fitted and the threshold used. For example, this analysis does not accurately account for tropical cyclone waves. More in-depth analysis is required to obtain results appropriate for designing coastal infrastructure and coastal hazard planning.

Figure 15.16:
Extreme wave distribution for Funafuti. The crosses represent the wave events that have occurred since 1979. The solid line is the statistical distribution that best fits past wave events. The dashed lines show the upper and lower confidence limits of the fit. There is a 95% chance that the fitted distribution lies between the two dashed lines. Note that the annual return interval is in logarithmic scale.

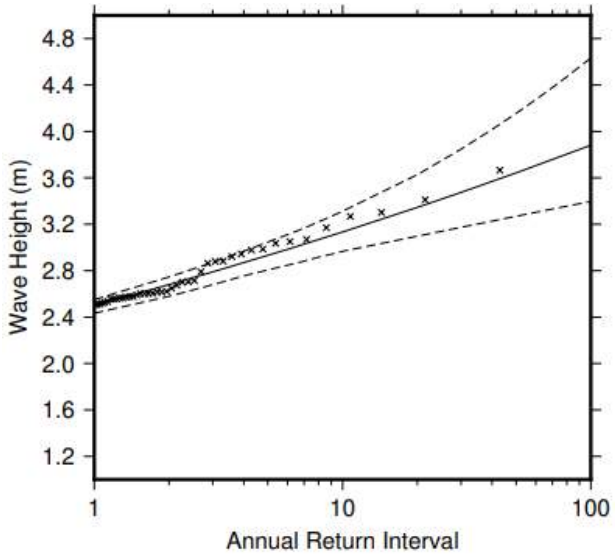

Table 15.4:
Summary of the results from extreme wave analysis in Funafuti

Large wave height (90th percentile)	1.67 m
Severe wave height (99th percentile)	2.13 m
1-year ARI wave height	2.50 m
10-year ARI wave height	3.13 m
20-year ARI wave height	3.35 m
50-year ARI wave height	3.64 m
100-year ARI wave height	3.88 m

16 Vanuatu

© SPC

16.1 Summary

16.1.1 Climate

- Changes in air temperature from season to season are relatively small and strongly linked to changes in the surrounding ocean temperature. Vanuatu has two distinct seasons – a warm wet season from November to April and a cooler dry season from May to October.
- The seasonal cycle is strongly affected by the South Pacific Convergence Zone (SPCZ), which is most intense during the wet season.
- Warming trends have been evident in annual and seasonal air temperatures at Aneityum and Port Vila-Bauerfield Airport since 1951. Hot days have also occurred more than twice as frequently in recent years compared to the middle of the 20th century.
- There has been little change in annual and seasonal rainfall at Aneityum and Port Vila, although the number of wet days each year has decreased at Aneityum.
- Tropical cyclones usually affect Vanuatu between November and April. Over the period 1969–2018, an average of 24 cyclones passed within the Vanuatu exclusive economic zone (EEZ) per decade. Tropical cyclones were most frequent in El Niño years and least frequent in La Niña years. Year-to-year variability is large, ranging from no tropical cyclones in some seasons to six in 1971/72 and 1991/92.
- There has been little change in the total number of tropical cyclones in the Southwest Pacific since 1981/82. The number of severe tropical cyclones has declined over the same period/region.

16.1.2 Ocean

- Highest sea levels typically occur in the months October–March.
- Sea-level rise within the EEZ, measured by satellite altimeters from 1993 to mid-2020, ranges from 3.5 to 5 mm per year.
- Monthly average ocean temperature, as measured by the Port Vila tide-gauge, ranges from 25.5 °C in August to 29 °C in February/March. However, monthly temperatures in any given year can be ±2 °C of these averages.
- The sea surface temperature (SST) trend in the EEZ is 0.23 °C per decade.
- Wave height is fairly consistent throughout the year, while wave period has a definitive peak in May.
- Dominant wave direction is from 182° (south), with an average significant wave height of 0.55 m and average wave period of 9.63 s.
- Severe wave height was defined as 1.83 m, with an average of 2.8 severe events per year.

16.2 Country description

The Republic of Vanuatu is located in the tropical South Pacific Ocean between latitudes 13°S and 21°S, and longitudes 166°E and 171°E (Figure 16.1). The nation consists of 83 islands (65 of them inhabited), with a distance of 1300 km between the most northern and southern islands. Fourteen of Vanuatu's islands have surface areas of more than 100 km^2, including, from largest to smallest: Espiritu Santo, Malakula, Efate, Erromango, Ambrym, Tanna, Pentecost, Epi, Ambae or Aoba, Gaua, Vanua Lava, Maewo, Malo and Aneityum. Vanuatu has a total land area of 12,189 km^2 and an EEZ of 0.7 million km^2. The highest point in Vanuatu is Mount Tabwemasana, at 1879 m, on the island of Espiritu Santo.

The population is approximately 307,000 and predominantly rural. Efate, which includes the capital Port Vila, has a population about 51,000.

Figure 16.1:
Vanuatu and the locations of the climate stations used in this report

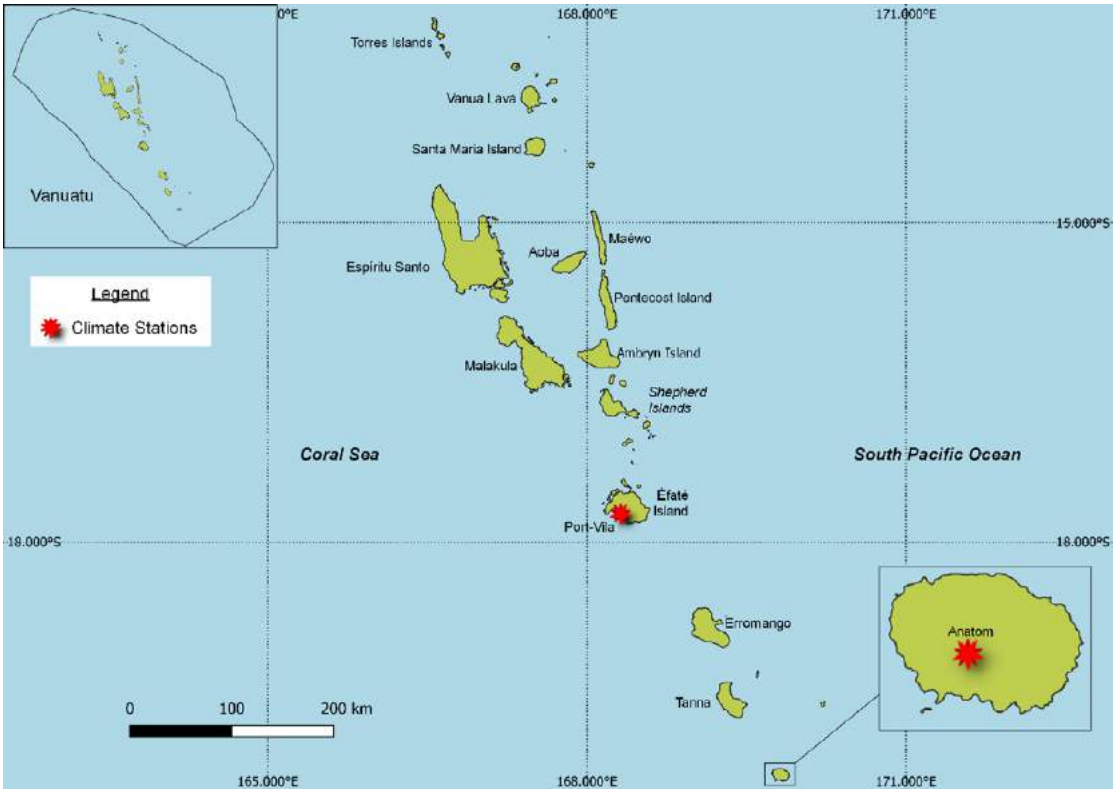

16.3 Data

Daily historical rainfall for Port Vila, air temperature records for a Port Vila-Bauerfield Airport (henceforth Port Vila) composite and Aneityum from 1951 were obtained from the Vanuatu Meteorological Service. These records have undergone data quality and homogeneity assessment. Where the maximum or minimum air temperature records were found to have discontinuities, these records have been adjusted to make them homogeneous (further information is provided in Chapter 1). Additional information on historical climate trends for Vanuatu can be found in the Pacific Climate Change Data Portal http://www.bom.gov.au/climate/pccsp.

Tropical cyclone data and historical tracks starting from the 1969/70 season are available from the SHTC Data Portal http://www.bom.gov.au/cyclone/history/tracks/index.shtml.

SST covering the EEZ was obtained via the daily Optimum Interpolation SST version 2.1 (OISST v2.1) dataset from NOAA (Reynolds et al. 2007; Banzon et al. 2016). In situ ocean temperature data were obtained from the PSLGM Project tide-gauge located at Port Vila, with data spanning from 1993 to 2021.

Wave data were obtained from the PACCSAP wave hindcast (Smith et al. 2021), available hourly from 1979 to 2021, with a grid resolution near Vanuatu of 7 km.

Regional sea level data were obtained from CSIRO satellite altimetry (updated by Benoit Legresy, Church and White 2011), with correction for seasonal signals, inverse barometer effect and glacial isostatic adjustment. Tide-gauge data were sourced from the Port Vila tide-gauge station, spanning from 1993 to 2021 at hourly intervals.

16.4 Rainfall

16.4.1 Seasonal cycle

Rainfall in Vanuatu is strongly influenced by the SPCZ. During the wet season (December–May), the SPCZ intensifies and moves further south, bringing higher rainfall to Vanuatu and leading to about 65% of Aneityum's and 67% of Port Vila's rain to fall during this period (Figure 16.2). Low pressure systems embedded in this band of heavy rainfall often become tropical cyclones during the cyclone season.

Mountains also play a role in variations in rainfall across some islands. During the wet season, rainfall is particularly high on the windward (southeast) side of mountain ranges of the bigger islands and scarce on the leeward (northwest) sides, especially during the dry season.

Figure 16.2:
Mean annual rainfall at Port Vila and Aneityum

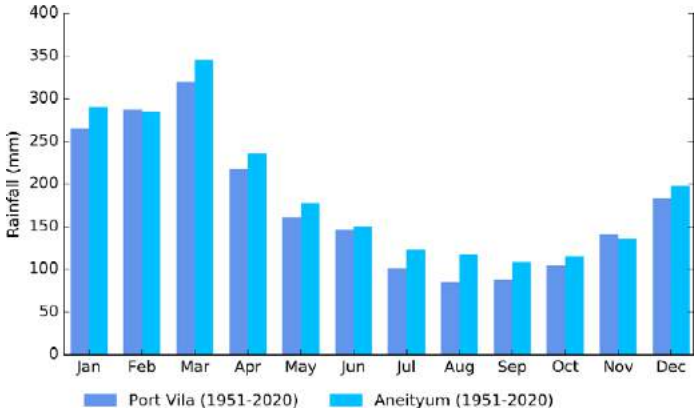

16.4.2 Trends

Trends in annual and seasonal rainfall since 1951 are not statistically significant at Aneityum and Port Vila (Figure 16.3, Table 16.1). This means there has been little change in annual and seasonal rainfall at these sites. While trends in annual and seasonal rainfall are not significant, the number of wet days each year has decreased at Aneityum. Annual rainfall has varied from approximately 1000 to 3800 mm at Aneityum and from approximately 900 to 3500 mm at Port Vila. Notable year-to-year variability associated with El Niño–Southern Oscillation (ENSO) is evident, with both sites typically experiencing higher rainfall during La Niña years compared to El Niño years.

Figure 16.3:
Annual rainfall (bar graph) and number of wet days (where rainfall is at least 1 mm; line graph) at Aneityum (left) and Port Vila (right). Straight lines indicate linear trends for annual rainfall (in black) and number of wet days (in blue). The magnitudes of the trends are presented in Table 16.1. Diamonds indicate years with insufficient data for one or both variables.

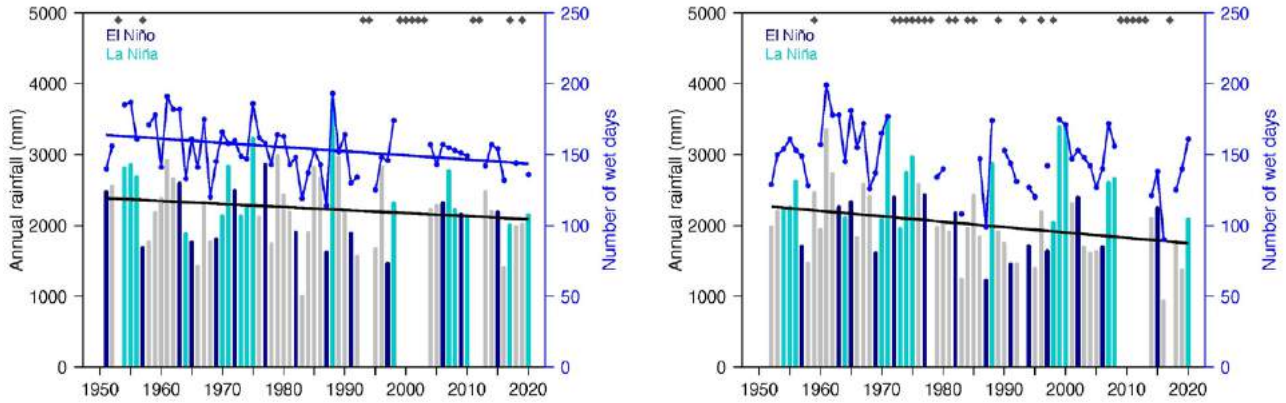

Table 16.1:
Trends in annual, seasonal and extreme rainfall at Aneityum (left) and Port Vila (right). The 95% confidence intervals are shown in parentheses, and trends significant at the 95% level are shown in bold. Criteria for statistical robustness were not met for determining linear trends for rainfall extremes at Port Vila. The contribution to total rainfall from extreme events and the standardised rainfall evapotranspiration index are measured relative to 1961–1990 (see Chapter 1 for details).

	Aneityum	Port Vila
	1951–2020	
Annual rainfall (mm/decade)	-43.22 (-111.51, +40.48)	-75.88 (-177.17, +28.27)
November–April (mm/decade)	+8.86 (-63.81, +60.77)	-45.59 (-115.57, +29.19)
May–October (mm/decade)	-24.94 (-65.70, +7.39)	-28.11 (-70.69, +17.96)
Number of wet days (days/decade)	**-2.94** (-6.26, -0.20)	-
Contribution to total rainfall from extreme events (%/decade)	-0.20 (-2.20, +1.84)	-
Consecutive dry days (days/decade)	+0.36 (-0.62, +1.41)	-
Maximum one-day rainfall (mm/decade)	+5.08 (-3.21, +13.66)	-
Standardised rainfall evapotranspiration index (November–April)	0.00 (-0.11, +0.11)	-0.14 (-0.31, +0.01)
Standardised rainfall evapotranspiration index (May–October)	-0.15 (-0.33, +0.03)	-0.09 (-0.23, +0.07)

Numerous gaps in daily data at Port Vila prevent the robust calculation of trends in rainfall extremes (Table 16.1). At Aneityum trends in rainfall extremes are not significant. Similar to annual rainfall, Figure 16.4 shows variability associated with ENSO at both sites, with longer dry spells typically experienced during El Niño years compared to La Niña years.

Figure 16.4:
Annual longest run of consecutive dry days (bar graph) and maximum daily rainfall (line graph) at Aneityum (left) and Port Vila (right). Straight lines indicate linear trends for dry days (in black) and maximum daily rainfall (in blue). The magnitudes of the trends are presented in Table 16.1. Criteria for statistical robustness were not met for determining linear trends at Port Vila. Diamonds indicate years with insufficient data for one or both variables.

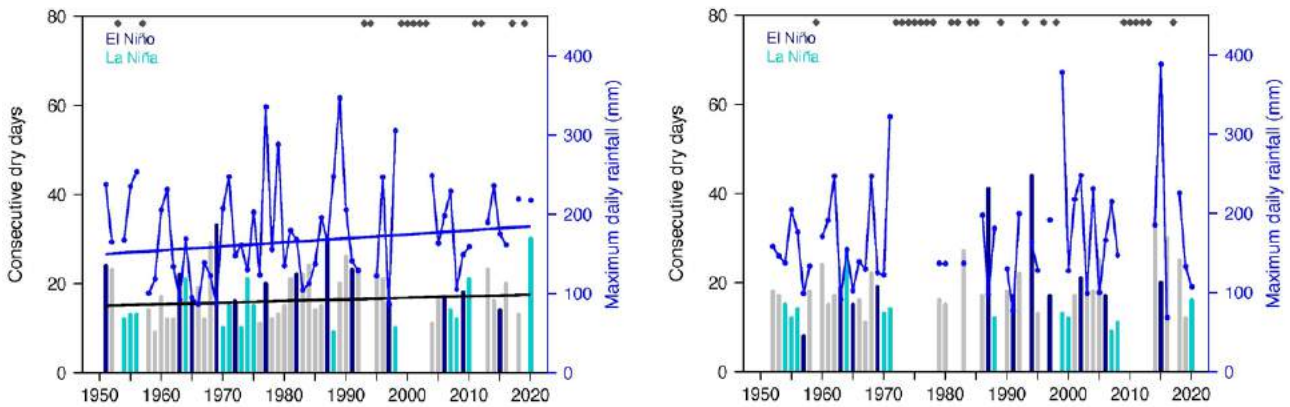

16.5 Air temperature

16.5.1 Seasonal cycle

Seasonal temperature changes in Vanuatu are strongly connected to changes in the surrounding ocean temperature. The country has two distinct seasons – a warm wet season from December to May and a cooler dry season from June to November (Figure 16.5).

The range in average monthly maximum temperatures throughout the year is about 4 ºC for Port Vila and 5 ºC for Aneityum. There has been a clear shift towards warmer average monthly temperatures between the climatology periods of 1961–1990 and 1991–2020 (Figure 16.5), with warmer average maximum temperatures occurring in all months throughout the year for both Port Vila and Aneityum. The range in average monthly minimum temperatures is 5 °C for both Port Vila and Aneityum.

Figure 16.5:
Maximum and minimum air temperature seasonal cycle for Port Vila (purple) and Aneityum (green), and for the periods 1961–1990 (dotted lines) and 1991–2020 (solid lines)

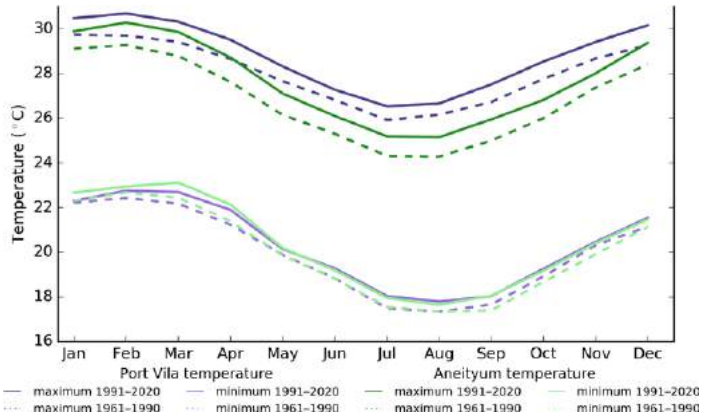

16.5.2 Trends

Average annual and seasonal temperatures have increased at Aneityum and Port Vila (Figure 16.6). All temperature trends at both sites are statistically significant, except for May–October minimum temperatures at Aneityum (Table 16.2). November–April temperatures have increased faster than May–October temperatures, and maximum temperatures have increased faster than minimum temperatures, particularly at Aneityum.

Figure 16.6:
Average annual, November–April and May–October temperatures for Aneityum (left) and Port Vila (right). Straight lines indicate linear trends. The magnitudes of the trends are presented in Table 16.2. Diamonds indicate years with insufficient data for one or more variables.

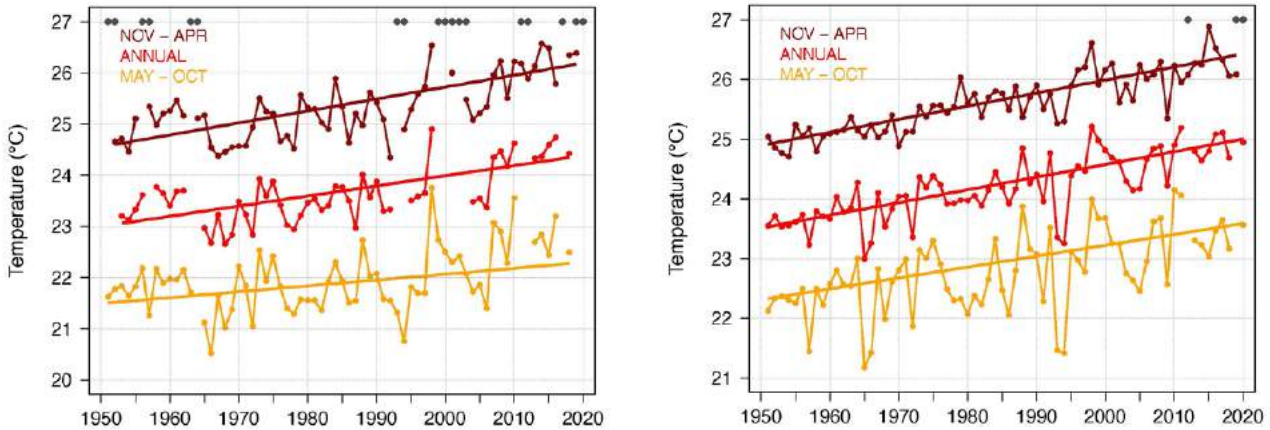

Table 16.2:
Trends in annual and seasonal air temperatures at Aneityum (top) and Port Vila (bottom). The 95% confidence intervals are shown in parentheses, and trends significant at the 95% level are shown in bold.

	Aneityum Tmax (°C/decade)	Aneityum Tmin (°C/decade)	Aneityum Tmean (°C/decade)	Port Vila Tmax (°C/10yrs)	Port Vila Tmin (°C/10yrs)	Port Vila Tmean (°C/10yrs)
	1951–2019			1951–2020		
Annual	**+0.33** (+0.17, +0.47)	**+0.14** (0.00, +0.25)	**+0.20** (+0.08, +0.32)	**+0.24** (+0.20, +0.29)	**+0.17** (+0.10, +0.23)	**+0.21** (+0.16, +0.25)
November–April	**+0.30** (+0.17, +0.44)	**+0.18** (+0.07, +0.28)	**+0.23** (+0.13, +0.34)	**+0.26** (+0.22, +0.31)	**+0.17** (+0.12, +0.22)	**+0.22** (+0.19, +0.25)
May–October	**+0.21** (+0.08, +0.32)	+0.06 (-0.08, +0.22)	**+0.11** (+0.01, +0.24)	**+0.21** (+0.15, +0.28)	**+0.16** (+0.06, +0.27)	**+0.18** (+0.10, +0.27)

Figure 16.7 shows the number of hot days and cold nights at Aneityum and Port Vila. Numerous gaps in daily data prevent the robust calculation of trends in most temperature extremes. However, the number of cold nights at Port Vila is decreasing significantly. Hot days have also occurred more than twice as frequently in recent years at both sites compared to the beginning of their records. This is consistent with the increases in annual and seasonal temperatures (Figure 16.6) as well as trends in temperature extremes for neighbouring Pacific Island countries.

Figure 16.7:
Annual number of hot days and cold nights at Aneityum (left) and Port Vila (right). The straight line indicates the linear trend. Criteria for statistical robustness were not met for determining linear trends at Aneityum and for hot days at Port Vila. Diamonds indicate years with insufficient data for one or both variables.

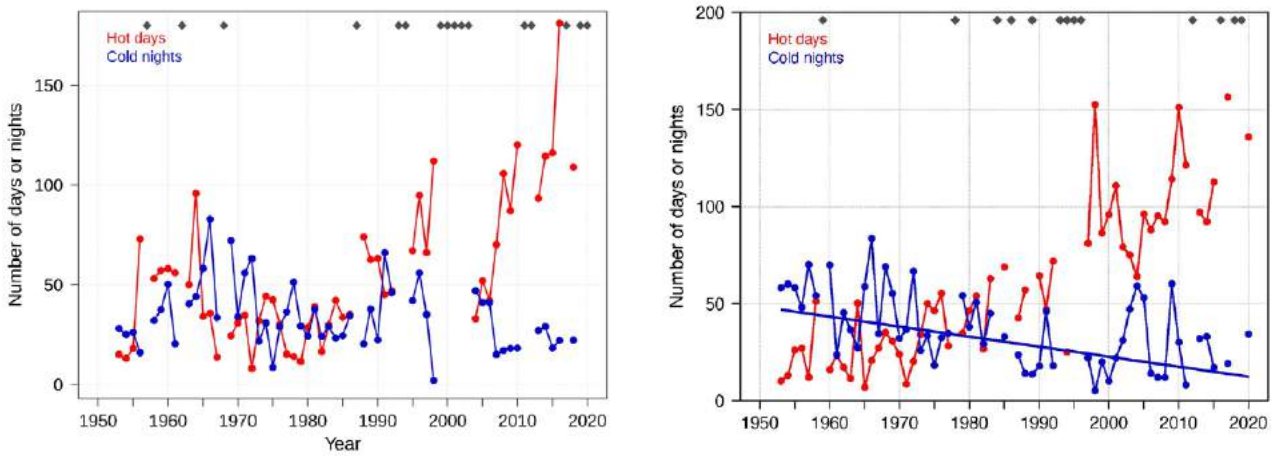

16.6 Tropical cyclones

16.6.1 Seasonal cycle

Tropical cyclones usually affect Vanuatu during the southern hemisphere tropical cyclone season, which is from November to April, but also occasionally occur outside the tropical cyclone season. The Southern Hemisphere Tropical Cyclone Archive indicates that between the 1969/70 and 2017/18 seasons, 117 tropical cyclones (Figure 16.8) passed within the EEZ. This represents an average of 24 cyclones per decade. Tropical cyclones were most frequent in El Niño years (28 cyclones per decade), followed by La Niña years (26 per decade) and least frequent in neutral years (20 cyclones per decade).

Interannual variability in the number of tropical cyclones in the EEZ is large, ranging from zero in some seasons to six in 1971/72 and 1991/92, and five in 1984/85, 1986/87 and 1997/98 (Figure 16.8). High interannual variability and the small number of tropical cyclones occurring in the EEZ make reliable identification of long-term trends in frequency and intensity difficult.

Some tropical cyclone tracks analysed in this section include the tropical depression stage (sustained winds ≤34 knots) before and/or after tropical cyclone formation.

Figure 16.8:
Number of tropical cyclones passing within the Vanuatu EEZ per season. Each season is defined by the ENSO status, with light blue being an El Niño year, dark blue a La Niña year and grey showing a neutral ENSO year. The 11-year moving average is presented as a purple line and considers all years.

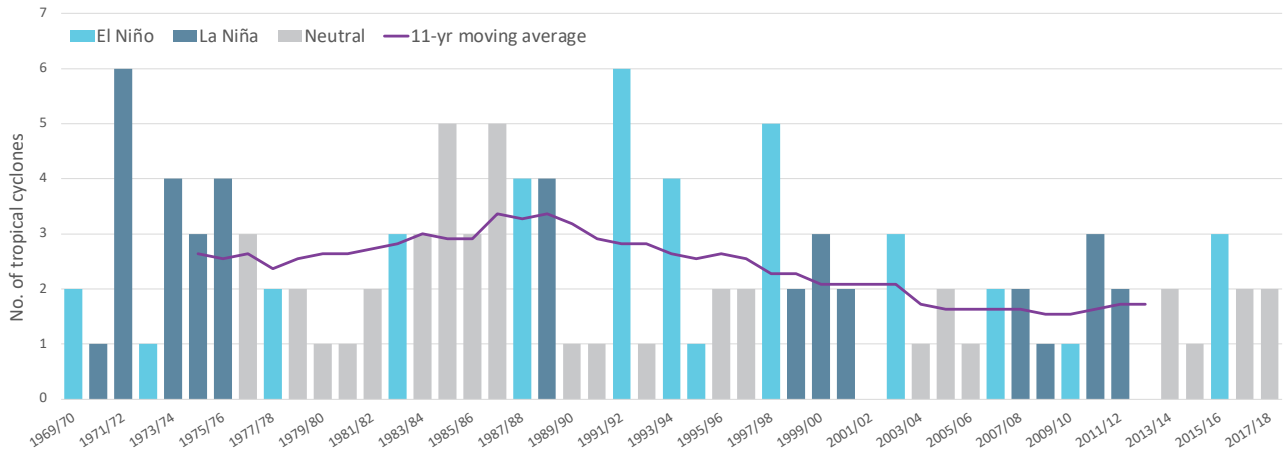

16.6.2 Trends

Trends in total number of tropical cyclones (<995 hPa) and severe tropical cyclones (<970 hPa) are presented for the period 1981/82–2020/21 for the greater Southwest Pacific (135°E–120°W; 0–50°S). Trends are presented at a regional scale as the number of tropical cyclones occurring within Pacific Island EEZs is insufficient for reliable long-term trend analysis.

For the total number of tropical cyclones, the trend (and 95% confidence interval) is -0.92 (-1.85, 0.01) tropical cyclones/decade. There has been little change/marginal decline in the total number of tropical cyclones over the last 40 seasons. This trend is not statistically significant.

For the total number of severe tropical cyclones, the trend is -0.80 (-1.32, -0.29) tropical cyclones/decade. There is a negative trend in the number of severe tropical cyclones over the last 40 seasons. There has been little change/marginal decline in the proportion of tropical cyclones reaching severe status. The trend is -0.04 (-0.08, 0.00) tropical cyclones/decade. The negative trend is statistically significant.

Records of tropical cyclones exist from the late 1800s in some countries in the Southwest Pacific, but trends in tropical cyclones have only been presented from 1981/82. Satellite-based observations began in the Southwest Pacific in the early 1970s, but consistent coverage and reliable intensity estimates have only been available since the early 1980s. Confidence in tropical cyclone trends is moderate as the definition of a tropical cyclone has changed and satellite observation methods have continued to improve over the last 40 years.

16.7 Sea surface temperature

16.7.1 Seasonal cycle

Ocean temperature, as measured by the Port Vila tide-gauge from 1993 to 2021, reaches on average a maximum of 29 °C in February/March, but individual months can get as high as almost 31 °C in January–March (Figure 16.9). Minimum average temperature is 25.5 °C in August. Hourly temperatures can be up to 2 °C higher or lower than these monthly averages, although 50% of hourly observations fall within 1 °C of the average.

Figure 16.9:
Annual temperatures measured at the Port Vila tide-gauge. Blue dots show the monthly average, and shaded boxes show the middle 50% of hourly observations. Lines show the top and bottom 25% of hourly observations.

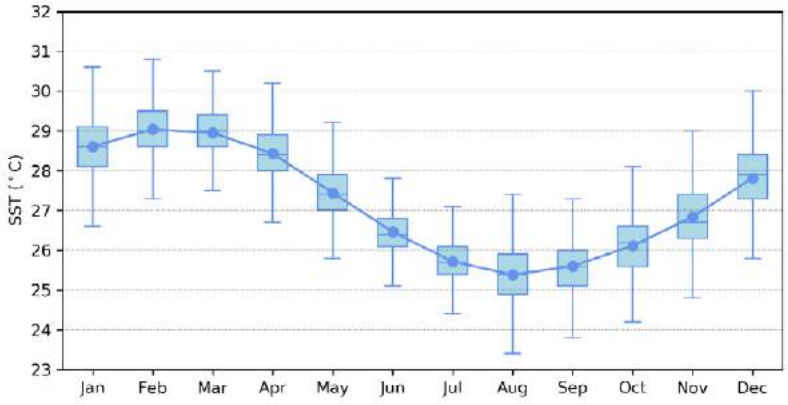

16.7.2 Trends

Figure 16.10 shows the 1981–2021 SST from satellite observations averaged over the EEZ. The data show a trend of 0.23 °C per decade with a 95% confidence interval of ±0.1 °C.

Figure 16.10:
Sea surface temperature from satellite observations averaged across the Vanuatu EEZ, shown as the orange line. The blue line shows the linear regression trend.

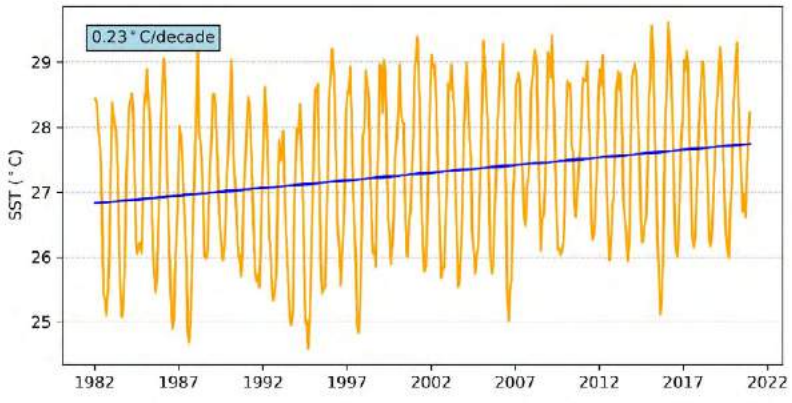

16.8 Sea level

16.8.1 Seasonal cycle

Vanuatu experiences a semidiurnal tidal cycle, meaning two high and two low tides per day, although high and low tides are often asymmetrical on a given day. The highest predicted tides of the year typically occur during the wet season months of November–February. Figure 16.11 shows the number of hours the 99th percentile (1.63 m) sea level threshold is exceeded per month across the entire sea level record at Port Vila. Peak sea levels typically occur from October to March.

Figure 16.11:
Number of hours exceeding 99th percentile sea level threshold per month from 1993 to 2021 at the Port Vila tide-gauge. Blue shading indicates the number of hours, and the final row provides a percentage summary of all the years.

Number of hours exceeding 1.63 m (Port Vila, Vanuatu)

	Jan	Feb	Mar	Apr	May	Jun	Jul	Aug	Sep	Oct	Nov	Dec	Annual
1993	0	0	0	0	0	0	0	0	0	0	0	0	0
1994	0	0	0	0	0	0	0	0	0	0	0	0	0
1995	0	0	0	0	0	0	0	0	0	0	2	0	2
1996	8	0	0	0	0	0	0	0	0	2	0	1	11
1997	5	0	12	0	0	0	0	0	0	0	0	0	17
1998	0	0	0	0	0	0	0	0	0	0	0	0	0
1999	0	0	0	0	0	0	0	0	0	0	0	0	0
2000	0	0	0	0	0	0	0	0	0	0	2	1	3
2001	1	1	0	2	0	0	0	0	0	1	1	3	9
2002	0	0	3	0	0	0	0	0	0	2	0	0	5
2003	0	0	0	0	0	0	0	0	0	0	0	0	0
2004	0	0	0	0	0	0	0	0	0	0	0	0	0
2005	0	1	0	0	0	0	0	0	0	0	0	0	1
2006	4	0	0	0	0	0	0	0	0	0	0	0	4
2007	0	0	0	0	0	0	0	0	0	8	8	0	16
2008	0	0	0	1	1	0	0	0	0	6	14	1	23
2009	14	0	4	0	0	0	0	0	2	5	0	0	25
2010	0	0	2	0	0	0	0	0	0	0	0	0	2
2011	0	0	0	1	0	0	0	0	5	8	0	5	19
2012	0	0	0	0	0	0	0	0	0	0	0	2	2
2013	1	0	0	0	0	0	0	0	0	0	0	0	1
2014	0	0	0	0	0	0	0	0	0	1	0	0	1
2015	0	0	2	0	0	0	0	0	0	0	0	0	2
2016	0	0	0	0	0	0	0	0	0	0	0	0	0
2017	0	0	0	0	0	0	0	0	0	0	0	0	0
2018	3	0	0	0	0	0	0	0	0	0	0	0	3
2019	0	1	0	0	0	0	0	0	0	0	0	0	1
2020	0	0	0	0	0	0	0	0	0	2	0	3	5
2021	0	0	0	0	0	0	0	0	0	2	4	5	11
Monthly Totals (%)	22	2	14	2	1	0	0	0	4	23	19	13	

16.8.2 Trends

Sea level at Vanuatu, measured by satellite altimeters (Figure 16.12) since 1993, has risen between 3.5 and 5 mm per year across the EEZ, with a confidence interval of ±0.4 mm in the south and up to ±1.0 mm in the north. Most of the EEZ exhibits sea-level rise that is larger than the global average of 3.1 ± 0.4 mm per year (von Schuckmann et al. 2021). This rise is partly linked to a pattern related to climate variability from year to year and decade to decade.

Trend estimates at the Port Vila tide-gauge over a similar time span to the altimetry observations (January 1993 to July 2020) are provided in the PSLGM Monthly Data Report for July 2020 (http://www.bom.gov.au/ntc/IDO60101/IDO60101.202007.pdf). For Port Vila, the trend is reported as 0.3 mm per year, much less than the altimetry trends shown in Figure 16.12 (tide-gauge indicated by star symbol). Vanuatu is one of the few places in the Southwest Pacific that has islands experiencing geodetic uplift (rising land) (Brown et al. 2020). The tide-gauge fixed to land shows the trend relative to the rising land and therefore offsets the effects of sea-level rise.

Figure 16.12: Satellite altimetry annual trend for the Pacific from 1993 to 2020, with the Vanuatu EEZ highlighted. The star symbol indicates the location of the tide-gauge at Port Vila.

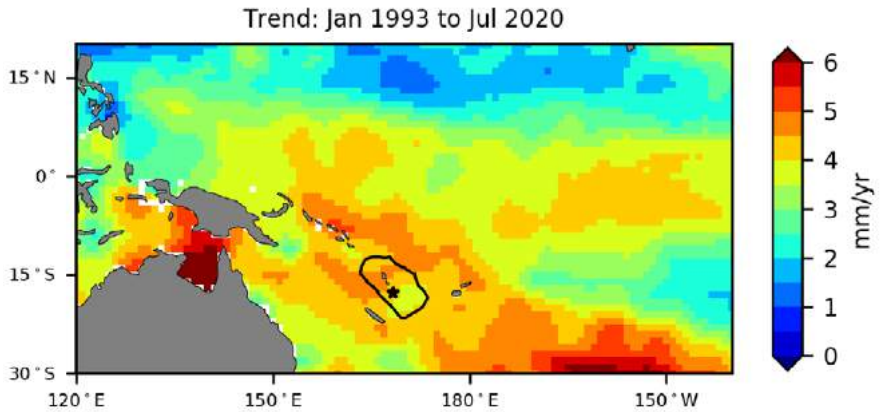

16.9 Waves

16.9.1 Seasonal cycle

The average wave climate at Port Vila is defined by the significant wave height, peak period and peak direction. The significant wave height is the mean wave height (from trough to crest) of the highest one third of waves and corresponds to the wave height that would be reported by an experienced observer. Peak period is the time interval between two waves of the dominant wave period. Peak direction is the direction from which the dominant waves are coming.

The average sea state is dominated by wind seas from the south. The annual mean wave height is 0.55 m, the annual mean wave direction is 182° and the annual mean wave period is 9.63 s. In the Pacific, waves often come from multiple directions and for different periods at a time. In Port Vila, there are often more than four different wave direction/period components coming from the southeast to southwest (Figure 16.13).

Figure 16.13:
Annual wave rose for Port Vila. Note that direction is where the wave is coming from.

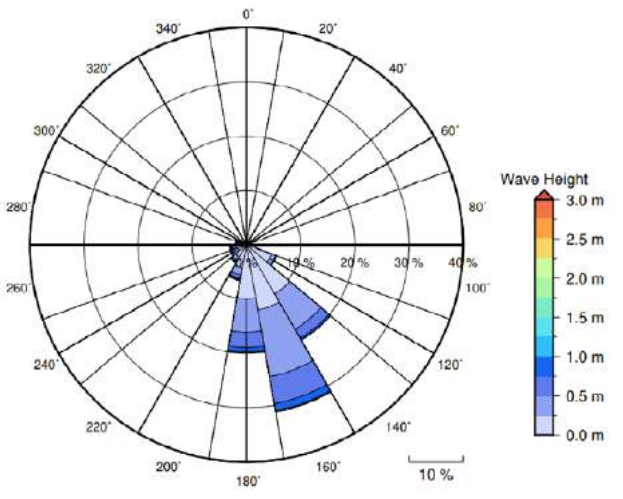

Seasonal wave height remains relatively consistent throughout the year. Wave period has a definitive peak in May (Figure 16.14).

Figure 16.14:
Monthly wave height (black line), wave period (red line) and wave direction (arrows). The grey area represents the range of wave height between calm periods (10% of lowest wave height) and large wave events (10% of highest wave height).

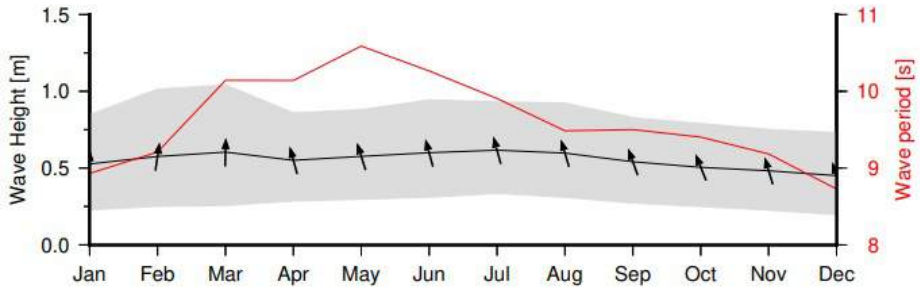

16.9.2 Trends

Waves change from month to month with the seasons, but they also change from year to year with climate oscillations. Typically, these changes are smaller than the seasonal changes but can be important during phenomena such as ENSO. In Port Vila, the mean annual wave height has remained unchanged since 1979 (Figure 16.15). The mean annual wave height in Port Vila is not significantly correlated with the main climate indicators of the region.

Figure 16.15:
Annual wave height (black line), wave period (red line) and wave direction (arrows). The grey area represents the range of wave height between calm periods (10% of lowest wave height) and large wave events (10% of highest wave height).

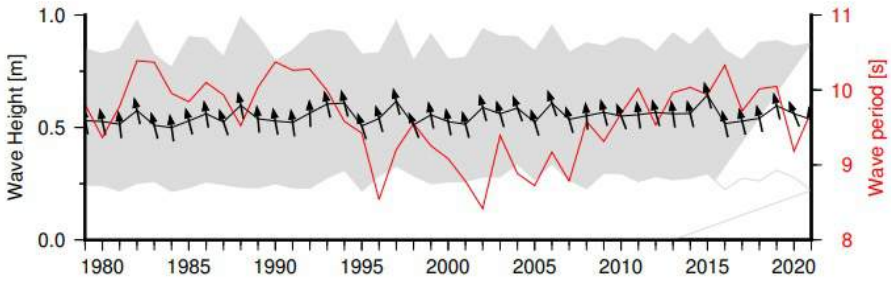

16.9.3 Extreme waves

Extreme wave analysis completed for Port Vila was done by defining a severe height threshold and fitting a generalized Pareto distribution (GPD). The optimum threshold selected was 1.83 m. In the 42-year wave hindcast, 116 wave events reached or exceeded this threshold, averaging 2.8 events per year. The GPD was fitted to the largest wave height reached during each of these events (Figure 16.16, Table 16.4). Extreme wave analysis is a very useful tool but is not always accurate because the analysis is very sensitive to the data available, the type of distribution fitted and the threshold used. For example, this analysis does not accurately account for tropical cyclone waves. More in-depth analysis is required to obtain results appropriate for designing coastal infrastructure and coastal hazard planning.

Figure 16.16:
Extreme wave distribution for Port Vila. The crosses represent the wave events that have occurred since 1979. The solid line is the statistical distribution that best fits past wave events. The dashed lines show the upper and lower confidence limits of the fit. There is a 95% chance that the fitted distribution lies between the two dashed lines. Note that the annual return interval is in logarithmic scale.

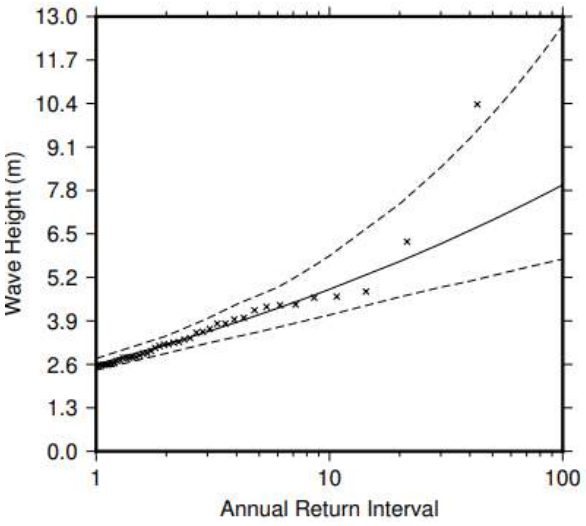

Table 16.4:
Summary of the results from extreme wave analysis in Port Vila.

Large wave height (90th percentile)	0.87 m
Severe wave height (99th percentile)	1.59 m
1-year ARI wave height	2.59 m
10-year ARI wave height	4.84 m
20-year ARI wave height	5.68 m
50-year ARI wave height	6.92 m
100-year ARI wave height	7.97 m

References

Australian Bureau of Meteorology and CSIRO. 2011. Climate Change in the Pacific: Scientific Assessment and New Research. Volume 1: Regional Overview. Volume 2: Country Reports. https://www.pacificclimatechangescience.org/publications/reports/report-climate-change-in-the-pacific-scientific-assessment-and-new-research/

Australian Bureau of Meteorology and CSIRO. 2014. Climate Variability, Extremes and Change in the Western Tropical Pacific: New Science and Updated Country Reports. Pacific-Australia Climate Change Science and Adaptation Planning Program Technical Report, Australian Bureau of Meteorology and Commonwealth Scientific and Industrial Research Organisation, Melbourne, Australia. https://www.pacificclimatechangescience.org/publications/reports/climate-variability-extremes-and-change-in-the-western-tropical-pacific-2014/

Banzon, V., Smith, T.M., Chin, T.M., Liu, C., and Hankins, W. 2016. A long-term record of blended satellite and in situ sea-surface temperature for climate monitoring, modelling and environmental studies, Earth Syst. Sci. Data, 8, 165–176, https://doi.org/10.5194/essd-8-165-2016

Bronaugh, D. and Werner A. 2019. Zhang + Yue-Pilon Trends Package for R. Version 0.10-1.1, 2019. https://cran.rstudio.com/web/packages/zyp/index.html

Brown, N. J., Lal, A., Thomas, B., McClusky, S., Dawson, J., Hu, G., and Jia, M. 2020. Vertical motion of Pacific Island tide gauges: combined analysis from GNSS and levelling. Record 2020/03. Geoscience Australia, Canberra. http://dx.doi.org/10.11636/Record.2020.003

Church, J.A., White, N.J. 2011. Sea-Level Rise from the Late 19th to the Early 21st Century. Surv Geophys, 32, 585–602. https://doi.org/10.1007/s10712-011-9119-1

Hersbach, H, Bell, B, Berrisford, P, et al. 2020. The ERA5 global reanalysis. Q J R Meteorol Soc. 146, 1999–2049. https://doi.org/10.1002/qj.3803

Kuleshov, Y., Fawcett, R., Qi, L., Trewin, B., Jones, D., McBride, J., and Ramsay, H. 2010. Trends in tropical cyclones in the South Indian Ocean and the South Pacific Ocean. J. Geophys. Res., 115, D01101, https://doi.org/10.1029/2009JD012372

McGree, S., Herold, N., Alexander, L., Schreider, S., Kuleshov, Y., Ene, E., Finaulahi, S., Inape, K., Mackenzie, B., Malala, H., Ngari, A., Prakash, B., & Tahani, L. 2019. Recent Changes in Mean and Extreme Temperature and Precipitation in the Western Pacific Islands, Journal of Climate, 32(16), 4919-4941. https://doi.org/10.1175/JCLI-D-18-0748.1

Nicholls, N., Landsea, C., Gill, J. 1998. Recent trends in Australian region tropical cyclone activity, Meteorolo. Atmos. Phys., 65, 197–205. https://doi.org/10.1007/BF01030788

Pacific Climate Change Monitor: 2021. Marra, J.J., Gooley, G., Johnson, M-V, Keener, V., Kruk, M.K., McGree, S., Potemra, J.T., and Warrick, O. 2022. Pacific Islands - Regional Climate Centre Network (PI-RCC) Report to the Pacific Islands Climate Service (PICS) Panel and Pacific Meteorological Council (PMC). April 18, 2022. https://www.pacificmet.net/sites/default/files/inline-files/documents/PICC%20Monitor_2021_FINALpp_0.pdf

Reynolds, R.W., Smith, T.M., Liu, C., Chelton, D.B., Casey, K.S., and Schlax, M.G. 2007. Daily High-Resolution-Blended Analyses for Sea Surface Temperature. J. Clim. 20(22), 5473–5496. https://journals.ametsoc.org/view/journals/clim/20/22/2007jcli1824.1.xml

Sen, P, K. 1968. Estimates of the Regression Coefficient Based on Kendall's Tau. Journal of the American Statistical Association, 63:324, 1379–1389. DOI: 10.1080/01621459.1968.10480934

Smith, G.A., Hemer, M., Greenslade, D., Trenham, C., Zieger, S., & Durrant, T. 2021. Global wave hindcast with Australian and Pacific Island focus: From past to present. Geosci. Data J., 8(1), 24– 33. https://doi.org/10.1002/gdj3.104

University of New South Wales (UNSW). 2022. Climpact. Version 3.1.1. https://climpact-sci.org/

von Schuckmann, K., Le Traon, P.Y., Smith, N., Pascual, A., Djavidnia, S., Gattuso, J. P., et al. 2021. Copernicus marine service ocean state report, issue 5. J. Oper. Oceanogr. 14, 1–185. https:/doi.org/10.1080/1755876X.2021.1946240

Glossary

A

Altimetry
see *Satellite altimetry*

Anthropogenic
Resulting from or produced by human beings.

Anthropogenic emissions
Emissions of greenhouse gases, greenhouse gas precursors and aerosols associated with human activities, including the burning of fossil fuels, deforestation, land use changes, livestock, fertilisation, etc.

Anomaly
In climate science, a deviation from the normal value of a variable. It is usually the deviation of a variable from the average value at a specific place and time.

Austral
see also *Boreal*
Relating to the southern hemisphere.

Average return interval
An annual return (or recurrence) interval is sometimes also known as 'return period'. It is the average number of years that it is predicted will pass before an event of a given magnitude occurs. For example, a 50-year ARI event would happen, on average, every 50 years.

B

Boreal
see also *Austral*
Relating to the northern hemisphere.

C

Climate
Climate in a narrow sense is usually defined as the average weather, or more rigorously, as the statistical description in terms of the mean and variability of relevant parameters over a period of time ranging from months to thousands or millions of years. The classic period for averaging these variables is 30 years, as defined by the World Meteorological Organization (WMO). The relevant quantities are most often surface variables such as temperature, precipitation and wind. Climate in a wider sense is the state, including a statistical description, of the climate system. In various parts of this report, different averaging periods, such as a period of 20 years, are also used.

Climate change
see also *Climate variability*
Climate change refers to a change in the state of the climate that can be identified (e.g., by using statistical tests) by changes in the mean and/or the variability of its properties and that persists for an extended period, typically decades or longer. Climate change may be due to natural internal processes or external forcing, or to persistent anthropogenic changes in the composition of the atmosphere or in land use.

Climate projection
see also *Projection*
A projection of the response of the climate system to emission or concentration scenarios of greenhouse gases and aerosols, or radiative forcing scenarios, often based upon simulations by climate models. Climate projections are distinguished from climate predictions in order to emphasise that climate projections depend upon the radiative forcing scenario used, which are based on assumptions concerning, for example, future socioeconomic and technological developments that may or may not be realised and are therefore subject to substantial uncertainty.

Climate variability
see also Climate Change, Modes of climate variability
Climate variability refers to variations in the mean state and other statistics (such as standard deviations, the occurrence of extremes, etc.) of the climate on all spatial and temporal scales beyond that of individual weather events. Variability may be due to natural internal processes within the climate system, or to variations in natural or anthropogenic external forcing.

Climatology
a. The description and scientific study of climate. b. The long-term average state of a particular climate variable or process (e.g., the 30-year average temperature at a location). Climatology is used in this context within this report.

Climate and Ocean Support Program in the Pacific (COSPPac)
COSPPac, extended for five years from 2018, builds on the success of the first phase from 2012. In Phase 2, the program is funded by the Australian Government with additional investment from New Zealand Aid. Implementation partners include: Bureau of Meteorology (The Bureau), Pacific Community (SPC), Secretariat of the Pacific Regional Environment Programme (SPREP), Geoscience Australia (GA) and National Institute of Water and Atmospheric Research (NIWA). Phase 2 continues the collaborative partnership between 15 Pacific Island countries and territories in the western tropical Pacific and the implementation partners. The program includes three projects: the Pacific Sea Level and Geodetic Monitoring (PSLGM) Project – continuing a 30-year South Pacific Sea Level and Climate Monitoring Project (SPSLCMP) to establish high-quality data records for the Pacific region; the Climate Data for the Environment (CliDE) and Services Client (CliDEsc) Project – to archive meteorological data locally in 15 countries and territories and provide sector-specific products; and the Seasonal Prediction Project (SPP), which supports seasonal and intraseasonal climate and ocean monitoring and prediction services. The three projects are supported by training and communications that build capability and climate resilience and incorporate traditional knowledge.

Convergence
In meteorology, where winds flow from different directions towards each other, thus meeting at one point or along one line. Similarly, in oceanography, where water currents flow towards each other and meet. Horizontal convergence usually forces vertical motion to occur, such as convection.

Coral bleaching
Coral bleaching results from a breakdown of the symbiotic relationship between corals and unicellular algae (zooxanthellae). The symptoms of bleaching include a gradual loss of colour as the algae are expelled from the coral tissue. In severe cases, it can result in the death of the coral. The stress factor most commonly associated with bleaching is elevated sea temperature, although it also occurs in response to any number of environmental pressures, whether natural or anthropogenic, such as changes in solar radiation, salinity (freshwater input), disease, sedimentation, nutrients and pollution.

D

Driver (of climate)
Any natural or human-induced factor that directly or indirectly causes a change.

E

El Niño
see also El Niño–Southern Oscillation (ENSO), La Niña
This is the warm phase of the El Niño–Southern Oscillation (ENSO). El Niño events occur on average once every two to seven years. They are associated with basin-wide warming of the tropical Pacific Ocean east of the dateline and a weakening of the Walker Circulation.

El Niño–Southern Oscillation (ENSO)
see also El Niño, La Niña, neutral
The term El Niño was initially used to describe a warm water current that periodically flows along the coast of Ecuador and Perú, disrupting the local fishery. It has since become identified with a basin-wide warming of the tropical Pacific Ocean east of the dateline. This oceanic event is associated with a fluctuation of a global-scale tropical and subtropical surface pressure pattern called the Southern Oscillation. This naturally occurring, coupled atmosphere–ocean phenomenon, with timescales of approximately two to seven years, is known as the El Niño–Southern Oscillation (ENSO). The state of ENSO is often measured by the Southern Oscillation Index (SOI) and sea surface temperatures in the central and eastern equatorial Pacific. During an ENSO event, the prevailing trade winds weaken, reducing upwelling and altering ocean currents such that the sea surface temperatures warm, further weakening the trade winds. This event has a great impact on the wind, sea surface temperature and precipitation patterns in the tropical Pacific. It has climatic effects throughout the Pacific region and in many other parts of the world. The cold phase of ENSO is called La Niña.

ERA5
see also Reanalysis
ERA5 is the fifth generation European Centre for Medium-Range Weather Forecasts (ECMWF) atmospheric reanalysis of the global climate covering the period from January 1950 to present. ERA5 is produced by the Copernicus Climate Change Service (C3S) at ECMWF. ERA5 provides hourly estimates of a large number of atmospheric, land and oceanic climate variables. The data cover the Earth on a 30 km grid and resolve the atmosphere using 137 levels from the surface up to a height of 80 km. ERA5 includes information about uncertainties for all variables at reduced spatial and temporal resolutions.

Evapotranspiration
Evapotranspiration is the sum of evaporation from land surface (e.g., from the soil and bodies of water such as lakes and rivers) and transpiration from vegetation.

Exclusive economic zone (EEZ)
An exclusive economic zone, as prescribed by the 1982 United Nations Convention on the Law of the Sea, is an area of the sea in which a sovereign state has special rights regarding the exploration and use of marine resources, including energy production from water and wind. It stretches from the baseline out to 200 nautical miles from the coast of the state in question.

External forcing
see Forcing

Extreme weather event
An event that is rare at a particular place and time of year. An extreme weather event would normally be as rare as or rarer than the 10th or 90th percentile of the observed distribution. For example, warm nights or hot days are those exceeding the 90th percentile of temperature, while cold nights or days are those falling below the 10th percentile.

G

Generalized Pareto distribution
In statistics, the generalized Pareto distribution (GPD) is a family of continuous probability distributions. It is often used to model the tails of another distribution. It is specified by three parameters: location, scale and shape.

Glacial isostatic adjustment
The last Ice Age occurred just 16 000 years ago, when great sheets of ice, two miles thick, covered much of Earth's northern hemisphere. Though the ice melted long ago, the land once under and around the ice is still rising and falling in reaction to its Ice Age burden. This ongoing movement of land is called glacial isostatic adjustment.

Gridded datasets
see also Reanalysis
A set of climate data that are given for the same time or average period on a regular grid in space. Data at each grid point represent the average value over a grid box whose size is determined by the spacing between the grid points (also called the grid resolution). Global climate model and reanalysis data are produced as gridded data.

H

Hindcast
see also Reanalysis
A statistical calculation determining probable past conditions. In this case, reanalysis wind data (i.e., wind data which has been calculated for a regular global grid based on directly and indirectly measured data on an irregular grid) is applied to a wave model to compute the likely wave structure over a historical time period in lieu of directly sensed wave data.

Homogenisation
see also Inhomogeneities
Climate data homogenisation aims to adjust data if necessary, so that all variations in the data series are caused by real changes in the climate and are not due to artificial changes in the way or location at which the data were recorded.

Humidity
see Relative humidity

I

Index/indices
A number representing a measure of a particular feature of the climate system at a given time, varying with time and used as a measure of variability.

Inhomogeneities
see also Homogenisation
Inhomogeneities in climate data are caused when artificial changes affect the climate observations through time. These changes may be abrupt or gradual. The main causes of inhomogeneities are changes in instrumentation, station moves, changes in the local environment such as urbanisation, or the introduction of different observing practices. These inhomogeneities can interfere with the proper assessment of any climate trends and extremes. To account for these artificial changes, homogenisation methods are applied to the data.

Interannual
From year to year.

Interdecadal Pacific Oscillation (IPO)
see also Pacific Decadal Oscillation (PDO)
The Interdecadal Pacific Oscillation is a natural recurring pattern of variability in tropical Pacific Ocean sea surface temperatures occurring over periods of about 15 years and longer. While defined differently, the IPO and PDO (Pacific Decadal Oscillation) describe essentially the same variability.

Intertropical Convergence Zone (ITCZ)
see also Trade winds
An east–west band of low-level wind convergence near the equator where the southeast trade winds of the southern hemisphere meet the northeast trade winds of the northern hemisphere. It has an associated band of heavy rainfall as the winds converge and moist air is forced upward.

L

La Niña

see also El Niño, El Niño–Southern Oscillation (ENSO), neutral

The most common of several names given to cold phase of the El Niño–Southern Oscillation (ENSO). La Niña is the counterpart to the El Niño warm event, although La Niña events tend to be somewhat less regular in their behaviour and duration. La Niña is associated with large-scale cooling of the surface waters of the eastern tropical Pacific Ocean and a strengthening of the Walker Circulation.

M

Madden–Julian Oscillation (MJO)

The Madden–Julian Oscillation is the major fluctuation in tropical weather on weekly to monthly timescales. The MJO can be characterised as an eastward moving 'pulse' of cloud and rainfall near the equator that typically recurs every 30 to 60 days.

Mean sea level

see also Relative sea level, Sea level change/rise

Mean sea level is normally defined as the average relative sea level over a period, such as a month or a year, long enough to average out transients such as waves and tides.

Meridional

see also Zonal

In meteorology, a flow in a direction that is parallel to a line of longitude; along a meridian; northerly or southerly; as opposed to zonal.

Modes of climate variability

see also Climate variability

Natural variability of the climate system, in particular on seasonal and longer timescales, predominantly occurs with preferred spatial patterns and timescales through the dynamical characteristics of the atmospheric circulation and through interactions with the land and ocean surfaces. Such patterns are often called regimes or modes. Modes of variability often involve a connection between a remote driver and a local effect, termed a teleconnection. An example is the El Niño–Southern Oscillation (ENSO).

N

Neutral (ENSO)

see also El Niño, El Niño–Southern Oscillation (ENSO), La Niña

In the neutral state (neither El Niño nor La Niña), trade winds blow east to west across the surface of the tropical Pacific Ocean, bringing warm moist air and warmer surface waters towards the western Pacific and keeping the central Pacific Ocean relatively cool. The thermocline is deeper in the west than the east.

P

Pacific–Australia Climate Change Science Adaptation Planning program (PACCSAP program)

see also PCCSP

The 2011–2014 Pacific–Australia Climate Change Science Adaptation Planning program (PACCSAP) built on the success of the 2009–2011 Pacific Climate Change Science Program (PCCSP). With support from Australian Aid (AusAID), the Department of the Environment, the Bureau of Meteorology and the Commonwealth Scientific and Industrial Research Organisation (CSIRO), PACCSAP continued the collaborative partnership between Australian scientists, 14 Pacific Island countries and East Timor, and regional and non-government organisations in the western tropical Pacific. Using climate observations, projections and targeted communication, it has helped fill the climate information and knowledge gap and generated scientific insight into the state of climate change in the Pacific region.

Pacific Climate Change Science Program (PCCSP)

see also PACCSAP

The Pacific Climate Change Science Program (PCCSP) was a collaborative research partnership between the Bureau of Meteorology and CSIRO, Australian government agencies (AusAID and the Department for Climate Change and Energy Efficiency), 14 Pacific Island countries and East Timor, and regional and international organisations which ran from 2009 to 2011. It provided critical climate scientific research and was instrumental in building the capacity of Pacific Island countries to manage the effects of climate change.

Projection

see also Climate projection

The term 'projection' is used in two senses in the climate change literature. In general usage, a projection can be regarded as any description of the future and the pathway leading to it. However, a more specific interpretation has been attached to the term 'climate projection' by the IPCC when referring to model-derived estimates of future climate.

R

Reanalysis

see also Gridded data, Hindcast

An analysis combining many irregular meteorological or oceanographic observations from close to the same time into a

physically consistent, complete gridded dataset for a given time and usually for the whole globe. A reanalysis may be used to drive a hindcast.

Relative humidity
Relative humidity is defined as the amount of water vapour in the air, relative to the maximum amount of water vapour that the air is able to hold, without it condensing (expressed as a percentage).

Relative sea level
see also Mean sea level
Relative sea level is sea level measured by a tide-gauge with respect to the land upon which it is situated.

Relative sea-level change/rise
see also Mean sea level, Sea-level change/rise
Relative sea-level rise occurs where there is a local increase in the level of the ocean relative to the land, which might be due to ocean rise and/or land level subsidence.

S

Satellite altimetry
for sea-level change/rise
An altimeter measures how high something is. Satellite radar altimeters measure the ocean surface height (sea level) by measuring the time it takes a radar pulse to make a round-trip from a satellite to the sea surface and back.

Sea-level change/rise
see also *Mean sea level, Relative sea-level change/rise*
Sea level can change, both globally and locally, due to: (1) changes in the shape of the ocean basins; (2) changes in the total mass of water; and (3) changes in water density. Factors leading to sea-level rise under global warming include both increases in the total mass of water from the melting of land-based snow and ice, and changes in water density from an increase in ocean water temperatures and salinity changes.

Seasonal cycle
As the Earth moves around the sun, it spins on its axis at a constant angle. Due to this angle, the northern and southern hemispheres are tilted away from the sun at opposite points of the year. When a hemisphere is tilted away from the sun, it experiences cooler days and nights and longer nights. When a hemisphere is tilted towards the sun, it experiences warmer days and nights and longer days. At the equator, daylight patterns remain fairly consistent throughout the year there is less variation in temperature.
In climatology, the seasonal cycle also refers to variation in climate (for one or more parameters) through the year.

Sea surface temperature (SST)
The temperature of the ocean surface. The term 'sea surface temperature' is generally representative of the upper few metres of the ocean as opposed to the skin temperature, which is the temperature of the upper few centimetres.

Significant wave height
The significant wave height is defined as the mean wave height (from trough to crest) of the highest one third of waves and corresponds to the wave height that would be reported by an experienced observer.

Southern Oscillation
see also El Niño-Southern Oscillation (ENSO)
Fluctuation of a global-scale tropical and subtropical surface pressure pattern.

Southern Oscillation Index (SOI)
The Southern Oscillation Index (SOI) is calculated from the monthly or seasonal fluctuations in the air pressure difference between Tahiti and Darwin.

South Pacific Convergence Zone (SPCZ)
A persistent and greatly elongated zone of low-level convergence extending from approximately 140°E near the equator to approximately 120°W at 30°S. The zone is not quite linear but is oriented more west to east near the equator and has a more diagonal orientation (northwest to southeast) at higher latitudes.

Storm surge
The temporary increased height of the sea above the level expected from tidal variation alone at that time and place due to extreme meteorological conditions.

Surface mass balance
The mass balance is the net gain or loss of ice and snow for an ice sheet. It is related to difference between snow accumulation versus melt, run-off and iceberg calving.

Subsidence
The sinking of the land. In Pacific Island countries, this is usually caused by the natural event of tectonic movements often brought on by earthquakes. Subsidence can also be caused by human activity such as removing groundwater or other mining activities.

T

Thermal expansion
see also *Sea-level change/rise, Mean sea level*
The increase in volume (and decrease in density) that results from warming water.

Timeseries
The values of a variable generated successively in time. Graphically, a timeseries is usually plotted with time on the horizontal axis (x-axis) and the values of the variable on the vertical axis (y-axis).

Trade winds
see also *Intertropical Convergence Zone (ITCZ)*
The wind system occupying most of the tropics that blows from subtropical high-pressure areas towards the equator.

Tropical cyclone
A tropical cyclone is a tropical depression of sufficient intensity to produce sustained gale force winds (at least 63 km per hour). A severe tropical cyclone produces sustained hurricane force winds (at least 118 km per hour). Severe tropical cyclones correspond to the hurricanes or typhoons of other parts of the world.

W

Walker Circulation
Warm sea surface temperatures in the western Pacific pump heat and moisture into the atmosphere above. In a process known as atmospheric convection, this warm air rises high into the atmosphere and, if the air is moist enough, causes towering cumulonimbus clouds and rain. This now drier air then travels east before descending over the cooler eastern tropical Pacific. The pattern of air rising in the west and falling in the east with westward moving air at the surface is referred to as the Walker Circulation.

Warm Pool (also known as West Pacific Warm Pool)
An extensive pool of the world's warmest water, with temperatures exceeding 28–29 °C, extending from the central Pacific to the far eastern Indian Ocean.

Wave period
The wave period is usually reported in seconds as a peak or an average time interval between two waves. Swell waves are energetic and faster waves that are often defined as having periods of 8 to 20 seconds. Smaller choppy waves are referred to as wind sea and have a period of between 3 and 8 seconds.

West Pacific Monsoon (WPM)
A monsoon is a tropical and subtropical seasonal reversal of both surface winds and associated rainfall caused by differential heating between a continental scale land mass and the adjacent ocean. The West Pacific Monsoon is the eastern edge of the Indonesian or Maritime Continent Monsoon and the southern extension of the larger Asian–Australian Monsoon system.

Z

Zonal
see also *Meridional*
In meteorology, latitudinal, that is, easterly or westerly; opposed to meridional.

Produced by the Pacific Community (SPC)

Pacific Community
B.P. D5 - 98848 Noumea Cedex, New Caledonia

Telephone: +687 26 20 00
Email: spc@spc.int
Website: www.spc.int